CORROSION AND TRIBO-CORROSION BEHAVIOUR OF METALLIC ORTHOPAEDIC IMPLANT MATERIALS

by

Yu Yan

Submitted in accordance with the requirements for the degree of

Doctor of Philosophy

The University of Leeds

School of Mechanical Engineering

September 2006

ACKNOWLEDGEMENTS

I would like to express my deepest gratitude to my Ph.D supervisor, Professor Anne Neville for her constant guidance and endless encouragement. Her enthusiasm, her inspiration and her great efforts to explain things clearly and simply, make this thesis possible.

I am grateful to the present and past members of the Corrosion and Surface Engineering Research Group (CoSERG), in particular, Ardian, Tomasz, Chen, Yanmeng, Djico, Simon, Chun, Kent, Haque, Faisal, Aurelie, Anne-Lise, John, Ley, Kuldeep, Inga, Rupesh, Penny, Jacky, Greg, Myrna and Ole. The discussion of not only my project but also the meaning of many things is interesting and helpful.

I would like to thank Professor Duncan Dowson for his efforts into this study. The knowledgeable remarks and discussion from him can not be overstated. The support from Professor John Fisher and Dr. Sophie Williams is also acknowledged.

I am indebted to the secretaries and technicians in the two mechanical engineering departments in the Heriot-Watt University and the University of Leeds, for helping me run this study smoothly and for assisting me in many different ways. Marian, David and Ann Blyth from the Heriot-Watt University, Keith, Paul, Lucci, Graham, Devon, Adrian, Jackie, Cath and Debra from the University of Leeds deserve special mention. I wish to thank my friends in Leeds, Edinburgh and China for their encouragement, friendship and company through my Ph.D study.

Last but certainly not least, I would like to dedicate this work to my parents and stepparents. Their unreserved love and support are the most important reason to keep me moving forward. Without their encouragement, I would not have carried out this study.

ABSTRACT

Since the introduction of medical implants into human bodies, corrosion and wear have been regarded as key issues for their long-term durability. There has been a recent renewed interest in the use of large diameter metal-on-metal (MoM) hips, primarily because of the reduced volumetric wear compared with the well-established polyethylene-on-metal joints. Long term durability of MoM joints relies on control of both their *corrosion resistance* (relating to ion release) and *wear behaviour* (relating to creation of nanometre-scale wear debris). Concerns about the potential risk of released metal ions to the biological environment (patient) are of great importance. In this respect tribocorrosion is a serious consideration in joint performance.

An integrated electrochemical cell on a reciprocating tribo-meter was employed to evaluate the corrosion and tribocorrosion behaviour in a protein rich solution (Bovine Serum), a cell culture solution (DMEM) and a saline solution (NaCl) with the attempt to isolate the organic species effects. Three commonly used orthopaedic materials were involved in this study. A High Carbon Cobalt-Chromium-Molybdenum alloy, a Low Carbon Cobalt-Chromium-Molybdenum and UNS S31603 Stainless Steel (316L).

A range of electrochemical methods were used in the assessment of materials under biotribocorrosion systems and results were supported by surface analysis and bulk solution analysis techniques. The material degradation rate is strongly dependent upon the charge transfer (*corrosion*), the mechanical damage (*tribology*) and also their interactions (*tribocorrosion*) in these simulated biological environments.

CONTENTS

LIST OF FIGURES

LIST OF TABLES

NOMENCLATURE

a	Contact circle radius (m)
AP	Anodic Polarization
BE	Binding Energy (eV)
c_p	Heat capacity ($J\ g^{-1}K^{-1}$)
C'	Volume loss due to corrosion in the absence of wear (mm^3)
CE	Counter Electrode
CoC	Ceramic-on-Ceramic
CoCrMo	Cobalt-Chromium-Molybdenum
CoM	Ceramic-on-Metal
CP	Cathodic Protection
C_w	Volume loss due to the wear effect on corrosion (mm^3)
DMEM	Dulbecco's Modified Eagle's Medium
E	Young's modulus (GPa)
E_b	Breakdown potential (V)
E_{corr}	Free corrosion potential (V)
EHL	Elasto-hydrodynamic-lubrication
ESEM	Environmental Scanning Electron Microscope
f	Contact frequency (Hz)
F	Faraday's constant
h	Thermal input per unit area
h_{min}	Minimum film thickness (m)
H	Hardness
HC	High carbon
i	Current density ($\mu A/cm^2$)
i_{max}	Maximum current density ($\mu A/cm^2$)
I	Current (A)
ICP	Inductively Coupled Plasma
k	Wear coefficient
K	Thermal conductivity ($W\ m^{-1}K^{-1}$)
l	Sliding distance (m)
LC	Low carbon
M_{at}	Material atomic weight
MoC	Metal-on-Ceramic
MoM	Metal-on-Metal
MoP	Metal-on-Polyethylene
n	Valence number
N_A	Avogadro's number
OCP	Open circuit potential (V)
p_0	Maximum contact pressure (Pa)
p_m	Mean contact pressure (Pa)

P_e	Peclet number
Q	Charge (C)
R	Radius (mm)
R_a	Average roughness (μm)
RE	Reference Electrode
S	Synergy of corrosion and wear
t	Time duration (s)
T	Total weight loss (g)
THR	Total Hip Replacement
TJR	Total Joint Replacement
TKR	Total Knee Replacement
UHMWPE	Ultra High Molecules Weight Polyethylene
u	Velocity (mm/s)
v	Poisson's ratio
V	Total volume loss (mm^3)
w	Wear rate ($m^3 N^{-1} m^{-1}$)
W	Load (N)
W	Volume loss due to wear in the absence of corrosion (mm^3)
W_c	Volume loss due to the corrosion effect on wear (mm^3)
WE	Working Electrode
WLI	White Light Interferometry
XPS	X-ray Photoelectron Spectroscope
β_a	Anodic Beta Tafel constant
β_c	Cathodic Beta Tafel constant
δ	Thickness of the passive film
ΔG	Free energy change
κ	Thermal diffusivity ($m^2 s^{-1}$)
γ_{ls}	Liquid-solid surface tension
γ_{lv}	Liquid-vapour surface tension
γ_{sv}	Solid-vapour surface tension
η	Lubricant viscosity (Pa s)
λ	Lambda ratio
Θ	Temperature (°C)
τ	Shear stress
μ	Friction coefficient
θ	Contact angle (°)
ρ	Density (g/cm^3)

LIST OF PUBLICATIONS ARISING FROM THIS THESIS

[1] Yu Yan, Anne Neville and Duncan Dowson, *Understanding the role of corrosion in the degradation of metal-on-metal implants*, Proceeding of The Institution of Mechanical Engineers Part H: Journal of Engineering in Medicine, 2006, **220**, pp.173-180

[2] Yu Yan, Anne Neville, Duncan Dowson and Sophie Williams, *Tribocorrosion in implants - assessing high carbon and low carbon Co-Cr-Mo alloys by in-situ electrochemical measurements*, Tribology International, 2006, **39**, pp.1509-1517

[3] Yu Yan, Anne Neville and Duncan Dowson, *Biotribocorrosion - an appraisal of the time dependence of wear and corrosion interactions - Part I: The role of corrosion*, Journal of Physics D: Applied Physics, 2006, **39**, pp.3200-3205

[4] Yu Yan, Anne Neville and Duncan Dowson, *Biotribocorrosion - an appraisal of the time dependence of wear and corrosion interactions - Part II: Surface analysis*, Journal of Physics D: Applied Physics, 2006, **39**, pp.3206-3212

[5] Yu Yan, Anne Neville and Duncan Dowson, *Tribo-corrosion properties of Cobalt-based medical implant alloys in simulated biological environments*, submitted to Wear for a special issue of WOM 2007

[6] Yu Yan, Anne Neville and Duncan Dowson, Isolating the effect of proteins on corrosion, tribology and tribocorrosion material loss mechanisms on CoCrMo orthopaedic implant materials, submitted to Proceeding of The Institution of Mechanical Engineers Part J: Journal of Engineering Tribology, 2006

CHAPTER 1

INTRODUCTION

1.1. Background of Arthroplasty Implant

Arthritis causes long term health problems for more than one in seven adults and is the second most common cause of absence from work in both men and women [1]. 10% of the population did and will receive one (or more) joint replacement(s) during their lifetime in the UK [2]. Several million total hip replacements with a market value of about 2 billion pounds are implanted annually worldwide. Figure 1-1 summarizes the implant market by the Swedish National Hip Arthroplasty Register in 2004 [1]. 25,000 hip replacements (91% primary and 9% revision) and 22,000 knee replacements (94% primary and 6% revision) had been made in England in 2003 (between April and December) [2]. The major group receiving joint implants in the UK is the population of age range from 45-70 (Figure 1-2). However, more and more young and active patients demand to have their joint (hip/knee) replaced due to arthritis and accidental damage. It requires the replacement to last longer and 'safer'. Therefore, new generation Metal-on-Metal (MoM) joint replacements have been considered as an alternative to the commonly used Metal-on-Polyethylene (MoP) implants [3-5].

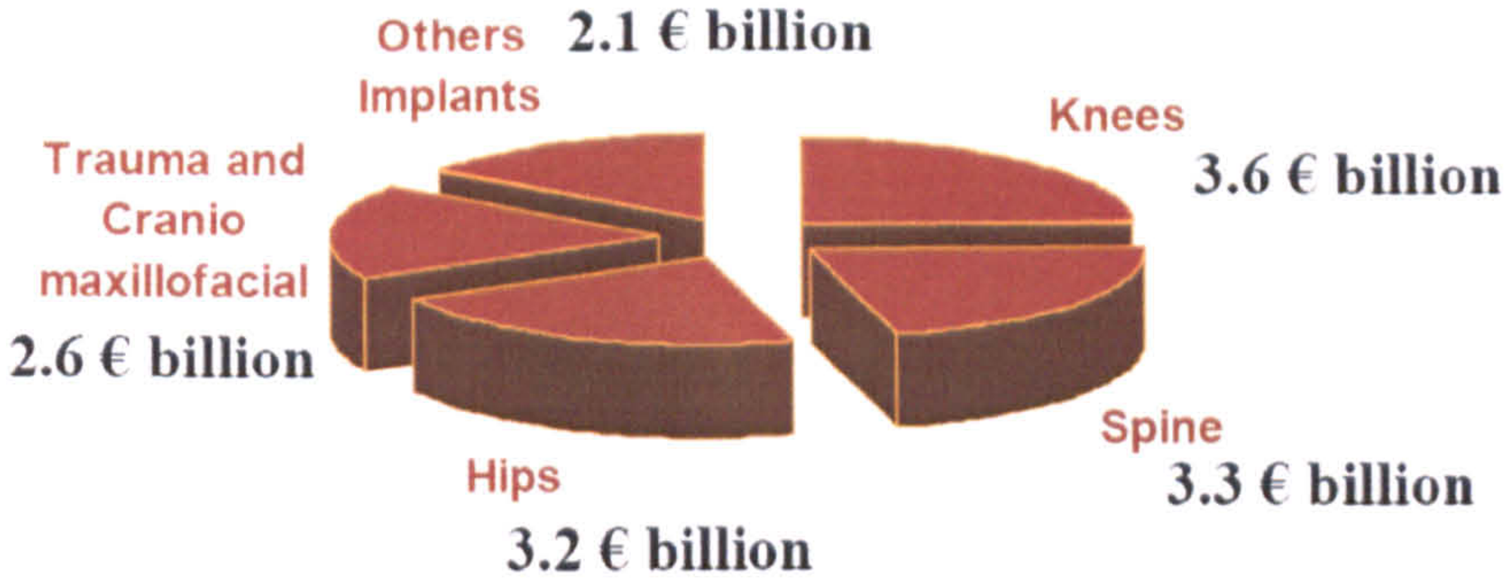

Figure 1-1 Summary of the implant market worldwide [1]

Figure 1-2 Age range of hip replacement recipients in the UK in 2003 [2].

1.2. Challenges and Concerns of The Use of MoM Implants

A survey by NJR (National Joints Registry of the UK) shows the most popular femoral head material is metal, which was implanted in 76.3% primary hip replacements [2]. Some concerns remain regarding the levels of metallic ions released *in vivo* from these MoM prostheses. Even though the implant is expected to last 10-20 years or longer, 10% of the implants need revision within 5 years due to various reasons [1-5]. However, wear is one of the major reasons attributed to the failure or revision of implants. Corrosion is regarded as the source of released ions.

Therefore, to improve the wear resistance and biocompatibility of implant materials is the focus of most implant industries and manufacturers (Figure 1-3).

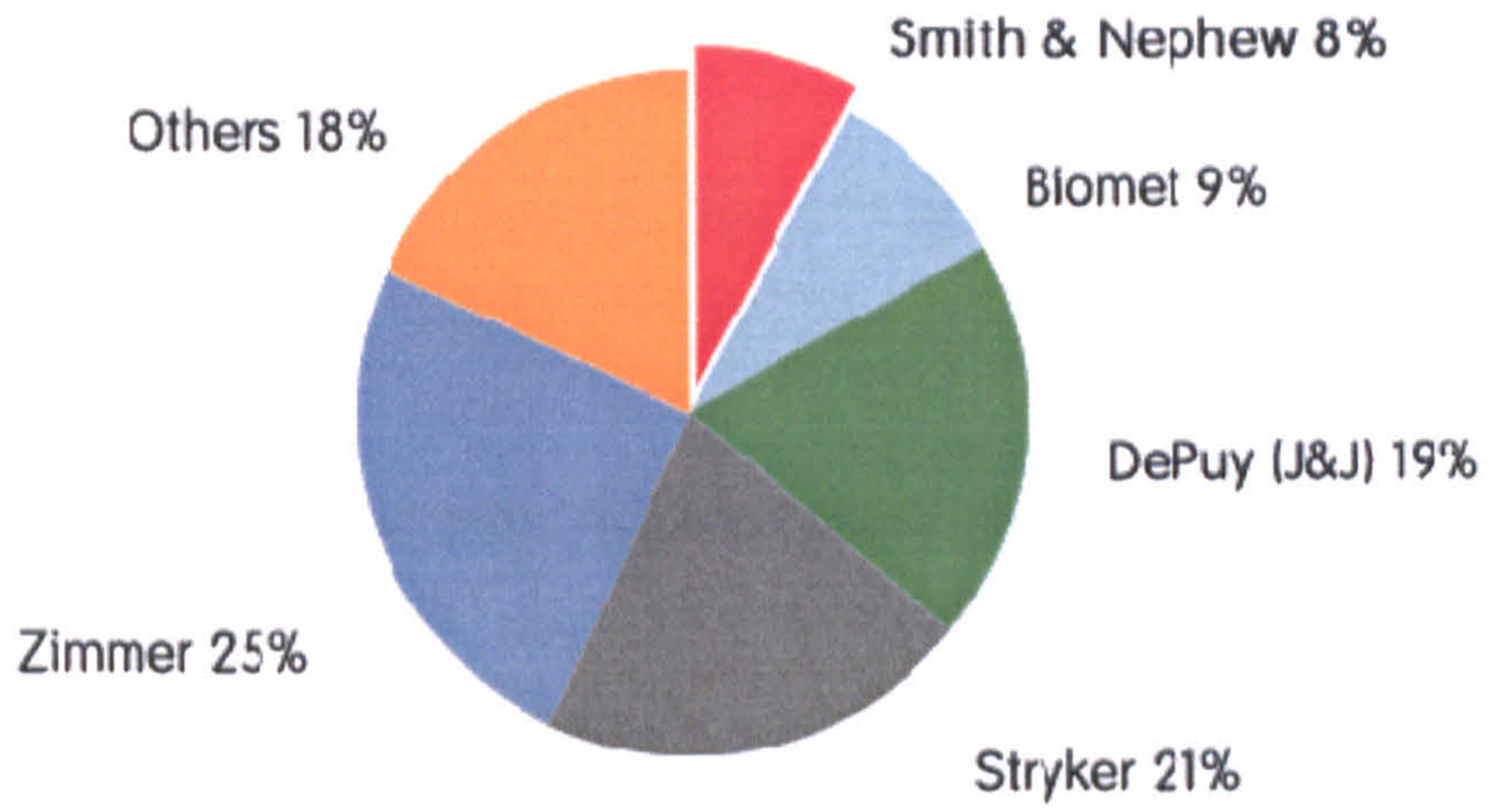

Figure 1-3 Major manufacturers of implant [2].

1.3. Objectives of This Study

Although, wear and corrosion are considered as important issues for implants, few studies have been focused to understand their joint effect – tribocorrosion for load bearing implants. Therefore, the aim of this work is to improve the understanding in the area of tribocorrosion behaviour for some widely used implant materials. It can give a better insight into material degradation processes in tribocorrosion systems and ultimately contribute to the selection and development of implant materials. The main objectives of this study can be summarized as:

- To analyze the tribology, corrosion and tribocorrosion behaviour in simulated synovial fluids by combining tribology and electrochemical tests.
- To analyze tribofilm formation and link it with tribocorrosion performance.
- To analyze the metal ion release process (corrosion) and link it with tribological performance.

- To analyze the parameters which can influence materials tribocorrosion behaviour.

1.4. Thesis Outline

This thesis contains nine chapters. Some basic theories are presented in Chapter Two covering the areas of corrosion and tribology. Electrochemical reactions and lubrication regimes are discussed.

An extensive review of literature is presented in Chapter Three. Related topics such as the development of joint replacement, the current research status and the understanding of tribocorrosion and the role of protein on implant materials are reviewed.

In Chapter Four, the sample preparation, experimental methodologies, procedures and equipment used in this study are described.

Chapter Five, which describes the material characterization and their corrosion behaviour in static conditions, is followed by the effect of tribology and corrosion on each other and their synergetic effect – tribocorrosion behaviour (Chapter Six and Chapter Seven). An integrated tribo-electrochemical technique is used to study the tribocorrosion phenomenon. X-ray Photoelectron Spectroscopy (XPS) is used to chemically characterize the tribofilm while a laser interferometer is used to characterize topographical features and material loss during the tests. Contact angle measurements are also employed to analyze the effect of surface energy and the protein adsorption on the tribocorrosion behaviour.

The discussion of the results of relevance to the findings from this work and their general relation to the published literature are presented in Chapter Eight. The main conclusions from this study and the possible future work which could be carried out as a result of the main findings from this work are given in Chapter Nine.

CHAPTER 2

BASIC THEORIES OF CORROSION AND TRIBOLOGY

2.1. Corrosion Principles and Corrosion Reactions

Corrosion is defined as the reaction of a material with its surrounding environment with a consequent deterioration in properties of the material. The reaction can be chemical, electrochemical, physical or their combination [6]. The materials can be metals, ceramics and polymers and the environments can be aqueous and non-aqueous liquids and gases. However, corrosion is often referred to metallic materials. To study the corrosion phenomenon, three factors from the definition of corrosion can be summarized: the material (metal), the environment and the material/environment interface. In this study, the electrochemical reaction of materials under tribological contact is the focus.

2.1.1. Thermodynamics aspects of corrosion

Thermodynamics can be applied to determine which processes can occur and how strong the relative tendency is for these changes to take place (i.e., for the metals to corrode). The degradation of metallic materials due to corrosion in aqueous environments usually exhibits an electrochemical nature. Thermodynamics provides a means of prediction the equilibrium state of a system of specified components, but provides no information on the detailed course of the reaction or of the rate at which the system proceeds to equilibrium [7]. The rate of reaction can be described by

kinetic theory. Thermodynamics is concerned with energy states. The original metallic ores are seen to be in a state of low energy. External energy is applied in the conversion of the ores to usable metals and alloys, transforming them to a higher energy state [6]. They tend to revert to a lower (more stable) energy state by reacting with a corrosive environment.

$$\Delta G = -NFE_{cell} \qquad \text{(Eq.2-1)}$$

Where ΔG is the free energy change. N means the numbers of electrons being transferred. F is the Faraday constant (96485 C mol $(e^-)^{-1}$). E_{cell} represents the cell potential and can be determined by the difference of the electrode potential of cathodic and anodic ($E_{cathodic}$-E_{anodic}). If ΔG <0 (negative) the tendency for a metal to react with species in solution will be high, but whether or not the reaction proceeds to any extent will depend on kinetic factors; if ΔG>0 (positive) the metal is stable and no further consideration need to be given to kinetics; if ΔG=0, the system is at equilibrium and will not proceed in either direction [7].

2.1.2. Electrochemical reactions

Most corrosion phenomena are electrochemical in nature. They basically imply two reactions: the anodic oxidation reaction of metal, which involves the dissolution of metal; the cathodic reaction, which includes the reduction of an oxidising agent [8].

Eq. 2-2 represents the generalized anodic reaction that corresponds to the rate-determination step of corrosion.

$$M \rightarrow M^{n+} + ne^- \qquad \text{(Eq.2-2)}$$

M represents a metal. For example for iron, the anodic reactions can be following two:

$$Fe \rightarrow Fe^{2+} + 2e^- \qquad \text{(Eq.2-3)}$$

$$Fe^{2+} \rightarrow Fe^{3+} + e^{-} \qquad \text{(Eq.2-4)}$$

The formation of corrosion products, the solubility of corrosion products in the electrolyte and the formation of passive films all affect the overall rate of the anodic metal dissolution process and cause deviations from simple rate equations. For passive materials, passive films distinguish themselves from corrosion products, in the sense that these films tend to be more tightly adherent and can provide higher degree of protection from corrosive attack [6].

Eq. 2-5 represents a cathodic reaction, which is well known as the oxygen reduction process.

$$O_2 + 2H_2O + 4e^{-} \rightarrow 4OH^{-} \qquad \text{(Eq. 2-5)}$$

In the case of metal in acid conditions, the electrons combine with hydrogen ions at the surface of the metal. Atomic hydrogen is formed. Most of it combines to form molecular hydrogen gas but some may dissolve in the metal [7].

$$2H^{+} + 2e^{-} \rightarrow H_2 \qquad \text{(Eq. 2-6)}$$

2.1.3 Electrochemical corrosion rate

A log current versus potential plot is also called a Tafel Plot. The Tafel Plot in Figure 2-1 is generated directly from the Butler-Volmer equation (Eq. 2-7). Tafel-curve extrapolation uses experimental data taken typically within $\pm$ 50 mV of E_{corr} (the open circuit potential) (a linear relationship of the log(current) and potential normally lasts for at least 1 decade for the log(current)) where the corrosion process is less disturbed corrosion-product (anodic reaction) or diffusion-limiting process (cathodic reaction) [6]. The Tafel analysis is performed by extrapolating the linear portions of a log current versus potential plot back to their intersection (Figure 2-1). The value of either the anodic or the cathodic current density at the intersection is i_{corr}.

$$i = i_{corr}(\exp(\frac{2.3(E-E_{corr})}{\beta_a}) - \exp(\frac{2.3(E-E_{corr})}{\beta_c})) \qquad \text{(Eq.2-7)}$$

where i is the measured cell current density, i_{corr} is the corrosion current density from Figure 2-1. E is the electrode potential and E_{corr} is the free corrosion potential. β_a is the anodic Beta Tafel constant while β_c is the cathodic Tafel constant.

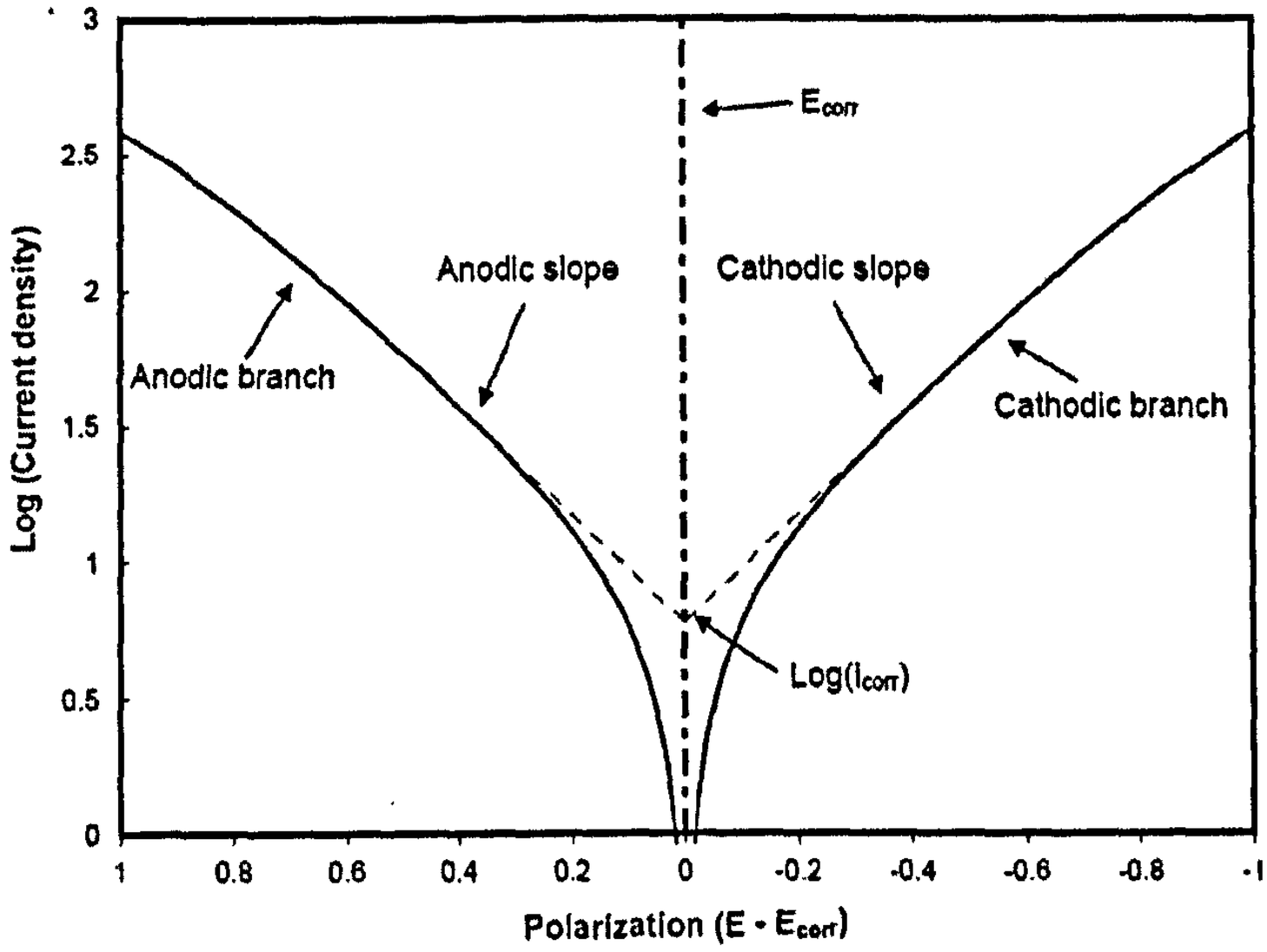

Figure 2-1 Schematic experimental polarisation curves with the Tafel analysis [8].

2.1.4. Potentiodynamic polarization

Several methods may be used in polarization of specimens for corrosion testing. Figure 2-2 illustrates the ideal linear polarization resistance measurement. The polarization resistance (R_p) of a material is defined as the slope of the potential-current density plot.

$$R_p = \frac{\Delta E}{\Delta i} = \frac{\beta_a \beta_c}{2.3(\beta_a + \beta_c) i_{corr}} \qquad \text{(Eq. 2-8)}$$

Potentiodynamic polarization is a technique in which the potential of the electrode is varied at a selected rate by application of a current through the

electrolyte. It is probably the most commonly used polarization testing method for measuring corrosion resistance and is used for a wide variety of functions Figure 2-3 shows a hypothetical potentiodynamic polarization for a passive material. The potential range is typically of the order of 10-20mV.

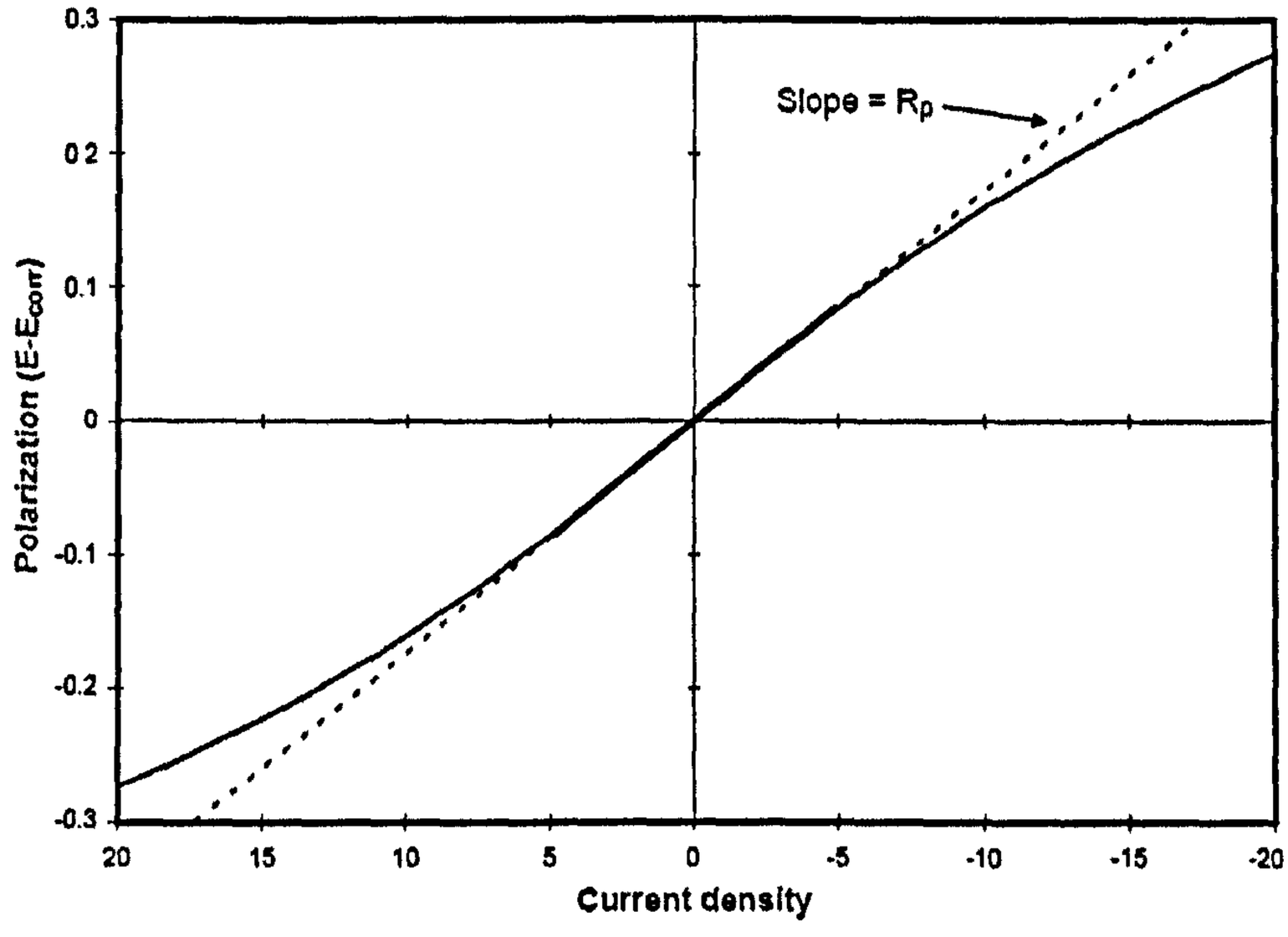

Figure 2-2 Hypothetical linear polarization plot [8].

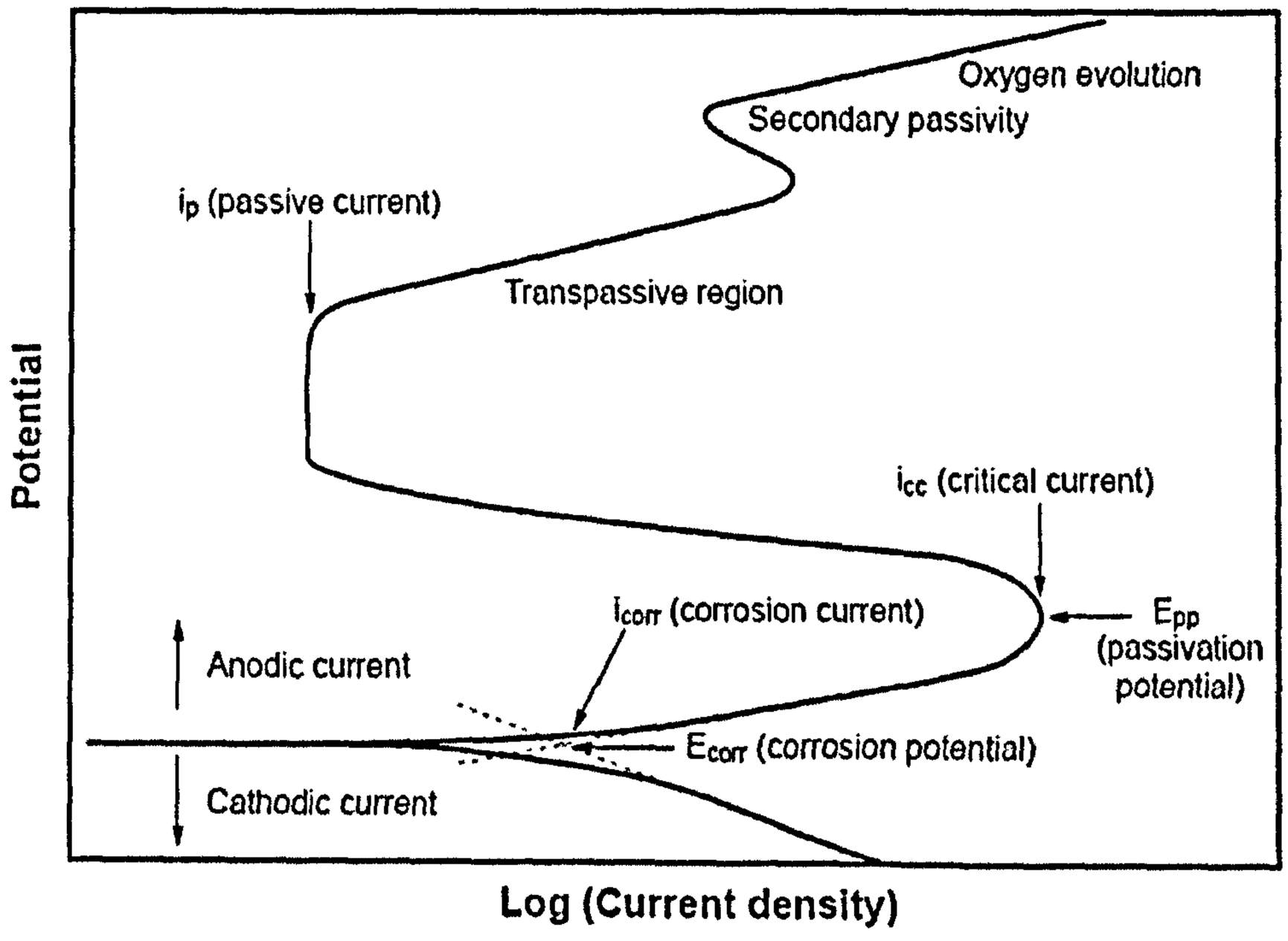

Figure 2-3 Hypothetical polarization diagram for a passivable system with anodic and cathodic branches [7].

2.1.5. Types of corrosion and corrosion protection

The corrosion classification can be considered from the extension of the damaged region. If a large area of the metallic surface is corroded, this is an indication of general corrosion. If small regions are the only ones damaged, this is referred to as localised corrosion [6-8]. Some types of corrosion are summarized below:

- General corrosion: General or uniform corrosion is a form of electrochemical corrosion that occurs with equivalent intensity over the entire exposed surface and often leaves behind a scale or deposit.
- Pitting corrosion: Pitting is a kind of localised corrosion which selectively attacks area of a metal surface where there is a surface scratch, an emerging dislocation or a compositional heterogeneity. When the metal corrodes in the pit, dissolved metal ions generate an environment with low pH and chloride ions migrate into the pit to balance the positive charge of the metal ions. Thus the environment inside a growing pit gradually becomes more aggressive and repassivation becomes less likely. As a result, pitting attacks often penetrate at a high rate, thereby causing corrosion failure in a short time.
- Galvanic corrosion: Galvanic corrosion tends to occur when dissimilar conducting materials are connected electrically and exposed to an electrolyte. The corrosion rate of the more active material is accelerated.
- Crevice corrosion: Crevice corrosion is a localised form of corrosive attack. Crevice corrosion occurs at narrow openings or spaces between two metal surfaces or between metals and non-metal surfaces. A concentration cell forms with the crevice being depleted of oxygen. This differential aeration between the crevice (microenvironment) and the external surface (bulk environment) gives the crevice an anodic character which can contribute to a highly corrosive condition in the crevice.

Due to the serious cost and failures of corrosion, some protection can be applied to minimize corrosion [8].

- Coatings: Protective coatings are probably the most widely used products for corrosion control. They are used to provide long-term protection under a broad range of corrosive conditions. The main function of a protective coating is to isolate structural reactive elements from environmental corrosives.
- Cathodic protection (CP): Cathodic protection (CP) is a technique to control the corrosion of a metal surface by making that surface the cathode of an electrochemical cell. Through the application of a cathodic current onto a protected structure or material, anodic dissolution is minimized. There are two ways to produce the cathodic current: i) by connecting sacrificial anodes to create a galvanic cell. ii) by applying an external power current source.
- Anodic protection: It is based on the formation of a protective film (passive film) on metals by externally applied anodic currents.

2.2. Tribology

Tribology is defined as the science and technology of interacting surfaces in relative motion and related subjects and practices. It focuses on friction, wear and lubrication of interaction surfaces in relative motion [9].

Wear is the progressive damage, which occurs on the surfaces of a component or components as a result of their motion [10].

Friction is the resistance encountered when one body moves over another with which it is in contact [9].

Lubrication occurs when opposing surfaces are completely separated by a lubricant film. The applied load is carried by pressure generated within the fluid, and frictional resistance to motion arises entirely from the shearing of the viscous fluid [9, 10].

2.2.1. Lubrication regimes

Lubrication regime is defined by the lambda ratio. The lambda ratio is the minimum film thickness in relation to the composite RMS surface roughness:

$$\lambda = \frac{h_{\min}}{\sqrt{R_{a1}{}^2 + R_{a2}{}^2}} \qquad \text{(Eq. 2-9)}$$

Stribeck [9] demonstrated that the coefficient of friction is directly proportional to the viscosity of lubricant and the difference in speed and inversely proportional to the pressure which is exerted on the contact surfaces. Figure 2-4 shows the Stribeck curve which is the friction coefficient against $\mu\omega/p$ (lubricant viscosity (η), speed (ϖ) and contact pressure (p)). There are three regimes as defined from the Stribeck diagram: boundary lubrication, mixed lubrication and hydrodynamic lubrication.

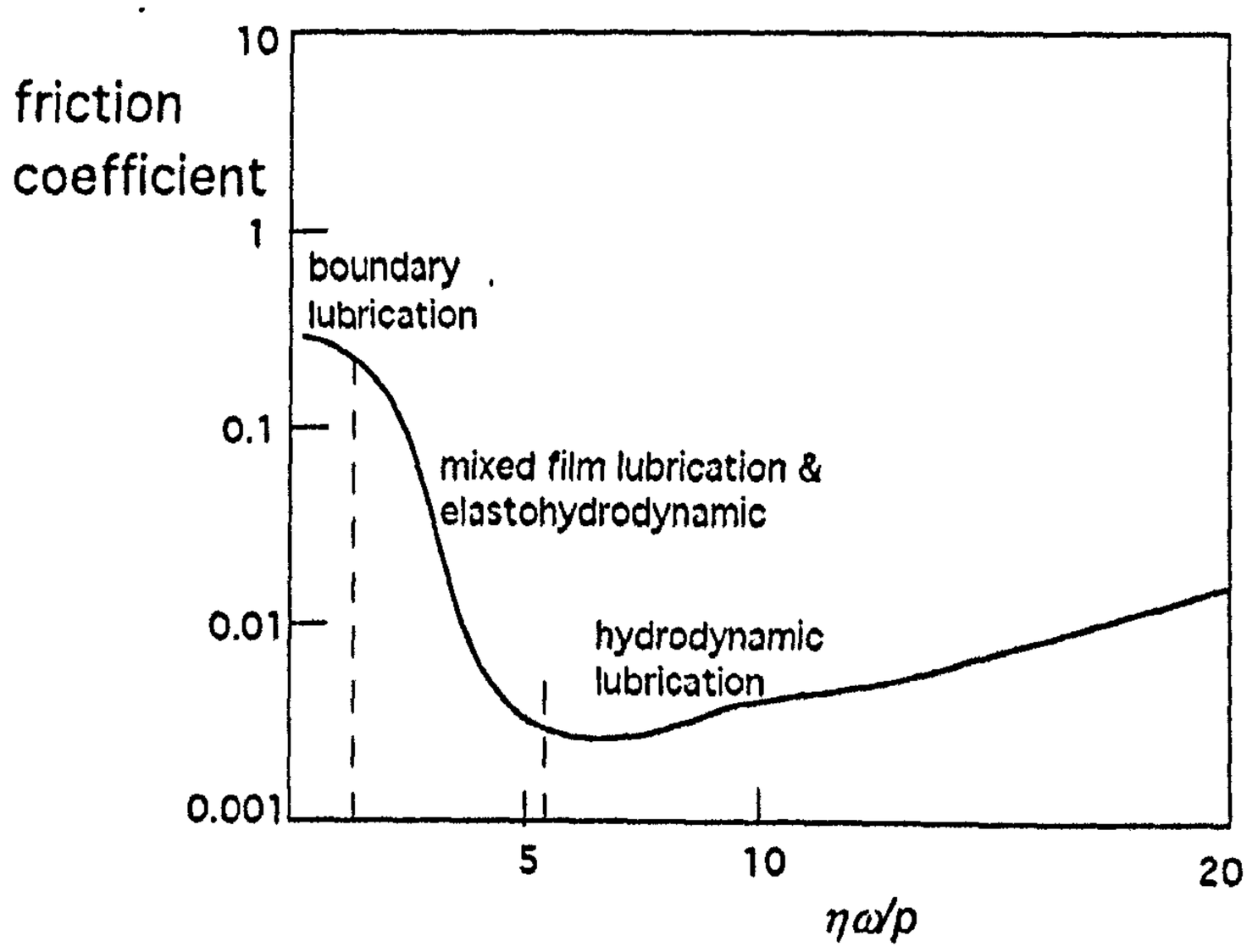

Figure 2-4 Friction coefficient as a function of the bearing number [9].

2.2.1.1. Boundary lubrication

At lambda ratio values lower than 1, it is conventionally supposed that asperity interaction becomes more severe and that the shear properties of the films on the solid surfaces, whether formed by adsorption or reaction, become significant. This regime is called boundary lubrication. In the boundary lubrication regime, the physical properties of the bulk lubricant such as density and viscosity are not as important as the chemical properties of the lubricant and the properties of the surfaces in contact. In animal or human joints and some hip replacements, the lubrication regime is in boundary lubrication [11]. However, for other hip replacements, the lubrication regime can be mixed lubrication [12]. Therefore, the boundary and mixed lubrication regimes are of primary importance in this thesis.

2.2.1.2. Hydrodynamic lubrication

If the lambda ratio is very much greater than unity, so that the film is thick, then the traction or friction force will be a function of the bulk rheological properties of the lubricant at the appropriate operating conditions of load, temperature, shear rate and so on. The influence of the surface roughness will be negligible. This regime is called full film lubrication or hydrodynamic lubrication. Fluid film lubrication is the most desirable form of lubrication. In this case the surfaces are not in contact so the resistance to their tangential motion, friction force is dependent primarily on the viscosity of the lubricant [9]. Also since there is essentially in theory no contact between surfaces, no wear should occur.

2.2.1.3. Mixed lubrication

When the film thickness and the surface roughness are of comparable dimensions ($1<\lambda<5$), then the traction will still be determined by the bulk properties

of the lubricant but the local contact conditions of asperity interaction will need to be consider [9]. Since the lubrication is a mix of full film lubrication and some asperity contact, the regime is called the mixed lubrication regime. On further decreasing the speed and at very high specific loads, full film lubrication is difficult to maintain and despite the presence of micro elasto-hydrodynamic-lubrication (EHL) there will be some mechanical interactions between opposing surface asperities. In this regime, the lubricant film provides partial separation [10]. The contact load is shared between the contacting asperities and the film when mixed lubrication prevails.

2.2.2. Wear between surfaces of solids

It has been suggested by Archard [9] that the total wear volume (V) is proportional to the real contact area (A_r) times the sliding distance (l) as shown in Eq. 2-10.

$$V = KA_r l = K\frac{W}{H} = klW = wl \qquad \text{(Eq. 2-10)}$$

the "K" coefficient also known as the "Archard coefficient" is widely used as an index of wear severity. In practical engineering situations the hardness of the uppermost layer of material (H) in contact may not be known with any certainty and consequently a rather more useful quantity than the value of "K" alone is the ratio k ($k = \frac{K}{H}$). This is known as the dimensional wear coefficient "k" and is usually quoted in units of $m^3N^{-1}m^{-1}$. The wear rate in Eq. 2-10 is w.

2.2.3. Wear mechanisms

In materials science, wear is the erosion of material from a solid surface by the action of another solid. There are four principal wear processes: adhesive wear,

abrasive wear, corrosive wear and fatigue wear [9, 10]. However, other forms of wear also present such as cavitation wear, fretting wear and diffusive wear..

2.2.3.1. Adhesive wear

Adhesive wear is also known as scoring, galling or seizing. It occurs when two solid surfaces slide over one another under pressure. Surface projections, or asperities, are plastically deformed and eventually welded together by the high local pressure [13]. As sliding continues, these bonds are broken, producing cavities on the surface, projections on the second surface, and frequently tiny, abrasive particles- all of which contribute to future wear of surfaces. The strong adhesion observed between metals can be explained by electron transfer between contacting surfaces. Numerous free electrons are present in metals and on contact electrons may be exchanged between the two solids to establish binding. High hardness, large elastic modulus and surface energy of the metal can suppress adhesion [9].

2.2.3.2 Abrasive wear

If the film material consists of hard particles or merely flows against one body without providing support against another body, then a form of wear which sometimes can be very rapid known as abrasive wear occurs. It occurs whenever a solid object is loaded against particles of a material that have equal or greater hardness [10]. The mechanisms of abrasive wear can be:

- Microcutting;
- Fracture;
- Ploughing or
- Grain pull-out.

Two modes are involved and they are two body and three body abrasive wear [13].

2.2.3.3. Corrosive wear

In some practical situations the film material is formed by chemical attack of either contacting body and while this may provide some lubrication, significant wear is virtually inevitable [13]. If a material (metal) is corroded to produce a film on its surface while it is simultaneously subjected to a sliding contact then one of the three following processes may occur:

- A durable lubricating film which inhibits both corrosion and wear may be formed:
- A weak film which has a short life-time under sliding contact may be produced and a high rate of wear may occur;
- The protective surface films may be worn (e.g. by pitting) and a galvanic coupling between the remaining films and the underlying substrate may result in rapid corrosion of the worn area on the surface [9].

2.2.3.4. Fatigue wear

When the intervening films are partially effected then milder forms of wear and these are often initiated by fatigue processes due to repetitive stresses under either sliding or rolling. These milder forms of wear can be named fatigue wear. Wear under theses conditions is determined by the mechanics of crack initiation, crack growth and fracture [10]. Worn surfaces contain very high levels of plastic strain compared to unworn surfaces. This strain and the consequent modification of the materials' microstructure have a strong effect on the wear processes [13].

CHAPTER 3

REVIEW OF LITERATURE – ORTHOPAEDIC IMPLANTS AND TRIBOCORROSION

3.1. Introduction

In this chapter, the literature is reviewed with the specific objective of addressing these issues:

- How implants affect their operating environments
- How biological environments influence implantable material and devices.

Firstly an overview of materials used for implants is given. This chapter also reviews the common combinations of materials in Total Joint Replacement (TJR). Metal-on-Metal (MoM) artificial human joint replacements are emphasized being most relevant to the current study. The review then focuses on the existing literature on their wear and corrosion evaluation and in particular the combination of wear and corrosion (tribocorrosion). The performance of different implant materials *in vitro* and *in vivo* is also discussed. The effect of proteins on wear and corrosion behaviour of metallic implant materials is reviewed.

3.2. Biomaterials

Biomaterials are defined by Williams [14] as non-viable materials used in medical devices, intended to interact with biological systems. Biomaterials cover all

classes of materials for various needs (e.g. dental, orthopaedic and cardiovascular). Implantable devices intended for major load-bearing applications (primarily in orthopaedic and dentistry) are made mainly from metals, ceramics or polymers [15-17].

3.2.1. Metals

Metals and alloys have a wide range of applications in biomedical devices. Devices from metals and alloys can be used for fracture fixation, partial and total joint replacement, external splints and heart valves [15]. Their high modulus, yield point and ductility make them suitable for such applications. Although pure metals are sometimes used, alloys frequently provide improvement in material properties. The disadvantage of metals is that they are susceptible to chemical and electrochemical degradation. However, polymers and ceramics can also be subjected to corrosion attack [16]. Three groups dominate biomedical metals: iron-based stainless steel, cobalt-based alloys and Titanium and Titanium alloys.

3.2.1.1. Stainless Steel

Stainless steels were the first metals to be used in orthopaedics [15,17]. Although several types of stainless steels are available for implant use, in practice the most common are austenitic 316 and 316L stainless steels. Cr, Ni and Mo in stainless steel enhance corrosion resistance by forming a resistant passive film. Carbon and other alloying elements also affect the mechanical properties of steels through the alteration of their microstructures. The key function of the chromium is to permit the development of a strongly adherent surface oxide (passive film Cr_2O_3) . Molybdenum is ferrite stabilizer. To counter this tendency to form ferrite, nickel is added to stabilize the austenitic phase. Between them, 316L is considered more biocompatible than 316 due to this lower carbon content [17]. One recognized

limitation of the stainless steel is associated with its susceptibility to crevice and pitting corrosion. This characteristic has limited some of the possible applications of the alloy, such as orthopaedic fracture plates, dental implants and cranial palates [16]. Therefore, 316L was employed only for a short time in orthopaedic hip implants in their early development of the use of total hip replacement [15]. Ortron 90 is now widely used as an load bearing impant material du to its superior corrosion and corrosion fatigue resistance.

3.2.1.2.Cobalt-based alloys

From the very wide range of Cobalt-based alloys, there are currently two major categories used as implant alloys [18]:

- Cobalt-Chromium-Molybdenum (CoCrMo) alloys and
- Cobalt-Nickel-Chromium-Molybdenum (CoNiCrMo).

However, the dominant Co-based alloys are CoCrMo alloys. CoCrMo alloys are regarded as highly biocompatible materials and have been employed in the fabrication of prostheses since the 1940s. Since then, they have been extensively used in orthopaedic fracture plates, joint replacement prostheses and heart valves [16]. For cast Co-based alloys, they typically consist of a Co-rich matrix (alpha phase) with inter-dendritic grain boundary carbides (primarily M23C6 where M represents Cr or Mo). Different processing treatments have been used to improve the mechanical properties of Co-based alloys such as forging and HIPing (Hot Isostatic Pressing) [18]. Details of CoCrMo alloys in hip replacement implants will be discussed later in this chapter.

3.2.1.3.Titanium and titanium alloys

Commercially-Pure (CP) titanium and titanium alloys have shown excellent electrochemical corrosion properties and tissue biocompatibility for static implant conditions [15, 17]. One titanium alloy, Ti6Al4V is widely used to manufacture implants. With a nano scale (10 nm) thin oxide film (TiO_2) Titanium and its alloys show excellent corrosion resistance in biological fluids. Their good biocompatibility is also verified in clinical results. However, the V (vanadium) from Ti6Al4V is a concern in relation to be toxicity to humans [17]. Titanium and titanium alloys also have poor shear strength and relatively less resistance to wear compared to Co-base alloys, making it less desirable for load bearing implants. It also tends to gall or seize when in sliding contact with itself or another metal [15]. The softness of Ti alloys is also a drawback when being considered as a load bearing material. Ti6Al4V is reported to be >15% softer then CoCrMo [17]. Newly developed Ti alloys such as Ti5Al2.5Fe and Ti6Al17Nb have shown improved fatigue strength while maintaining their corrosion resistance.

3.2.2. Ceramics

Ceramics are inorganic components which can be classified into five categories of biomaterials; carbon, alumina, zirconium, glass ceramics and calcium phosphate [19]. Ceramics generally display good resistance to chemical attack and they are resistant to the effects of elevated temperature [15]. Alumina and zirconia are used for orthopaedic implant materials. They are relatively inert and resist the assaults of the body's defence mechanisms. The low tensile strength and fracture toughness are limitations of ceramics by being used under heavy load [16, 18]

3.2.3. Polymers

Polymeric materials are the most widely used materials in biological applications (orthopaedic, dental, soft tissue), due to their close resemblance to

natural polymeric tissue components [18]. The constituent atoms of classic polymers are usually carbon and are joined in a linear chainlike structure by covalent bonds. Various forms of polymers are considered for implant applications such as fibres, textiles, rods and viscous liquids. They are the choice for cardiovascular devices as well as for replacement and augmentation of various soft tissues [17]. Examples of current uses include heart valves, contact lenses, intraocular lenses, blood substitute and joints replacement. However, because of biochemical and mechanical factors in the body environment, polymers suffer great degradation resulting in ionic attack leading to tissue irritation and decreased mechanical properties [17].

For hip and knee replacements, Ultra-high-molecular-weight polyethylene (UHMWPE) is used due to its improved strength compared to other normal classified polyethylene in the modern artificial joints design, but it still suffers great deformation under cyclic loading. Cross-linked chains in UHMWPE can reduce degradation [20]. Improved performance in terms of wear rate has been reported [15]. However, the debris from such materials is the major cause for osteolysis and loosening of devices.

3.3. Total Joint Replacement

Total Joint Replacement (TJR), or joint arthroplasty, is a surgical procedure in which the entire joint is removed and replaced with a prosthetic joint. Some typical TJR implants are shown in Figure 3-1. Due to the increasing osteoarthrosis and similar disabling conditions, total artificial replacement of human joints has become a widely used treatment. It is performed to release pain and improve joint function [21]. In TJR, the most popular types are Total Hip Replacement (THR) (Figure 3-1(a) and (b)) and Total Knee Replacement (TKR) (Figure 3-1(d)). TJR as normally only performed on patients who were over 60 years old in the early periods. However, nowadays, more and more young and active patients are requiring TJR surgeries. Improvement and development of safer, longer lasting and better functioning implants are expected for such applications [20, 21].

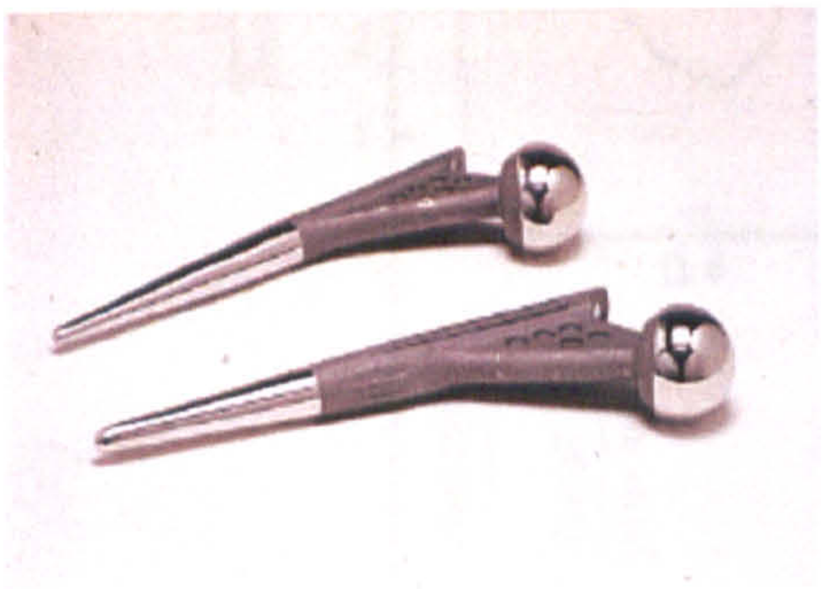

(a)

(b)

(c)

(d)

(e)

(f)

Figure 3-1 Typical TJR implants (a) (b) total hip replacement (c) shoulder replacement (d) knee replacement (e) elbow replacement (f) ankle replacement

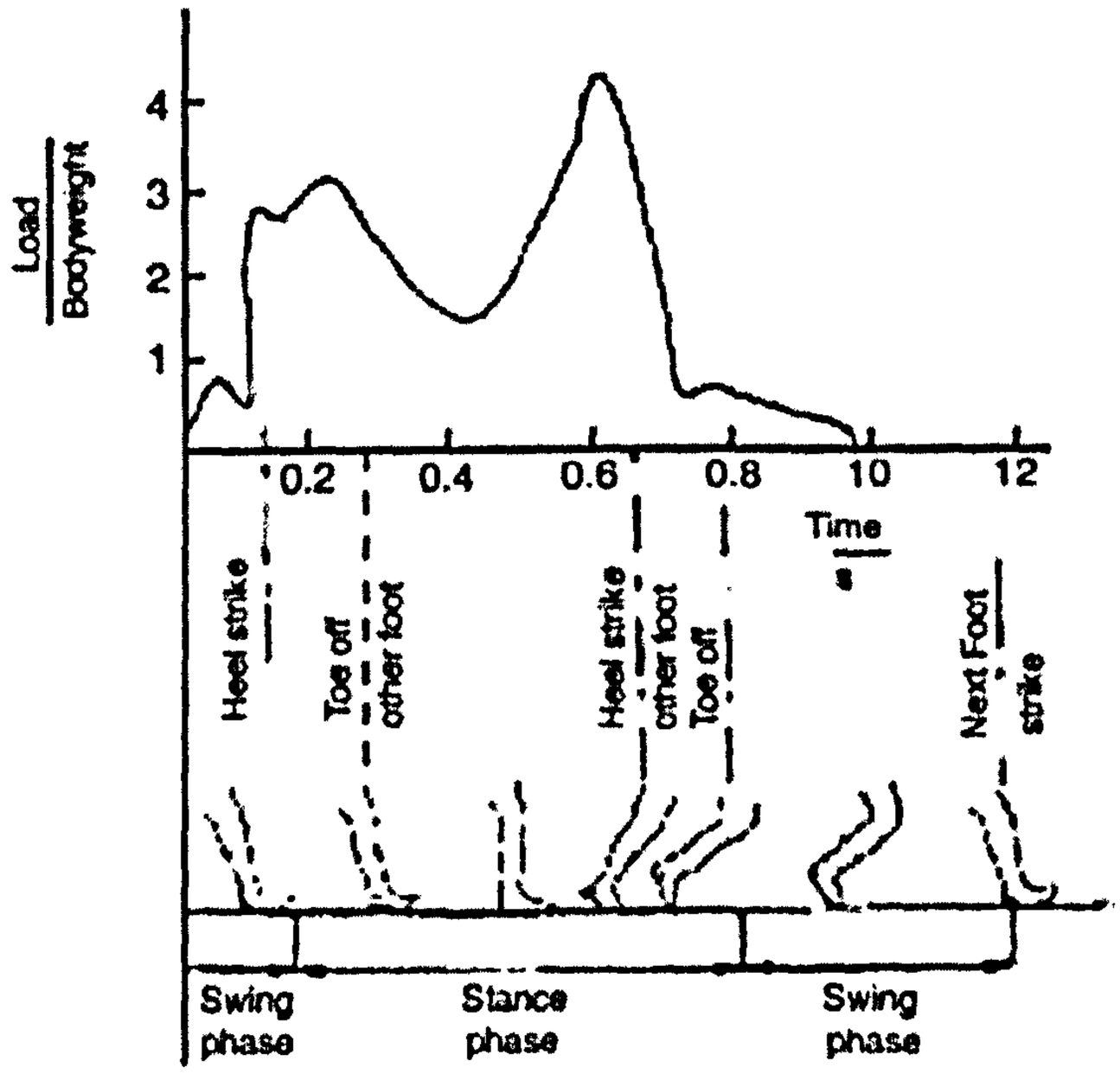

Figure 3-2 Hip joint force during one cycle of walk [10].

Because TJR are under the fluctuating and cyclically repeated forces caused by gravity and muscular action, mechanical characteristics such as strength elasticity, toughness and ductility are relevant factors [22]. Figure 3-2 shows the force change during a cycle of walk. A peak load of more than 4 times bodyweight was obtained when the action of heel strike was made. Two phases in the human hip joint are classified during a normal walking cycle. In the stance phase, the hip joint carries very high load and the relative movement in the joint (between femoral head and socket) is little. In the swing phase, even though the load on the joint is lower than in the stance phase, the movement of the joint is greater. Some authors believe that the material degradation progresses (wear) severely in this phase [23]. The correct counterface, material combinations, surface finish, diameter of femoral head and clearance are important aspects in minimizing friction, wear and corrosion [22]. Low friction, low wear and good biocompatibility are desirable characteristics for TJR prostheses.

From a historical study, the first recorded attempt to replace the hip joint was made by Gluck from Berlin in 1880. The prosthesis was made of ivory. Then the designs intended to just replace femoral head by different materials. In this period, acrylic materials and metals were involved [23]. The TJR have developed largely over approximately the last 60 years. In the early period of TJR, a number of configurations of Metal-on-Metal (MoM) hip prostheses were invented and used. They are normally referred to as *the first generation MoM bearings*, which were manufactured from as-cast cobalt chromium alloys. Among them, the McKee-Farrar prosthesis was the most widely used design [24]. While some of the early McKee implants experienced short term failures, others survived for service periods of 20 or 30 years [25]. In the late 1950s and early 1960s, Charnley tried polyethylene (PTFE and UHMWPE) as an alternative acetabular material, a design which remains to this day. It achieved low friction and it involved a stainless steel (later cobalt chromium alloy) femoral component [26]. However, problems of loosening and osteolysis are associated with this Metal-on-Polyethylene (MoP) design. The drive to improve the long-term service life of TJR has resulted in interest in using hard-on-hard bearing couples. Developed and modified Ceramic-on-Ceramic (CoC), MoM and Ceramic-on-Metal (CoM) bearing systems were introduced and have attracted many investigations [27].

Alumina and zirconia ceramics were introduced into orthopaedic surgeries in the early 1970s. From clinical and laboratory results, for CoC types of TJR, especially THR, low wear rates were noticed. CoC benefits from higher scratch resistance properties and better wettalility and therefore enhanced lubrication properties [28]. However, complications due to the ceramic brittle fracture, acetabular loosening and ceramic degradation have been reported. In addition, it is very difficult to remove all of the ceramic fragments from the surrounding tissues if CoC fails and revision surgery is required [27]. Modification of surfaces of CoC components has been attempted and results are promising [28]. Many authors believe that CoC prostheses are an effective option for younger and more active patients. The history of hip replacement is shown in Figure 3-3.

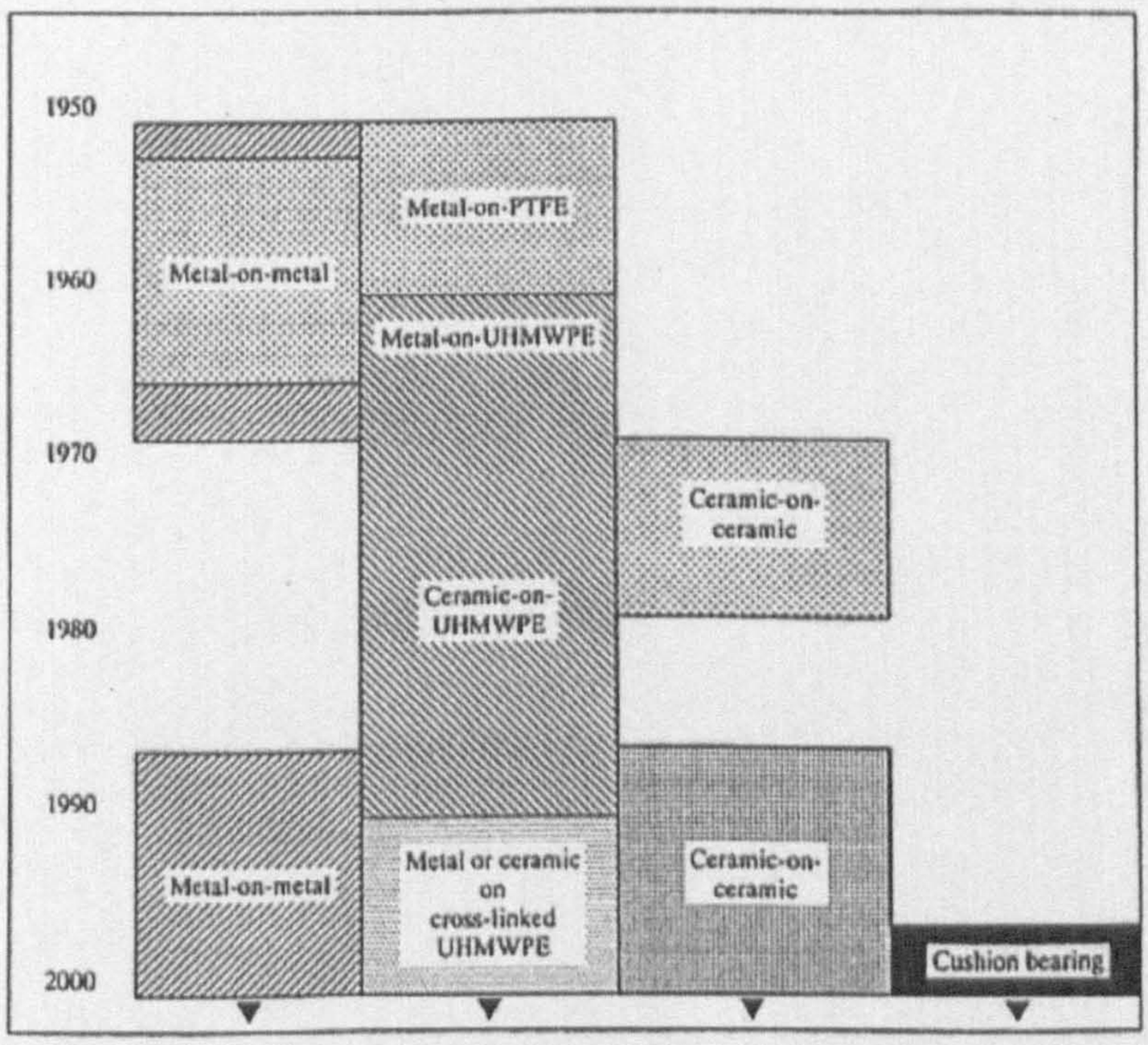

Figure 3-3 History of hip replacement from 1950 to 2000 [30].

Hip and knee simulators in laboratories are widely used to test materials and designs before they go to clinical trials. Such simulator tests and simple wear tests are always referred to as *in vitro* tests, while *in vivo* tests are that experiments performed in the living organism. Comparison of various material combinations for THR in terms of wear rate (mm^3/year) both *in vitro* and *in vivo* is made in Table 3-1. 1 million cycles *in vitro* is equivalent to approximately 1 year of service *in vivo*. Therefore, in this table, *in vitro* results are calculated in mm^3/year instead of original mm^3/million cycles. Clearly, even for the same material combination, the wear rate varies from different laboratories and researchers. It is due to the different designs of THR used in those studies. It indicates that the design of the replacement is as important as the material selection.

Generally, CoC gives the lowest wear rate among the material combinations in THR. However, MoM (CoCr-on-CoCr) replacements show longer duration of the devices and well documented clinical results have been reported.

Table 3-1 Wear rate of different combinations of THR from literatures for both *in vitro* and *in vivo*

Material combination	wear rate (mm^3/year)	Ref.
SS-on-UHMWPE	120	[25] (*in vitro*)
CoCr-on-UHMWPE	32	[26] (*in vitro*)
	102	[28] (*in vivo*)
	22	[16] (*in vivo*)
Ti-on-UHMWPE	35	[16] (*in vivo*)
Alumina-on-UHMWPE	50	[27] (*in vitro*)
	30	[28] (*in vitro*)
	32	[29] (*in vivo*)
Zirconia-on-UHMWPE	53	[31] (*in vitro*)
	63	[31, 32] (*in vitro*)
CoCr-on-CoCr	1.5	[33] (*in vitro*)
	2	[34] (*in vitro*)
	2.3	[34] (*in vivo*)
	1.3	[35] (*in vitro*)
	0.12	[36] (*in vitro*)
	0.5	[37] (*in vivo*)
	0.75	[38] (*in vitro*)
Alumina-on-Alumina	0.6	[19] (*in vitro*)
	0.2	[27] (*in vitro*)
	0.05	[39] (*in vitro*)

3.4. Metal-on-Metal TJR

As discussed in the previous section, the first generation Metal-on-Metal (MoM) implants were gradually abandoned in the 1970s due to the high revision rates (75%-90% at 5 years) and the arrival of MoP prostheses. The reasons for the high failure rate were primarily a lack of clearance at the articulation and the poor finishing (roughness) of the articulations. For the second generation MoM implants, wrought/forged cobalt chromium alloys were used due to a greater hardness and a more homogenous microstructure without residual porosity. However, studies by Devine *et al.* [40] have shown a very small difference between cast and wrought cobalt chrome alloys in terms of material loss. It suggests therefore that the difference of hardness between cast and wrought alloys may not be as important as expected for MoM bearings. In the TJR implants market, products are made from both wrought and cast by different manufacturers. Larger femoral heads and smaller clearance mean that MoM implants are seen as a promising development [32].

Even though Titanium and Ti alloys have very high corrosion resistance and excellent biocompatibility, their application for MoM joint replacement is still not recommended by some authors [22, 41] due to their poor resistance to wear and clinical reason of high hypersensitivity [42]. However, as a counterpart material, Ti alloys are used with polyethylene or ceramics for MoP or MoC joint replacement. In addition, Ti alloys are largely involved with bone-cemented or cementless femoral head stems. Studies have been carried out for Ti alloys toward involving surface modification in order to apply them in a MoM joint replacement [43]. Because Ti alloys still have serious limitations, CoCrMo alloys are still the primary choice for MoM TJR.

It has been studied and proved that the most active (causing osteolysis) particles are in size range of 0.1 μm to 10 μm for polyethylene particles. For metal hip replacements, wear debris was isolated from previously implanted prosthetic

tissues and also from simulators. It has shown that the mean size of 50-80 nm particles is significantly too small to affect the resident macrophages and below the activation of the osteolytic size range [44, 45]. Germain *et al.* [44] found that most metallic particle sizes were 10-20 nm and they were uniform both in size and shape. However, the number of metallic wear particles greatly exceeds that of polyethylene particles. By isolating metal wear particles from tissues of several patents, an average of 7.0×10^{13} particles were produced per year and lead to loosening [20]. About 1×10^{6} particles are generated from each walking step or each cycle in THR. Volumetric wear in MoM hip replacement is less than $1/100^{th}$ of that of MoP counterpart [23]. As a consequence, MoM TJR is receiving significant attention from the orthopaedic community.

All metallic implants degrade to some extent over time, resulting in locally and systemically elevated levels of metal. Elevated levels of Cr, Co, and Ti have been reported in the serum of patients with both well and poorly functioning total joint replacement. Yang *et al.* [46] noticed that the metal ions can bind with albumin, and therefore be transported wherever albumin goes. Released metal ions may cause various phenomena: transportation, metabolism, accumulation in organs, allergy and carcinoma [47]. If a large amount of metal ions are released, it could be generally harmful for human health. Particularly, any release of Cr^{6+} could cause double and single DNA strand breaks, protein-Cr-DNA crosslinks and aneuploidy. Cr^{3+} is reported to be 1000 fold less toxic than Cr^{6+}, due to the fact that it has difficulties in entering cells. Co^{2+} itself can cause DNA strand breaks and in addition, it inhibits the incision and polymerization step in DNA repair. Therefore, both Cr^{6+} and Co^{2+} have potential risks to the patients who had MoM or MoP with Co-based alloy component(s) [48]. The increased levels of Co and Cr were eliminated in urine after MoM hip replacement [49]. It indicates that binding of metal ions with proteins is possibly reversible. However, at this stage, in TJR, more adverse biologic responses are reported for the polyethylene than metal replacements.

The ion release process is electrochemical in nature. In addition, wear, fretting or stress can significantly accelerate the release rate. In order to fully understand these processes and then to improve MoM joint replacements, in the next sections, the corrosion and tribocorrosion effects based on existing literature are reviewed.

3.5. Corrosion of Metallic Biomaterials

Corrosion has been considered as one of the major problems for metallic biomaterials [50-52]. When devices are implanted into the human body, they are immediately surrounded by biological fluids. Even though corrosion can occur on plastics, ceramics and glasses, the term is often associated with metals. In this section, corrosion of metallic bio implant materials is the focus. From a corrosion engineering point of view, these liquids are not as aggressive as some industrial process fluids, but the body is still a harsh environment due to the oxygenated saline solution and the involvement of organic species. Ever since metallic biomaterials were adapted for surgical use, studies have been done to assess corrosion resistance of those materials. Three major metallic materials; stainless steel, cobalt chromium alloys and titanium/titanium alloys are normally used and the understanding of their performance and improvement has been under investigation for several years.

Corrosion can severely limit the fatigue life and ultimate strength of materials, leading to the mechanical failure of implants [53, 54]. Corrosion products have been implicated in causing local pain and swelling in the region of the implant and affect the performance of those implants resulting in failure and revision. The release of ions from implanted metallic biomaterials to the local host environment is also a great concern. Ions are released by chemical and electrochemical processes (*corrosion*). The potential effects of released Co^{2+} and Cr^{6+} have been discussed in the earlier section.

One point which should not be ignored is the corrosion of wear debris. Even though, nano-size metal debris is very difficult to be collected and analyzed, it is still a potentially important source of the metal ion release which has not largely been studied until now.

The corrosion mechanisms of these metallic materials for surgical use have been extensively investigated, from both *in vitro* experiments and *in vivo* observations [45, 53, 54]. They cover most of corrosion formations shown in Chapter 2. They were identified and shown as following:

- Pitting corrosion: Pitting corrosion is the most common type of localized corrosion. It was found on stainless steel implant materials resulting in extensive damage and caused release of significant amounts of metal ions [55]
- Crevice corrosion: Compared to the other types of metallic implant materials Type 316L stainless steel is highly susceptible to this corrosion attack. In the area of contact between stainless steel screw head and the bone plate, the occurrence of corrosion was found. It also induced crack propagation of bone plate [7, 55]
- Fretting corrosion: Fretting corrosion phenomena are associated with micromotions between components [50, 56]. When an oscillating rubbing action is continuously applied on two opposing surfaces such as bone plates and the screw heads of the prosthetic devices, fretting corrosion can occur [46]. It is the major factor to cause the initiation of cracks and fracture failures for surgical screws.
- Galvanic corrosion: When metals of different types from different devices are in physical contact in body fluid, galvanic corrosion can occur. For example, a bone screw and a bone plate made of dissimilar metals and alloys can form a galvanic couple.
- Wear corrosion: When implant materials are under cyclic loading, wear-corrosion is always present [57, 58]. Wear-corrosion resistance is

an important factor of consideration for load-bearing surgical implants such as hip and knee replacement implants. Details regarding to wear corrosion will be discussed separately in section 3.7.

These types of corrosion are the major reasons for metallic device failure. A survey in India has shown that 70% of failed stainless steel implants are associated with corrosion related to pitting and crevice attack [55].

Metallic materials used for bearing surfaces in hip arthroplasties normally rely on a stable passive film, which forms spontaneously in air, for their biocompatibility. The passive film can form a barrier which can efficiently separate the metal from the corrosive environment and protect it from further corrosion processes [6]. The passive film inhibits corrosion and keeps current flow and the release of corrosion products at a very low level. Nonetheless, the release of metal into the body is a well-documented fact [50-52]. Uniform passive dissolution resulting from the slow diffusion of metal ions through the passive film, transpassive dissolution under high oxidizing conditions, or the local breakdown of passivity as a consequence of localized forms of corrosion such as pitting or crevice corrosion, or as a consequence of mechanical events such as fretting and wear corrosion are all possible mechanisms.

XPS (X-ray Photoelectron Spectroscopy) and other surface analysis techniques have been used to determine the nature of passive films on Co-base alloys. Primarily Cr_2O_3, CoO and MoO_3 are found in the top layer (1.6nm) of the spontaneously formed passive film in air for CoCrMo alloys. The inner layer of the passive film contains Cr_2O_3 and Co and Mo metal species [48]. The total thickness of the passive film on CoCrMo alloys in the atmosphere is about 4-5 nm.

Hanawa *et al.* [60] examined the surfaces of metallic (Stainless steel, CoCrMo alloys and Titanium). A preferential release of Co ion for CoCrMo alloys and Fe ion

for stainless steel 316L were obtained. The release of Mo in CoCrMo was reported to be insignificant. A ratio of approximately 2.9/1 of Co/Cr for pin-on-disk tests on CoCrMo was reported [59]. However, from Jacobs *et al.* [61] work, Co was released from the cast CoCrMo alloys was very small in the biological solution and it was found that Ni release from 316L gradually decreased with increasing pH while Cr and Mo ions from CoCrMo were smaller at a pH of approximately 4 and higher. One thing should be noticed that in the natural body serum condition, the pH is around 7.4. Calcium phosphate was found as precipitates on implant metals and alloys surfaces. He also suggested that formation of oxide or hydroxides of metal ions were less toxic than the complex of protein-bond-metal [62].

The CoCrMo alloys are highly corrosion resistant with only a minimal susceptibility whilst stainless steel quite readily suffers crevice and pitting corrosion. CoCrMo alloys are considered biocompatible. However, very high levels (20-30 times as reference normal serum cobalt value (0.15μg/L) and serum chromium value (0.26μg/L)) of metal ions are reported cytotoxic with increasing concern over the biocompatibility of implant materials and especially in terms of the significance of corrosion, wear, hypersensitivity and carcinogenicity [63]. The quantity of organometallic production over longer periods after TJR, correlation with patient health medication and activity levels remain the objective of many studies [42]. There can be no doubt therefore that patients with MoM implants will be exposed to elevated levels of metal ions locally. The outstanding question remains the clinical impact of these elevated ion levels. Brondner *et al.* [64] examined patients with CoCrMo metal-on-metal THR and found that the Co and Cr concentration in blood serum and urine are high. They seem to fall after the initial 1 year running-in phase. Average preparative blood serum cobalt levels of 0.15 μg/L were cited as reference values for patients who had MoM hip implant from Muniz's studies on elements trace [65] and it is generally in line with the others [39]. Black *et al.* [66] showed a disagreement concerning 'normal' levels for these elements in serum. Because it is still unclear what constitutes a *normal* level for an individual patient and what the consequences are of transient or chronic deviations from that level, a question mark still exists over MoM implantation.

Visuri and Koskenvuo [67] showed that there was no increase in the risk of cancer in patients with McKee-Farrar type CoCrMo MoM THR and Willert [68] found no proof that the release of metal is teratogenic but did show possibility of hypersensitivity to metals. Koegel *et al.* and others [69] disagreed. An increased incidence in cardiomyopathy (a disease or disorder of the heart muscle) and tumours was found from animal tests. Because the numbers of patients with a MoM TJR for 10, 20 or longer years increases, it suggested that long-term studies are still required to fully address the issue of metal-ion associated diseases. Investigations to clarify the importance of toxicology are currently being undertaken by many researchers and clinicians [63].

Electrochemical methods have been employed to understand corrosion behaviour for implant materials and then to assess their biocompatibility. Many authors have been trying to monitor the performance of TJR by measuring metal levels [56, 58, 70].

At this stage, it is important that a more detailed understanding of the effects of implanted metals must be gained. A wide variety of serum proteins exist *in vivo* and it is reasonable to assume that many of these become rapidly adsorbed onto the metal surfaces upon implantation. It is suggested that the adsorbed proteins influence the material corrosion rate. Details of the effect of proteins will be discussed in section 3.8.2.

3.6. Tribology Behaviour of MoM TJR

The wear rates for MoM, particularly for CoCrMo MoM implants were shown in Table 3-1. The results are gathered from both *in vivo* and *in vitro* simulator tests. MoM implant material degradation is influenced by many factors such as macrogeometry (diameter and clearance), deviation from sphericity and alloy

composition. In this section, consideration of MoM implant configuration design, the role of materials and different testing methods are reviewed. The discussion of their effect on MoM tribology behaviour is made.

For most tests, wear means the total material degradation and is commonly accepted due to mechanical processes. Wear rate then refers to the volumetric or gravimetric material loss during certain periods of time. However, *wear* (mechanical process) and *corrosion* (chemical and electrochemical processes) can not be separated in real MoM implants therefore in this section, the term 'wear' refers to the damage caused due to both mechanical and electrochemical processes. Details of studies and attempts to separate these effects will be reviewed in the later section.

Before they go to the simulator testing stage, candidate materials should be assessed by more simplified methods to screen or rank materials tribological behaviour or combinations. From a tribological point of view, in MoM artificial joints, sliding wear is the dominant wear mechanism. Pin-on-disk or ball-on-disk tests have been extensively carried out worldwide [71, 72]. Materials which have high wear in pin-on-disk experiments are expected to have high wear rates when they used in joint replacement.

3.6.1. Material selection

As discussed in 3.3., in MoM TJR, Cobalt based alloys dominate the materials selection, due to their high wear and corrosion resistance [32]. Cr and Mo are always involved to improve their resistance to corrosion and metallurgical stabilities. The protective passive film is primarily composed of Cr oxides (mainly Cr_2O_3), which firstly prevents metal ions from being further released and secondly, protects any aggressive ions (Cl^-, SO_4^{2-} etc.) from attacking the substrate. Goldberg *et al.* [73] showed a stronger surface oxide on CoCrMo then Ti6Al4V. Then a higher interfacial adhesion strength of oxide film can make it more resistant to fracture.

Cr and Mo with carbon can form very complex combinations of M_7C_3, M_6C, and $M_{23}C_6$ carbides in the f.c.c (face centred cubic) Co-rich matrix [74]. Due to this structure, Cobalt based alloys are generally well suited as self-bearing materials, they are known to have the ability to polish out visible surface scratches with continued wear cycles. Wrought CoCrMo alloys can undergo strain induced transformation, an alteration in microstructure and more resistant crystallographic structures [75]. The reasons they have being used increasingly in orthopaedic implants are because of their hardness, strength, and resistance to corrosion and wear. In particular, the excellent wear properties make this the preferred alloy for the new generation of metal on metal bearing couples .

Two classes of CoCrMo alloys are commonly used in MoM implants. They differ in carbon content. The role of carbon in minimizing the amount of wear for MoM has attracted to different groups [76]. Franks *et al.* [77] compared a higher carbon content (0.2%) CoCrMo hip implant and a lower carbon content (0.05%) implant. They concluded that high carbon content seemed to reduce material wear resistance. However, many researches have shown that the alloy with the relative high carbon therefore having high carbide volume fraction has systematically low amount of abrasive wear [78, 79]. From Kato's work [78], HC (with carbon 0.24%) CoCrMo-on-HC CoCrMo showed 5 times less wear than LC (with carbon 0.05%) CoCrMo-on-LC CoCrMo and similar value for HC CoCrMo-on-LC CoCrMo. In another work which was carried out by Schmidt *et al.* [79], from pin-on-disk experiments, LC CoCrMo had three times more wear than HC CoCrMo. It was summarized that carbide containing CoCrMo alloys were more resistant to wear and recommended to be used under load and tribological contact. Liu *et al.* [80] also compared HC CoCrMo and LC CoCrMo in saline solution; better wear resistance was observed on HC CoCrMo due to the increase of carbon in this alloy and the enhancement of the elastic properties and stiffness of the alloy. A reduction of ductility was found and also if the carbon content is too high, poor wear resistance was suggested due to the over balanced carbides resulting in weak interfaces with the solid solution matrix.

A third-body effect was observed most *in vitro* and *in vivo* tests. Wear debris was released from counterface materials and could escape from the contact areas then cause abrasive scratches. Devine *et al.* [40] suggested that carbides in CoCrMo alloys were responsible for this phenomenon. The size of normal carbides is about several microns, and the wear particles observed from the MoM implants are nano-sized. It is unlikely that carbides are the major causes for the third body effect. One possibility is that carbides are pulled out from counterface material and crushed by mechanical contact, but with a very high hardness, carbides are difficult to be cracked. Further investigations are still needed to fill this gap.

In terms of manufacturing methods, Wrought, Forged and Cast CoCrMo are all in use by different manufacturers. Cast materials are easy to be shaped but poor in final surface finish. Wrought/forged alloys can achieve very low surface roughness ($R_a = 0.01\mu m$) then can get a better lubrication effect and reduce the possibilities of loosening [80]. Additionally, according to the Archard equation, the harder alloys have a better abrasive and adhesive wear resistance than less hard alloys. Normally, wrought or forge treatment is likely to achieve a harder surface. However, Cawley *et al.* [81] suggested that hardness between cast and wrought alloys may not be a fundamental factor for small diameter MoM implants. It is concluded that the carbides were instrumental in maintaining the integrity structure of the metallic Co rich matrix [75]. As discussed in section 3.3., debates are still ongoing on this topic.

3.6.2. The role of femoral head diameter and clearance

Dowson *et al.* [82] found that the predicted film thickness increased steadily as the implant diameter increased and by the time a film thickness of about 14 μm was established (femoral head diameter 36 mm), the wear rate is exceeding low (<0.08 mm^3/million cycles). Increase in the head diameter caused the wear rate to decline as the lubrication regimes developed from boundary to mixed. Another advantage of a

large diameter head is that it can prevent dislocation of the femoral ball when the operation is performed [83].

The amount of ball-socket clearance in MoM hip joint implant also can influence the wear rate of a metal-on-metal bearing. Jin *et al.* [11] suggested that a small clearance can achieve full fluid film lubrication between ball and socket, therefore increases the contact area and reduces friction and wear. The increase of the volumetric wear as a function of the decrease of clearance was confirmed by Scholes *et al.* [33]. However, the smallest clearance limit of 20 μm and optimal clearance of 100-150 μm are recommended [39].

3.6.3. The relationship with roughness

Several authors have been studying the relationship between femoral heads or acetabular cups roughness and wear [83, 84]. Some models were provided to simulate wear rate (k) by a given roughness (R_a from 0.05 to 0.7 μm).

The model from Wang *et al.* [83] is

$$k = 7.21\times10^{-6}(R_a)^{0.42} \qquad \text{(Eq.3-1)}$$

and the model from Hall *et al.* [84] is

$$k = 9.7\times10^{-6}(R_a)^{0.54} \qquad \text{(Eq.3-2)}$$

However, many other studies failed to show any relationships between these two factors: wear rate and roughness [85, 86]. Nonetheless the use of the parameter of the roughness R_a is questionable. Small roughness can achieve EHL (elastohydrodynamic lubrication) and reduce friction. In the first generation of MoM joint replacement, the poor surface finish was one reason for the early failures. For modern MoM implants, small roughness is believed to decline the wear rate.

3.6.4 Friction of MoM

High frictional torques was found to contribute to loosening of early MoM designs [87]. Therefore, the assessment of friction for MoM has been studied by many authors. Hall *et al.* [88] reviewed the work undertaken by numerous groups and individuals on the frictional resistance that arises in both established and experimental joint replacement. It is concluded that for MoM and MoP implants, McKee-Farrar (MoM) showed friction coefficients of 0.1-0.8 under dynamic loading in synovial fluid while CoCrMo-on-UHMWPE or Ti6Al4V-on-UHMWPE achieved the value of 0.05, while Kenneth's work [89] showed friction from MoM wear studies were 2 times less than MoP.

The relationship of friction and wear for MoP, CoC and CoM hip implants were compared with metal-on-metal bearings that contained either similar or dissimilar materials based on a number of studies [79]. It is summarized in Figure 3-4.

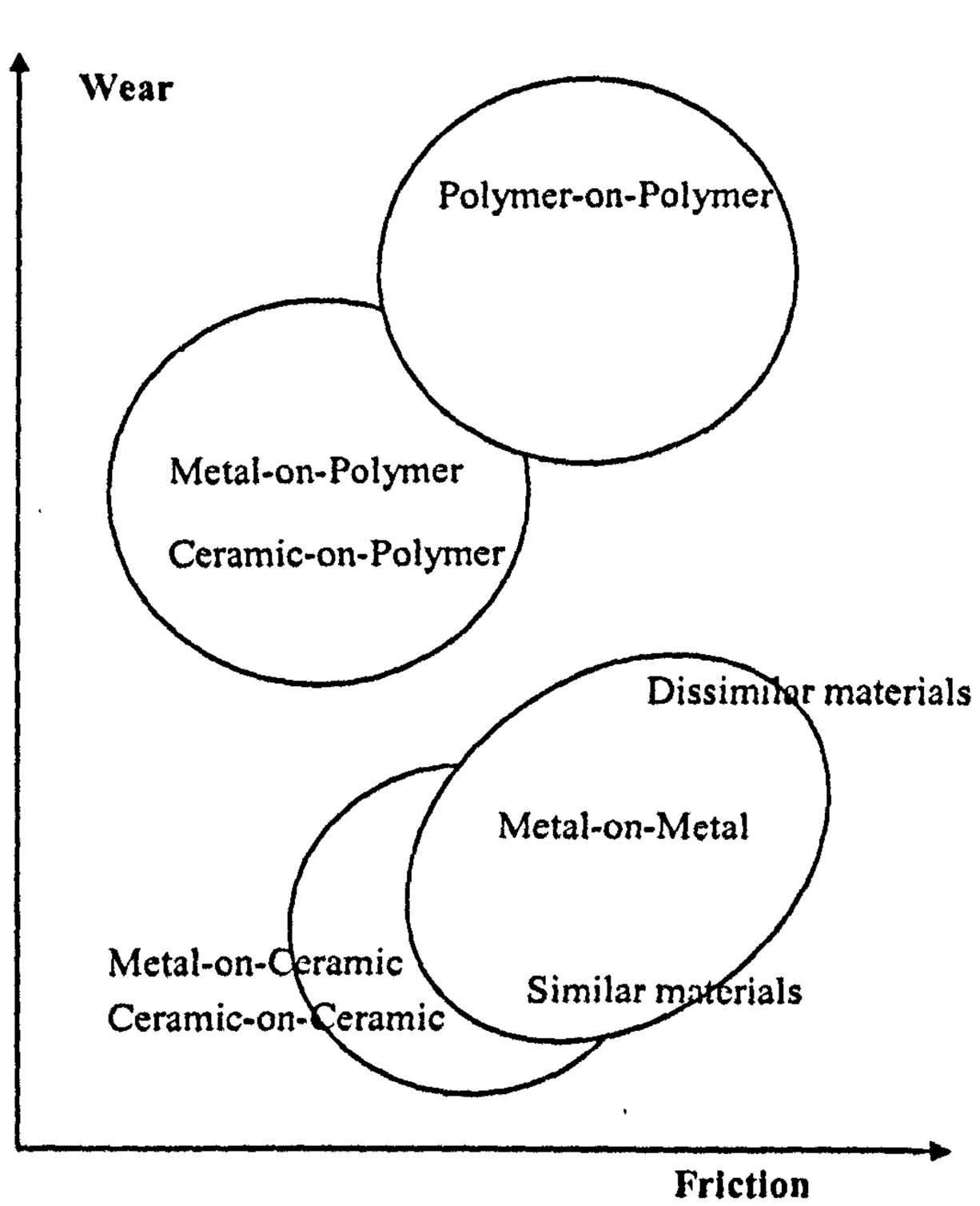

Figure 3-4 Wear and friction for different combinations of THR [79].

3.6.5. The running-in state and the steady state

The phenomena of running-in state and steady state have been recognized in many applications when wear is presented [90]. Many authors have been studying MoM wear behaviour *in vivo* and *in vitro*. Two distinct wear phases were discernible for MoM joints. A running-in (or bedding-in, wearing-in) stage is found, followed by a lower wear rate steady-state [90] (Figure 3-5). The length of running-in varies depending on the different simulators and geometry of contacts (pin-on-plate, ball-on-plate etc.) from thousands of cycles to about 1 million cycles [31, 59, 82]. Generally, after 1 million cycles *in vitro* and 1 year *in vivo*, implants are considered to reach a steady state. Small wear debris particles are mostly created in the running-in phase and cause abrasive wear. From clinical examinations, for the first few days after implantation of MoM joints, metal ions were found to increase dramatically. The metal ion level then stabilized [90-92], which is possibly related to the biphasic (running-in and steady-state) wear phenomena and the saturation of metal ions in the body. As shown in Figure 3-6, from clinical wear factor, a stable wear factor was reached in region A to B after the initial relatively high wear rate (before A). It is considered that a running-in process is present before point A. as mentioned previously, the duration is about 1 year. Then the wear was dramatically accelerated (region B-C) due to the failure of devices. Theoretical and experimental studies have been carried out by Scholes *et al.* [93], Dowson [82] and the others [59,65].

Some authors have studied the hypothesis that in the steady-state, calcium phosphate formed from the simulated biological synovial fluids (serum, etc.) can contribute to reduced friction [94] by acting like a solid lubricant then can also reduce wear. In contrast, some studies have shown that the formation of calcium phosphate can prevent a very important fluid film on sample surface [83]. For stainless steel and Ti alloys they have the preference of calcium phosphate formation both *in vivo* and *in vitro* [57]. It is because phosphate ion can be readily adsorbed on the hydrated Ti oxide surface or stainless steel surface by relieving proton. Then calcium phosphate forms when Ca is adsorbed on the adsorbed phosphate ion [19].

However, the transformation from the running-in state to the steady state is likely to be associated with the change of surface mechanical properties. The smoothening of surface can reduce the roughness and then achieve a lower wear rate in the steady state [94].

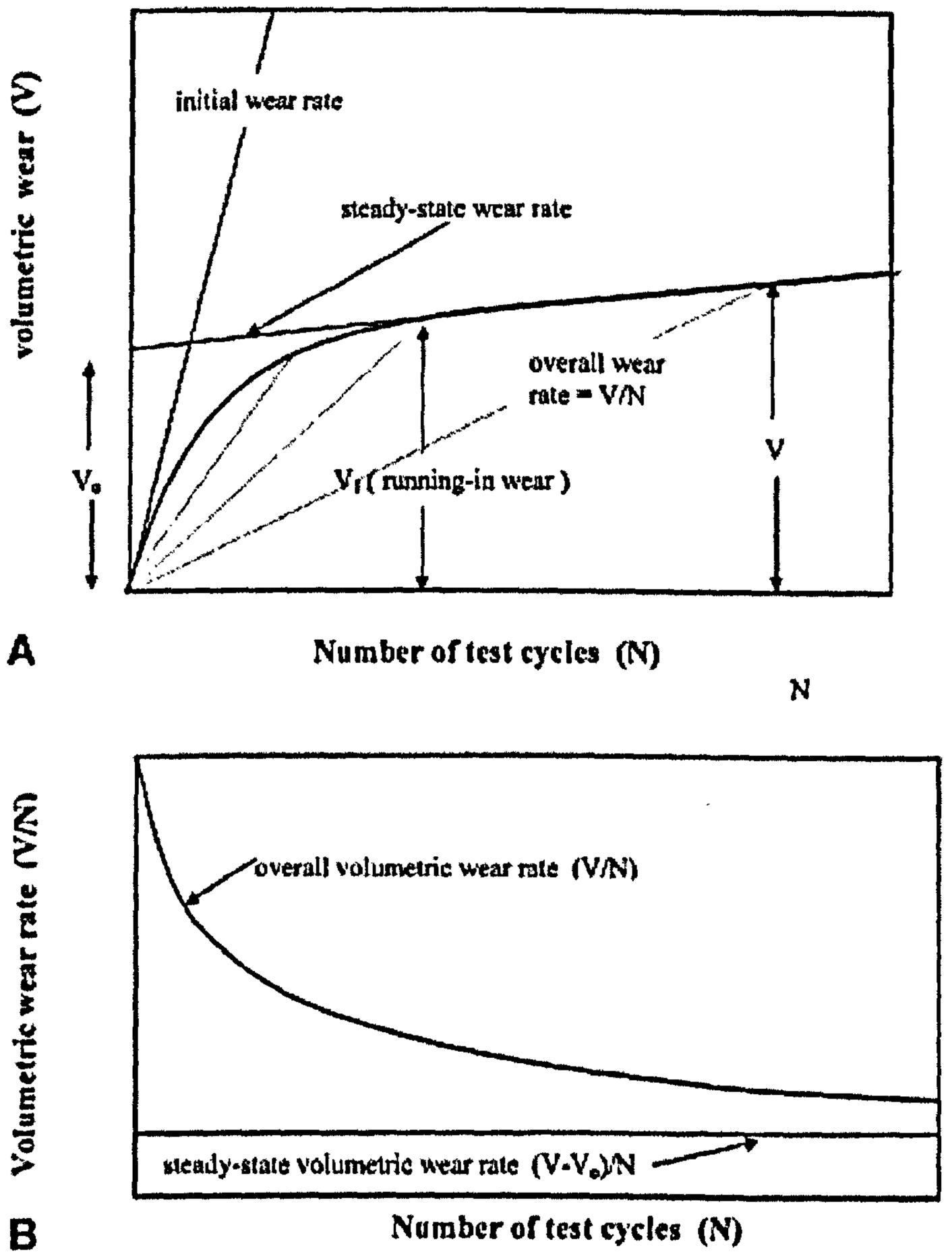

Figure 3-5 Basic features of volumetric wear and volumetric wear rate. (A) Volumetric wear. (B) Overall and steady-state wear rates [82].

From clinical results, a wear-in (running-in) was also found in about 1-2 years both in terms of a stabilized and low wear rate, and relative constant metal ions (Co, Cr and Ni) levels [48]. Declined serum Cr and Co levels and slightly increased Ni levels were also found after a few months of implantation of MoM THR by Black *et al.* [66]. A correlation between released ions levels and material loss was noticed by many authors [32] and then it was suggested to evaluate the implants performance

by monitoring the released ions [95]. The solubility of Co, Cr and Ni in serum is very low (0.002%). CoO has a solubility of 19.9% while $CoCl_2$ has a 100% solubility in serum [155]. It indicates that the traced Co, Cr or Ni ions are from electrochemical processes (corrosion).

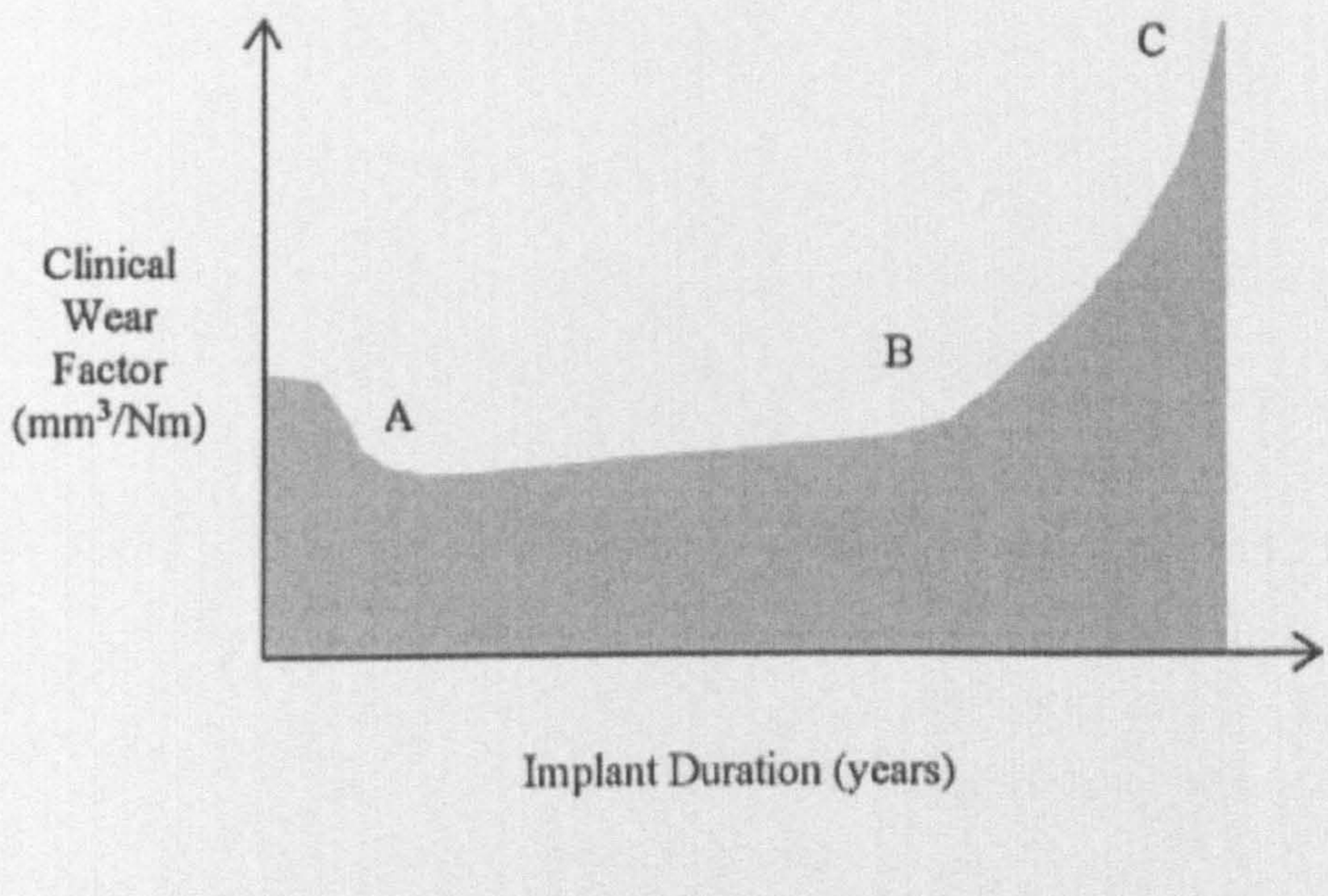

Figure 3-6 Clinical wear rate for THR [96]

3.7. Tribocorrosion

Tribocorrosion is defined as the chemical, electrochemical and mechanical processes leading to a degradation of materials under tribological contacts in a corrosive environment [97, 98]. It is an irreversible transformation.

Material degradation due to the combination of mechanical and electrochemical may occur under a variety of conditions. A sliding movement between two surfaces under two bodies or three bodies contact is a common cause of tribocorrosion. With micromotion involved, fretting-corrosion is a special type of

tribocorrosion. Tribocorrosion is also observed in ball bearing under rolling contact. Particle impact 'or impingement attack can also result in a combined mechanical, chemical, electrochemical attack of material.

As discussed earlier, a stable passive film on metallic materials surface can protect materials from corrosion attack. Under mechanical relative movement, oxide films on passive metals can be locally or even completely destroyed. An accelerated corrosion has been found by different studies [58, 98]. It is generally believed that wear will enhance corrosion rate.

The electrochemical approach offers the opportunities to control the surface chemistry of the material under tribological contact. Mischler *et al.* [97] monitored the current change by holding a certain potential. The oxides of materials were disrupted by mechanical movement. The fundamental work suggested that the passive film on mechanical degradation played an important role.

The relationship between friction and electrochemical processes attracted a number of authors. Okazaki [99] noticed that friction can change biomaterials corrosion behaviour. 316L, CoCrMo and Ti6Al4V showed current fluctuation under tribological contact. Ponthiaux *et al.* [100] believed that a decreased friction was due to a third-body effect by the released corrosion products particles. Higher friction was found where a large tendency to passivation prevails. One important conclusion from this work is that between unworn and worn area, a galvanic couple may take place.

Garcia *et al.* [101] promoted an equation to model the current flow between the two areas. An anodic potential assumed to be provided and it is expressed as:

$$I = fA_a \int_0^{\frac{1}{f}} i_a(t)dt + f(A - A_a) \int_0^{\frac{1}{f}} i_p(t)dt \qquad \text{(Eq.3-3)}$$

where I is the current flowing through an electrode of total area A. A_a it the worn are. A-A_a then presents the passive area without tribological contact. The repassivation current density is $i_a(t)$. The $i_p(t)$ corresponds to the anodic current density for passive material polarized at that given anodic potential. The contact frequency is f.

Goldberg *et al.* [73] suggested an equation by which the current transient and repassivation current by single scratch test could be modelled and predicted. Oxide film fractured due to a mechanical sliding.

$$I(t) = I_{peak} \exp\left[\frac{-(t-t_0)}{\tau}\right] + I_\infty \qquad \text{(Eq.3-4)}$$

where I_{peak} is the peak current ($I_{peak} = I_{max} - I_\infty$), τ is the time constant for repassivation, t_0 is the time to produce the scratch, and I_∞ is the baseline current at t $= \infty$. If sample had Tafel behaviour, the following equation was then given:

$$I_{peak} = j_{crit} A_0 \exp\left[\frac{\eta_f}{\beta_a}\right] + \frac{\delta \rho Z F A_0}{M_w \tau} \qquad \text{(Eq. 3-5)}$$

Where j_{crit} is the critical current density for passivation, A_0 is the initial scratched area, η_f is the film overpotential (the difference between passivation and potentiosatically held potential) β_a is the Tafel slope, δ is the thickness of the repassived oxide film, ρ is the oxide film density, Z is charge per cation, F = Faraday's constant and M_w is oxide film molecular weight. It described the relationship between the peak current, oxide film thickness and exchange current density for ionic dissolution. It suggests that greater contact area resulting from plastic deformation (an application of high contact load) results in enhancing ion rlease.

Mischler *et al.* [97] presented a model to describe the corrosive behaviour of passive metals sliding against a hard insulating body. The anodic current under wear, $I_{a,w}$ was influenced by wear track length, l, sliding frequency, f, applied load, W, and hardness of the material, H. The model is expressed as :

$$I_{a,w} = K_w lf\left(\frac{W}{H}\right)^{\frac{1}{2}} \int_0^{\frac{1}{f}} i dt \qquad \text{(Eq.3-6)}$$

where K_w is the proportionality factor.

However, in tribocorrosion systems, the material degradation is caused by the combination of tribological material removal and electrochemical processes. It is not simply sum of the two processes together. Synergistic effects play a very important role.

A number of works have been carried out in erosion-corrosion; another form of tribocorrosion process. Neville *et al.* [102] examined erosion-corrosion behaviour for materials under slurry conditions. Material degradation was evaluated. An equation (Eq. 3-7) was used to determine the mechanisms of material loss which caused by mechanical impact and electrochemical process.

$$T = E + C + S \qquad \text{(Eq.3-7)}$$

$$S = E_C + C_E \qquad \text{(Eq.3-8)}$$

$$T = E + C + E_C + C_E \qquad \text{(Eq.3-9)}$$

T is the total weight loss in erosion corrosion environments. The pure material degradation caused by erosion is referred as E. C is the material loss due to electrochemical corrosion process only. S is the synergy effect which involves E_C (corrosion effect on erosion) and C_E (erosion effect on corrosion). Cathodic protection was employed to obtain erosion damage. Electrochemical tests and Faraday's Law were used to determine material loss due to corrosion effect. It can be expressed as :

$$C_E = \frac{QM}{nF} \qquad \text{(Eq.3-10)}$$

where Q is the quantity of charge. M is the material molecular weight. The valence of the material is referred as n. F is Faraday's constant. Theoretically, the amount of charge can be calculated by the equation 3-11:

$$Q = \int_0^{t_f} (I - I_0)dt \qquad \text{(Eq.3-11)}$$

where t_0 is the time at tribological movement starts and the current is I_0, t_f is the time at which the relative movement is completed and at t_f the current is I.

Many studies for investigations of wear and corrosion have used those equations [6, 97]. A model was developed by Jiang *et al.* [103] to suit wear-corrosion under a aqueous sliding contact from Eqs. 3-6 and 3-9. It is able to simulate the synergy in a tribocorrosion system. The model is rather complex but covers the most important issues in a tribocorrosion system and provides a tool for further development. The effect of sliding distance, contact frequency, load and susceptibility of metals were related to this model and their effects on synergism were discussed. The low corrosion rate of orthopaedic materials relies on the protective passive film. When material under frequent mechanical motion, the protective barrier can be removed and re-form. In this sense, how fast the removal force is should be taken into account. Additionally, a wear map was constructed. A biphasic structure was concluded. One of them was called *wear-induced corrosion*, which is the equivalent to C_E in Eq. 3-9. It dominates the material degradation processes when low load and high contact frequency are applied. Another one was named *corrosion-induced wear*, which corresponded to E_C in Eq. 3-9. The tribocorrosion system was dominated by corrosion-induced wear under high load and low contact frequency. In addition, when the applied load was high and the contact frequency was low, corrosion-induced wear likely dominated the metals who had high passivation capabilities. The boundary of the biphase was determined by Eq. 3-12.

$$\frac{W}{H} = k_{cw}\left\{f\tau_0\left[1-\exp\left(\frac{-1}{f\tau_0}\right)\right]\right\}^2 \qquad \text{(Eq.3-12)}$$

Considering dental or joint implants, material degradation is a consequence of combined attack by corrosion and wear. The two mechanisms do not proceed separately. Therefore, the conjoint processes of wear and corrosion are of great importance in the design of orthopaedic prostheses.

Khan and Williams [104] examined the conjoint action of corrosion and wear for orthopaedic use Ti alloys. An increase weight loss due to the presence of corrosion is found in wear tests. However, with proteins, a weight gain was observed. It was explained that protein adsorption and the corrosion products adhering to the contact area were responsible. One concern from this work is that wear tests in distilled water were performed as a simulation of an environment where corrosion will not occur. However, dissolved oxygen in distilled water can cause corrosion attack. The study was useful and given some important information. Tribocorrosion behaviour for other implantable metallic materials lacks any advanced or extensive literature.

3.8. Protein Effects

3.8.1 Protein and Protein structure

Proteins are complex, high molecular weight organic compounds that consist of amino acids joined by peptide bonds. They have three-dimensional structures (Figure 3-7) [105]. Each type of protein has its own unique structure and function. The basic structure of an amino acid consists of four parts: an amino group ($-NH_2$), a carboxyl group (-COOH), a central carbon (C) and a side chain. A large number of amino acids then composes a single protein molecule. The formation of hydrogen bonds between amino acids in the chain causes bends and curves in the structure. According to biochemists, four distinct aspects of a protein structure are referred to [106]. They are primary structure, secondary structure, tertiary structure and quaternary structure. Protein native state is known as a protein naturally folds, which means the secondary structure remains its functional shape. A protein in its native state is often described as *folded*. A protein that is not in its native state is said to be denatured (*unfolded*). Denatured proteins generally have no well-defined secondary structure [107].

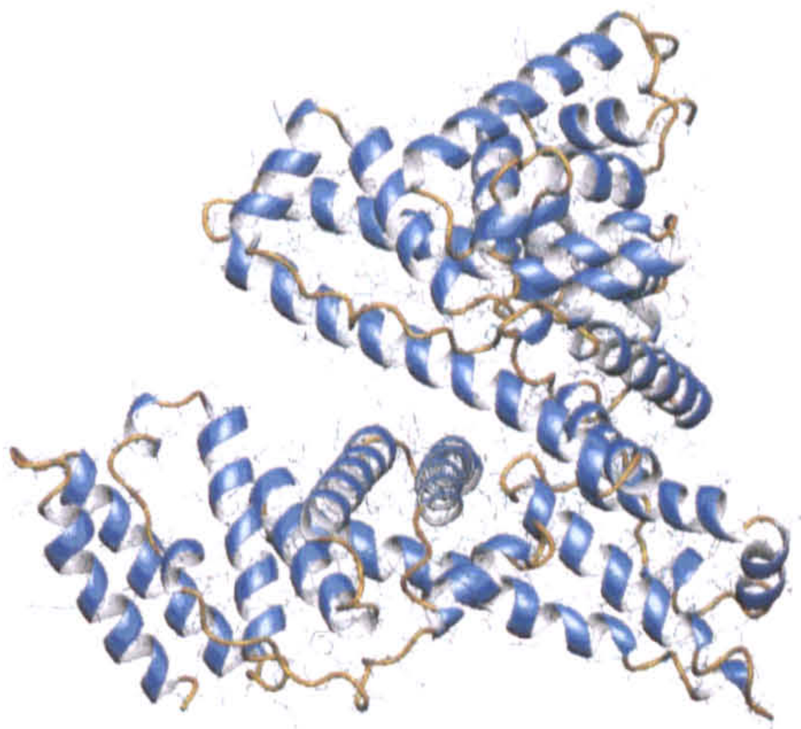

Figure 3-7 3-D structure of human albumin [107]

Synovial fluid is joint fluid (Figure 3-8). In human joints, a thin film of synovial fluid covers the surface of cartilage within the joint space. It consists of an ultrafiltrate of blood plasma plus hyaluronic acid and glycoproteins. It contains about 60% of Albumin [108]. Synovial fluid in joints has three major functions:

- To lubricate joints
- To provide nutrients to the cartilage.
- To protect the joint structure when subjected to large compressive forces.

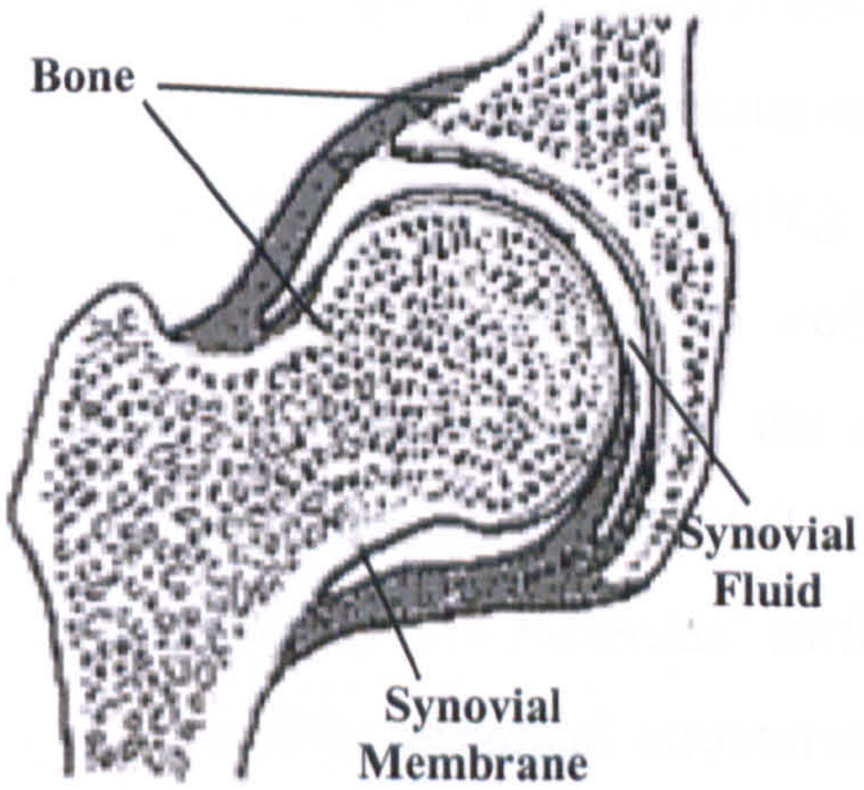

Figure 3-8 Structure of a normal human hip joint

For *in vitro* TJR simulator and wear tests, bovine serum has been employed as an equivalent or similar liquid as synovial fluid in human joints [39]. For MoM implants, they were considered to operate in the boundary lubrication regime by

Franks and others [11, 77]. In this regime, molecular components of synovial fluid, mainly proteins and lipids, can attach themselves by chemical or physical bonding to the metal surface. In addition, some authors suggested that mixed film lubrication [12] or fluid film lubrication (elastohydrodynamic lubrication) may occur. Medley [109] noted that healthy synovial fluid had approximately 30% less protein than serum. However, in another study by Walker [110], with a McKee-Farrar implant, the joint fluid had approximately ½ the amount of protein as serum. The protein concentration factor is critical due to the fact that proteins not only influence material wear behaviour but also corrosion behaviour. Thus, the appropriate concentration of serum should give a comparably similar protein level with them in the synovial fluid. The author summarizes and concludes that 30%-50% of serum should be employed as a testing liquid *in vitro*.

3.8.2. Protein adsorption and binding with metal ions

The interaction of biomolecules and cells with implants is determined by the chemical composition, surface energy, roughness and topography of the top surface layers that are in contact with body fluids (biological systems). Interaction between biomaterials and tissues occurs via a layer of proteins adsorbed at the surface of any implant. Adsorption is the process whereby molecules adhere to solid surfaces. Such proteins adsorption is an instantaneous process occurring on its first contact with biological fluids and tissues [113]. Protein adsorption studies have focused on the adsorption kinetics, dynamics and thermodynamics, the spectroscopic studies of protein structure and function in the adsorbed state [114]. The nature and amount of the protein adsorption layer depends on materials surface properties, such as wettability, polar or ionic interaction, chemical structures and topography of the surface.

- Texture: greater texture expose more surface area for the interaction with proteins.

- Composition: chemical characteristics of a surface will determine the intermolecular forces to the interaction with proteins
- Wettability: hydrophobic surfaces tend to bind more proteins then hydrophilic surfaces.
- Heterogeneity: nonuniformity of surface results in domains that can interact different with proteins.

It is reported that the primary structure of proteins relate to the surface activity. It means that the sequence of amino acids affects protein-surface interactions [113]. Another factor that should be considered is that proteins not only interact with surface of materials but also intend to interact with each other. The protein adsorption is greatly influenced by the pH value of the environment [115]. In an acid environment, the amino group ($-NH_2$) becomes to ($-NH_3^+$) and carries a positive charge. In an alkaline solution, the carboxyl group (-COOH) losses H and becomes ($-COO^-$). Proteins can interact with material surfaces with the electrostatic force but the force is rather weak.

Desorption is the reverse of adsorption. Molecules previously bound to a surface detach and return to the bulk. It is believed that protein adsorption is quite irreversible. The desoption processes request some dramatic changes such as lowered pH and use of detergents.

Proteins tend to unfold or denature on the surface of some materials due to the change of energy. It can result in generation of more adsorption sites to the surface [116], while the adsorbed layer of denatured proteins effectively passivates the surface and prevents adsorption of further proteins from the solution [114]. However, the denaturation of proteins on metal surface is still under investigation. Kasemo [117] provided a model for protein and cell adsorption. It was suggested that water first adsorbed on the material surface then the surface-water interaction constitutes a starting point to the later interaction that occurs with proteins, amino acids or lipids.

It was concluded that in general hydrophobic surfaces would interact strongly with hydrophobic proteins. Because amino acids are the basic building blocks of proteins, interest in amino acid-surface interaction has been increasing. Intralayer bonding between amino acids and then co-adsorption with water was suggested by Barlow [118].

Figure 3-9 shows some of the atomic and molecular level events that happen when a metallic implant is placed in the biological molecule-rich environment (body). As mentioned in section 3.5., it is well documented that Co, Cr, Fe and Ni can incorporate with Albumin at carboxylate and tyrosine positions or bind with the –SH group of a single cysteine residue [114, 116]. This formation could be responsible for the decrease of friction because of its polymer-like structure. Yang *et al.* [49] gave a possible binding mechanism of metal ions on proteins. It shows in primary structure for a branch of a single protein molecule which contains γ-glutamyl, cysteinyl and glycine (Figure 3-10). In normal human albumin, the n-terminal region comprised of the amino-acid sequence N-Asp-Ala-His-Lys has been shown to be a strong binding site for transition metals such as Co,Cu and Ni [119].

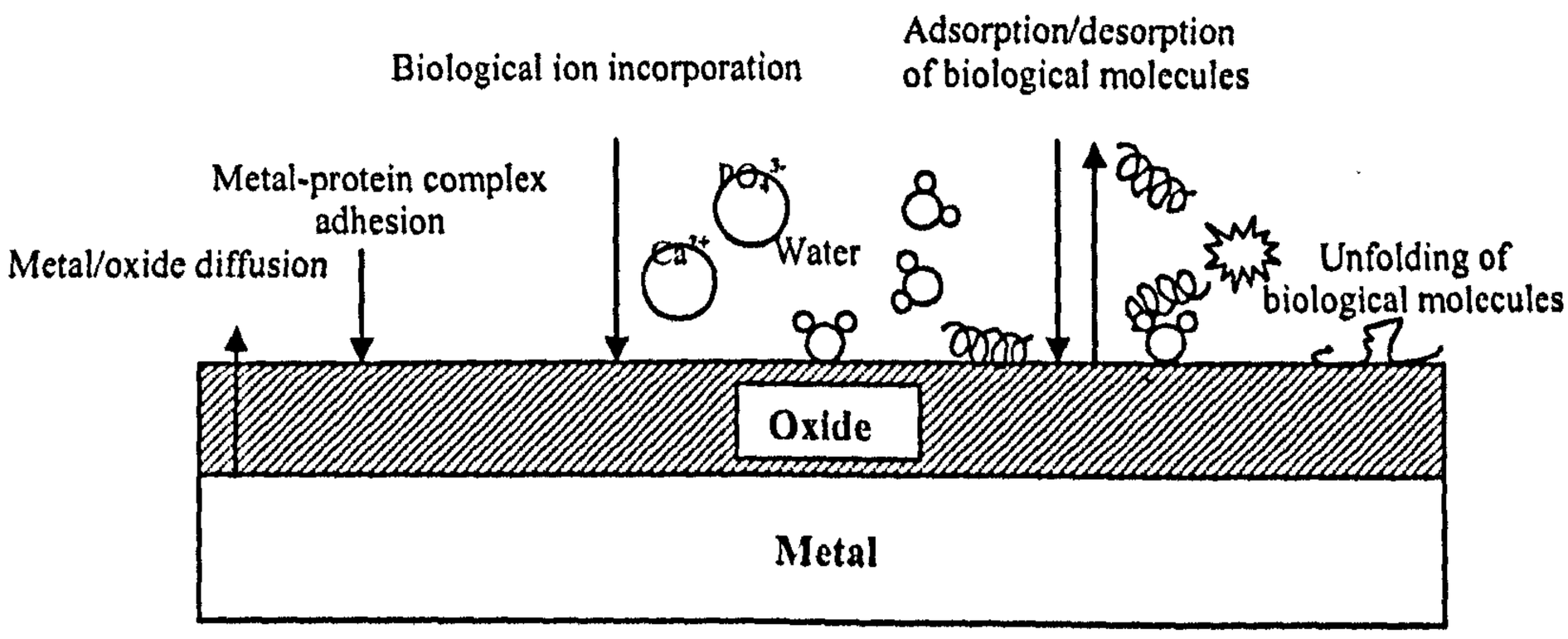

Figure 3-9 Possible interactions between proteins and a metal surface

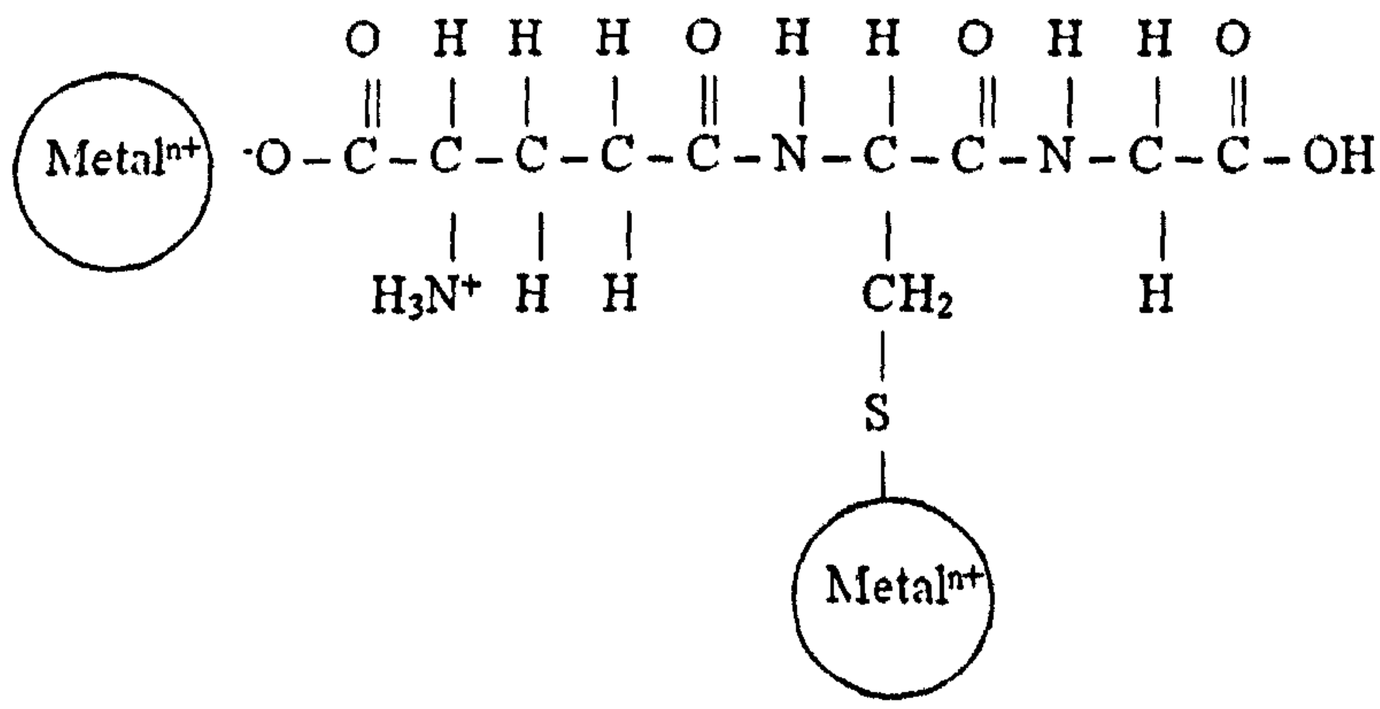

Figure 3-10 Schematic chemical structure for metal ions combining with protein

The protein layers act as a boundary lubricant and have a beneficial effect on the wear behaviour. They cover large areas of the surface and prevent adhesive and abrasive wear [120]. However, Hanawa [121] found that in the presence of proteins, metal ion dissolution from stainless steel is probably due to the effect of lubrication or adsorption. When negatively charged proteins in pH7-8 environments adsorbed on metallic materials surface, the corrosion rate of material can either be suppressed (for Ti alloys) or increased (Co alloys). The increased Co and Ni ions was due to the preference release/binding with negatively charged proteins. Heuberger *et al.* [112] concluded that hydrophobic surfaces preferentially adsorb denatured proteins and hydrophilic surfaces more prefer native proteins and have the potential to reduce boundary-lubricated friction. Hydrophilic surfaces selectively adsorb native proteins from a mixed solution, indicating that the driving force here is not the hydrophobic interaction but the ubiquitous Van der Waals force.

The role of proteins in a corrosive environment is governed by many factors such as the surface chemistry of the metal, protein adsorption characteristics, interaction of protein molecules with other ions present in electrolyte solution to produce organic complexes, and the transport of anionic and cationic charges around and away from local environment. Some points are summarized of how biological molecules influence materials corrosion behaviour:

- The stability of the passive layer depends on the availability of oxygen. The adsorption of proteins or cells onto the surfaces of materials could limit the diffusion of oxygen. This can cause the breakdown of the passive layer and preferential corrosion on the oxygen deficient regions [43].
- The lack of oxygen also can slow the cathodic reaction and then affect the anodic reaction. A decreased corrosion rate can be observed [123].
- As a contrast, an increased corrosion rate was explained due to the result from a greater oxygen concentration in the thin protein adsorbed film [124] and increased thermodynamic driving force for the electrochemical reactions is responsible.
- The adsorbed layer can prevent the diffusion of metal ions or oxide from the metal surface to the bulk environments by acting like a barrier [119]. Then an increased corrosion resistance is expected.
- The equilibrium of the corrosion reactions can be upset by the biomolecules through the electrical charged double layer [123]. Although, whether proteins can travel trough the electrical double layer and reach the substrate or interact with the out layer of the electrical double layer is still argued [52].
- The active reaction can be enhanced by the binding of proteins and metal ions. Then the formation transport them away form the implant surface.
- Some biological molecules, such as cells and bacteria can consume hydrogen in the bio environments. Hydrogen is involved with cathodic reaction in the corrosion process. The consumption of hydrogen can enhance the cathodic reaction then intend to increase the anodic dissolution [123].

Mixed results of the effect of proteins on materials corrosion behaviour from experimental work were observed. The work by Williams [124] show that in the presence of proteins, for Co, Cu and Ni metals, the corrosion rates increased, while Ag , Ti, Cr and Mo showed little changes or unaffected. In contrast, proteins gave V

a significant decrease of the corrosion rate. The binding of metal depredated products with proteins is believed to be a major reason for the increase of the corrosion rate [123]. Zhu *et al.* [113] also confirmed that an accelerated corrosion rate was observed on Cu in a protein-rich environment.

Khan *et al.* [104] showed that proteins can improve the corrosion resistance of Ti6Al 4V, but reduce the corrosion resistance of Ti13Nb13Zr and Ti6Al7Nb. Clark *et al.* [105] found that with protein (fibrinogen) involved, the corrosion rate for Co and Cu is significantly enhanced, but for Cr and Ni, the rates are moderately raised and for Mo, the corrosion rate decreases.

Contu *et al.* [55] observed an increased corrosion resistance for Co alloys in serum and explained that it was due to the inhibition effect of proteins on hydrogen evolution reaction. Adsorbed proteins generated a diffusion barrier which resulted in lowing the anodic dissolution of CoCrMo alloy.

It is in an agreement that albumin adsorption behaviour is different on different metal surfaces [115]. Therefore, the conclusion can be drawn that the change of corrosion rate in a biological environment is very much material and protein dependent.

Much research has been carried out to understand the relation between metal ions and proteins. There are some terms that define different types of interactions between them.

- Metalloprotein: it defines a certain protein, which contained in the normal structural and functional form a bounded metal ion.
- Metal-activated protein: it refers to a protein, which is activated to carry out a specific function only when a metal ion is bounded.

- Metal-binding protein: it refers to a protein of which function is to bind and release specific metal release specific metal ions.

Many metal ions can bind with proteins and form organometallic complexes, such as Fe^{3+}, Ca^{2+}, Mg^{2+}, Co^{2+}, Cr^{2+}, Zn^{2+} and Ni^{2+}. Figure 3-11 and Figure 3-12 show two typical metal-protein structures for Co and Fe. The binding between a metal ion and a protein is normal a ligand bind. A technique called the albumin cobalt binding test (ACB) is a new quantitative chemistry assay and used to determine myocardial ischemia [127].

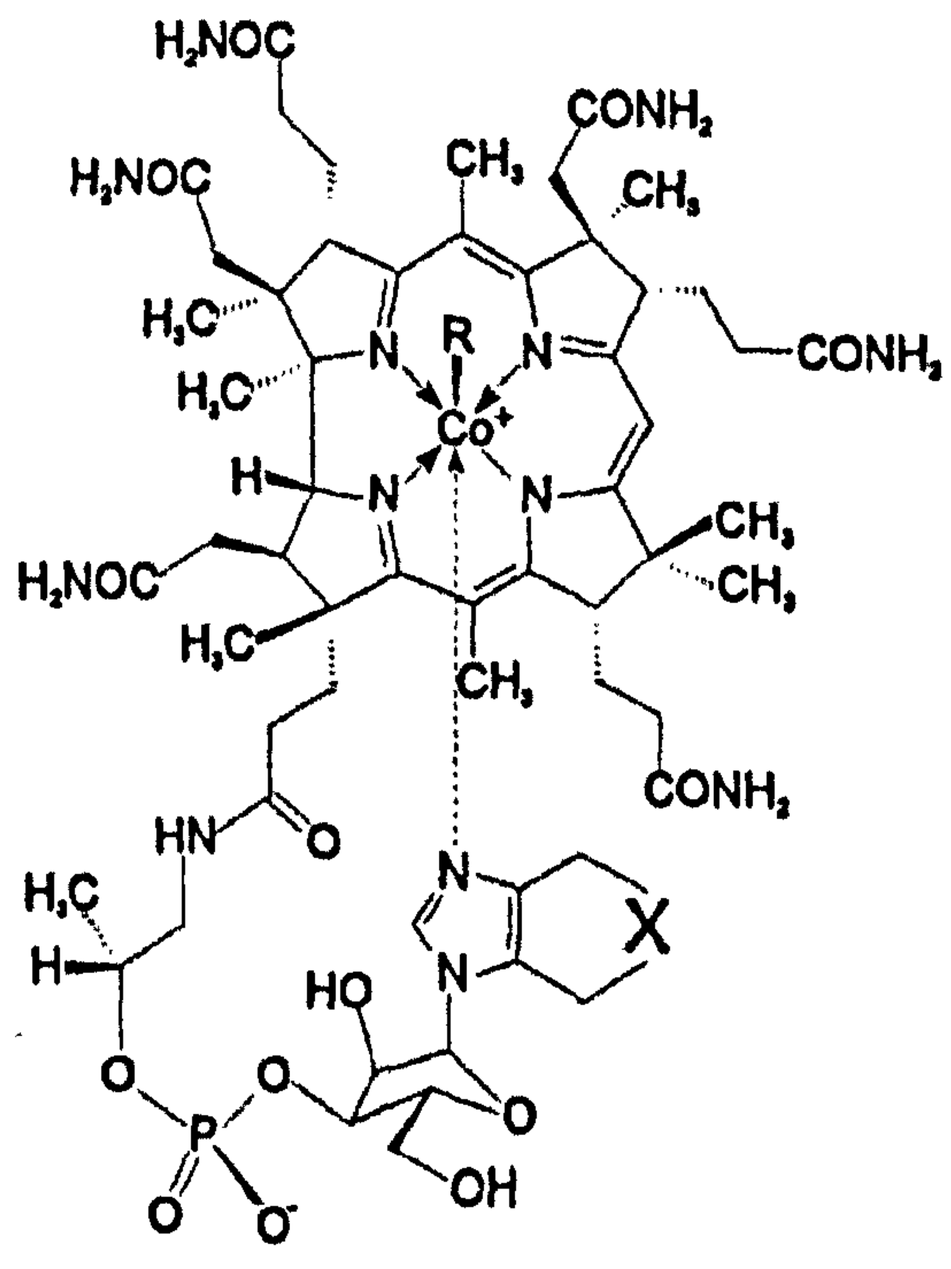

Figure 3-11 A typical vitamin B12 structure with Co

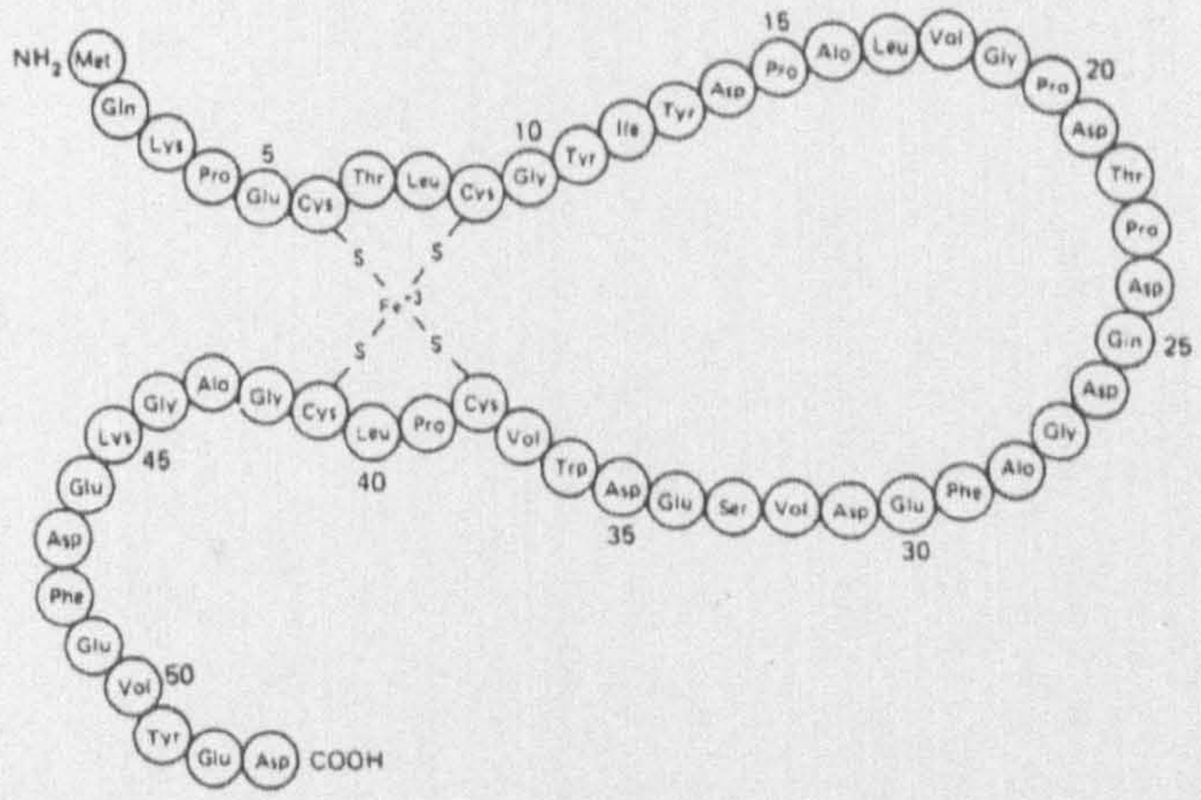

Figure 3-12 The amino-acid sequences of a iron-sulfur protein

3.9. Contact Angle

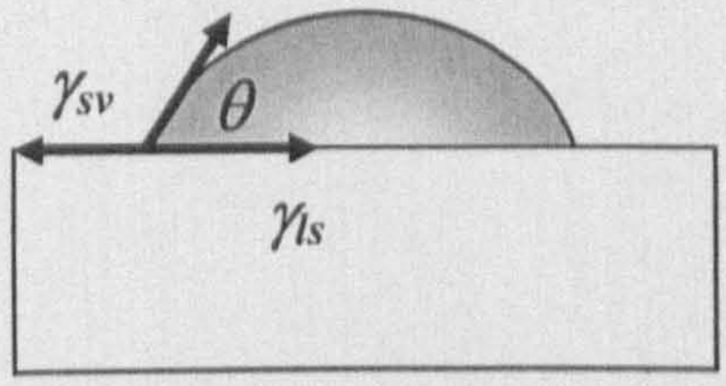

Figure 3-13 Contact angle measurement

Contact angle analysis involves measuring the angle of contact (θ in Figure 3-13) between a liquid and surface. Many methods can be used for contact angle measurements. The sessile drop measurement shown in Figure 3-13 is the most common one. It is widely used to evaluate adsorption of proteins. when a drop of liquid is placed on a surface, it spreads to reach a force equilibrium, in which the sum of the interfacial tensions in the plane of the surface is zero. From Young's Equation:

$$\gamma_{sv} - \gamma_{ls} - \gamma_{lv} \cos\theta = 0 \qquad \text{(Eq. 3-13)}$$

Where γ_{sv} represents the solid-vapour surface tension, γ_{ls} represents the liquid-solid surface tension and γ_{lv} represents the liquid-vapour surface tension. The contact

angle is an inverse measure of the ability of a particular liquid to 'wet' the surface [128]. Wettability is defined as the tendency for a liquid metal to spread on a solid surface. the interfacial energy that results from the imbalance of the surface and interface energies is the main driving force of wetting [129].

Although contact angle analysis provides knowledge about the way a surface interacts with gas or liquids, the information is not specific and can not indicate particular chemical characteristics. However, surface energy can represent the tendency of a fluid to form a monolayer film on a surface. Whether the film will grow beyond monolayer thickness depends on the interaction between the fluid and the surface covered by the monolayer film [130].

By using XPS and Raman Spectroscopy, it is concluded that with proteins in static condition, for CoCrMo alloys, the passive film contained Cr oxide and Mo oxide with a large number of OH^-. Meanwhile Co dissolved into the environment [48]. Without proteins or cells in the environment, passive film was found to comprise Co and Cr oxide with small amount Mo [131].

According to Hallab's work [132], albumin molecules showed preferential binding with Cr, Co and Ti implant degradation products. Williams [123] confirmed that in *in-vitro* wear tests, the protein molecules can form metal-protein-chloride complexes and change the oxide layer during repassivation.

3.10. Summary of The Literature Review

Orthopaedic implant materials, tribocorrosion, and protein adsorption were reviewed in this chapter. The MoM TJR was the particular focus. The effect of different materials and treatment on their overall performance was concluded from

various works. The fundamental results on wear, corrosion and tribocorrosion were carefully discussed. Based on clinical tests and bimolecular studies, the interaction of proteins and implant materials surface was also reviewed.

However, the two questions which were raised in the beginning of the introduction have not yet satisfactorily been answered. Research on analysis of tribocorrosion behaviour for implantable materials, especially load-bearing joint replacement materials, are still lacking. The role of proteins in the tribocorrosion system is still not fully understood. Studies are then needed to contribute to this topic.

CHAPTER 4

EXPERIMENTAL METHODS AND SURFACE ANALYSIS TECHNIQUES

4.1. Introduction

This chapter describes the main features of the experimental work, including integrated electrochemical measurement. It also reviews the analysis techniques involving surface analysis and bulk solution analysis. The preparation of samples and the test conditions are also given.

4.2. Test Conditions

Tests were conducted in three different fluids at 37 °C (normal human body temperature) in this study:

- 50% newborn bovine serum (Harlan ® SERA-LAB) with distilled water.
- Dulbecco's Modified Eagle's Medium (DMEM) (Sigma ® D5671)
- 0.36% NaCl solution;

The specific fluids were chosen to enable the effects of proteins and amino acid species in wear-corrosion to be isolated. Serum contains five different proteins, the primary constituent of which is albumin (Table 4-1). In this study, 0.1% sodium azide is added into serum as a preservative; since it effectively scavenges the dissolved oxygen from the serum solution, eliminating any electrochemical

inconsistencies due to oxygen-reduction and oxygen-evolution reactions [102]. It is found that the oxygen pressure in the human body is 1/6 to 1/2 of the normal oxygen pressure in the atmosphere [111]. Sodium azide also can provide conditions closer to the *in vivo* environment. DMEM is a type of cell culture medium. It contains 12 different amino acids and other ions comparable with serum (Table 4-2). 0.36% NaCl was chosen to have the same conductivity as 50% serum and DMEM, which is 0.68 mS/cm. The conductivity is an important factor to influence environment corrosiveness. Therefore in this study, all solutions maintained the conductivity at 0.68 mS/cm. For some studies, 0.9% sodium chloride solution was used, which is known as a physiological solution because it is isotonic with blood plasma [36, 59]. In this study, 50% serum has the comparable amount of proteins as synovial fluid and has the same conductivity with 0.36% NaCl solution.

Table 4-1 Serum quality profile from Harlan ® SERA-LAB (pH=7.2-7.4)

Elements	Quality profile	Elements	Quality profile
Sodium	140mmol/L	**AST**	32U/L
Potassium	8.0mmol/L	**ALT**	12U/L
Glucose	6.7mmol/L	**LDH**	809U/L
Urea	6.4mmol/L	**Amylase**	33U/L
Total protein	61.83g/L	**Triglyceride**	0.88mmol/L
Albumin	32g/L	**Cholesterol**	1.8mmol/L
Calcium	1.97mmol/L	**Magnesium**	1.22mmol/L
Phosphate	3.02mmol/L	**Iron**	19μmol/L
Total bilirubin	7μmol/L	**Immunoglobulins**	8.2g/L

Table 4-2 DMEM from Sigma ® D5671 (pH=7.6-7.7)

Component	g/L
Inorganic salts	
$CaCl_2 \cdot H_2O$	0.265
$Fe(NO_3)_3 \cdot 9H_2O$	0.0001
$MgSO_4$	0.09767
KCl	0.4
$NaHCO_3$	3.7
NaCl	6.4
NaH_2PO_4	0.109
14 Amino acids	0.4
8 Vitamins	0.01

The sliding wear tests were performed in a reciprocating wear tester which conformed to ASTM G133 and the three materials, High Carbon CoCrMo (HC CoCrMo), LC CoCrMo (LC CoCrMo) and stainless steel UNS S31603 (316L) were rubbed against a silicon nitride ball (12mm in diameter) at a normal load of 80N (Figure 4-1). Silicon nitride was chosen as the counterface material in this study due to its electrochemical stability – the key focus of the study being to measure the electrochemical response of the HC and LC CoCrMo alloys and stainless steel without any interference from an electrochemically active counter body. The frequency was controlled at 1Hz and the stroke length was 10 mm. All the specimens were disks with a diameter of 25 mm. All specimens have a surface roughness R_a value of about 0.01 μm which is consistent with the surface finish on most commercial hip replacement components. The friction force was measured by means of a load transducer with the combined error of 0.004N. Figure 4-2 shows the

friction force and the velocity of the reciprocating motion in 2 cycles. At the end of each wear test the volume loss was determined by interferometer using the WYKO NT3300S white light interferometer. The test duration was up to 48 hours.

A new material combination has to undergo stringent wear testing before being adopted as fit for use in manufacturing prosthetic joints. Simple configuration wear testing has been used extensively as an ideal method for screening novel materials, compared with existing ones for use in joint replacements, prior to more complex joint simulator tests. As a fractional cost of a full simulator wear test, the reciprocating ball-on-plate apparatus has enabled better control of the individual tribological variables, leading to a better understanding of how these tribological factors independently influence the wear mechanisms and corrosion behaviour. These simple tests also provide important information about the relative wear and wear-corrosion performance of bearing materials.

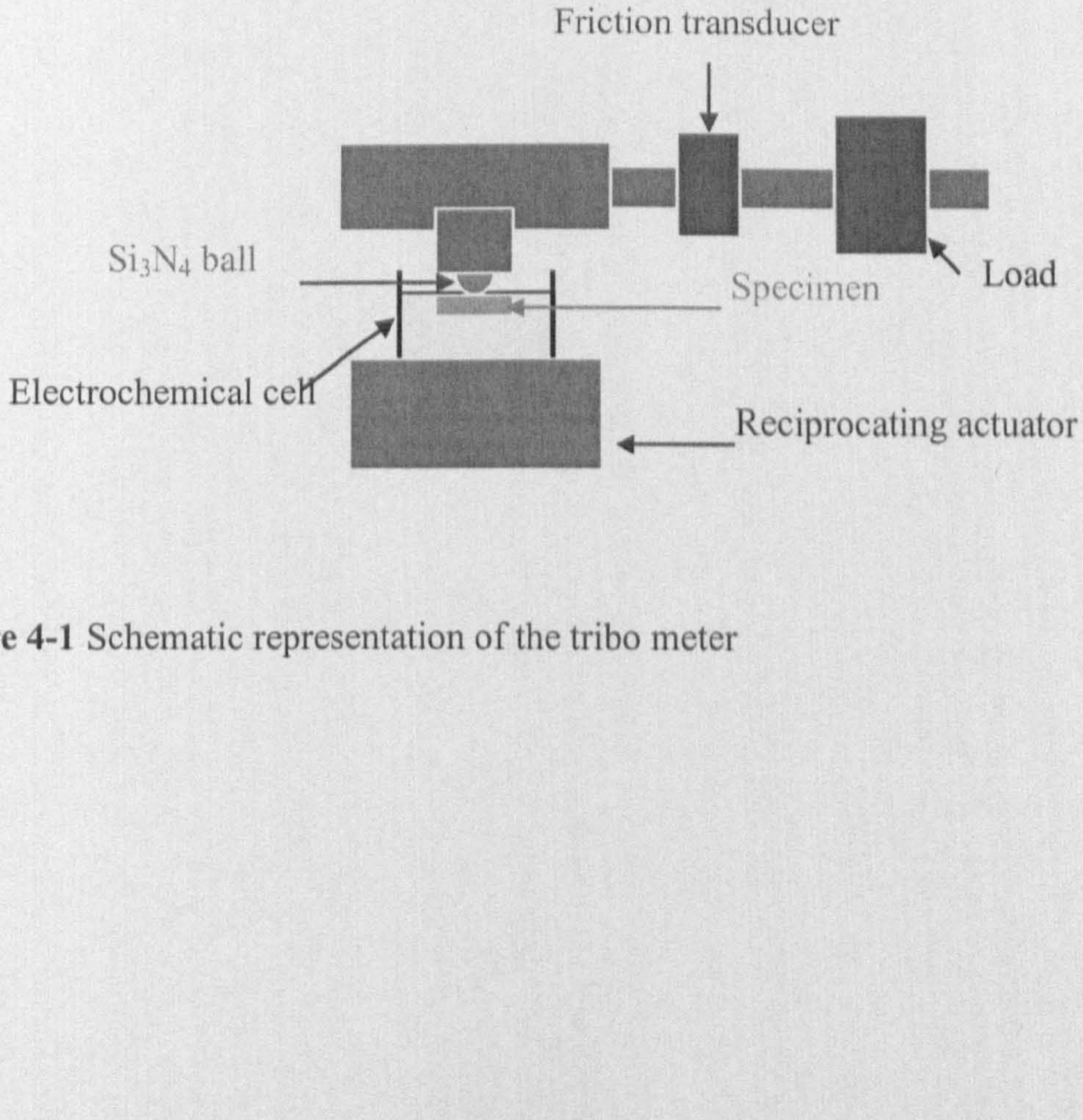

Figure 4-1 Schematic representation of the tribo meter

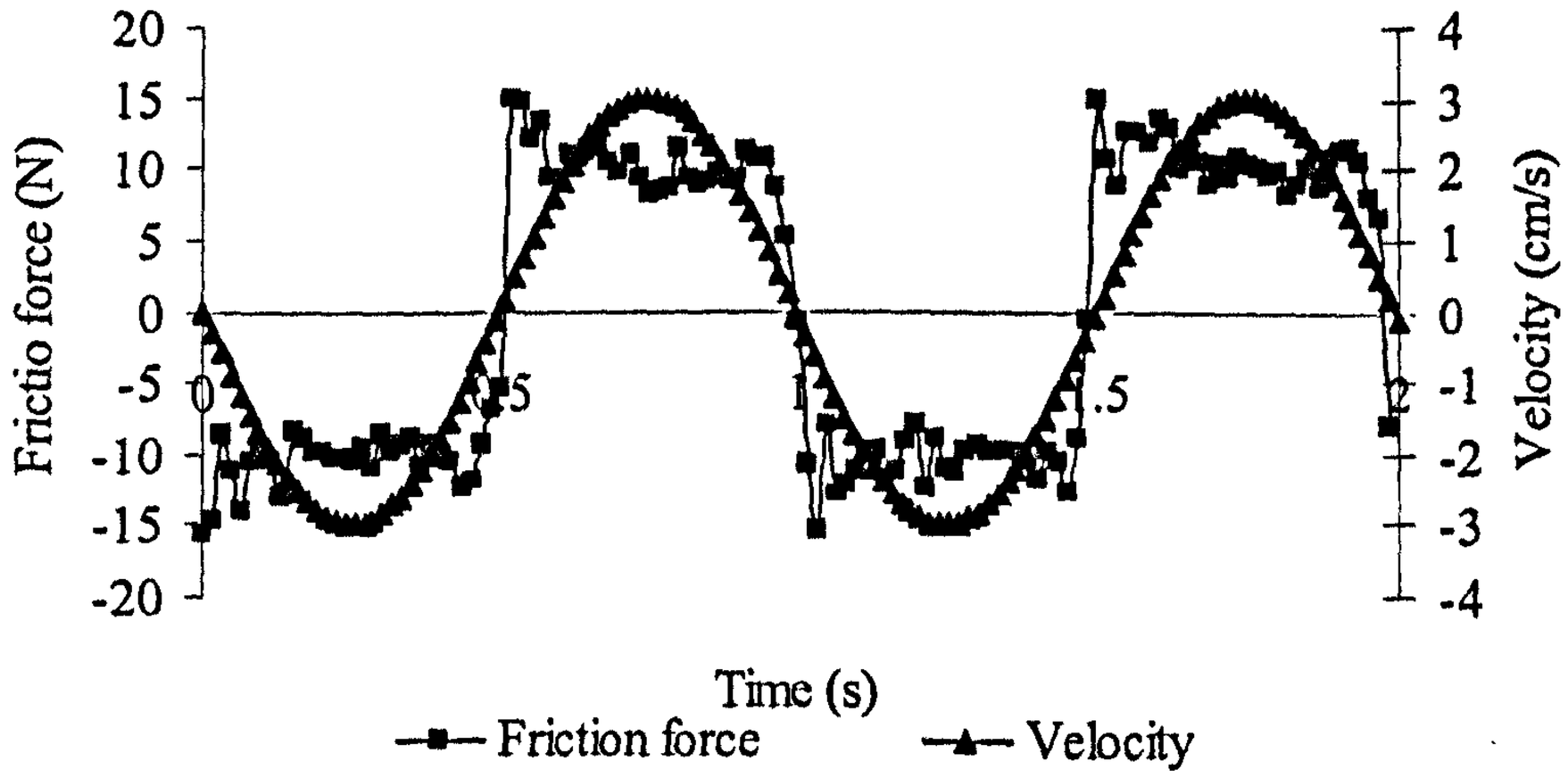

Figure 4-2 The friction force and the velocity of reciprocating motion

4.3. Electrochemical Measurements

In this study a few electrochemical measurements have been conducted such as the free corrosion measurement, anodic polarization, cathodic polarization, cathodic protection and linear polarization. Integrated three-electrode cell was used to determine electrochemical behaviour under tribological contacts (Figure 4-3). These three electrodes are:

- Working Electrode (WE): the specimen
- Reference Electrode (RE): single Ag/AgCl electrode
- Counter Electrode (CE): a platinum wire/mesh

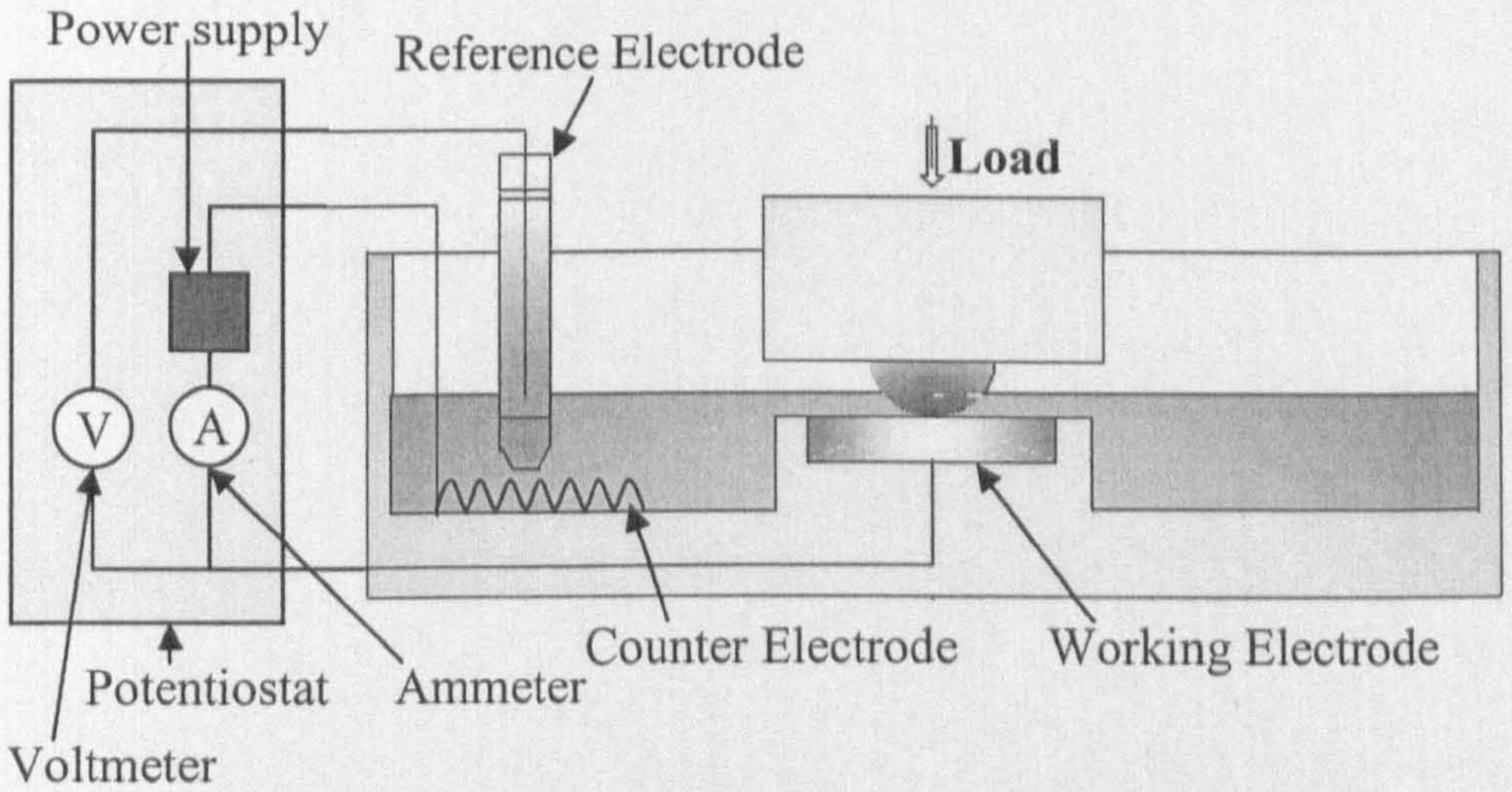

Figure 4-3 Schematic representation of the integrated three-electrode cell

4.3.1. The free corrosion potential measurement

At the free corrosion potential (E_{corr}), the anodic reaction rate is equal to the cathodic reaction rate and so there is no net current flow to or from the electrode The value of E_{corr} is often used to give a qualitative indication of the corrosion regime (active or passive) in which a material resides. It can provide a useful way to differentiate conditions of *active* corrosion from *passive* conditions. In this study measurement of E_{corr} was used to assess (a) how the action of a sliding counterface, against a passive alloy affects the passivity of the alloy and (b) how the material "recovers" once the sliding wear ceases and passivity is re-established. In this work E_{corr} was monitored in static conditions, under the action of sliding wear and once sliding wear ceased, as the material passivity was re-established.

4.3.2. Anodic polarization scans

In anodic polarization tests, the rate of metal dissolution (anodic) processes can be determined. In this study, the key purpose was to monitor the extent of passivity

of the surface. This is done by using a standard 3-electrode cell and involved using a computer-controlled potentiostat to shift (at a rate of 15mV/min) the potential of the Working Electrode (WE) from the free corrosion potential, E_{corr}, in the positive direction. This leads to the WE (sample) becoming a net anode and by analyzing the rate of charge transfer as a function of potential the corrosion behaviour can be evaluated. The overpotential (the shift from E_{corr}) is the driving force for passivity breakdown and the magnitude of the breakdown potential (E_b), defined as the potential where the current in the 3-electrode cell increases rapidly, gives a measure of the resistance of the passive film to localized corrosion initiation. For passive materials, the current will stay very low in the passive region, normally less than $10\mu A/cm^2$, because of the protective passive film. For active materials, where there is no protective film formed on the surface, the current will increase immediately on shifting the potential from E_{corr} (Figure 4-4).

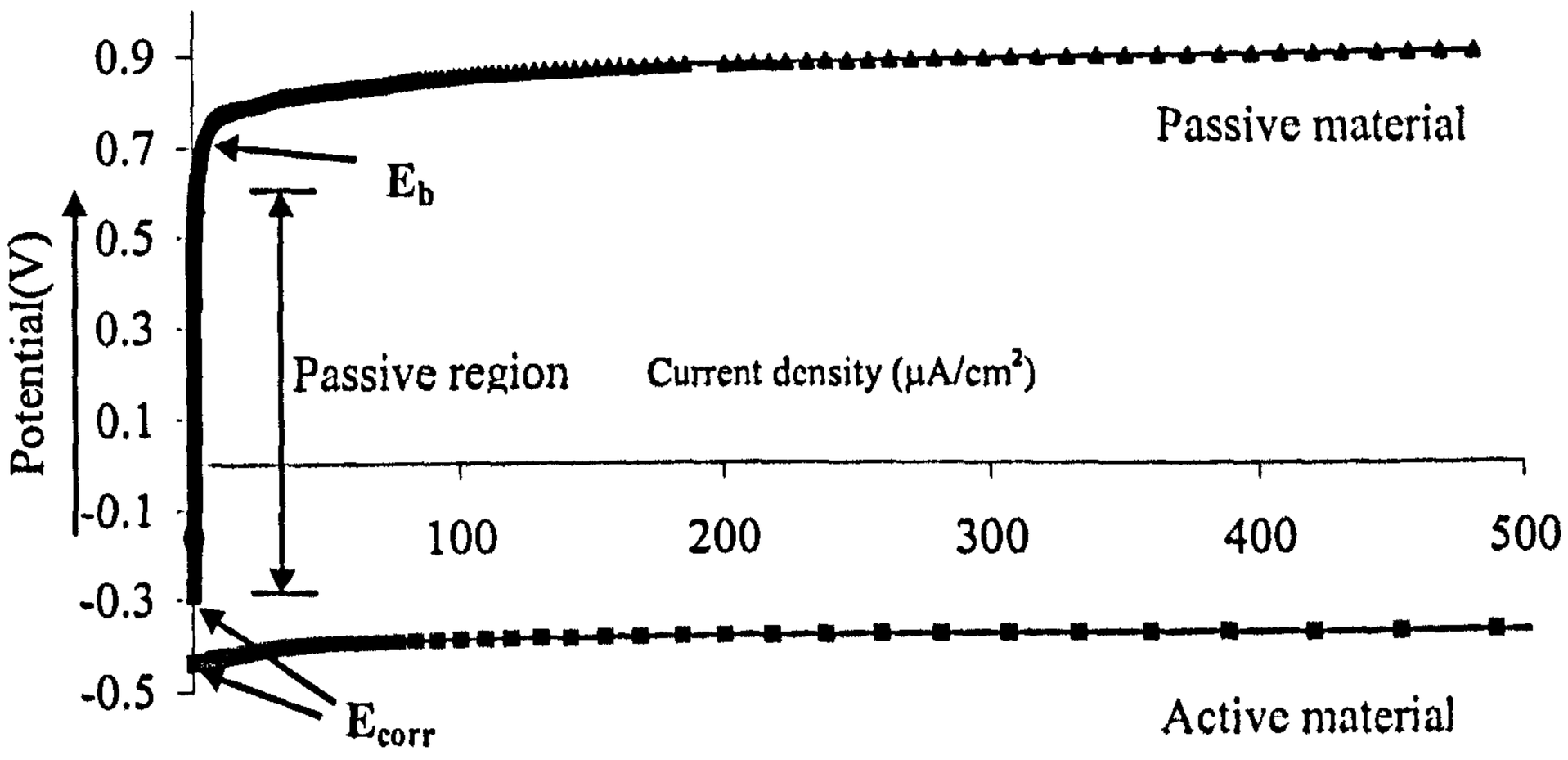

Figure 4-4 Typical anodic polarization for passive material and active material

4.3.3. Linear polarization resistance tests

Linear polarization resistance (LPR) test is a corrosion rate monitoring method and it can give an indication of the corrosion resistance of materials in an aqueous environment. In this study, LPR tests are performed both in the static conditions and under reciprocating motion. When material is under sliding, LPR tests are conducted

every hour up to 8 hours. In LPR tests, potential is shifted from 50 mV below E_{corr} (more negative than E_{corr}) to 50 mV more positive than E_{corr}. Current flow between the specimen and the counter electrode is monitored. A linear relationship of potential and current values can be observed. The value of $\Delta E/\Delta i$ is calculated.

4.3.4. Cathodic protection

One of the main aims of the work was to establish the extent of interactions between wear and corrosion processes on these three alloys in three saline solutions. The most effective means of achieving isolation of the *wear* component of degradation is to completely stop any charge transfer (corrosion) at the working electrode surface. Cathodic Protection (CP), by the impressed current method, is a widely used technique to control corrosion and in this study sliding wear tests under CP have enabled the wear material loss to be determined. The applied potential used was –0.8V (Ag/AgCl), chosen to be more negative than the equilibrium electrode potential for the Co/Co^{2+} reaction yet sufficiently noble enough to prevent hydrogen-evolution at the surface which would inevitably affect the wear process.

4.3.5. Potentiostatic tests

In tribocorrosion tests, the passive film is continuously removed by the sliding movement. By applying a positive potential (in the passive regime from anodic polarization scan), the mechanical depassivation and electrochemical repassivation can be monitored. In this study potential of 0.2V and 0.4V was chosen. In these tests, anodic polarization scan was initially performed until the potential reached 0.2 V or 0.4 V. Then potentiostatic tests were then conducted and the current as a function of time was measured.

4.4. Chemical and Surface Analysis Techniques

In this study, various surface analysis techniques were adopted to determine the mechanical properties, wear mechanisms, corrosion behaviour and chemical nature of tribofilms. The released ions were also detected by ICP tests (Inductively Coupled Plasma).

4.4.1. Microhardness measurements

Hardness is usually defined as resistance to penetration. Many information related to the mechanical properties of the metal matrix composites can be associated with its microhardness properties. A Mitutoyo-MVK-Ha microhardness testing machine was used to measure materials microhardness. A load of 500 g was applied. Tests were carried out 50 times and the procedure was repeated at different sites.

4.4.2. Light microscope analysis

The light microscope was used to study the influence of microstructure on the corrosion and wear behaviour. A NIKON standard binocular metallurgical microscope was employed in this study. The objective lenses used were calibrated using a graticule and the individual magnification bar is shown in each photograph. A portable camera on the microscope enabled the observation to be recorded.

4.4.3 Scanning Electron Microscopy (SEM)

An Environmental Scanning Electron Microscope (Philips XL30 ESEM) has been used to identify the wear mechanisms. The ESEM is equipped with a LaB_6 gun and it is capable of operating as a conventional high-vacuum SEM, or under low vacuum in ESEM mode. The ESEM is fully equipped with a range of secondary electron (SE) and back-scattered electron (BSE) detector.

4.4.4. White light interferometry

White Light Interferometry (WLI) is a powerful technique for non-contact measurement of surface topography at high vertical and moderate lateral resolution. The Phase Shifting Interference (PSI) mode was used and the resolution for this mode is 0.3 nm. The Wyko has a range of objectives from 2X-50X and has an additional zoom from 0.5-2X called the field-of-view (FOV) objective. Figure 4-5 shows typical wear scar images by using the interferometer. The volume value of the wear scar can be determined by Figure 4-5 (a).

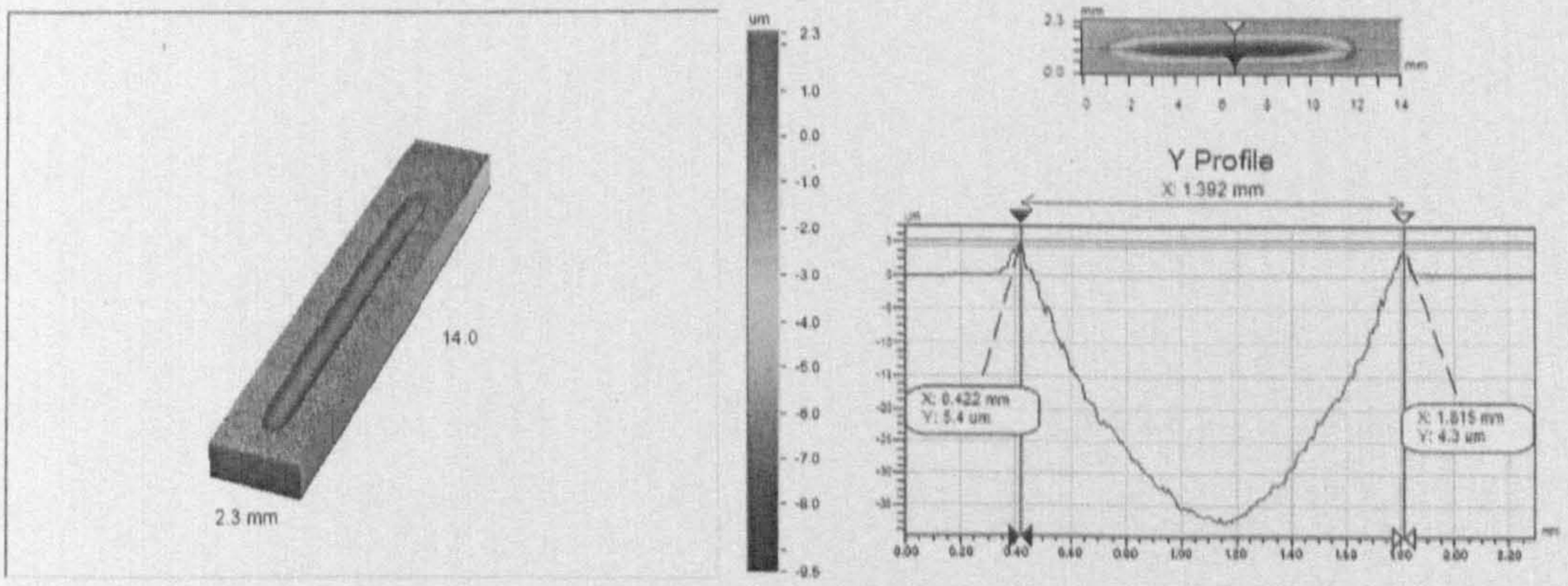

(a) (b)

Figure 4-5 Typical wear scar images obtained by using the Wyko white light interferometer (a) 3-D image of the wear scar (b) the cross section of wear scar

4.4.5. Contact angle measurements

Contact angles of liquids on material surfaces are widely used to predict wetting and adhesion properties of these solids by calculating their solid-vapour surface tension. While the theory is based on the equilibrium of an axisymmetric sessile drop on a flat, horizontal, smooth, homogeneous, isotropic, and rigid solid, it is generally found in practice that a whole range of contact angles is accessible experimentally causing wetting or contact angle hysteresis. The reason is that contact angle phenomena are very complicated. Contact angles on material surfaces are not only influenced by the interfacial tensions according to Young′s equation (Eq. 3-13) but also by many other phenomena, such as surface roughness, chemical heterogeneity, sorption layers, molecular orientation, swelling, and partial solution of the polymer or low-molecular constituents in the polymer material. These effects have to be considered when contact angle measurements are used to calculate the solid surface tension. In this study, contact angle measurement was used to determine the protein adsorption property. Distilled water was employed to measure contact angle of material surface. Samples were firstly immersed in the three environments. They were taken out every hour to measure contact angle. The interaction of protein molecules with protein adsorption layer on sample surface was also studied by using the serum droplet instead. Figure 4-6 shows a typical sessile drop method to measure contact angle.

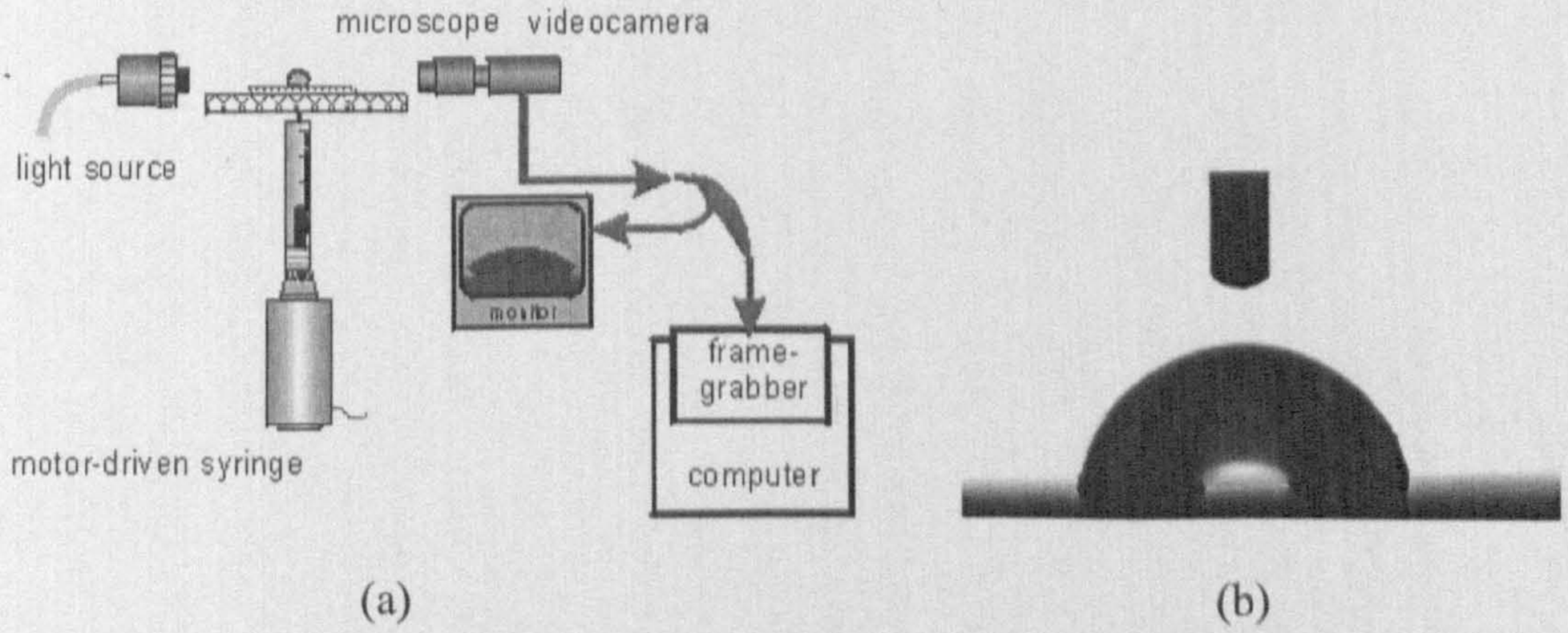

Figure 4-6 Contact angle measurement (a) a schematic picture of contact angle test system (b) a typical sessile drop on the surface

4.4.6. Inductively Coupled Plasma (ICP)

ICP (Inductively Coupled Plasma) tests were carried out for detecting and measuring released ions during the anodic polarization scan for three materials in different environments. A Thermo FI Maxim ICP-AES tester was employed. ICP is an analytical technique used for the detection of trace metals in environmental samples. It is a multi-element analysis technique that will dissociate a sample into its atoms and ions. The elements emit light of a characteristic wavelength which can then be measured and quantified. Samples were taken out during the anodic polarization scan at different potentials. They were nebulized and entrained in the flow of plasma support gas (Ar). The emitted light wavelength by a certain element was then converted to an electrical signal which could be measured quantitatively. The ICP tests were carried out on liquid samples collected at specific potential values during the anodic polarization tests in all three solutions for the three materials.

4.4.7. X-ray Photoelectron Spectroscopy (XPS)

XPS (X-ray Photoelectron Spectroscopy) data was obtained using the NCESS Scienta ESCA300 spectrometer at CCLRC Daresbury Laboratory as shown schematically in Figure 4-7. It is a powerful technique and widely used for surface analysis of materials. A high-power monochromatised Al K_α X-ray source ($h\nu$ = 1486.6 eV), high transmission electron optics and multi-channel detector were employed in this XPS machine [134]. *Survey scans* and more detailed *region scans* were run at 300 eV pass energy and 0.8 mm slit width. Although X-rays penetrate to a depth of several micrometers, ejected photoelectrons generally come from only the first several nanometres of material. In XPS the photon is absorbed by an atom in a molecule or solid, leading to ionization and the emission of a core (inner shell) electron. The binding energy (BE) is taken to be a direct measure of the energy required to remove the electron from its initial level to the vacuum level. In order to

assess the variation of composition as a function of depth the samples were subjected to argon-ion bombardment for various times. In this study, half minute and 5 minute argon-ion etching were applied on the sample surface both in the wear scar and outside of the wear scar.

The high X-ray power rotating anode has a maximum power rating of 8kW, a factor of 13 higher than a typical power of 600W for a conventional fixed anode source. A large, seven crystal, double focusing monochromator focus the X-ray to an area, 6mm by 0.3mm. The beam line is then focused in the middle of the wear scar in an area of 400 μm by 300 μm. The Al K_α (1486.7 eV) line profile has a Full Width at Half Maximum (FWHM) of 0.26 eV, a factor of 3 narrower than for an unmonochromated Al K_α source. The computer controlled lens system has two modes of operation: a high transmission mode for optimum acceptance of photoelectrons and an imaging mode for high spatial resolution with <50 μm lateral resolution. The detection system consists of a 300 mm radius hemispherical analyser and a multi-channel detector. This gives an overall instrument resolution of minimum 0.3 eV.

In typical XPS analysis, a survey scan is obtained first in order to identify elements present, and then the long scans of the selected peaks are obtained in order to determine a more comprehensive picture of the chemical composition. All the spectra were acquired in the spatial mode. Licensed CasaXPS software was used to fit the curves. Several XPS databases were referenced for the understanding of different binding energies [135-137].

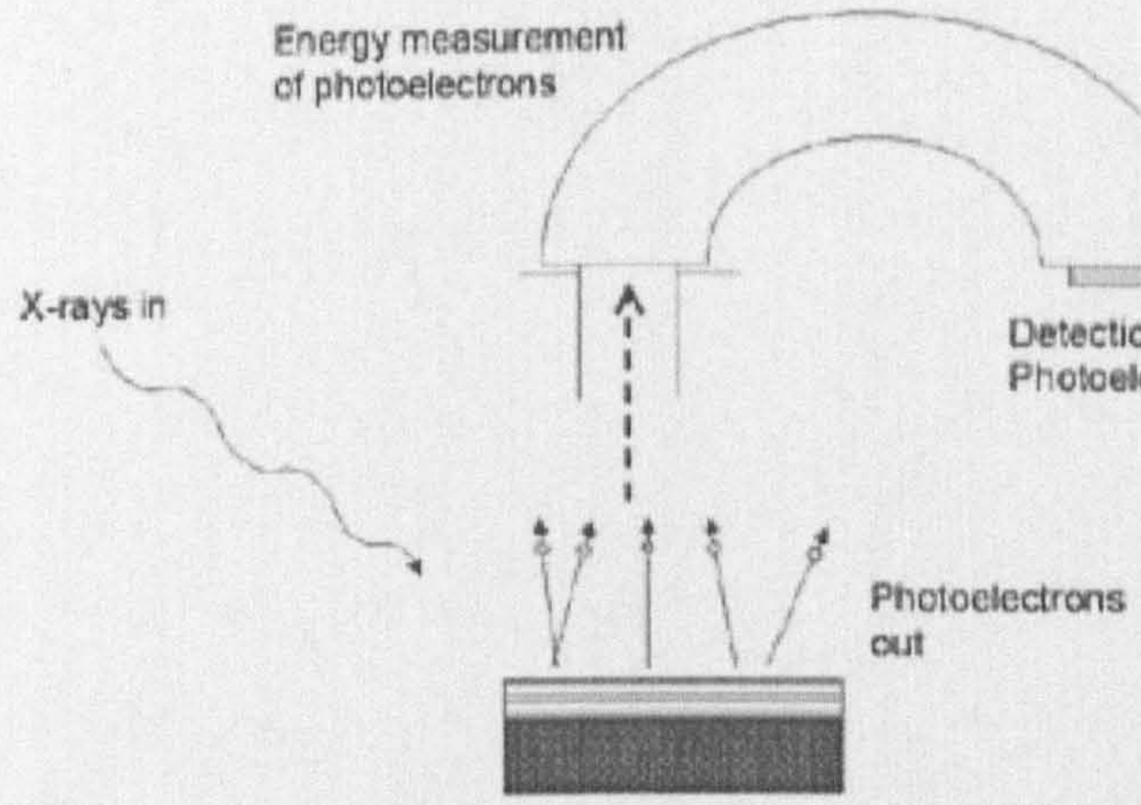

Figure 4-7 Schematic representation of XPS in a Scienta ESCA 300

4.5. Summary

The use of different physical and chemical analysis techniques makes it possible to have a comprehensive assessment of the tribofilm formed in a biotribocorrosion environment. The near surface analysis by XPS ensures that the very upper surface layer can be well defined. Corrosion behaviour and wear mechanisms were observed by using these techniques. The integrated electrochemical cell enables corrosion and tribology characterization separately and jointly.

CHAPTER 5

MATERIALS CHARACTERIZATION AND STATIC TEST RESULTS

5.1. Introduction

The performance of orthopaedic implants relies on their tribocorrosion resistance. The tribocorrosion system is a rather complex system as it involves tribological aspects *and* electrochemical reactions. How proteins affect implant materials in terms of lubrication, wear and metal ion release is still not entirely understood. In order to assess the tribocorrosion behaviour for candidate materials, electrochemical tests in static conditions were initially carried out in an attempt to understand their corrosion behaviour in absence of tribology.

In this chapter, the effect of proteins on HC CoCrMo, LC CoCrMo and 316L in static conditions was assessed. Different concentrations of serum were used in addition to DMEM and 0.36% NaCl solutions with the specific objective being to attempt to isolate the effects of proteins and amino acid species on static corrosion. The relationship between the wettability (surface energy) of candidate materials and their corrosion behaviour was also studied in this chapter.

Experiments were conducted at a temperature of 37°C. Samples were prepared as shown in Chapter 4. The three-electrode electrochemical cell was employed to assess their corrosion behaviour. The wettability was determined by a contact angle goniometry. Figure 5-1 shows a map of experiments for the work presented in this chapter to assist the reader in getting an overall picture of the experimental methodologies and how they fit together.

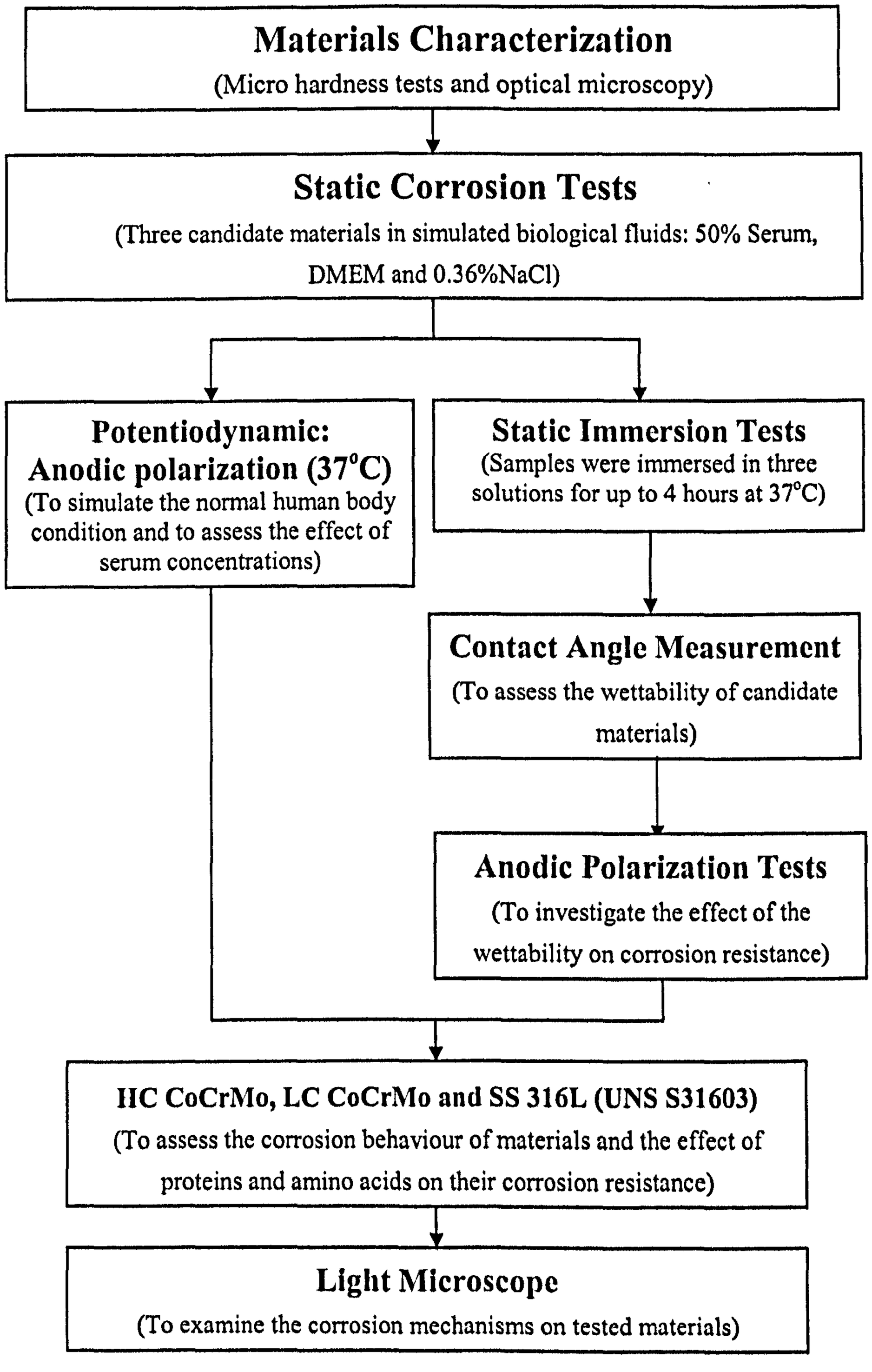

Figure 5-1 The map of experimental work presented in Chapter 5

5.2. Materials Characterization

The nominal chemical compositions of HC CoCrMo, LC CoCrMo and UNS S31603 (316L) stainless steel are shown in Table 5-1. The amount of Cr and Mo in the two CoCrMo alloys is similar. Samples were immersed in 15ml HCl, 10ml acetic acid and 10ml HNO_3 for 5 minutes and their microstructure can be seen in Figure 5-2. Backscattered SEM images showed two types of carbides: Cr-rich (dark) and Mo-rich (light) surrounded by the Co-rich matrix on HC CoCrMo (Figure 5-3). Microhardness tests were carried out repeatedly 50 times for each material. Figure 5-4 shows the average Vickers hardness under 500g load. HC content alloys produce large blocky carbides. The higher C content leads to more extensive carbide (Cr and Mo) formation and an increased hardness value as shown in Figure 5-3 and Figure 5-4, a few carbides can be observed on the LC CoCrMo alloy. However, there are notably fewer carbides and they are smaller than in the HC CoCrMo alloy. No Mo carbides were seen on LC CoCrMo. The stainless steel has a typical austenitic grain structure.

The importance of elemental compositions and the chemical state of the surface characterization for the implant cannot be overemphasized because it has a great influence on the performance of the implant through the surface layer-body tissue interaction and the possible release of metal ions from the surface to the surrounding body tissue.

Table 5-1 Chemical composition and micro hardness for all materials

Materials	C	Co	Cr	Mo	Fe	Ni	HV_{500g}
HC CoCrMo	0.19	Bal.	27.3	5.8	0.41	0.7	463±11
LC CoCrMo	0.05	Bal.	27.4	5.7	0.17	0.1	448 ±15
316L	0.03		17		Bal.	13	291 ±18

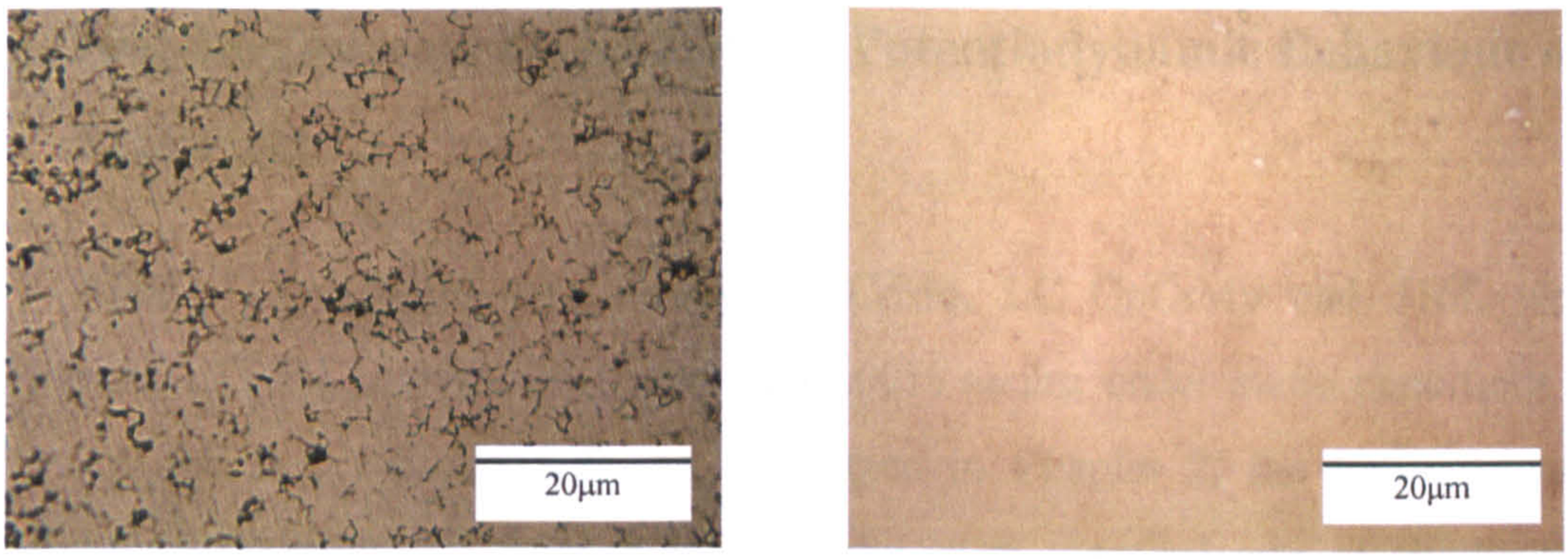

(a) (b)

Figure 5-2 Optical microscope images for (a) HC CoCrMo and (b) LC CoCrMo after 5 mins etching in 15ml HCl, 10ml acetic acid and 10ml HNO_3

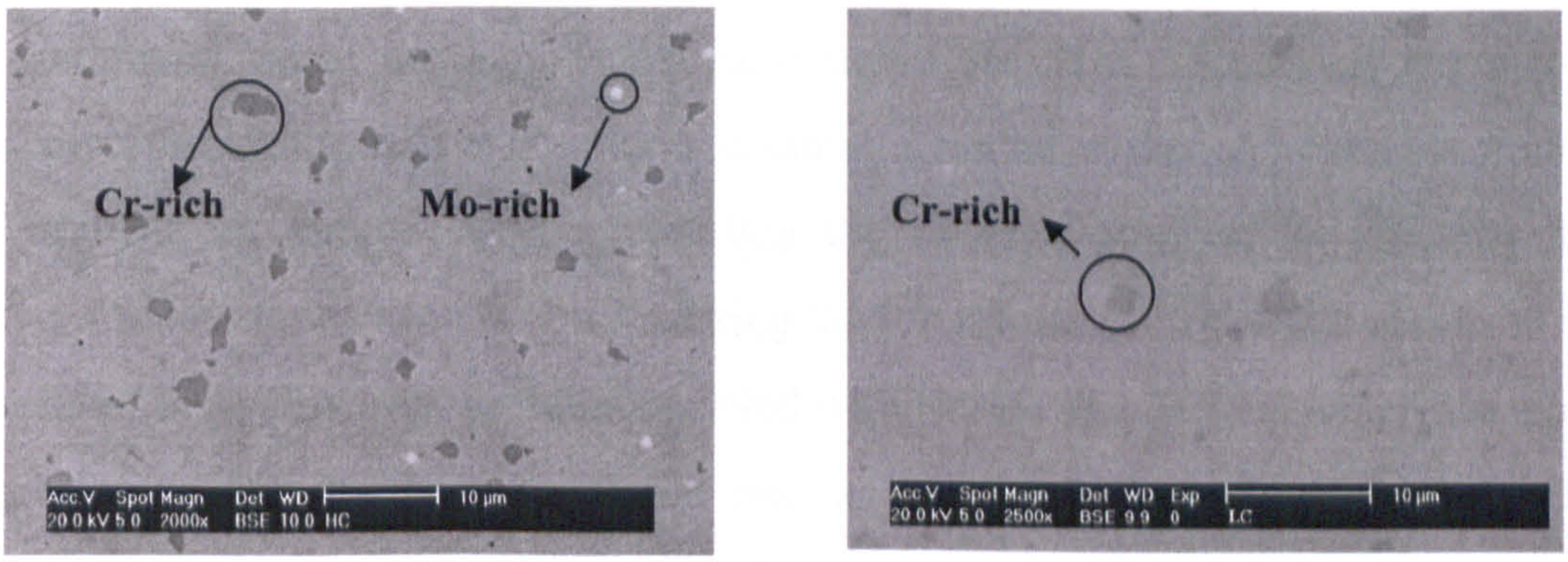

(a) (b)

Figure 5-3 Backscattered electron SEM images for (a) HC CoCrMo and (b) LC CoCrMo

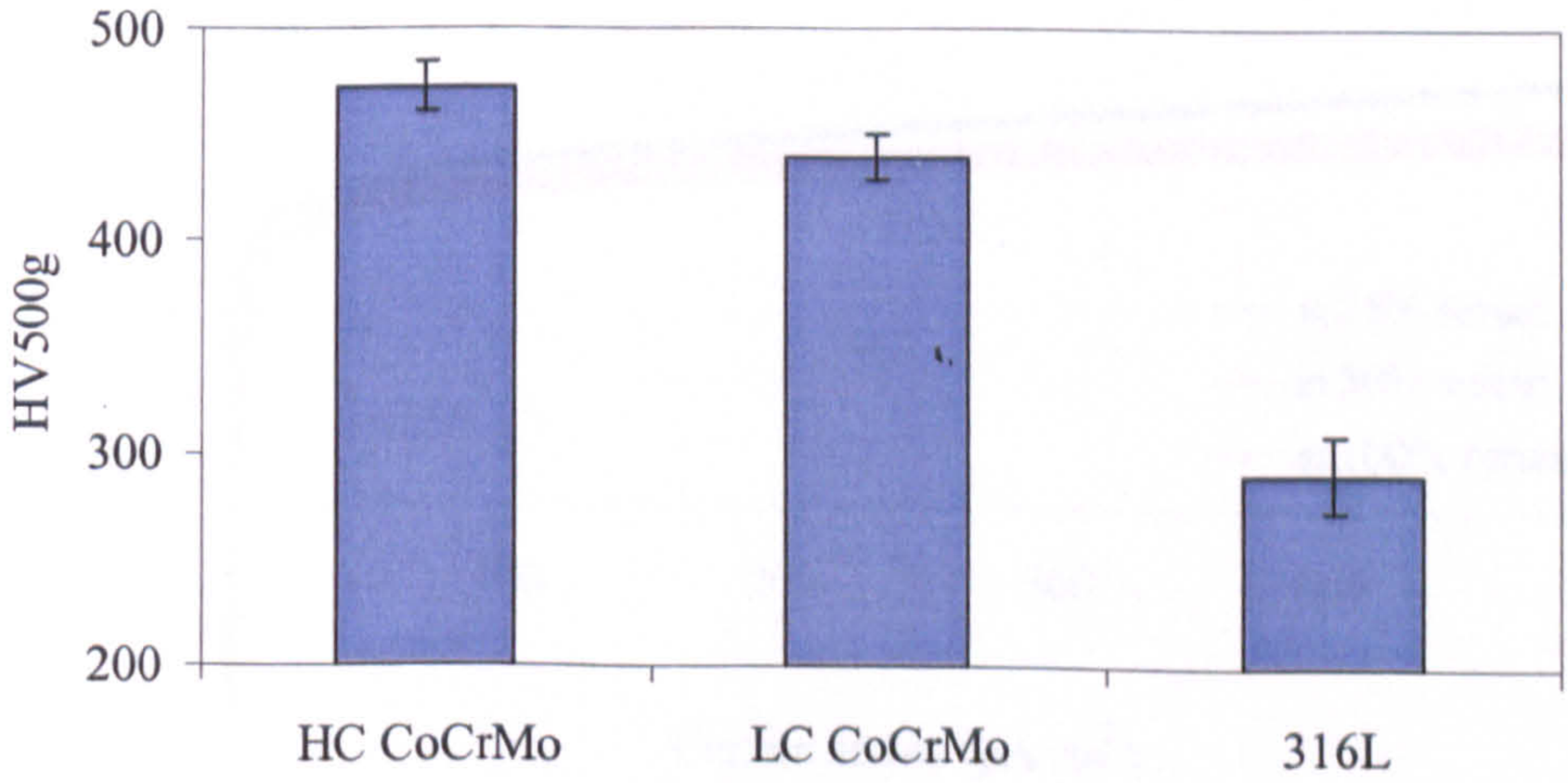

Figure 5-4 Microhardness for all three materials under load 500g

5.3. Protein Concentration Effect on Potentiodynamic Behaviour of Materials

Anodic polarization tests for HC CoCrMo, LC CoCrMo and 316L were performed in 25% serum, 50% serum and 100% serum under static conditions at 37°C (Figure 5-5, 5-6 and 5-7). As mentioned in Chapter 2, the free corrosion potential (E_{corr}) is the potential at which there is an identical rate of anodic and cathodic reactions.. In this study, the free corrosion potential (E_{corr}) for all materials in three concentrations of serum is shown in Figure 5-8. For both HC CoCrMo and LC CoCrMo, the potential moved in the negative direction as the concentration of serum changed from 25% to 50% and 100%. In contrast, the increase of protein concentration made the E_{corr} value more noble for 316L. Based on the mixed potential theory, the shift of E_{corr} for 316 samples can be explained by the adsorption of proteins on sample surface inhibiting the cathodic reaction by blocking the oxygen access to the sample and hindering the ion release [123], which results in an increased E_{corr}. However, proteins can bind with Cr, Co and Fe ions which are more likely to accelerate the ion release rate as more proteins are present in the environment. Due to the acceleration of anodic reaction, E_{corr} shifted to an active (negative) direction. Some researchers assumed that the adopted protein molecules could change the local pH, thus affecting the equilibrium and the corrosion rate [124].

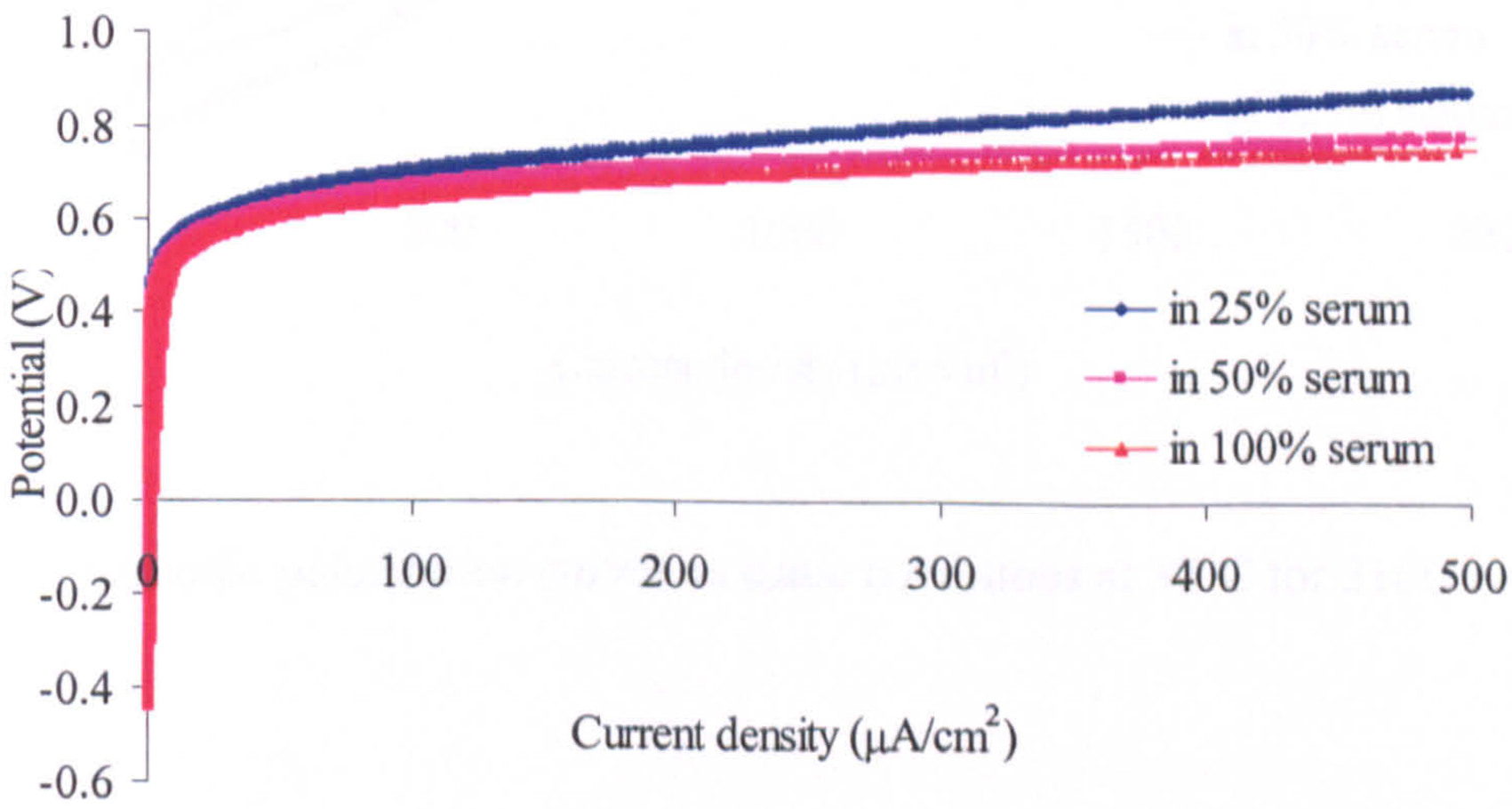

Figure 5-5 Anodic polarization curves in static conditions at 37°C for HC CoCrMo

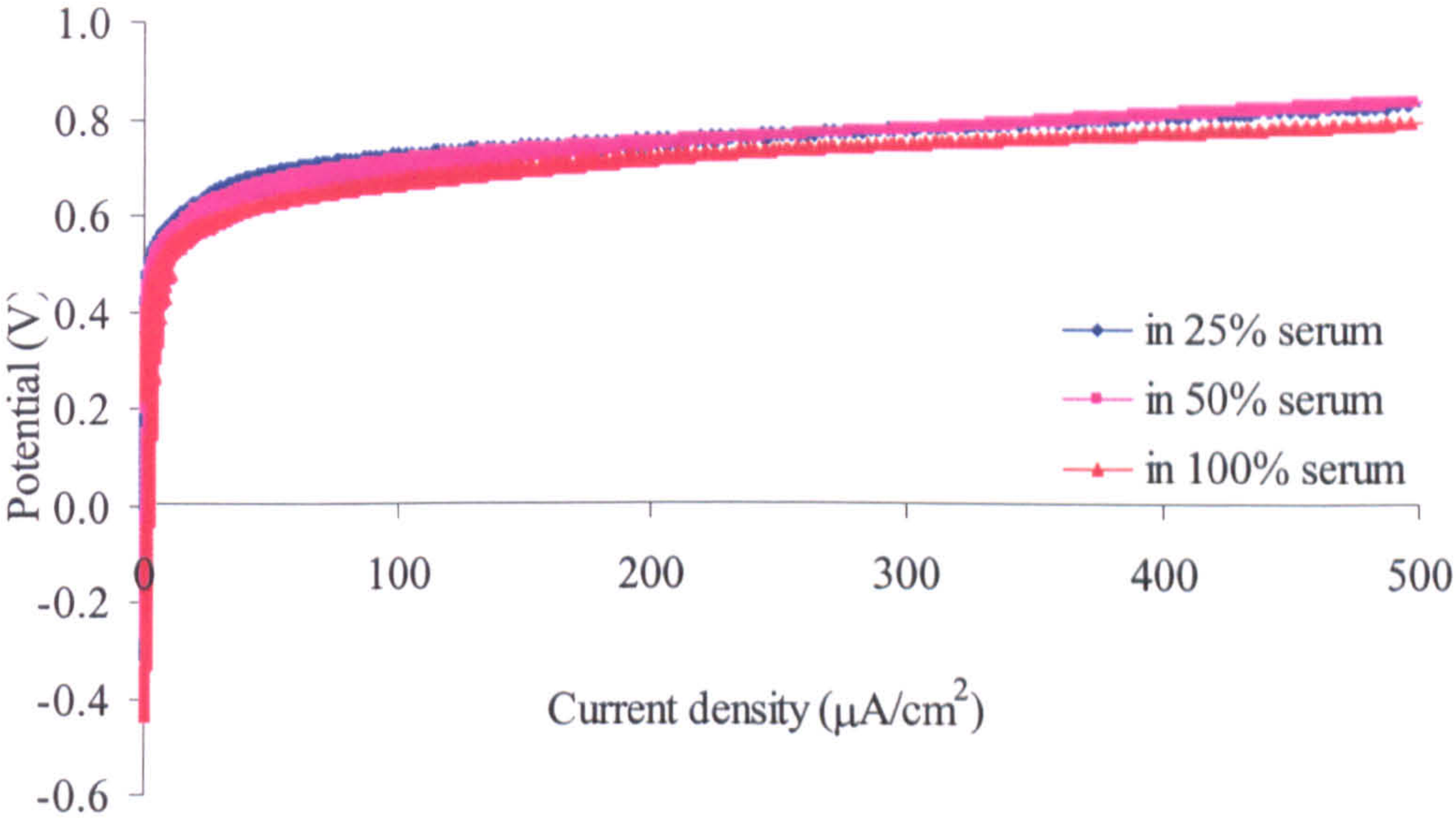

Figure 5-6 Anodic polarization curves in static conditions at 37°C for LC CoCrMo

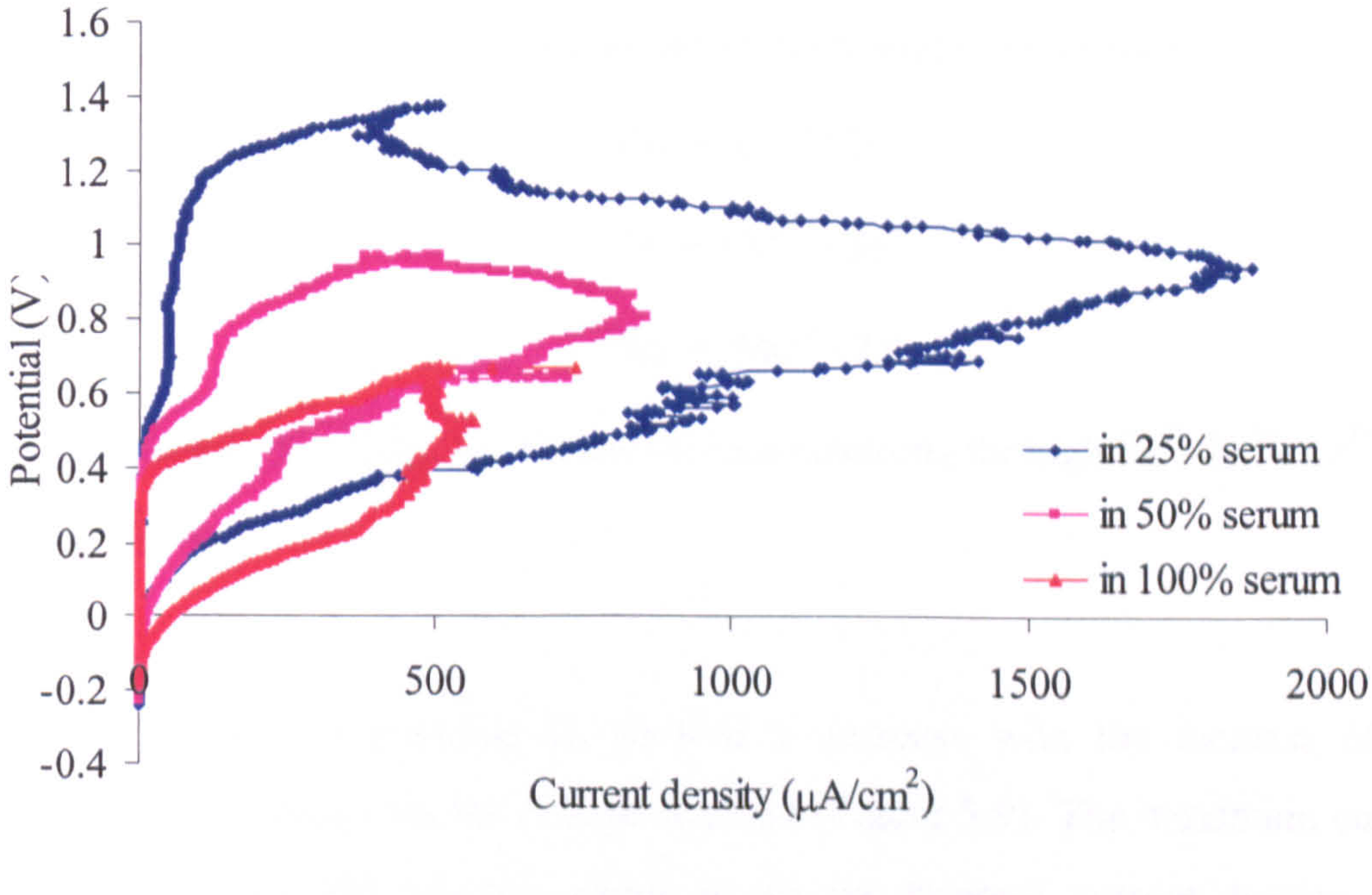

Figure 5-7 Anodic polarization curves in static conditions at 37°C for 316L

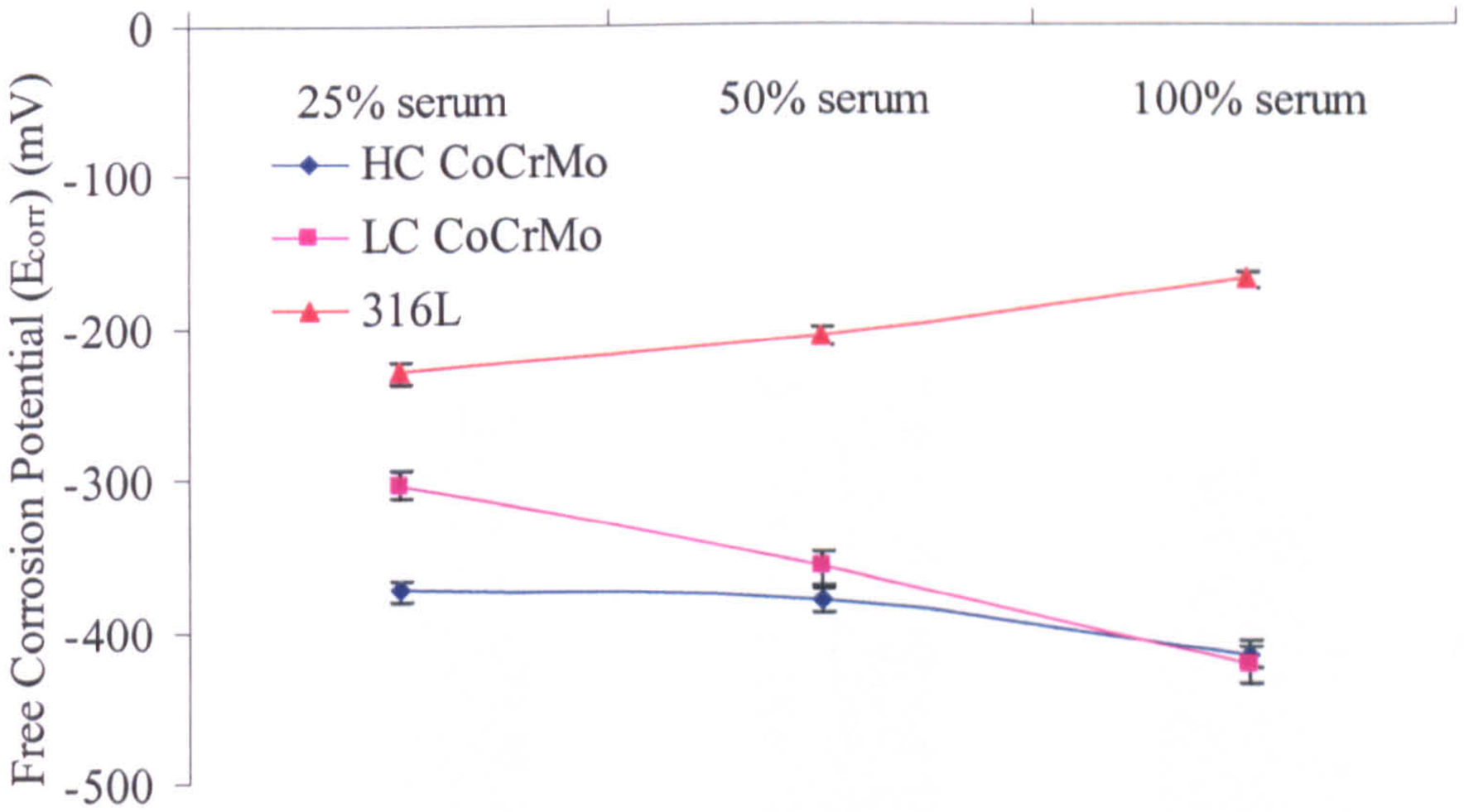

Figure 5-8 Free corrosion potential E_{corr} for the three materials in different concentration serum solution

The anodic reactions for CoCrMo alloys were suggested as shown below:

$$Co \rightarrow Co^{2+} + 2e^-$$

$$Cr \rightarrow Cr^{3+} + 3e^-$$

$$Mo \rightarrow Mo^{2+} + 2e^-$$

In addition, for 316L, Fe, Cr and Ni lose electrons through Fe^{2+}/Fe^{3+}, Cr^{3+} and Ni^{2+} reactions.

The breakdown potential E_b showed a decrease with the increase of the concentration of serum but the change is slight (Figure 5-9). The maximum current density (i_{max}) was 500 $\mu A/cm^2$, which is the set reversed current density. This suggests that once localized corrosion is forced to occur at E_b, no propagation appears on reversing the scan, which is supported by light microscopic images (Figure 5-10(a), (b)). For 316L in different solutions, the maximum current density (i_{max}) which can be used as a measure of the propagation of pitting corrosion declined with the increase of the concentration of serum. 316L showed the lowest

breakdown potential (E_b) and the highest maximum current density (i_{max}), confirming its lower corrosion resistance than the two CoCrMo alloys.

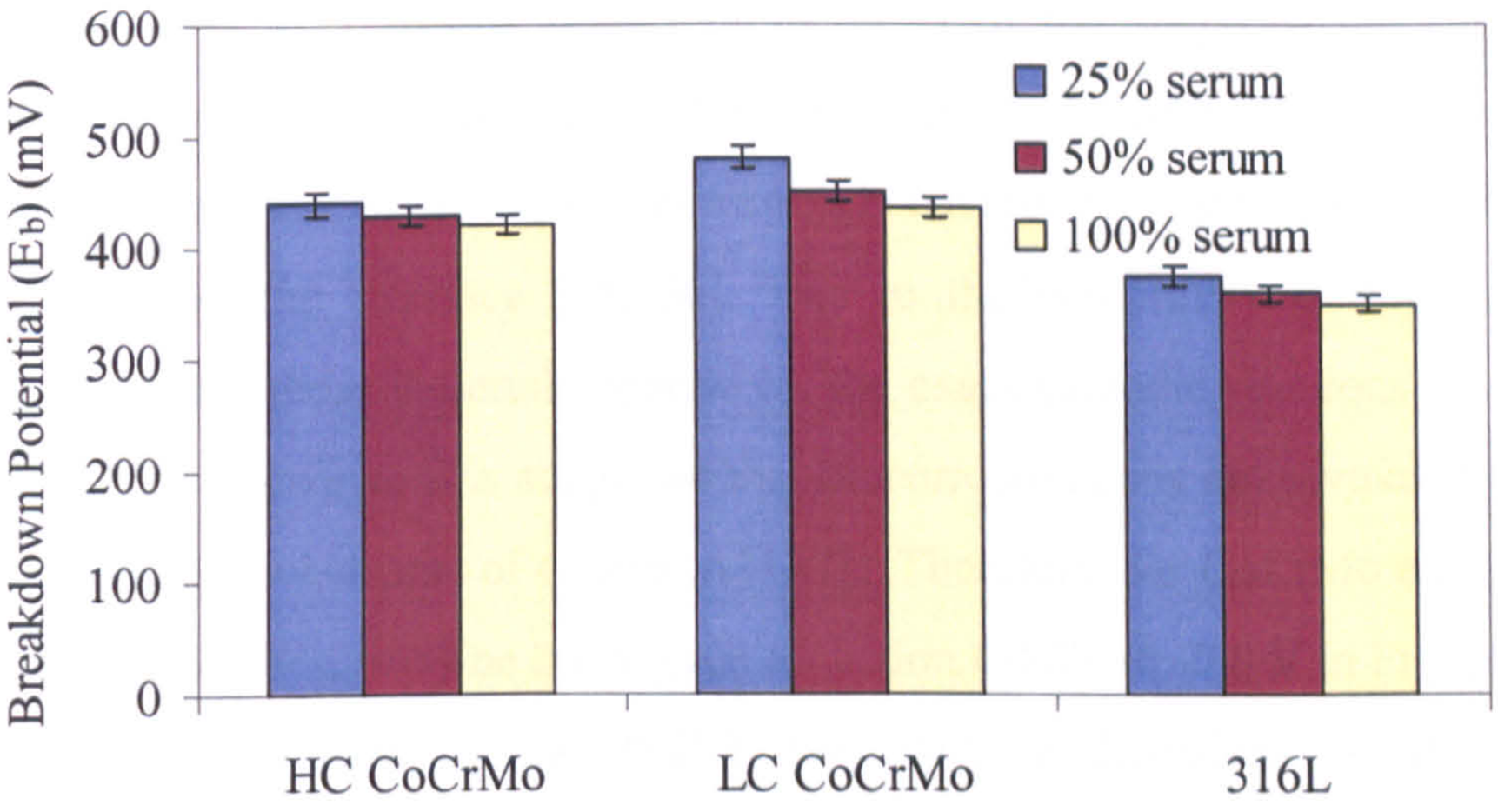

Figure 5-9 Breakdown potential E_b for the three materials in different serum concentration solutions

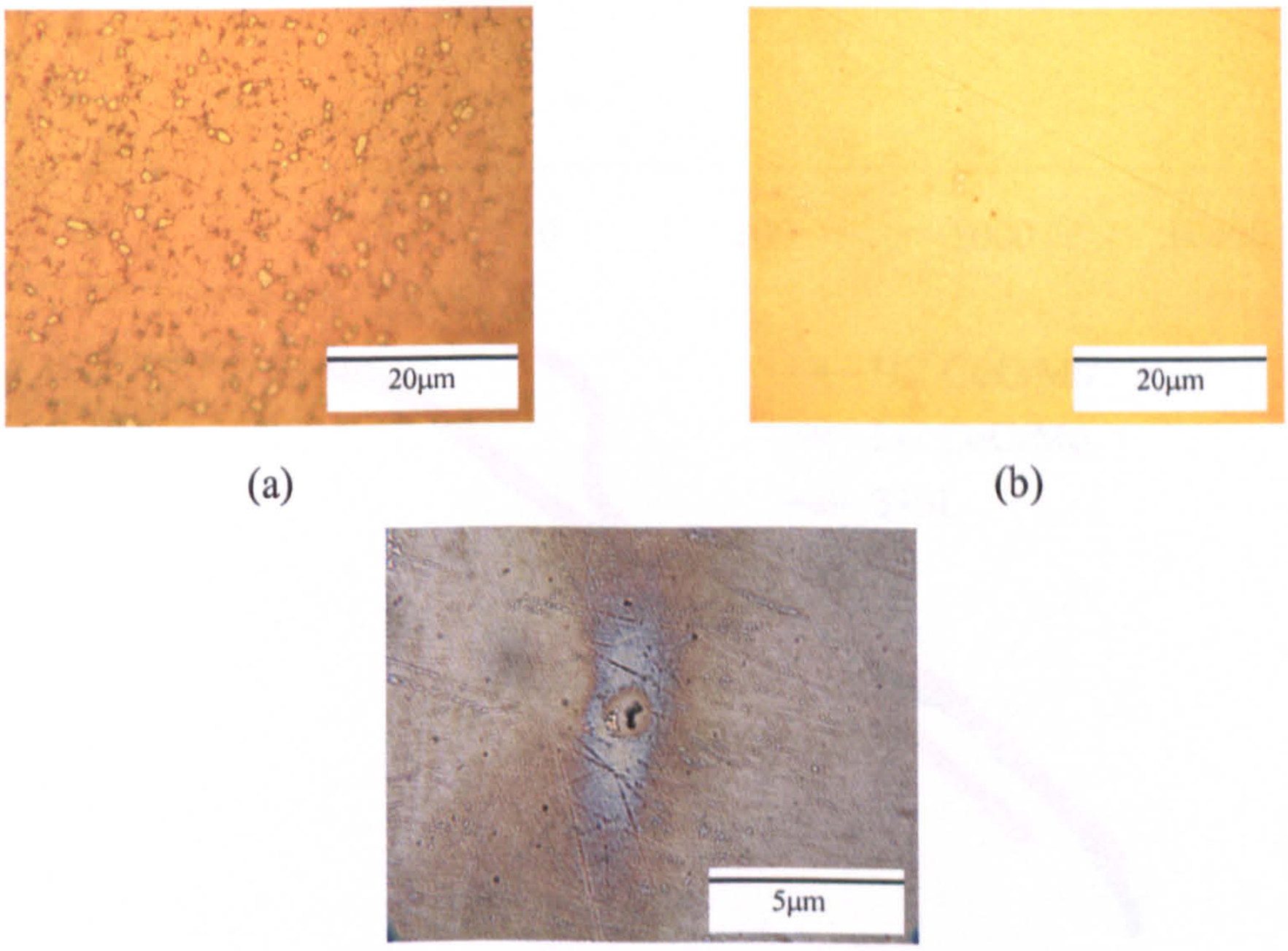

(a) (b)

(c)

Figure 5-10 Optical microscopy images for (a) HC CoCrMo (b) LC CoCrMo and (c) 316L in 50% serum after anodic polarization scan

As mentioned in Chapter 2, corrosion processes involve two reactions: anodic and cathodic reactions. Cathodic polarization tests were then carried out and the curves are shown in Figure 5-11 for all materials. HC CoCrMo and LC CoCrMo appeared to have very similar behaviour in terms of the shape of the curve. It indicates that they have similar reactions in serum. A lot of studies have been carried out to assess the effect of proteins on corrosion behaviour for metallic materials and the reactions on the interface [55,136]. Due to the complexity of the organic environments that those materials operate in, the exact cathodic reactions have not been elucidated. However it is suggested that biocorrosion does not invoke any new electrochemical mechanisms of corrosion [137]. Therefore, for CoCrMo alloys, the main cathodic reactions may be the oxygen reduction (-0.4V to -0.8 V in Figure 5-11) and hydrogen revolution (below -0.8V). For 316L, a diffusion-limited current density between -0.4V and -0.6V in Figure 5-11 was observed. Others believe that the cathodic reactions are complicated, which may involve the S-S bound scission during the protein denaturation and also possible hydrogen sulphide or nitrogen/nitric oxide reactions [114,138].

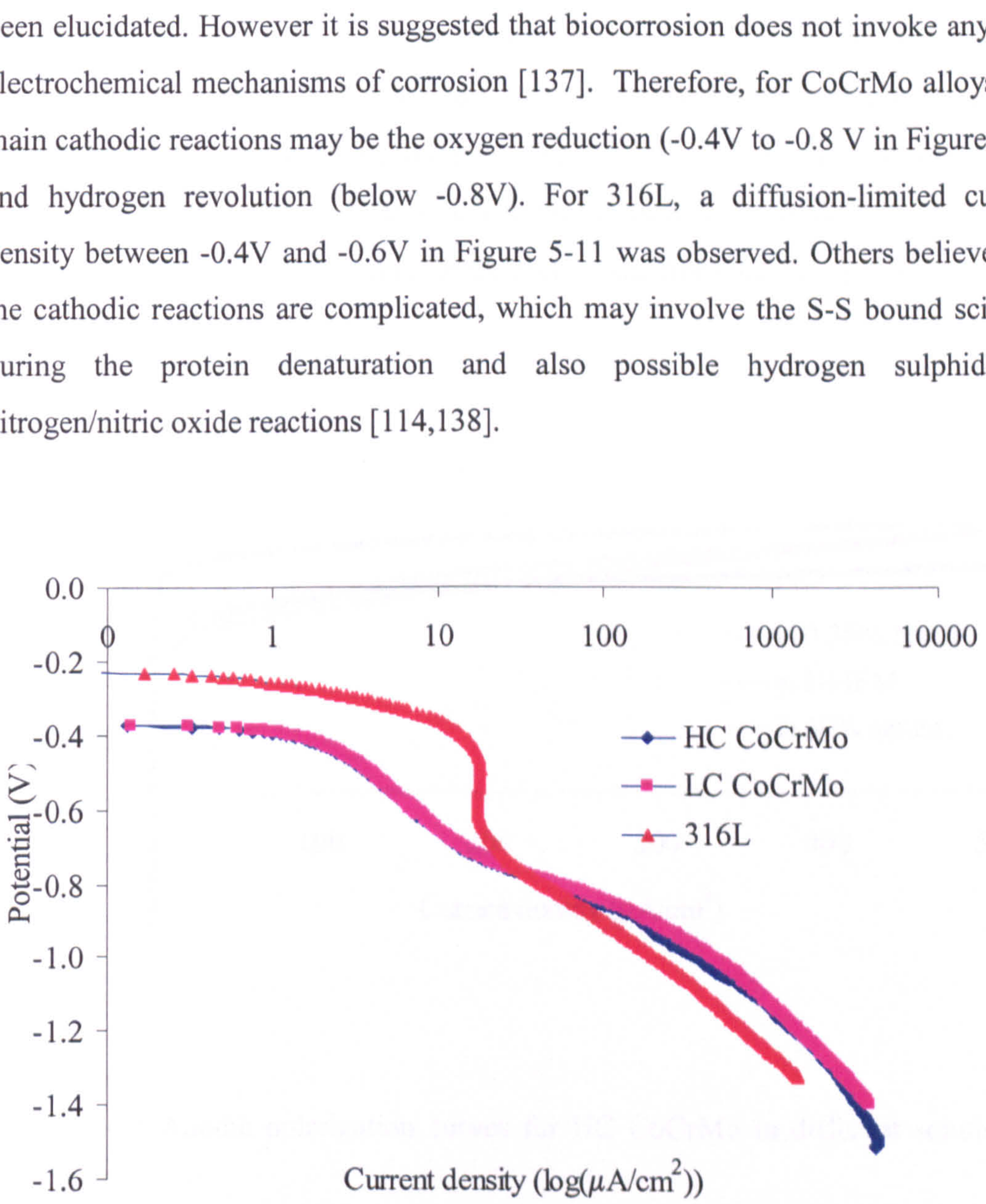

Figure 5-11 Cathodic polarization curves for the three materials in 50% serum

5.4. Organic Species Effect on Potentiodynamic Behaviour of Materials

Anodic polarization scans for the three materials in 50% serum, DMEM and 0.36% NaCl are shown in Figure 5-12, Figure 5-13 and Figure 5-14. In 0.36% NaCl, all three materials showed the most noble E_{corr} (Figure 5-15). With the presence of amino acids or proteins, both anodic and cathodic reactions were affected. Thus the equilibrium was shifted to more negative values. It is consistent with the results in the previous session, which with the increasing protein concentration, the E_{corr} moved towards a more active direction for CoCrMo alloys. The attachment of proteins or amino acids and the interactions between the organic species and the interface are primarily responsible for the shift of the free corrosion potential.

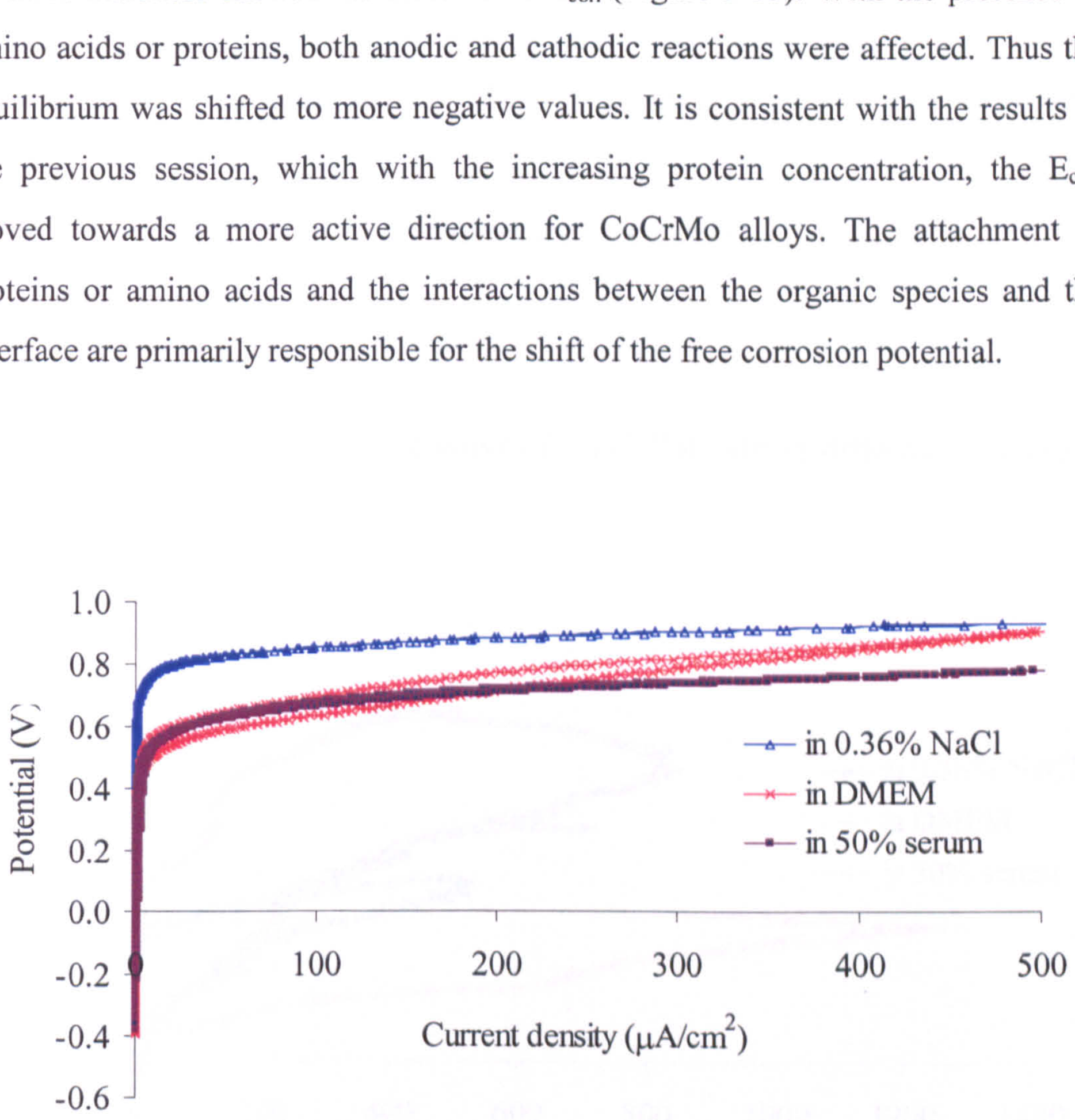

Figure 5-12 Anodic polarization curves for HC CoCrMo in different solutions at 37°C

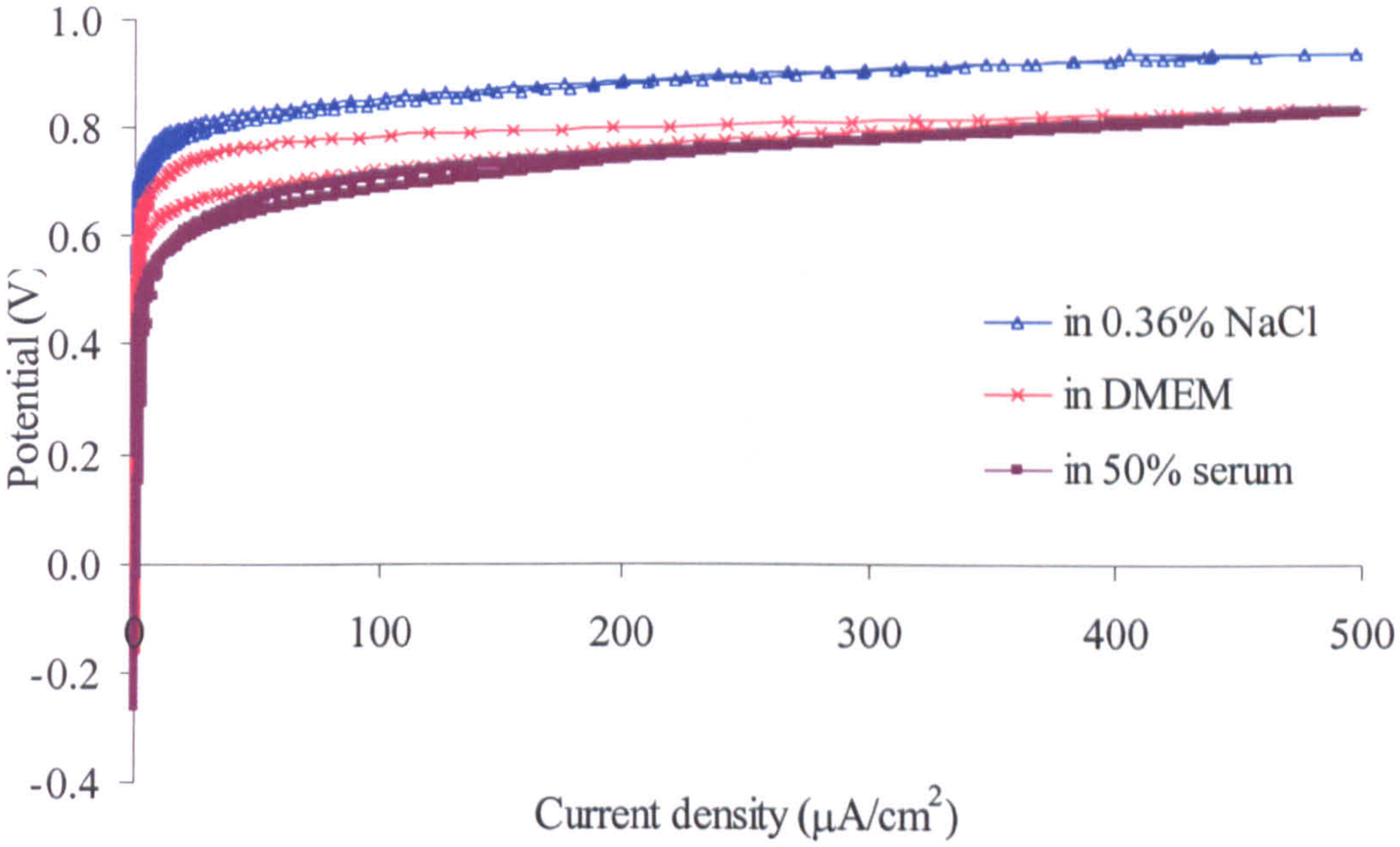

Figure 5-13 Anodic polarization curves for LC CoCrMo in different solutions at 37°C

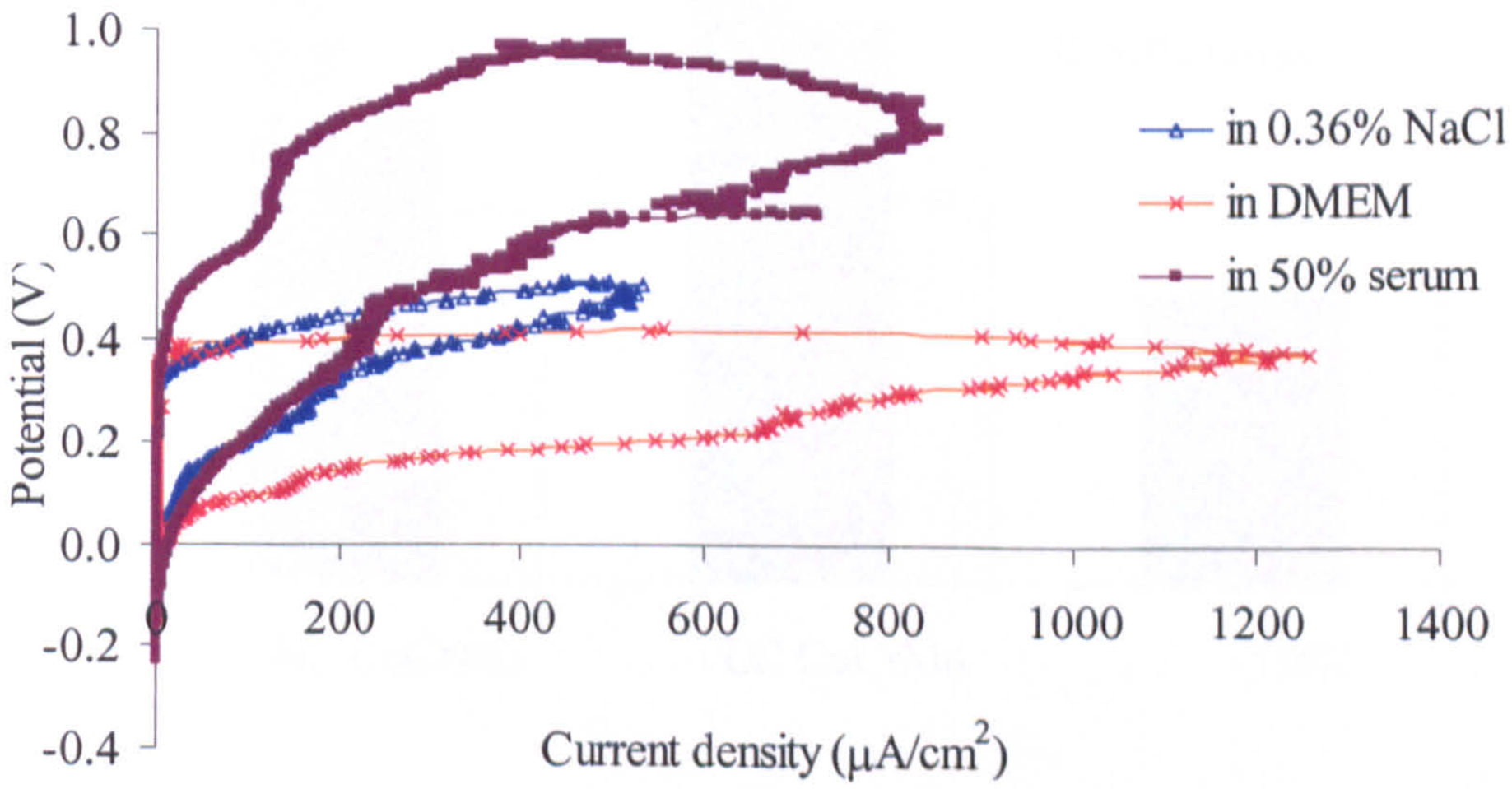

Figure 5-14 Anodic polarization curves for 316L in different solutions at 37°C

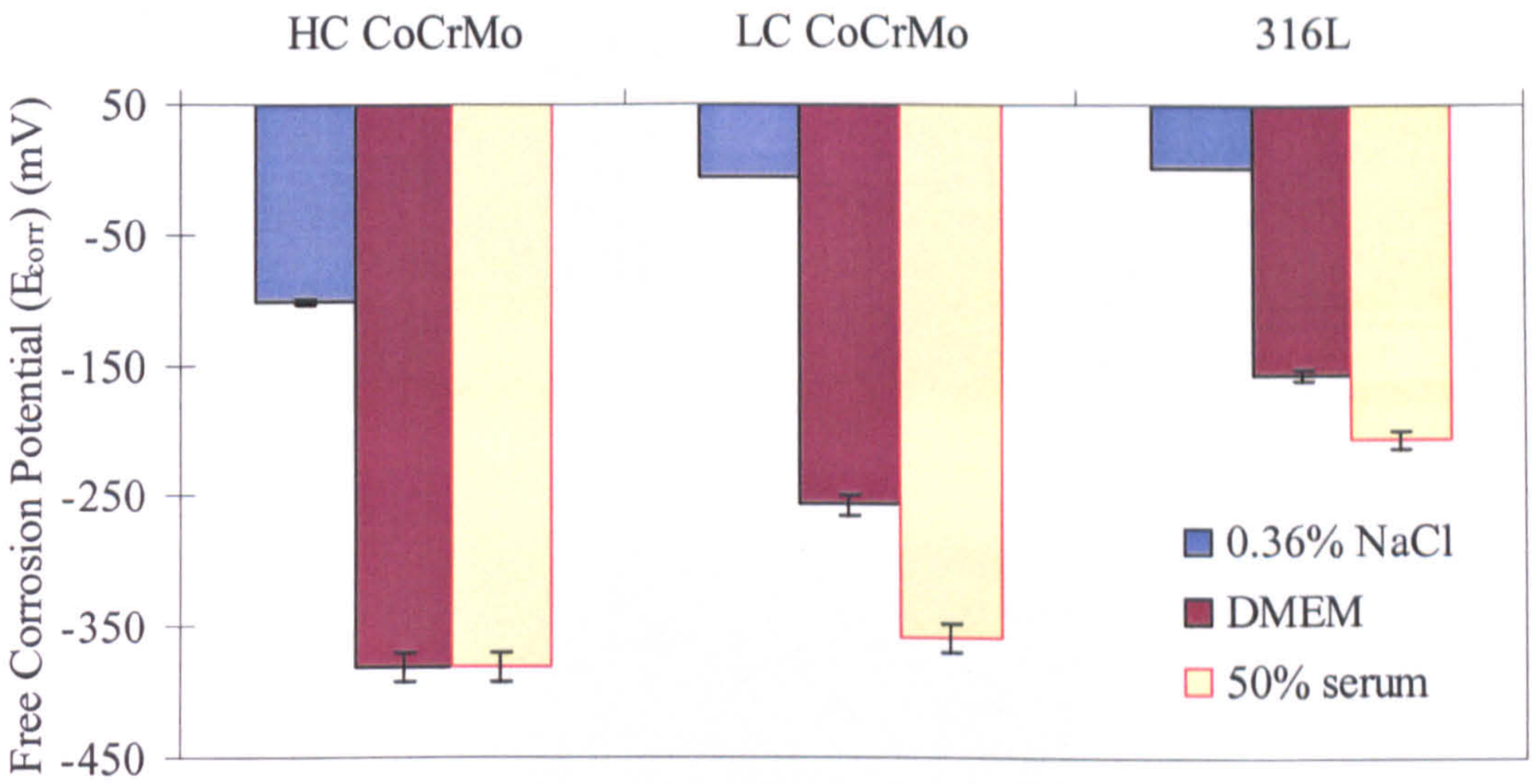

Figure 5-15 The free corrosion potential E_{corr} for the three materials

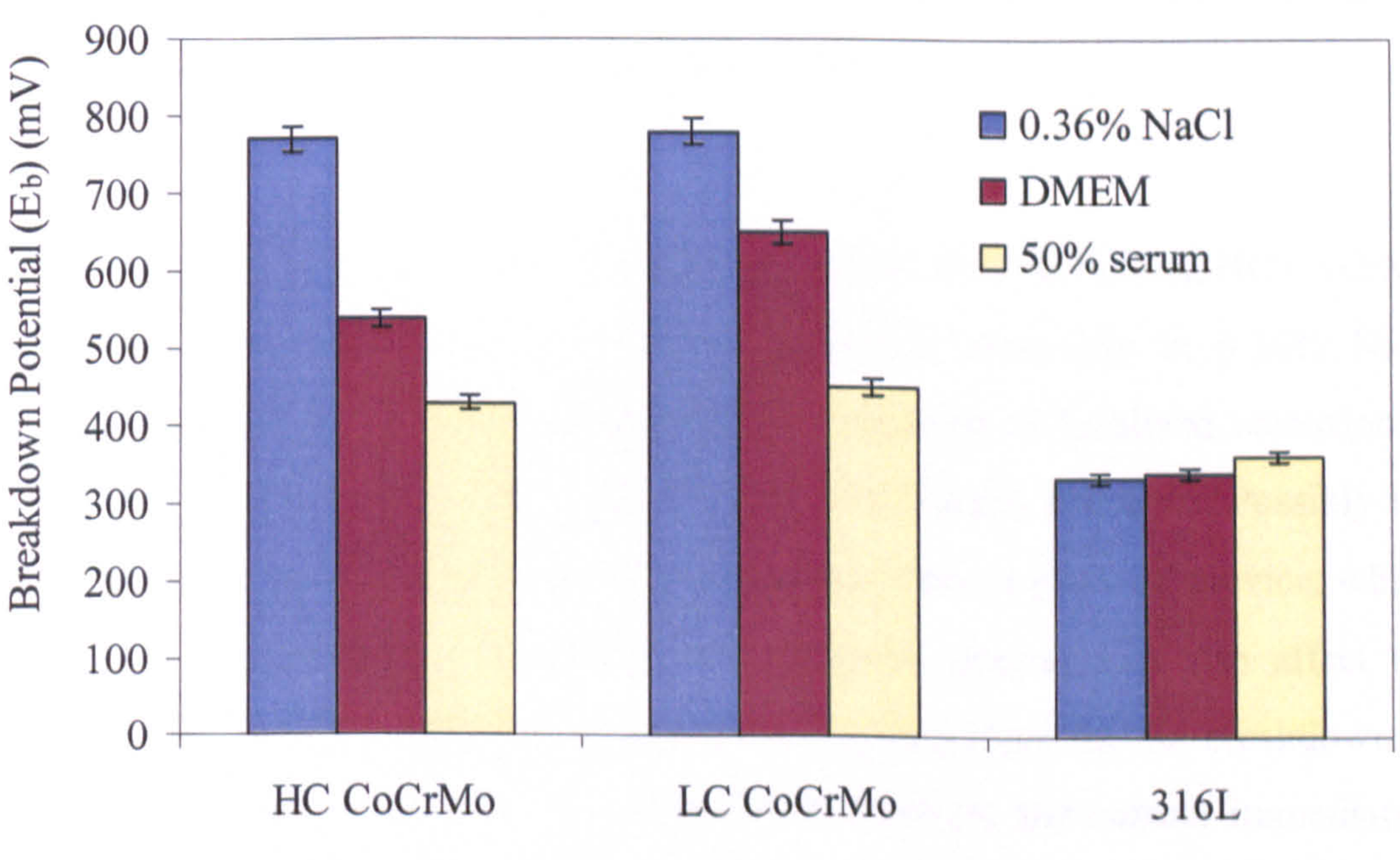

Figure 5-16 The breakdown potential E_b for the three materials in three solutions

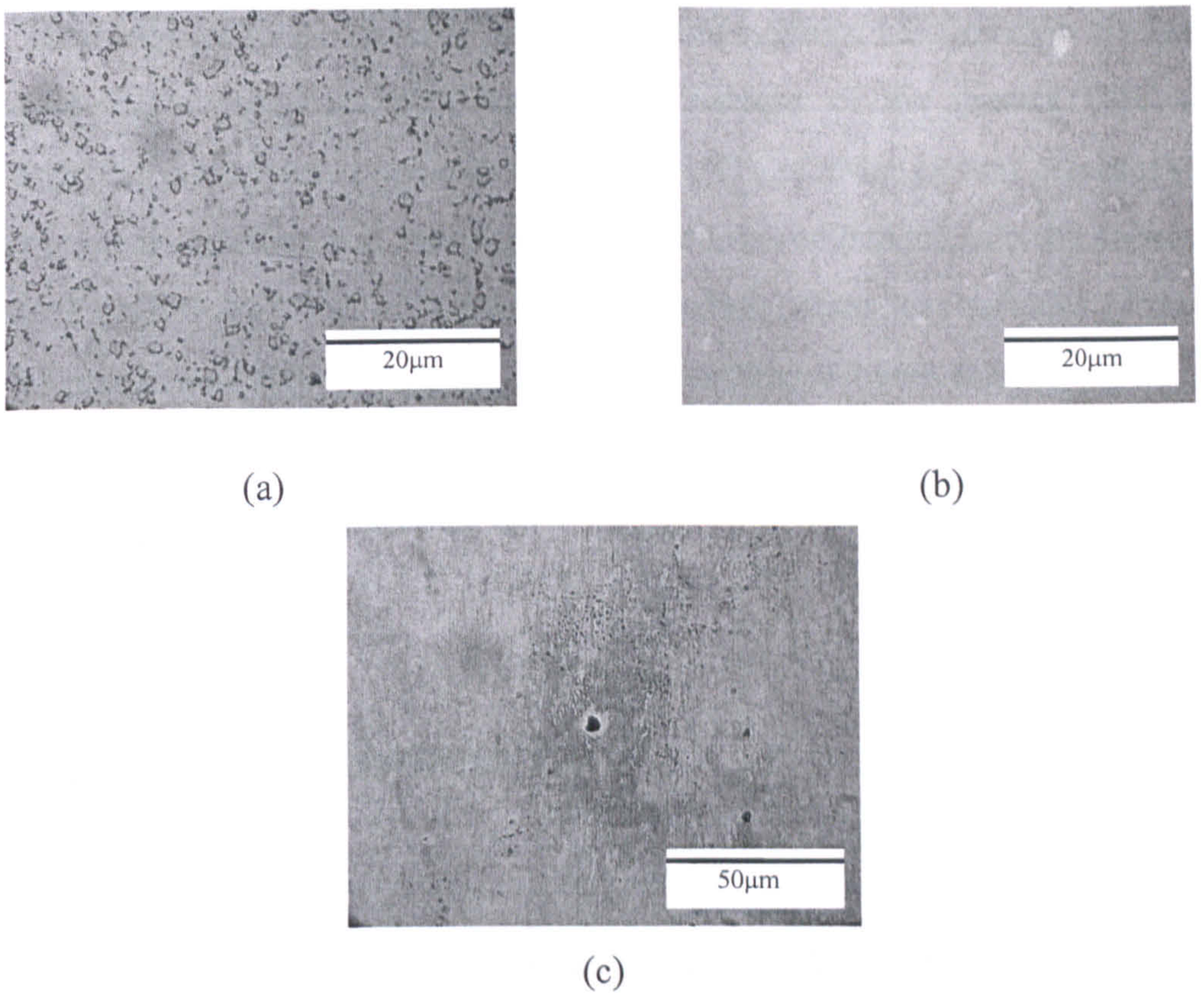

Figure 5-17 Optical microscopy images for (a) HC CoCrMo (b) LC CoCrMo and (c) 316L in DMEM after anodic polarization scan

Without proteins involved, in DMEM and 0.36% NaCl solutions, HC CoCrMo and LC CoCrMo show higher breakdown potentials especially in 0.36% NaCl solution (Figure 5-16), which suggests that the initiation of localized corrosion is more difficult in 0.36% NaCl than in the other two organic solutions. Possibly the presence of a layer (adsorbed protein molecules) can form a physical crevice, which resulted in a lowering E_b. It seems that the organic species can also affect the passivation process. Therefore, the extent of the driving force for the breakdown of the passive films was different. For both CoCrMo alloys, the current immediately decreased after it reached the reversal current density value ($500\mu A/cm^2$). No localized corrosion can be seen on the sample surface after the anodic polarization (Figure 5-17(a),(b)). For 316L, pitting corrosion was observed in all three environments(Figure 5-17(c)).

Comparing the HC CoCrMo and LC CoCrMo alloys, LC CoCrMo always had a higher E_b in every solution, presumably because of the greater Cr/C ratio. However, the difference is not significant. For HC CoCrMo, carbon combines with chromium/molybdenum and forms very fine carbides embedded into the cobalt rich matrix (Figure 5-2(a)). For LC CoCrMo, less carbon means less carbides formation. Instead chromium/molybdenum are uniformly distributed in the matrix, which gives a better capability to form a chromium oxide passive film to protect the bare metal surface from localized corrosion (Figure 5-2(b)).

5.5. Contact Angle Measurements

Contact angle measurement was carried out for all materials (HC CoCrMo, LC CoCrMo and 316L). The sample surface was polished to 0.01μm in an attempt to simulate the roughness of the wear scar under rubbing in tribocorrosion tests. Distilled water was used for the determination of the wettability. Serum was used to analyze the adsorption of proteins. The contact angle on samples which were immersed in 50% serum, DMEM and 0.36% NaCl for up to for 4 hours in static conditions at 37°C, was measured as described in Chapter 4. The values are shown in Table 5-2 for materials in DMEM and 0.36% NaCl. All three materials exhibited a hydrophobic surface (contact angle > 90° with water) after polishing. The mean values of contact angle for HC CoCrMo, LC CoCrMo and 316L were 93.8°, 98.3° and 98.9°. 316L showed the lowest surface free energy. After immersion in 50% serum and DMEM, the surface became hydrophilic for all materials, which indicates that an organic species adsorption layer had formed. Surfaces immersed in 0.36% NaCl remained hydrophobic.

Table 5-2 Contact angle for materials immersed in different solutions

Immersion time (hour)	Immersion solution	Contact angle (°)		
		HC CoCrMo	LC CoCrMo	316L
0	DMEM	62±0.7	73±1.0	91±1.2
	0.36% NaCl	94±1.4	98±1.5	99±1.3
1	DMEM	54±0.6	60±0.4	56±0.6
	0.36% NaCl	92±0.1	92±1.1	91±0.2
2	DMEM	54±0.5	59±0.2	57±0.6
	0.36% NaCl	9±0.2	92±0.7	92±0.5
3	DMEM	54±0.1	60±0.5	57±0.4
	0.36% NaCl	91±0.6	92±0..3	91±0.1
4	DMEM	53±0.4	60±0.6	56±0.3
	0.36% NaCl	92±0.6	92±0.4	91±0.3

For all materials, the contact angle for protein on the protein-layer is smaller than water on the protein-layer indicating that certain protein to protein reactions take place. From Figure 5-18, HC CoCrMo exhibits the lowest contact angle indicating the preference of protein adsorption on the HC CoCrMo surface (passive film). The contact angle dropped rapidly immediately the surface was immersed in the serum solution. After 1 hour, the contact angle is nearly constant for 316L and LC CoCrMo. For HC CoCrMo, the contact angle remained at a very low value and continued to reduce. It indicates that on 316L and LC CoCrMo, after adsorption and denaturation/unfolding of proteins (mainly Albumin), the surfaces were saturated with proteins. For HC CoCrMo, there are still sites onto which more proteins can be adsorbed or the force was not strong and stable, which means folded proteins could be detached from the surface.

The effect of protein adsorption on corrosion in static conditions was studied by anodic polarization tests (Figure 5-19). As soon as the sample was immersed into protein-rich serum, the breakdown potential (E_b) dropped. It is in an agreement with Williams [124]. It was noticed that albumin was adsorbed on Co and SS sample surfaces and remained constant from 1 hour throughout the time period of the experiment. It means that proteins can affect the formation of the passive film. A lower breakdown potential corresponds to a shorter passive region. The passive layer which interacts with proteins broke down in the simulated body fluid and the localized corrosion (pitting, crevice etc.) occurred. Overall, it has been suggested that proteins enhance corrosion rate for all materials, however for HC CoCrMo, the effect is insignificant. The contact angle measurement is an easy and assessable way to give an indication of protein adsorption and evaluate the possible corrosion resistance. It consists with Williams's work [140], which showed high surface energy alloys owned greater corrosion resistance.

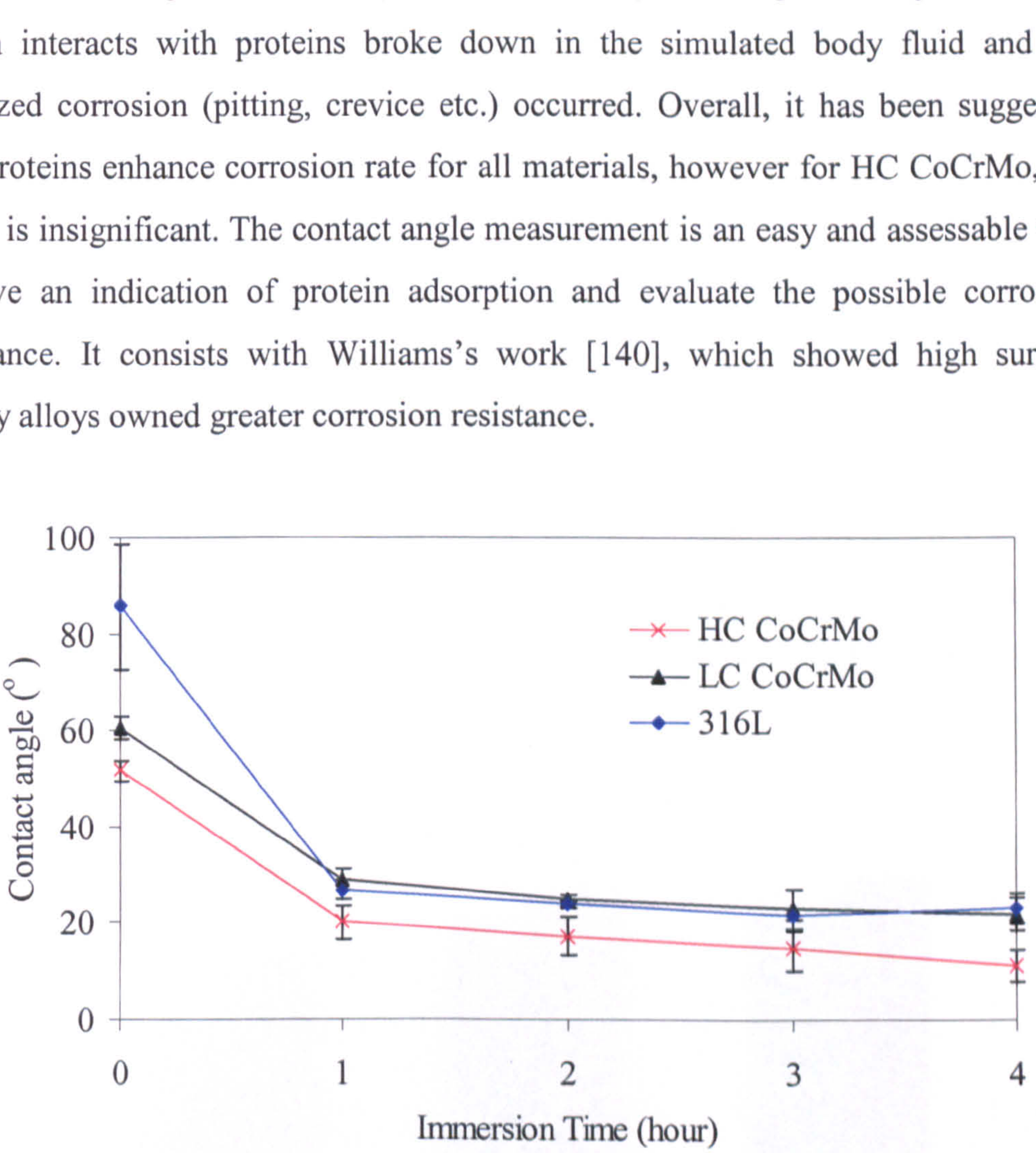

Figure 5-18 Contact angle for three materials after different immersion time in 50% Serum (measured with serum droplet)

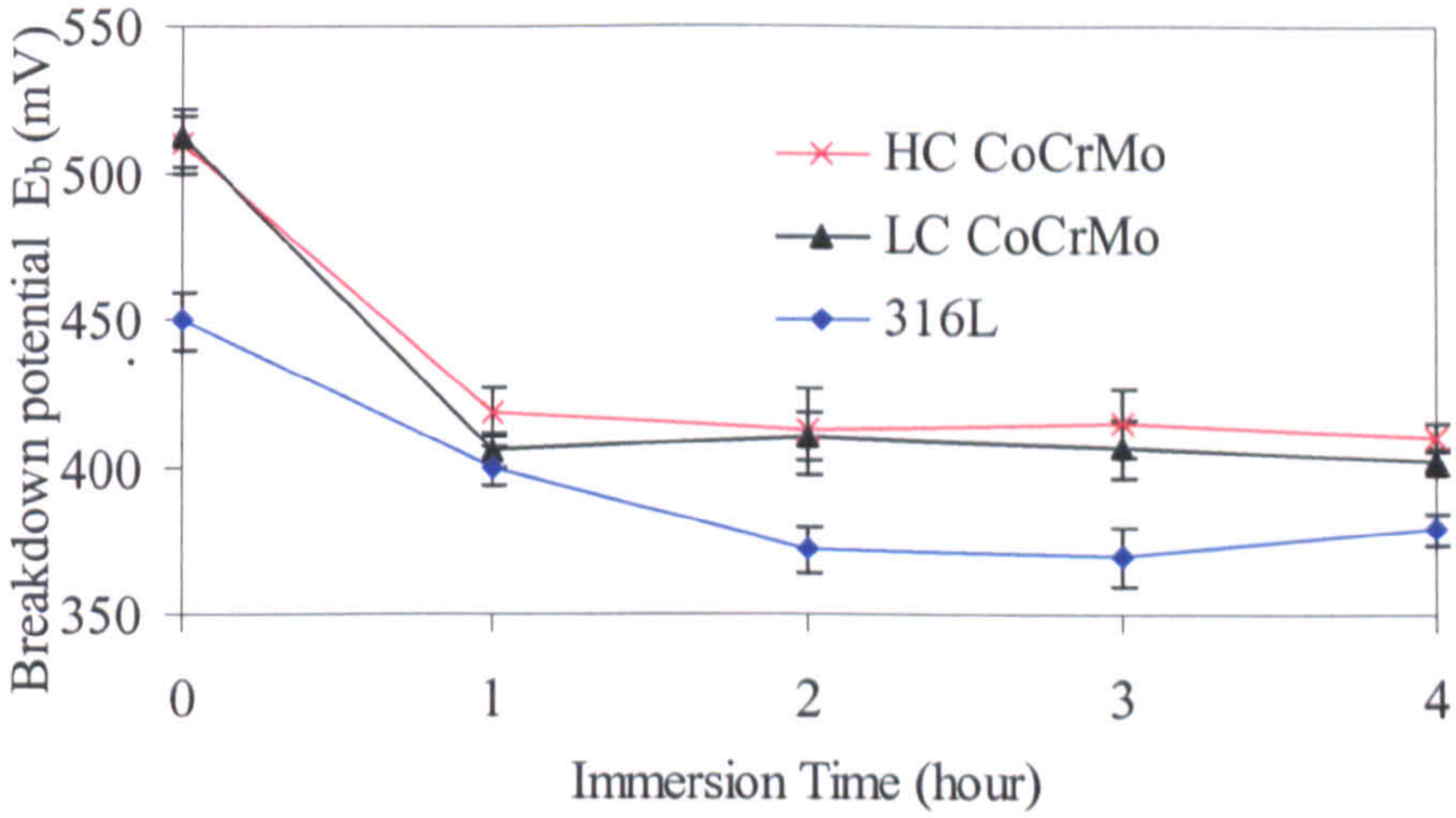

Figure 5-19 Breakdown potential (E_b) as a function of immersion time in Serum for all materials

Cathodic protection (CP) is a technique to prevent corrosion. Contact angle measurements also were conducted on sample surfaces after applying 1 hour CP in 50% serum and the results are shown in Figure 5-20. Higher contact angle indicates that less proteins adsorbed on material surfaces. It seems that CP can reduce the adsorption of proteins. However, the difference is small and further tests would be needed to confirm this as a significant effect.

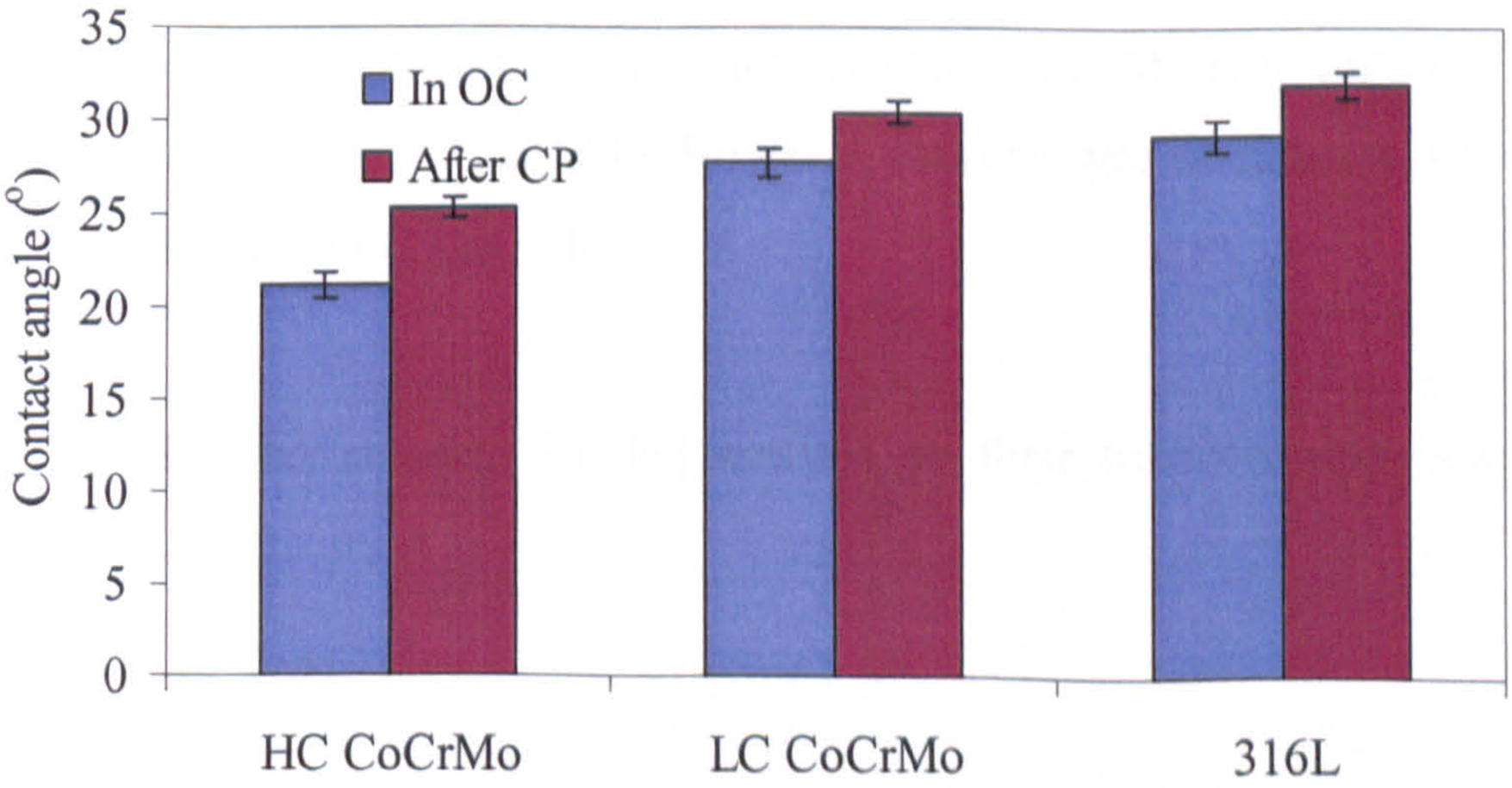

Figure 5-20 Contact angle for the materials in OC (open circuit) and 1 hour after CP in 50% serum

5.6. Summary

In this chapter, materials corrosion behaviour in static conditions have been assessed by using electrochemical methods. The contact angle measurements were used to determine the surface energy and wettability. Some findings can be summarized:

- A negative shift of E_{corr} can be observed in 50% serum comparing with E_{corr} values in 0.36% NaCl.
- Lower breakdown potential (E_b) was recorded for CoCrMo alloys in 50% serum and DMEM than in 0.36% NaCl, which indicates that proteins and amino acids exhibited great influence on passive film formation and localized corrosion initiation.
- Two CoCrMo alloys showed similar values of E_b. However, 316L appeared to have the least corrosion resistance in static condition in all three tested solutions
- Proteins adsorption occurred immediately when samples were immersed into the solution. The surfaces of all materials changed from hydrophobic to hydrophilic after the adsorption of proteins. Higher surface energy (HC CoCrMo among tested materials) intended to adsorb more proteins.
- Two types of carbides (Cr-rich carbides and Mo-rich carbides) can be observed on HC CoCrMo. However, just one type of carbides (Cr-rich) can be seen on LC CoCrMo.

In the next chapter, detailed analysis on their tribocorrosion behaviour is conducted.

CHAPTER 6

THE EFFECT OF TRIBOLOGY ON ELECTROCHEMICAL BEHAVIOUR AND SURFACE PROPERTIES OF MATERIALS

6.1. Introduction

After assessing candidate materials in static conditions, the next step was to understand their behaviour in tribocorrosion systems. For orthopaedic implants, especially for load bearing metallic implants, such as artificial hip or knee implants, they are not only exposed to an aggressive and corrosive environment but also to stress associated with tribological contact. Understanding tribocorrosion behaviour is necessary for material selection and development in such applications. From Chapter 5, proteins and amino acids appear to influence their electrochemical behaviour significantly in terms of passive film breakdown and corrosion propagation in the static environment. But how and to what extent can wear (tribology) affect the corrosion process? Moreover, what will be the corrosion response? In this chapter and the next chapter the effect of corrosion and wear on each other is studied. One important issue should be kept in mind is the interaction between wear and corrosion in such application is always presents. The interaction is a rather significant phenomenon and detailed discussion will be shown in Chapter 8.

In this chapter, the effect of tribology on the electrochemical process and the surface changes in three solutions are initially studied. The map of experiments for the work presented in this chapter is shown in Figure 6.1.

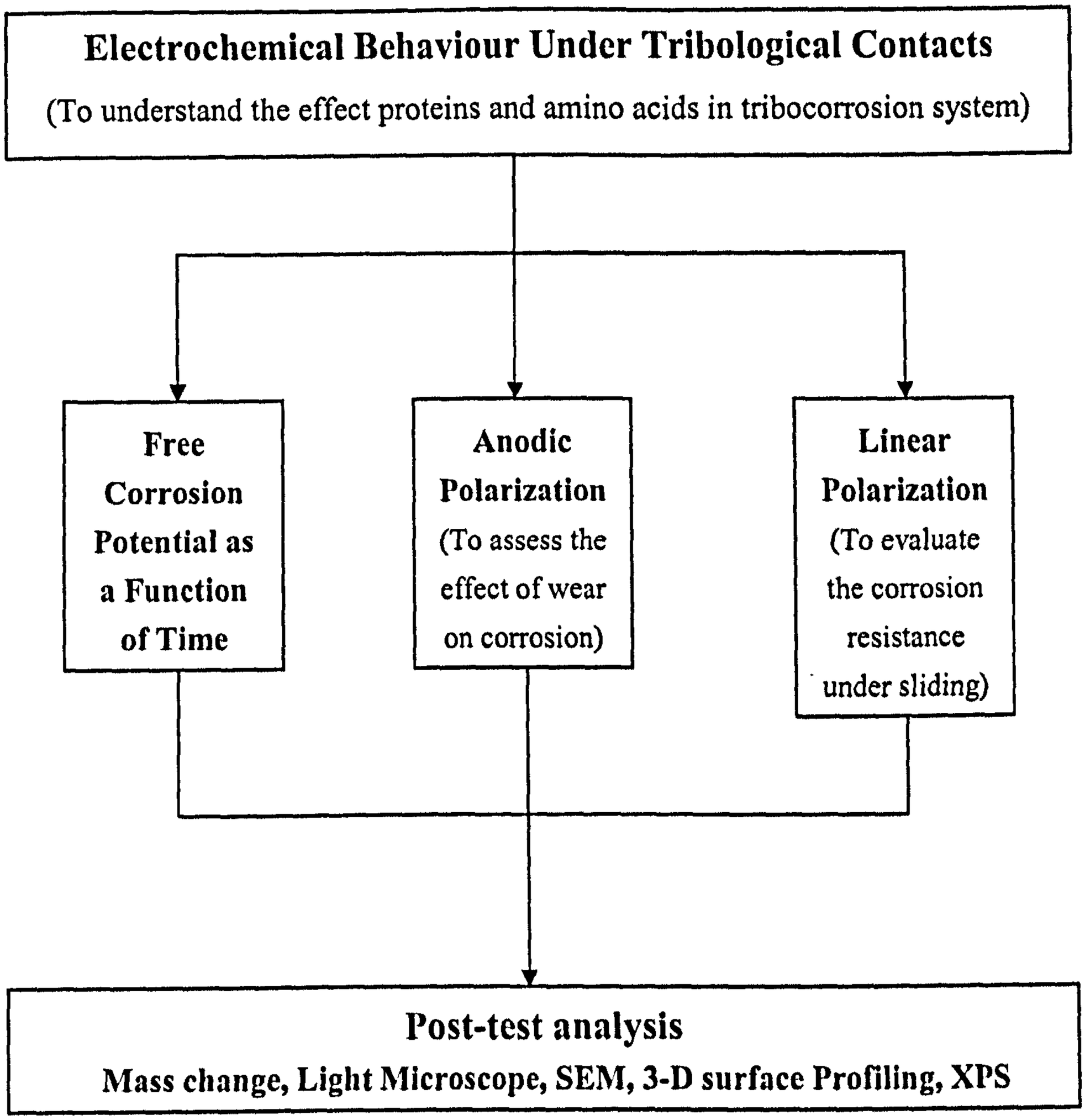

Figure 6-1 The structure of the experimental work in Chapter 6

6.2. Calculation of The Lambda Ratio

According to Eq. (6-1), the lambda ratio is related to the roughness of the counter pair and the minimum film thickness (Eq. (6-2)). In this study, tests were done on the ball on reciprocation plate tribometer, in which the contact is a point contact (Figure 6-2). The Hamrock and Dowson equation [10] for this configuration is Eq. 6-2. The starting lambda ratios for the three materials in 50% serum, DMEM and 0.36% NaCl are calculated and shown in Table 6-1. For the silicon nitride ball,

the Young's modulus E is 310 GPa and the Possion's ratio ν is 0.26. As tests progressed, the contact area becomes larger. The contact pressure reduces as the increase of wear on the ball.

$$\lambda = \frac{h_{\min}}{\sqrt{R_{q1}^{\ 2} + R_{q2}^{\ 2}}} \qquad \text{Eq. 6-1}$$

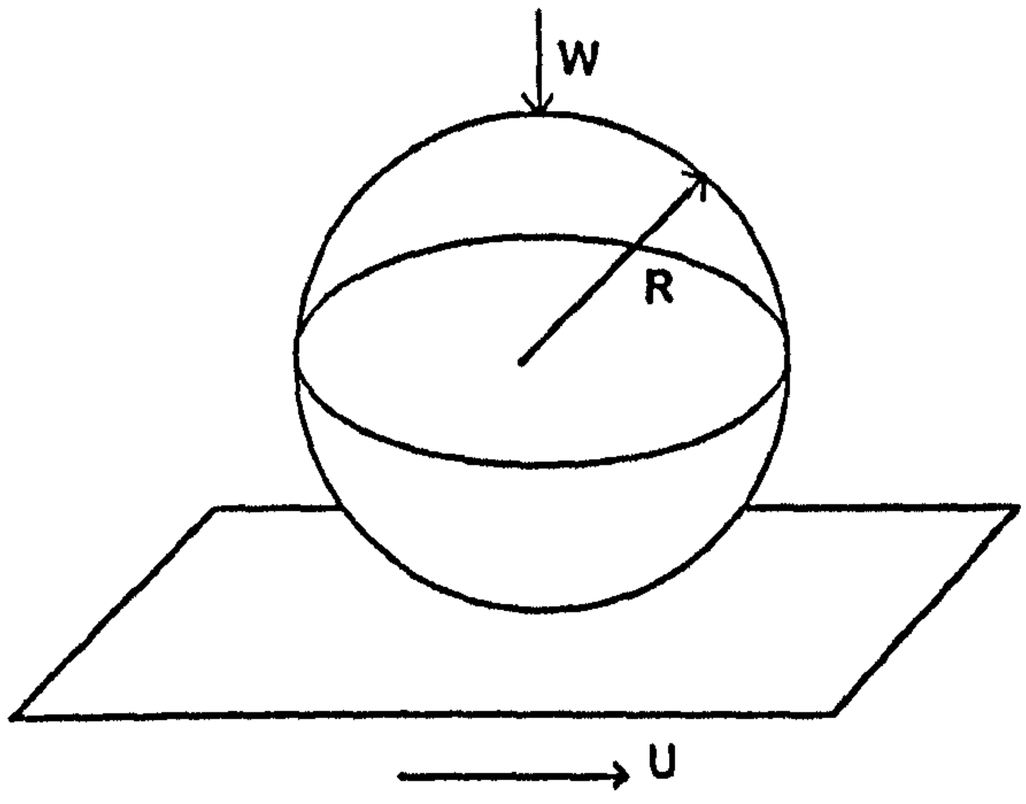

Figure 6-2 Configuration of ball on plate point contact

$$\frac{h_{\min}}{R} = 2.79\left(\frac{\eta u}{E'R}\right)^{0.65}\left(\frac{W}{E'R^2}\right)^{-0.21} \qquad \text{Eq. 6-2}$$

Where

$$\frac{1}{E'} = \frac{1-\nu_1^{\ 2}}{E_1} + \frac{1-\nu_2^{\ 2}}{E_2} \qquad \text{Eq. 6-3}$$

It shows that all materials in all environments are under the boundary lubrication regime in this study (λ less than 1). It is consistent with the lubrication conditions in MoM replacement [11, 12]. The lower lambda ratio for 0.36% NaCl is due to the lower viscosity comparing with 50% serum (0.01 Pa s). Moreover, for HC CoCrMo the lowest λ is because of the higher contact modulus.

$$p_0 = \frac{3W}{2\pi a^2} \qquad \text{Eq. 6-4}$$

Where $a = \left(\frac{3WR}{4E'}\right)^{1/3}$, and the mean contact pressure $p_m = \frac{2}{3}p_0$

Table 6-1 Lambda ratio for all materials in different solutions

		HC CoCrMo	LC CoCrMo	316L
***E* (GPa)**		220	214	180
v		0.32	0.32	0.30
***E'* (with Si_3N_4 ball) (GPa)**		140	138	123
λ	**Serum**	0.21	0.22	0.23
	DMEM	0.10	0.11	0.12
	0.36% NaCl	0.05	0.05	0.06

6.3. Effect of Proteins and Amino Acids on Electrochemical Processes

6.3.1. Effect of organic species on friction and the open circuit potential

From Chapter 5, clear passivity is shown for the three alloys in static conditions; expected due to the presence of a Cr_2O_3-containing film of several nm thickness spontaneously formed in air. One key issue with respect to tribo-corrosion is the behaviour of the film once a mechanical wearing/rubbing action is applied. One way to monitor the film (semi-quantitatively) is to measure E_{corr} (open circuit potential (OCP) or free corrosion potential) as the sliding action starts (and then stops).

In Figure 6-3 (a), for HC CoCrMo the trend in E_{corr} as a function of time is shown. From point 1, the sample was immersed into the solution (50% serum) under

static conditions. At this point the E_{corr} was stable. The reciprocating motion of the plate was started at point 2 but with no load added. Only the weight of the loading arm with the silicon nitride ball (<5N) in the holder acted on the plate. At this point a shift in E_{corr} in the active direction was recorded, consistent with removal of the passive film and an increase in the rate of the anodic reaction (as is expected when there is a removal of the charge transfer barrier). At position 3, the load on the silicon nitride ball was increased to 80N. At this point a significant shift in E_{corr} in the active (negative) direction was measured, followed by a transient period between points 3 and 4 during which the potential eventually stabilized. The steady state E_{corr} was reached when an equilibrium was reached between the rate of formation and the rate of removal of the passive film (depassivation versus repassivation) [6]. When load was added, plastic deformation occurred on the sample surface, which may contribute to the shift of potential. The initial transient period of potential moved at point 3 indicates the initiation of plastic deformation.

For LC CoCrMo in 50% serum, interestingly, friction coefficient dropped after about 2 hours and there was a corresponding increase in E_{corr} (Figure 6-3 (b)). This may be because the passive film recovery speed was slowly increasing comparing to the speed of the passive film damage by the mechanical rubbing then made the E_{corr} increase and friction coefficient drop. The transition of the running-in state to the steady state may be responsible for this phenomenon. The passive film acted as a solid lubricant. In addition, a third body effect might be involved in the first two hours of tests. Debris from the surface of LC CoCrMo alloy could cause abrasive wear and relatively high friction.

For 316L (Figure 6-3 (c)) in 50% serum, the same general trend of E_{corr} was seen but with more potential oscillations than for the CoCrMo alloys. Figure 6-4 and Figure 6-5 show the free corrosion potential and friction coefficient in DMEM and in 0.36% NaCl with the same experimental procedure as described above. Some similarities and differences can be seen.

- The friction coefficient and the free corrosion potential response correspond to each other very well.
- The transition period (when load was added) can be obtained for all tests. It indicates that an initial impact was occurred due to the load. Possibly there was an initial formation of tribofilm. However, the recovery from the impact in 50% serum seems quicker than in 0.36% NaCl. It may not be a simple passive (oxide) film recovery. Likely, it is an organic molecule-passive film interaction.
- 316L exhibited potential and friction coefficient oscillations in all three environments, especially in 50% serum. CoCrMo alloys, on the other hand, showed rather stable behaviour.
- In 50% serum, all materials showed an initial decrease of friction coefficient followed by an increase until the friction stabilized. In 0.36% NaCl, the friction coefficient increased from the start then reached a steady value. It may be caused by the removal of adsorbed proteins from the sample surface in 50% serum.
- In all solutions, after the load was removed, the removal of the passive film ceased and the protective barrier reformed. The final potential for CoCrMo was always more noble than the initial potential before load was applied. In contrast, the final recovery potential of 316L was more active (lower/more negative) than the stable free corrosion potential in the beginning of the tests (Figure 6-3 and Figure 6-4).

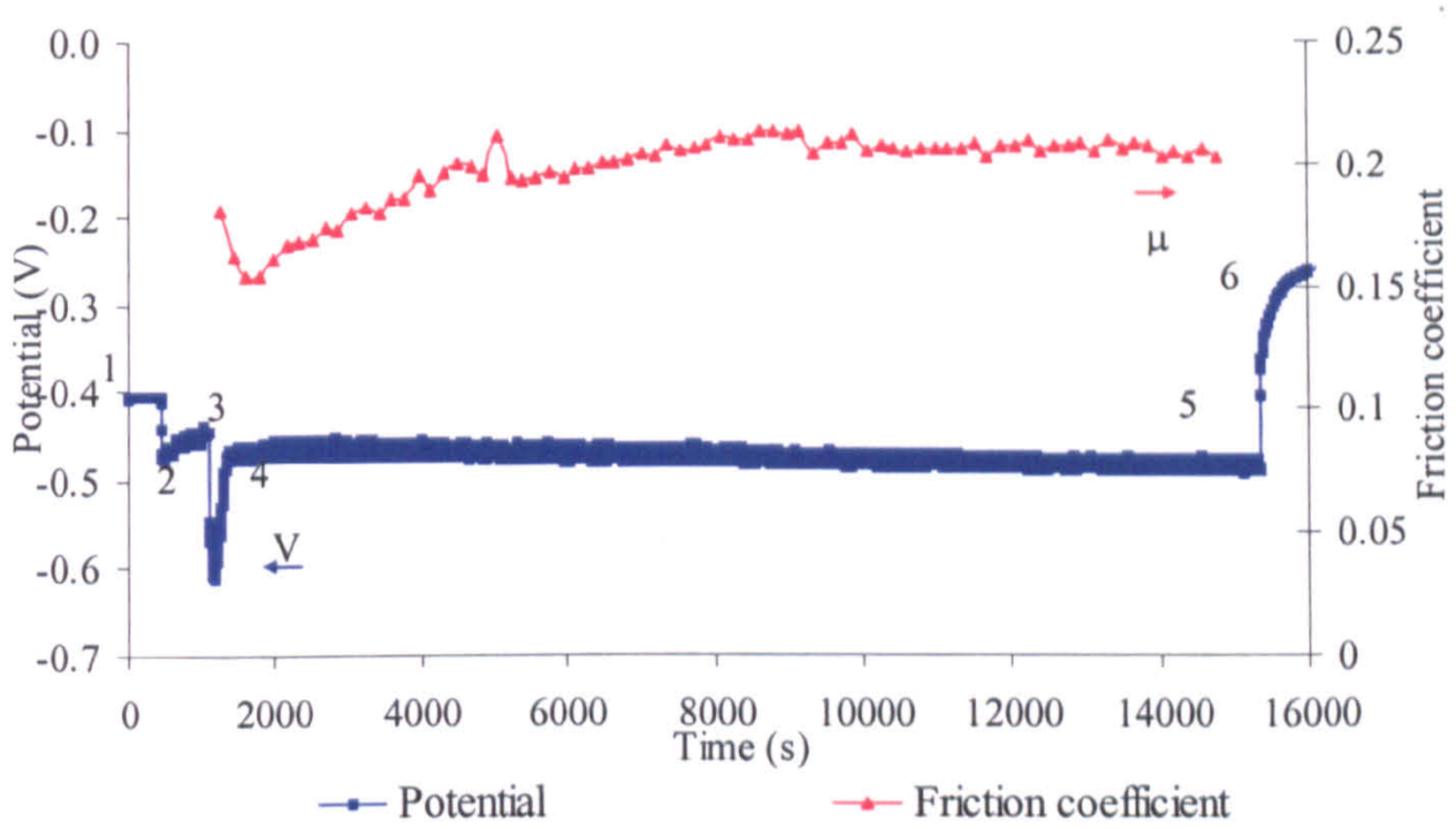
0.0
-0.1
-0.2
-0.3
-0.4
-0.5
-0.6
-0.7
Potential (V)
0.25
0.2
0.15
0.1
0.05
0
Friction coefficient
μ
1
2
3
4
5
6
V
0
2000
4000
6000
8000
10000
12000
14000
16000
Time (s)
Potential
Friction coefficient

(a)

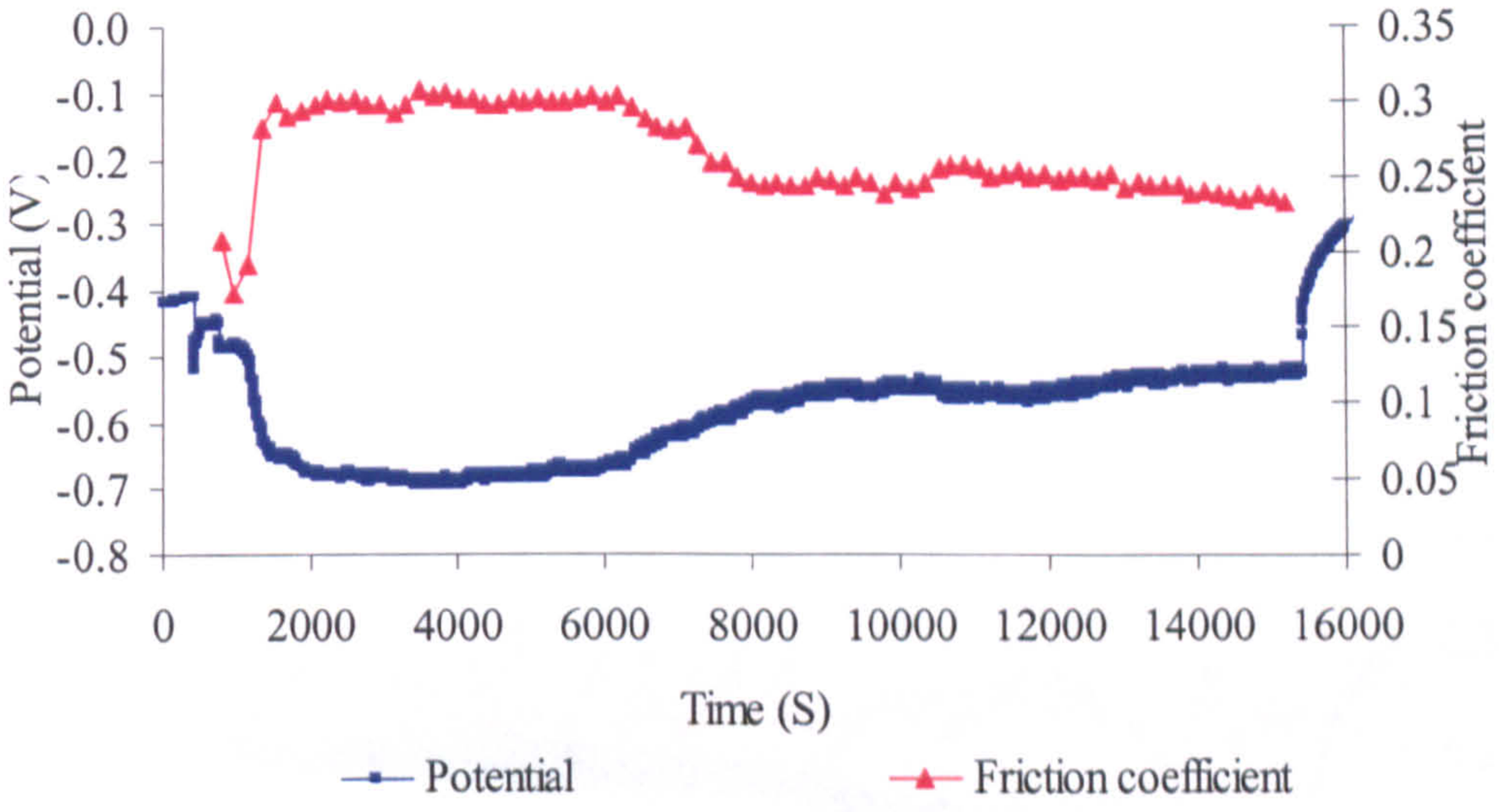
0.0
-0.1
-0.2
-0.3
-0.4
-0.5
-0.6
-0.7
-0.8
Potential (V)
0.35
0.3
0.25
0.2
0.15
0.1
0.05
0
Friction coefficient
0
2000
4000
6000
8000
10000
12000
14000
16000
Time (S)
Potential
Friction coefficient

(b)

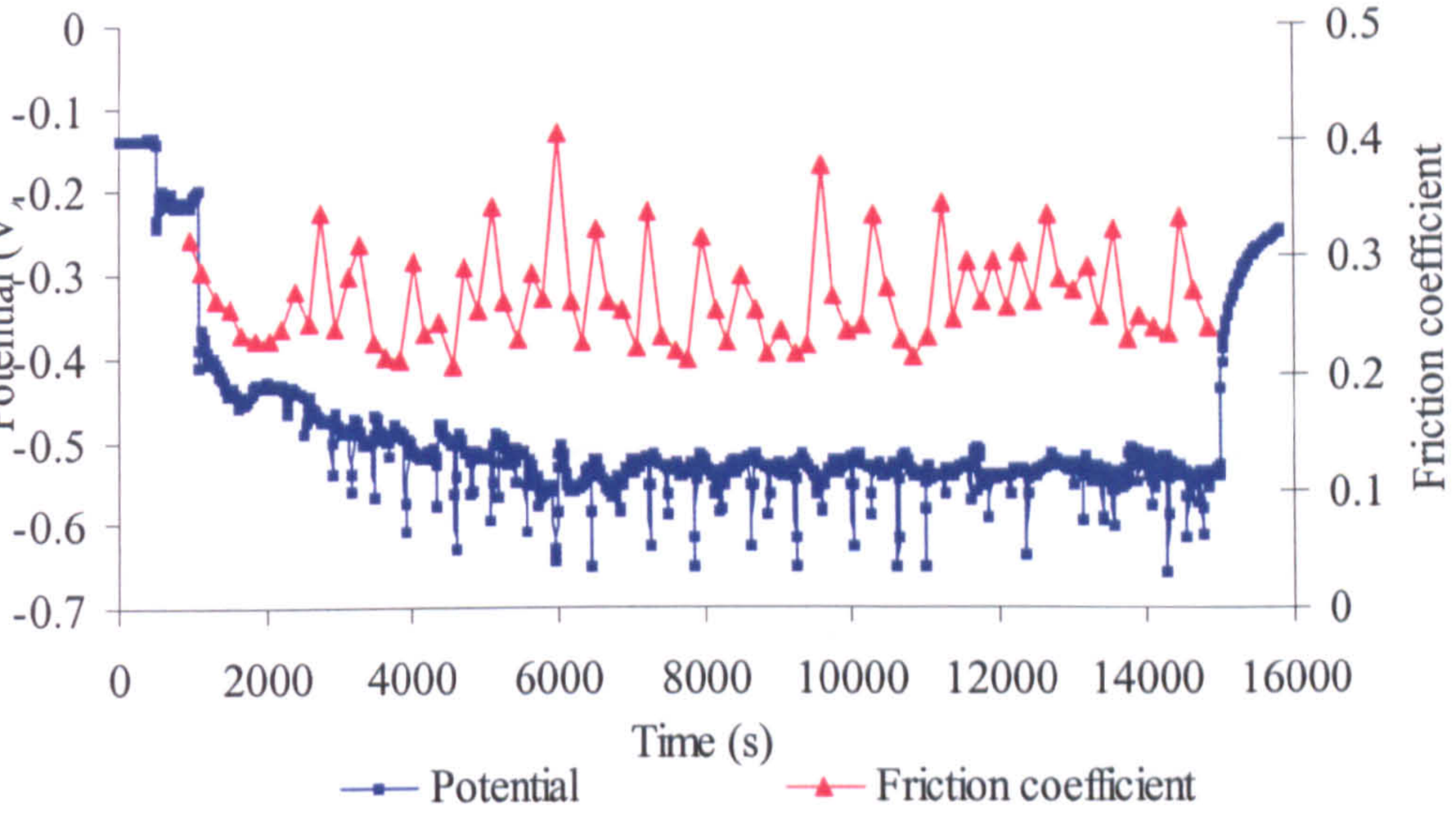

(c)

Figure 6-3 E_{corr} and μ versus time for (a) HC CoCrMo (b) LC CoCrMo (c) 316L in 50% serum for 4 hr tests

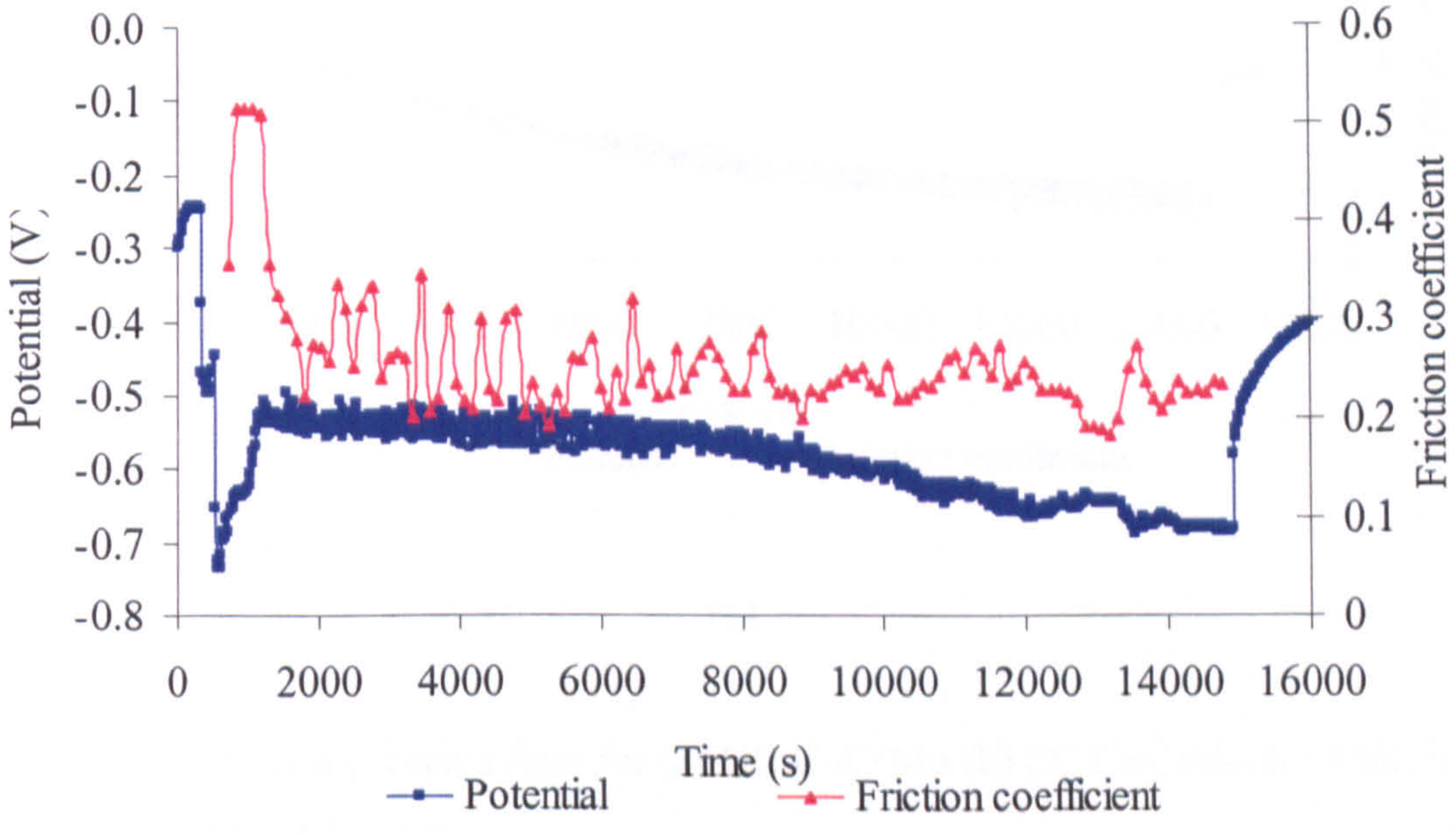

(a)

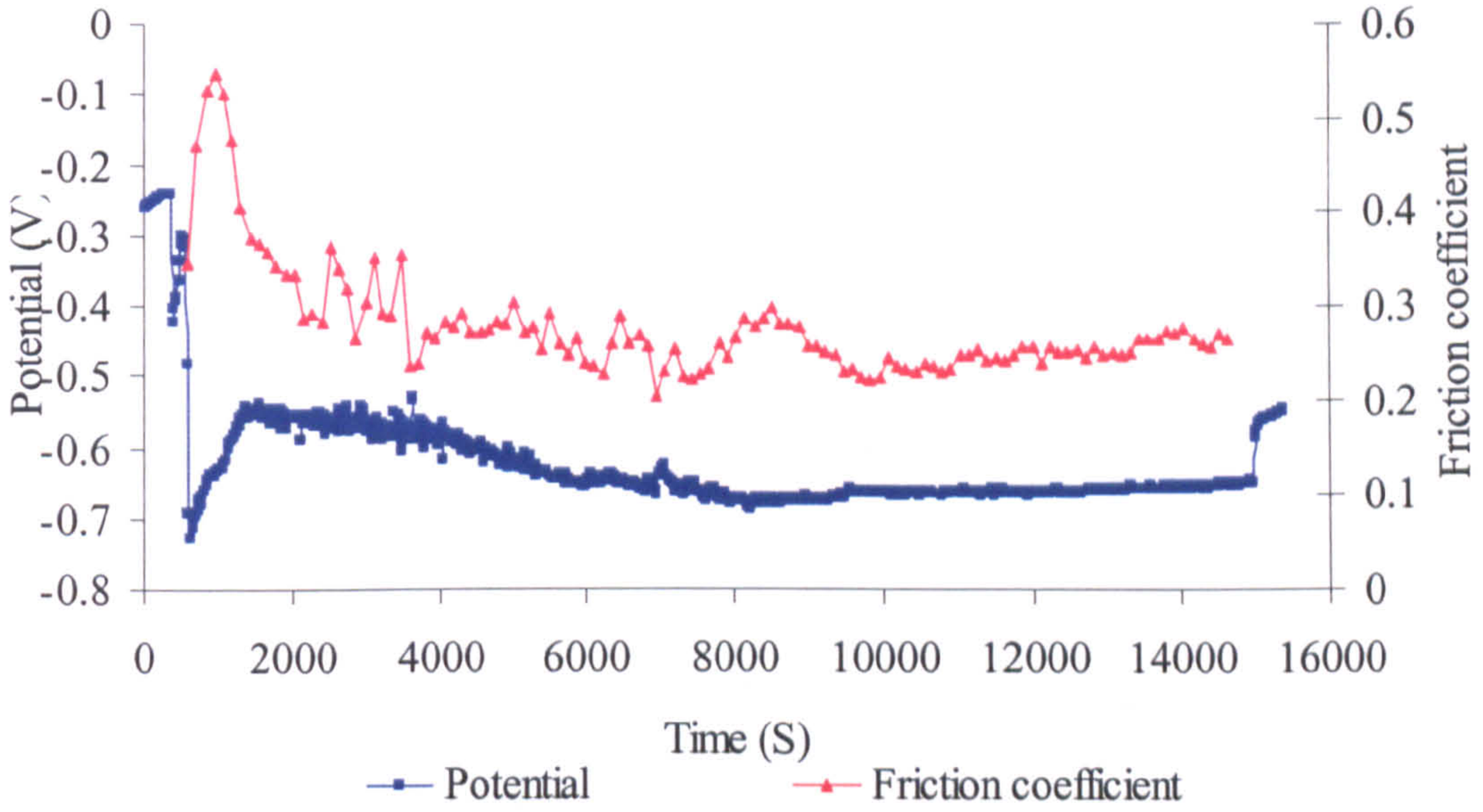

(b)

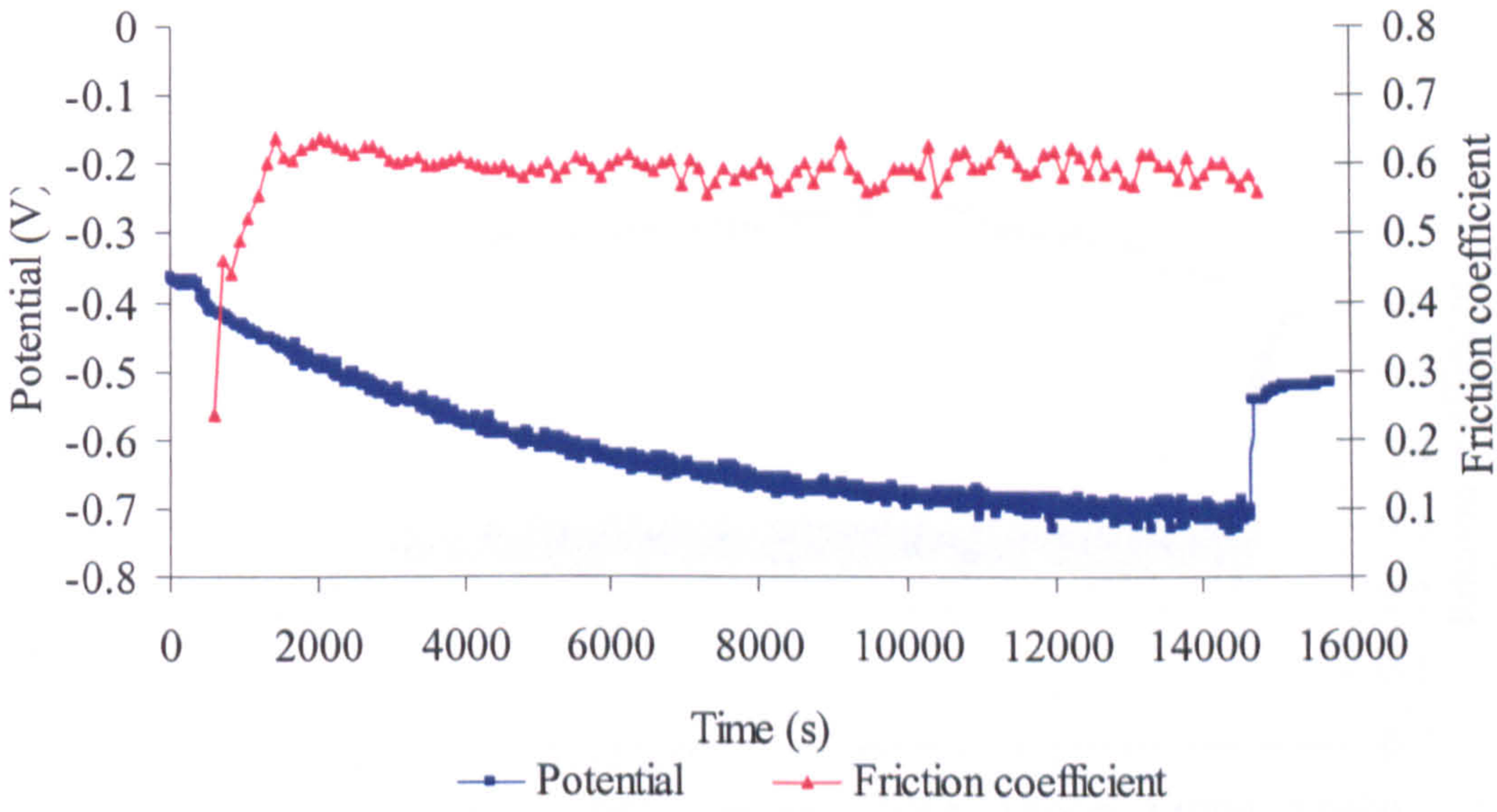

(c)

Figure 6-4 E_{corr} and μ versus time for (a) HC CoCrMo (b) LC CoCrMo (c) 316L in DMEM for 4 hr tests

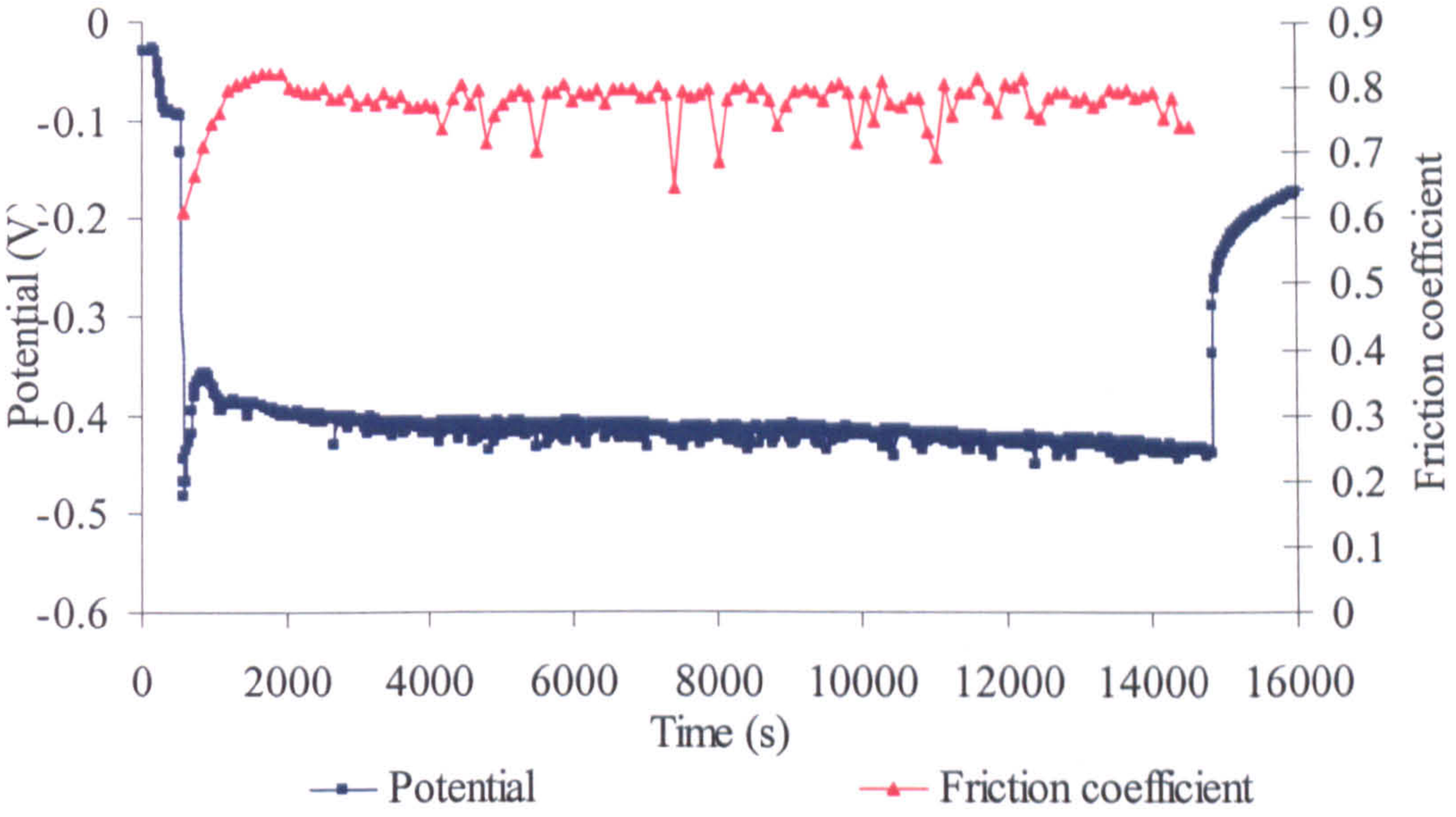
0
-0.1
-0.2
-0.3
-0.4
-0.5
-0.6
Potential (V)
0.9
0.8
0.7
0.6
0.5
0.4
0.3
0.2
0.1
0
Friction coefficient
0
2000
4000
6000
8000
10000
12000
14000
16000
Time (s)
Potential
Friction coefficient

(a)

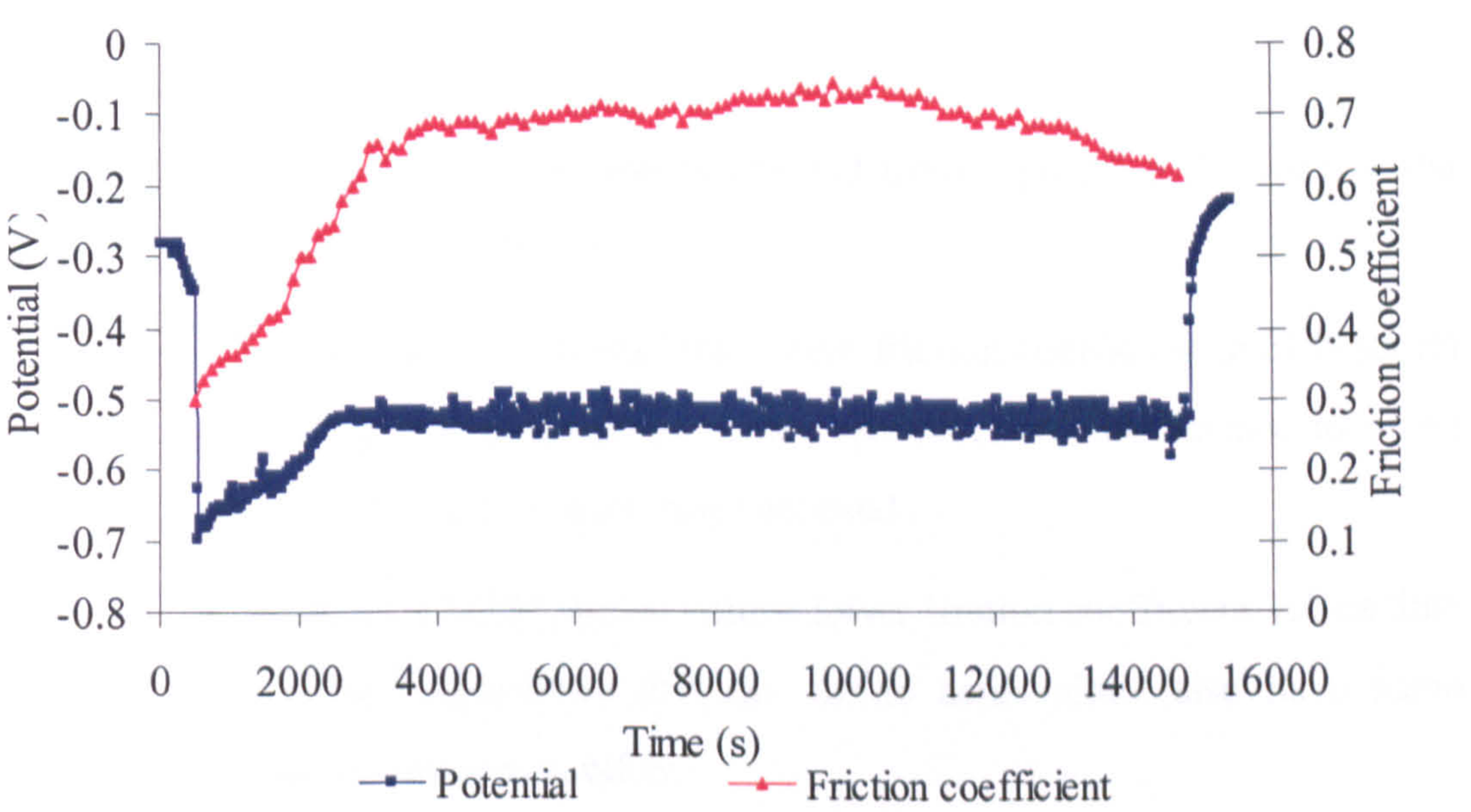
0
-0.1
-0.2
-0.3
-0.4
-0.5
-0.6
-0.7
-0.8
Potential (V)
0.8
0.7
0.6
0.5
0.4
0.3
0.2
0.1
0
Friction coefficient
0
2000
4000
6000
8000
10000
12000
14000
16000
Time (s)
Potential
Friction coefficient

(b)

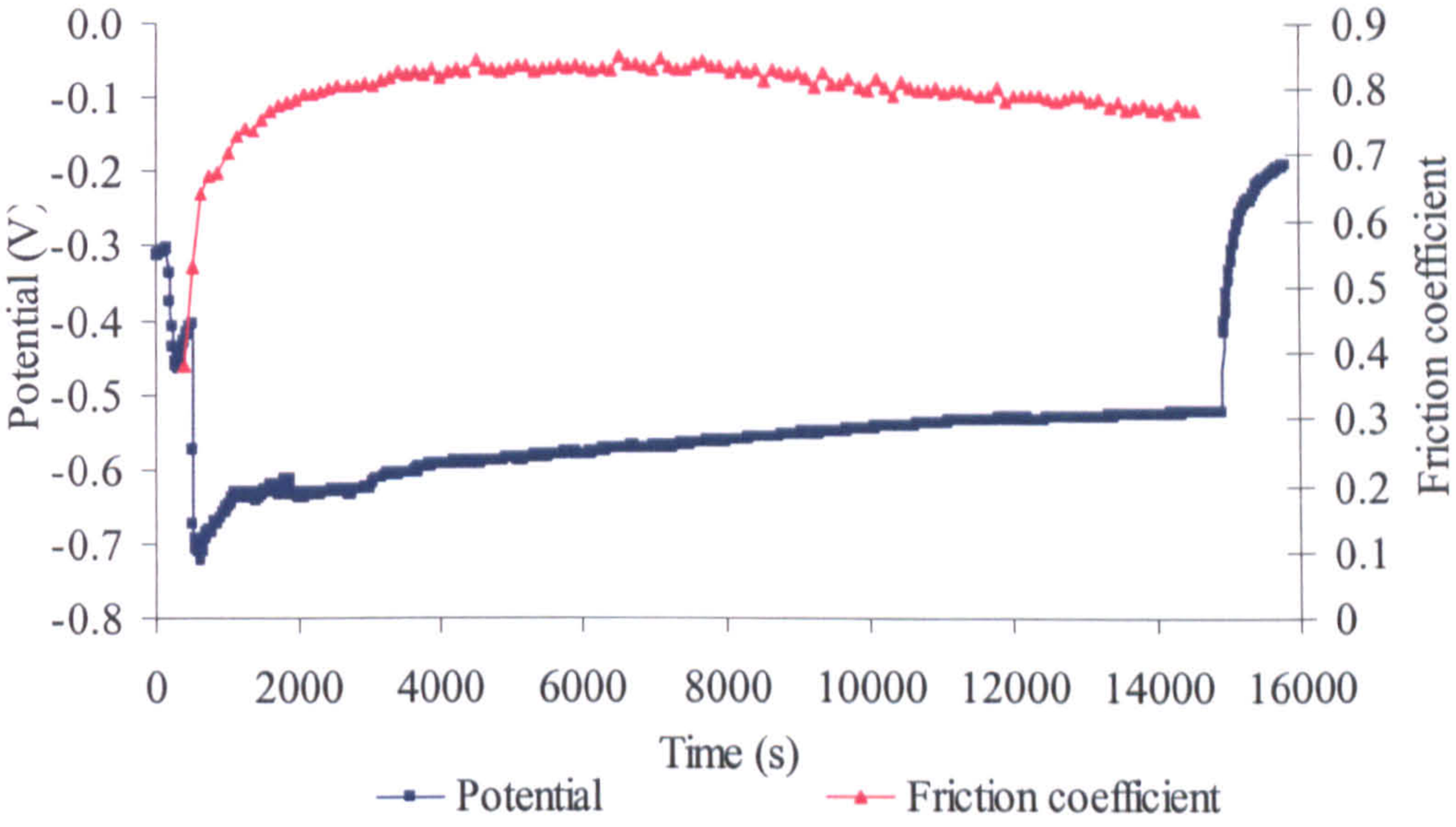

(c)

Figure 6-5 E_{corr} VS. time for (a) HC CoCrMo (b) LC CoCrMo (c) 316L in 0.36% NaCl for 4 hr tests

Some observations of the friction coefficient from Figure 6-3, Figure 6-4 and Figure 6-5 can be summarized below:

- All three materials showed the lowest friction coefficient in 50% serum indicating that proteins in serum can lubricate the surface to some extent under the test conditions adopted.
- In addition, DMEM showed much lower friction coefficient values than 0.36%NaCl suggesting that the amino acids alone also have some friction reducing capability.
- HC CoCrMo appeared to have the lowest friction coefficient and the most noble OCP with organic species involved (50% serum and DMEM). It seems that HC CoCrMo received a better lubrication benefit from proteins and amino acids.
- In 50% serum and DMEM, a more noble free corrosion potential corresponded a lower friction coefficient. However, in 0.36% NaCl, 316L had an exception. The behaviour may be related to the adsorption

of organic species and the passive film removal and re-formation mechanisms.

No carbide pluck out can be observed by optical microscopy and SEM. Figure 6-6 shows the wear groove for three materials in 50% serum. HC CoCrMo had a smooth groove (R_a 1.2μm) and the 316L wear scar was quite rough (R_a 6.3 μm). Figure 6-7 shows images taken from SEM. For LC CoCrMo, debris was observed in the wear scar and they seem to be ploughed. 316L appeared as a much rougher surface and cracks of the film can be seen (Figure 6-7 (c)). Images were also captured for the edge of the wear scar (Figure 6-8). HC CoCrMo showed a smooth transition from the scar to the un-rubbed surface (Figure 6-8 (a)). Slight plastic deformation can be seen on LC CoCrMo (Figure 6-8 (b)). For 316L, severe deformation was observed and some debris has been generated (Figure 6-8 (c)).

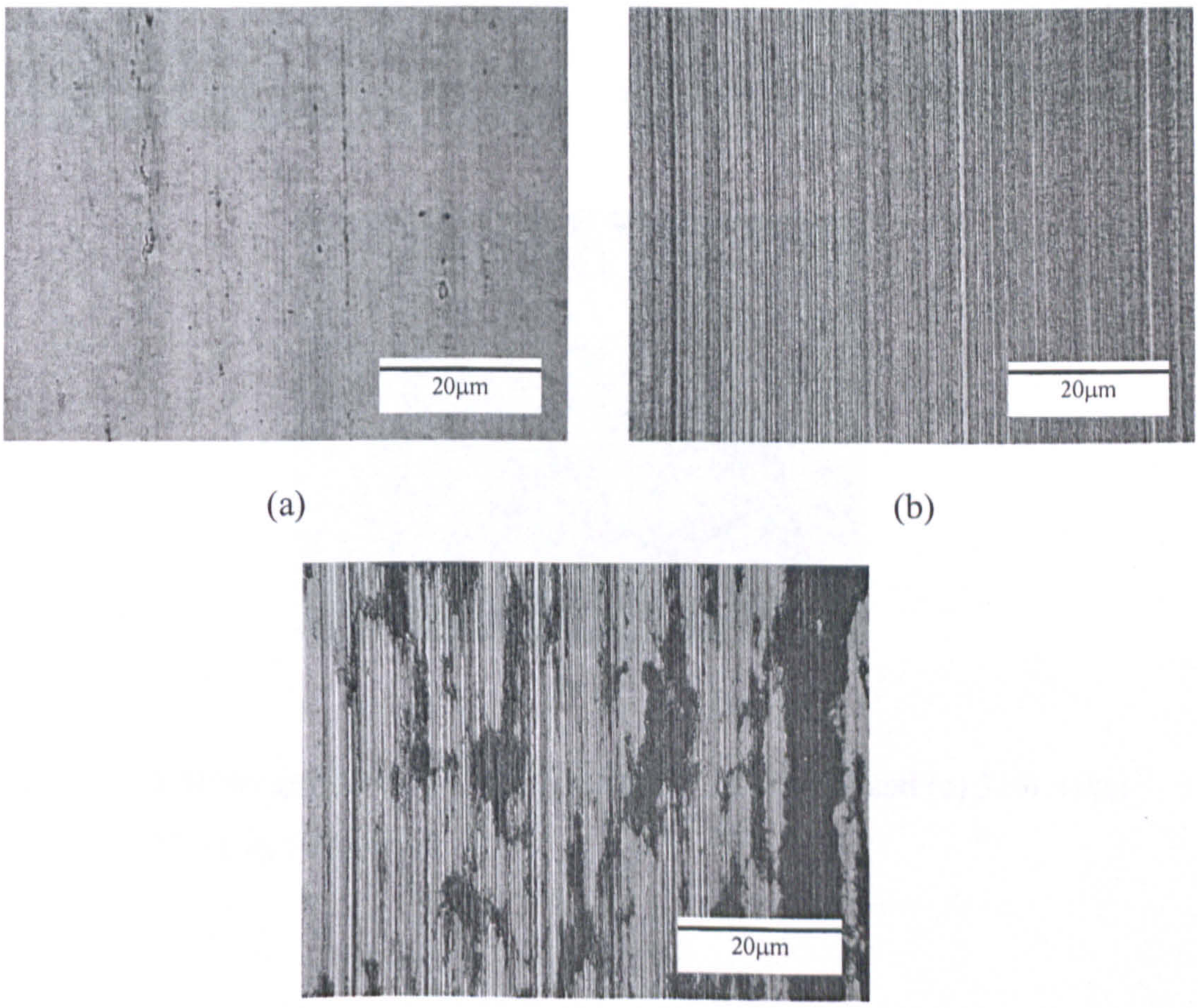

(a) (b)

(c)

Figure 6-6 Optical images for (a) HC CoCrMo (b) LC CoCrMo and (c) 316L taken after rubbing in 50% serum

At the free corrosion potential (E_{corr}) the passive film is being continually removed and reformed on the wear track. Corrosion processes were occurring under these conditions – the ionic species were released due to the charge transfer at the interface and it can potentially interact with the biological fluid constituents and affect the friction and wear response of that interface.

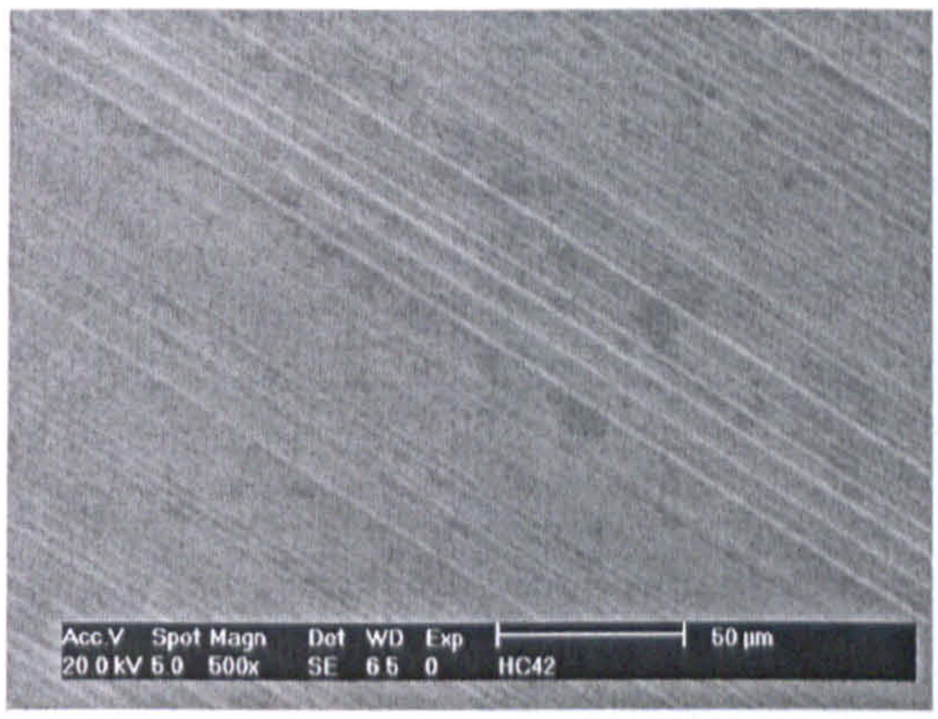

(a)

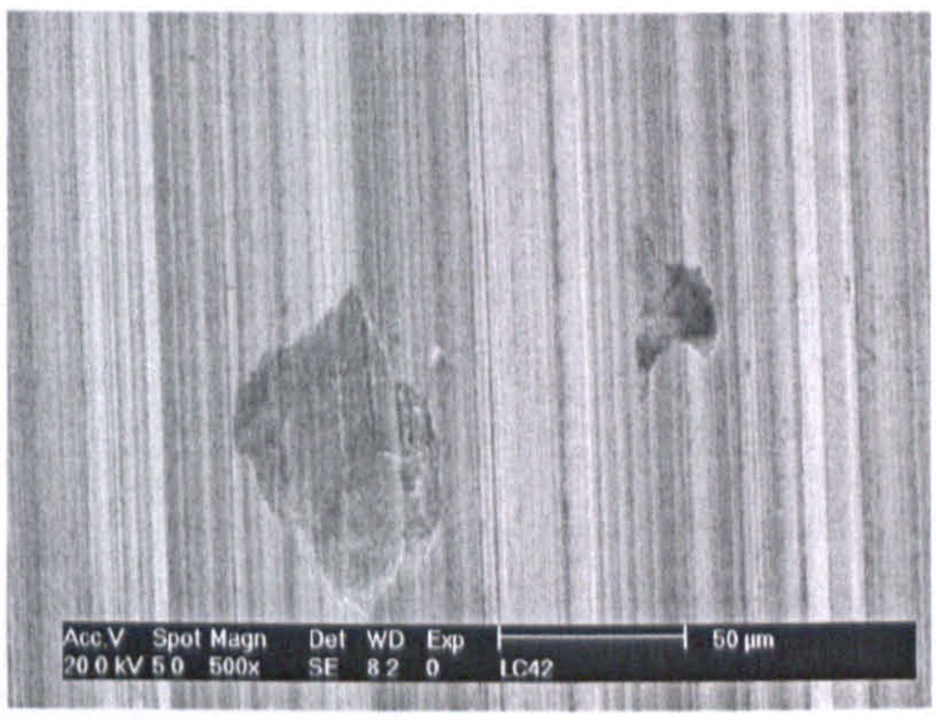

(b)

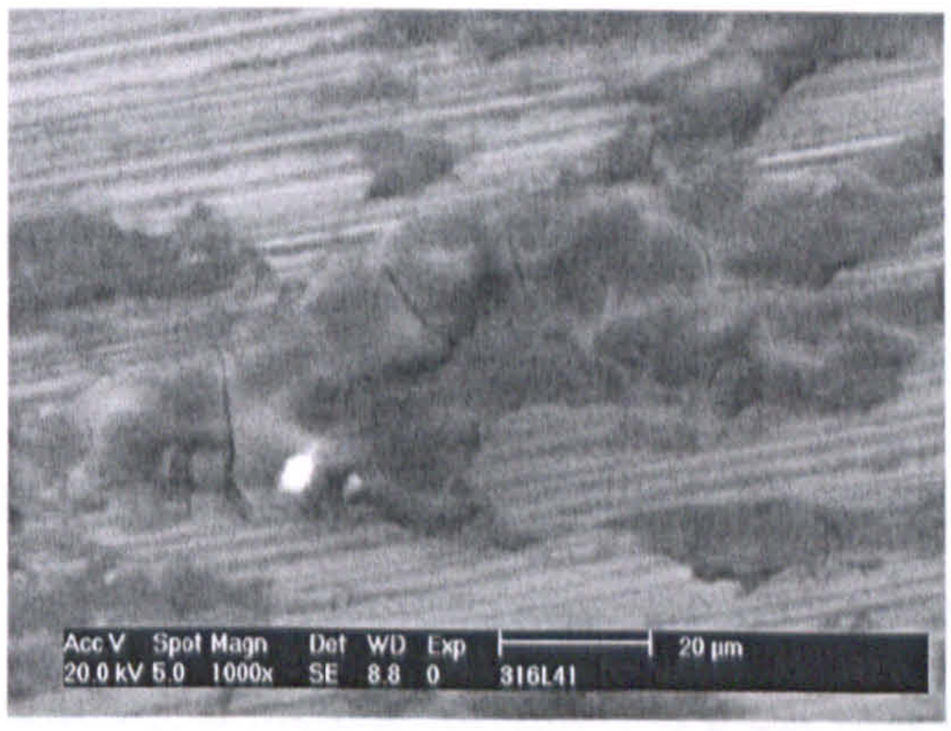

(c)

Figure 6-7 SEM images for (a) HC CoCrMo (b) LC CoCrMo and (c) 316L taken after rubbing in 50% serum

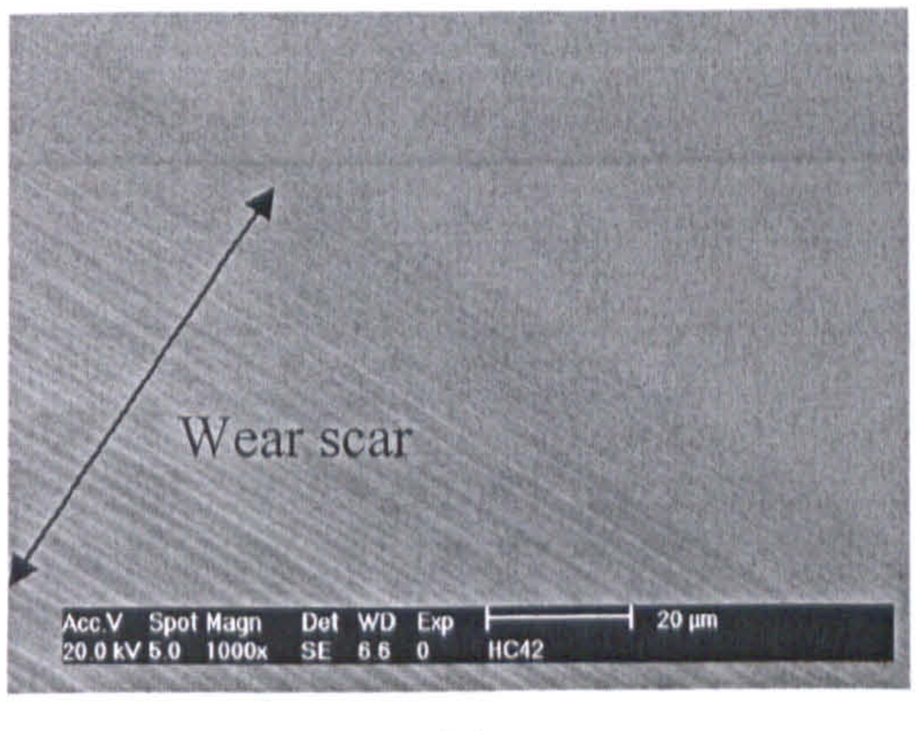

(a)

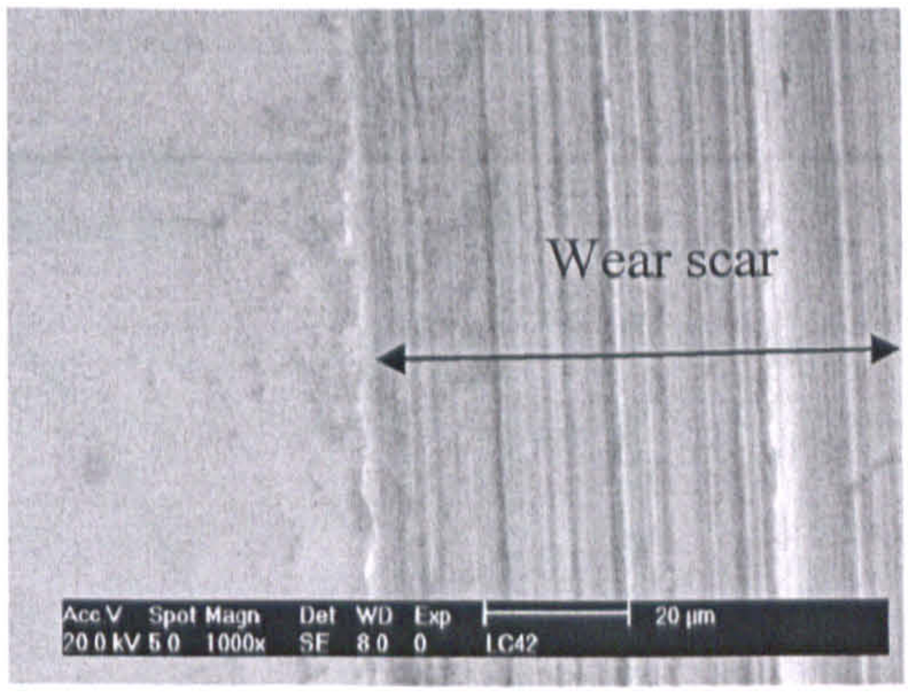

(b)

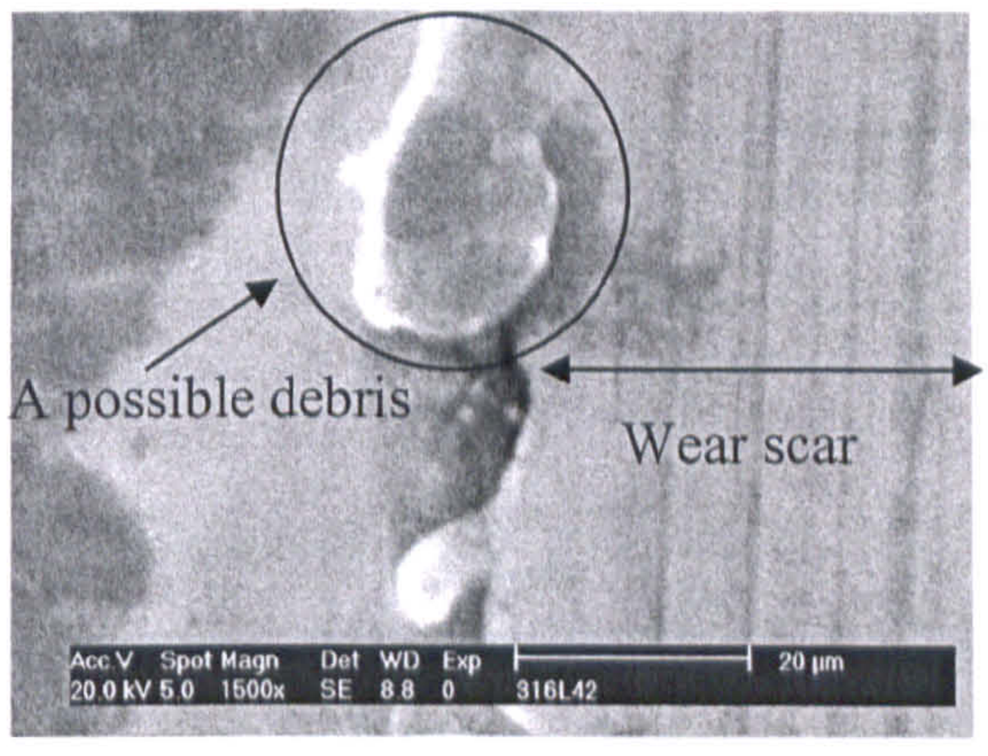

(c)

Figure 6-8 SEM images for the wear scar edge of (a) HC CoCrMo (b) LC CoCrMo and (c) 316L taken after rubbing in 50% serum

In Figure 6-9, the relationship between the friction force and the specimen potential and displacement over one cycle is shown. In terms of synchronising tribological and electrochemical measurements it is clear that there is a link between potential changes and friction/wear. The potential shifted in the active direction as the sliding started. As soon as the ball started to slow down (the sliding velocity decreased), the sample had an opportunity to rebuild the passive film (or win the competition between forming a passive film and the film being rubbed off) and hence the potential ennobled until the velocity returned to zero.

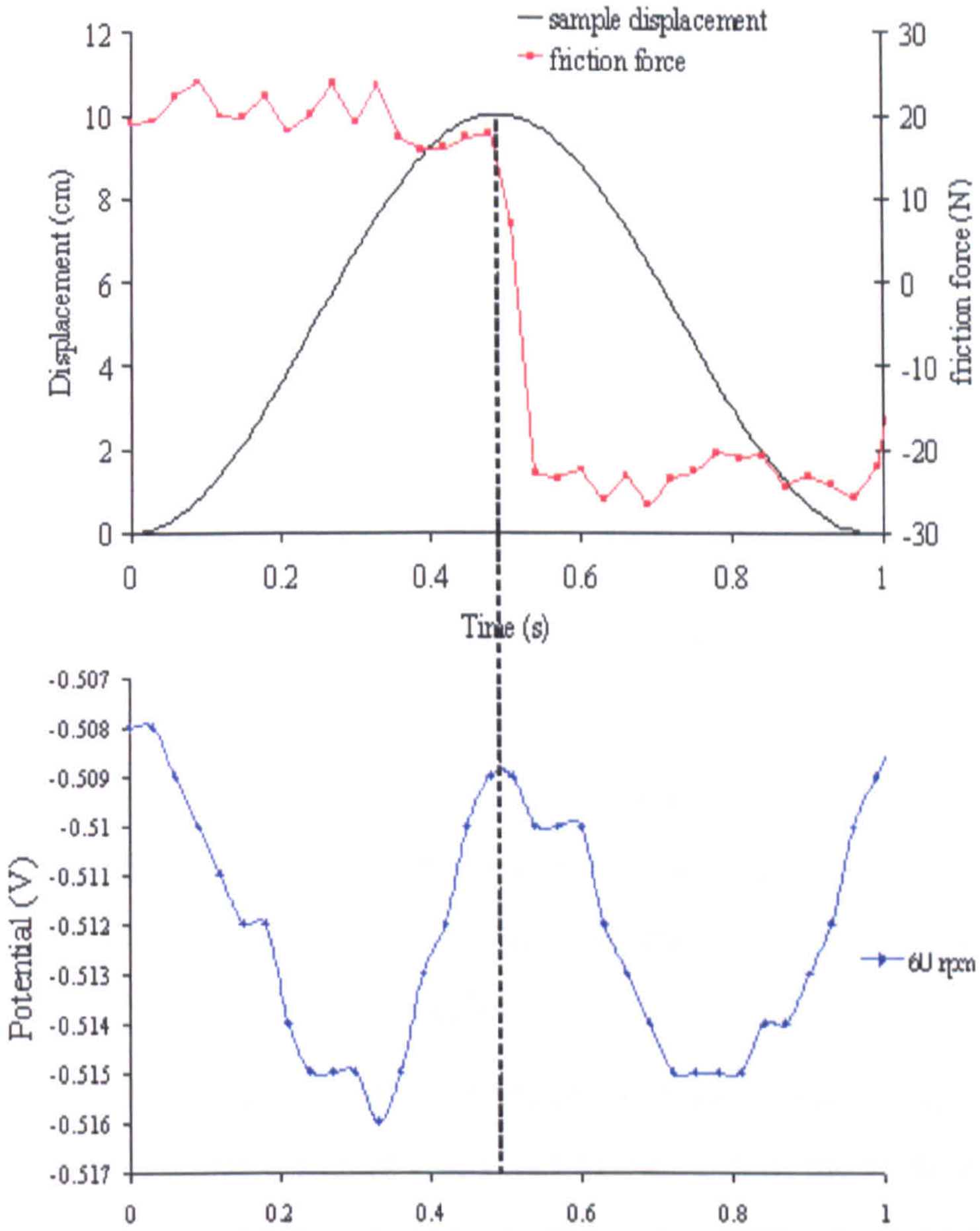

Figure 6-9 The relationship of potential, friction force and sample displacement in one cycle of reciprocation

6.3.2. Effect of wear on anodic polarization

Anodic polarization tests were carried out under sliding wear for the three materials in the three environments. These tests are able to tell whether

- the material corrosion behaviour changes compared to static conditions.

- the material degradation process (ion release) affected by tribological contacts.

Figure 6-10 shows the curves in both static conditions and under sliding for HC CoCrMo in 50% serum and 0.36% NaCl and the electrochemical response for this alloy is comparable for the other two alloys in 50% serum. The key aspect of the electrochemical response under sliding is the transition from passive to active behaviour.

Three clear regions can be determined from the anodic polarization scans as shown in Figure 6-10.

- In region 1, the current increased immediately as the potential is scanned from E_{corr} until the current reached a maximum value and starts to reverse. The continuous metal ion release was due to the tribological contacts and the electrochemical driving force.
- In region 2, the current remained at a low value but clearly the base line of the curve under sliding was close to the scan in the static condition. This has been reported to be the case in erosion-corrosion, cavitation-corrosion and abrasion-corrosion studies by numerous authors and is due to the removal of the passive film (i.e. the charge transfer barrier) [140]. But in erosion-corrosion etc. under water and sands impingement the current values are substantially greater than the passive currents under static conditions. In addition, oscillations in current were observed, again associated with the depassivation/repassivation transient current response [141] (Figure 6-10 (a)).
- In region 3, the passive film brokedown therefore there was a significant enhancement of corrosion due to wear. This is one important aspect of the corrosion/wear interactions as discussed later.

In the potential range between 0V and 0.4V (region 2) in Figure 6-10 (a) an interesting pseudo-repassivation regime can be seen. This is likely to be due to the enhanced binding of proteins as the wear process accelerates release of Co^{2+}. The proteins then act to block charge transfer at the metal/solution interface by forming a corrosion product (crystalline) or an organometallic complex. In comparison to Figure 6-10 (b), in 0.36% NaCl, though there were still three regions obtained, in region 2, the current remained the level at which the maximum value which materials in region 1 had achieved at. Due to just oxides/hydroxides (passive film) presented in region 2 in 0.36% NaCl, no severe reduction of current can be observed. It confirms again that there was a passive film with an organometallic complex on samples surface when materials were in 50% serum and DMEM.

In terms of the passive film breakdown, even through when materials were under tribological contact, the passive films was continuously and locally removed/damaged, repassivation was rapidly taking place in region 2. When the potential reached a certain value (E_b), the passive film (including both in the wear track and out of the wear track) broke down. However, it seems that when tribology was involved, the overall breakdown potential was lower than in static conditions for materials in all solutions. The value of the breakdown potential under tribology contact is the mixed breakdown potential of the wear scar and the area outside of the wear scar. With organic species involved, such as in 50% serum and DMEM, beside the passive film breakdown on the wear area and un-worn area, E_b also represents the breakdown of the organometallic layer. It may result in the release of metal ions from the organometallic formation.

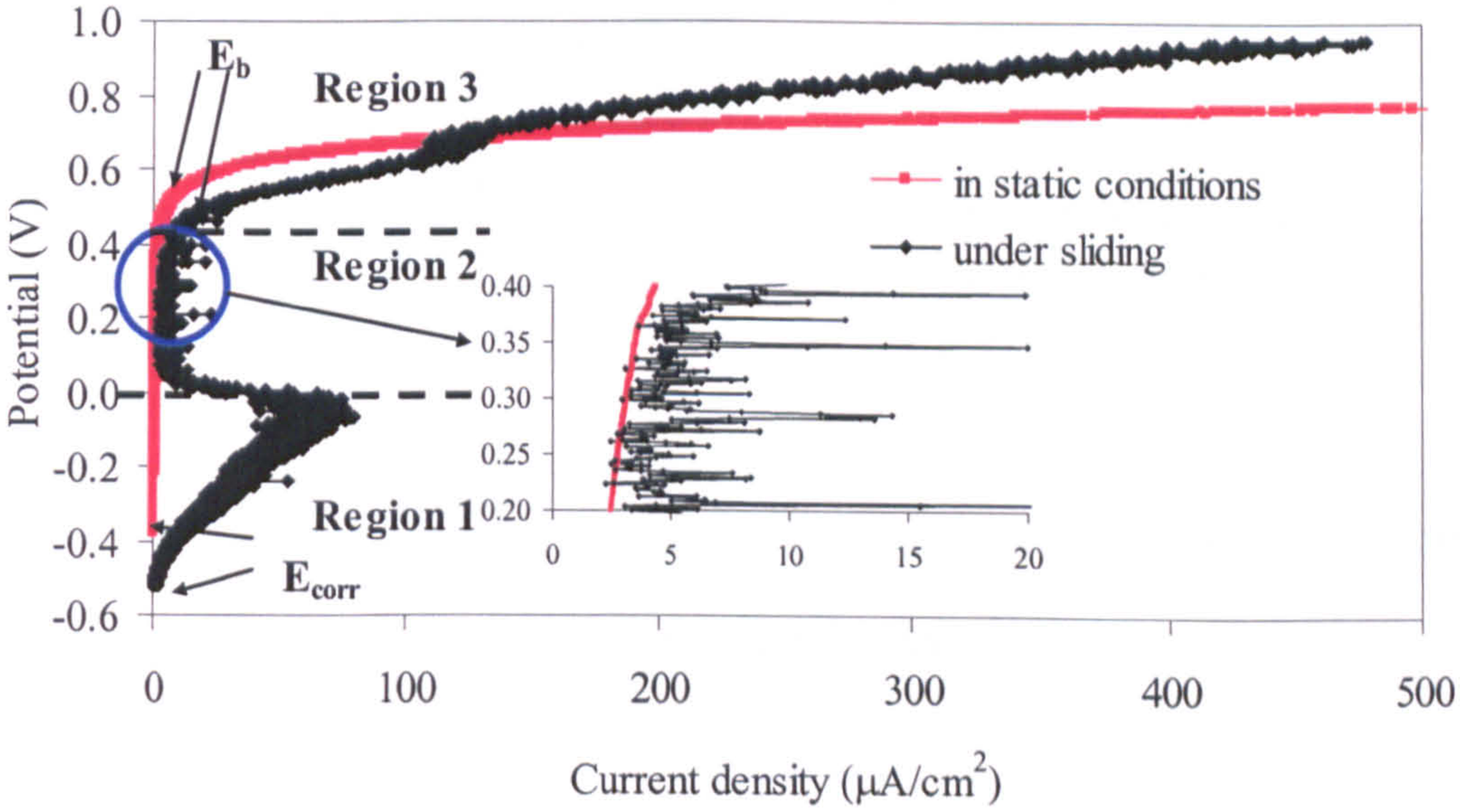
Potential (V)
Current density (μA/cm²)
Region 1
Region 2
Region 3
E_b
E_corr
in static conditions
under sliding

(a)

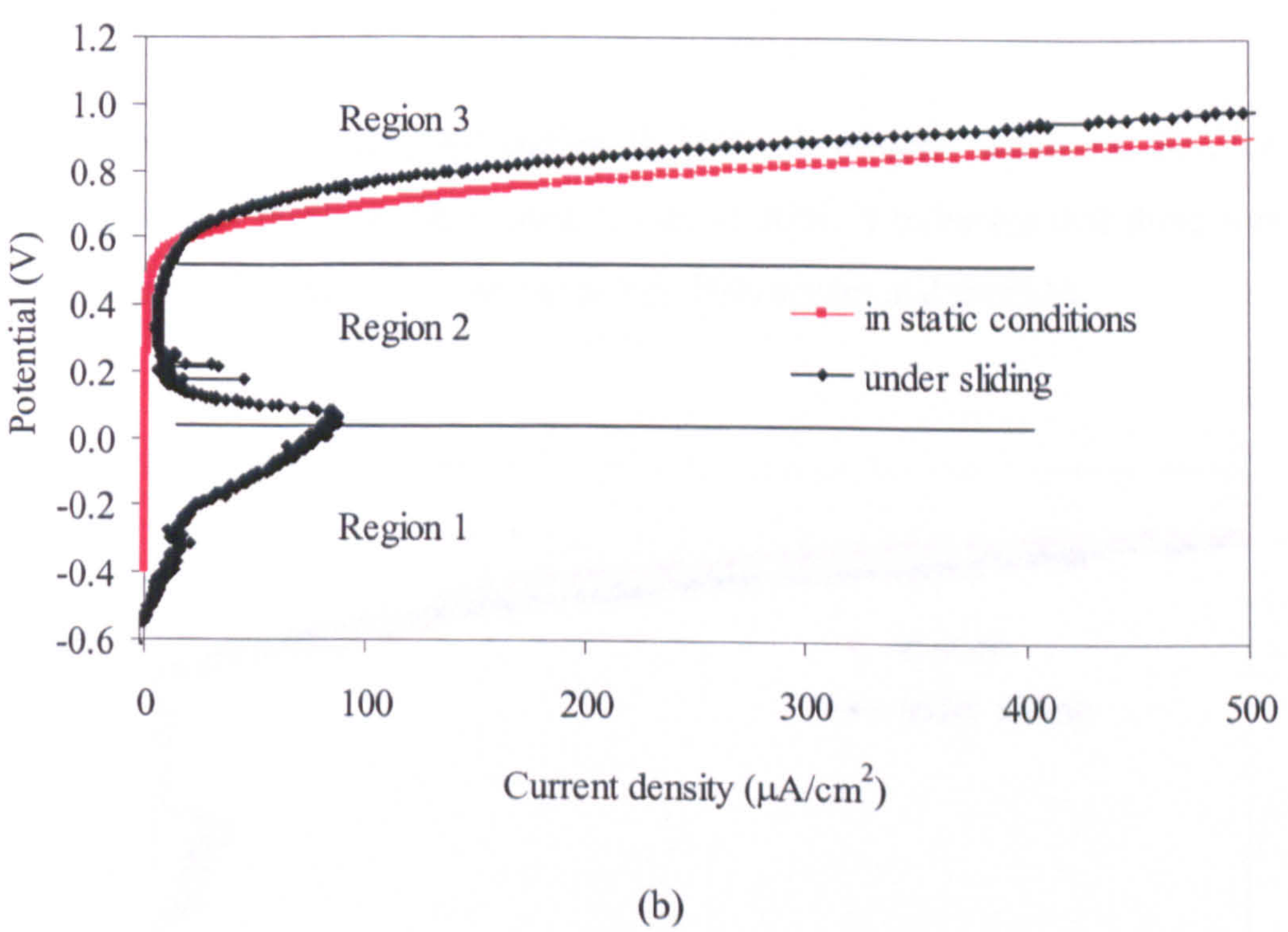
Potential (V)
Current density (μA/cm²)
Region 1
Region 2
Region 3
in static conditions
under sliding

(b)

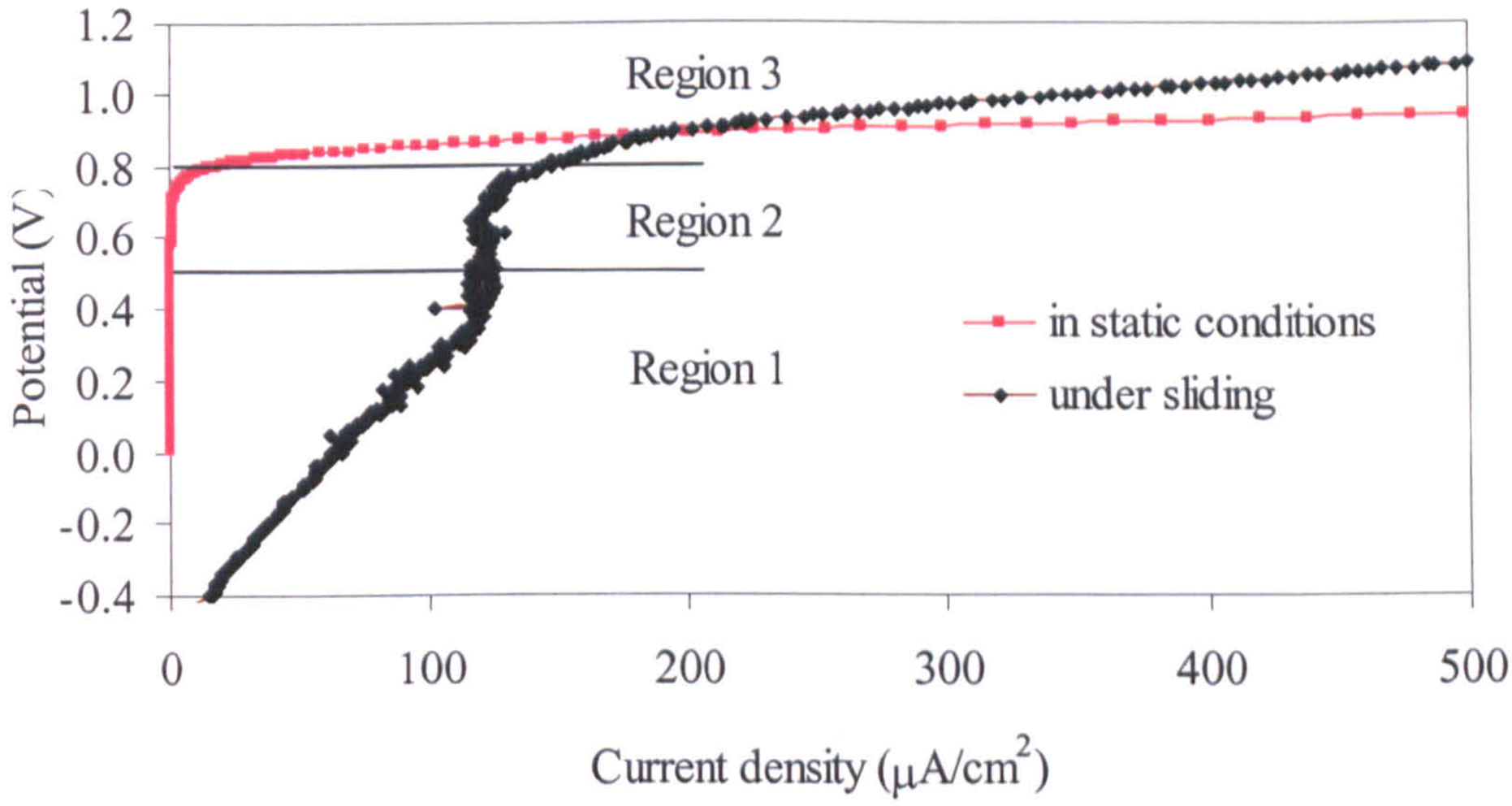

(c)

Figure 6-10 Comparison of HC CoCrMo anodic polarization in static and under sliding for in (a) 50% serum, (b) DMEM and (c) 0.36% NaCl

Figure 6-11 presents AP curves of 316L in different solutions. Similar with CoCrMo alloys, there are three regions can be seen. It indicates that there was also an organometallic formation during tests in 50% serum and DMEM.

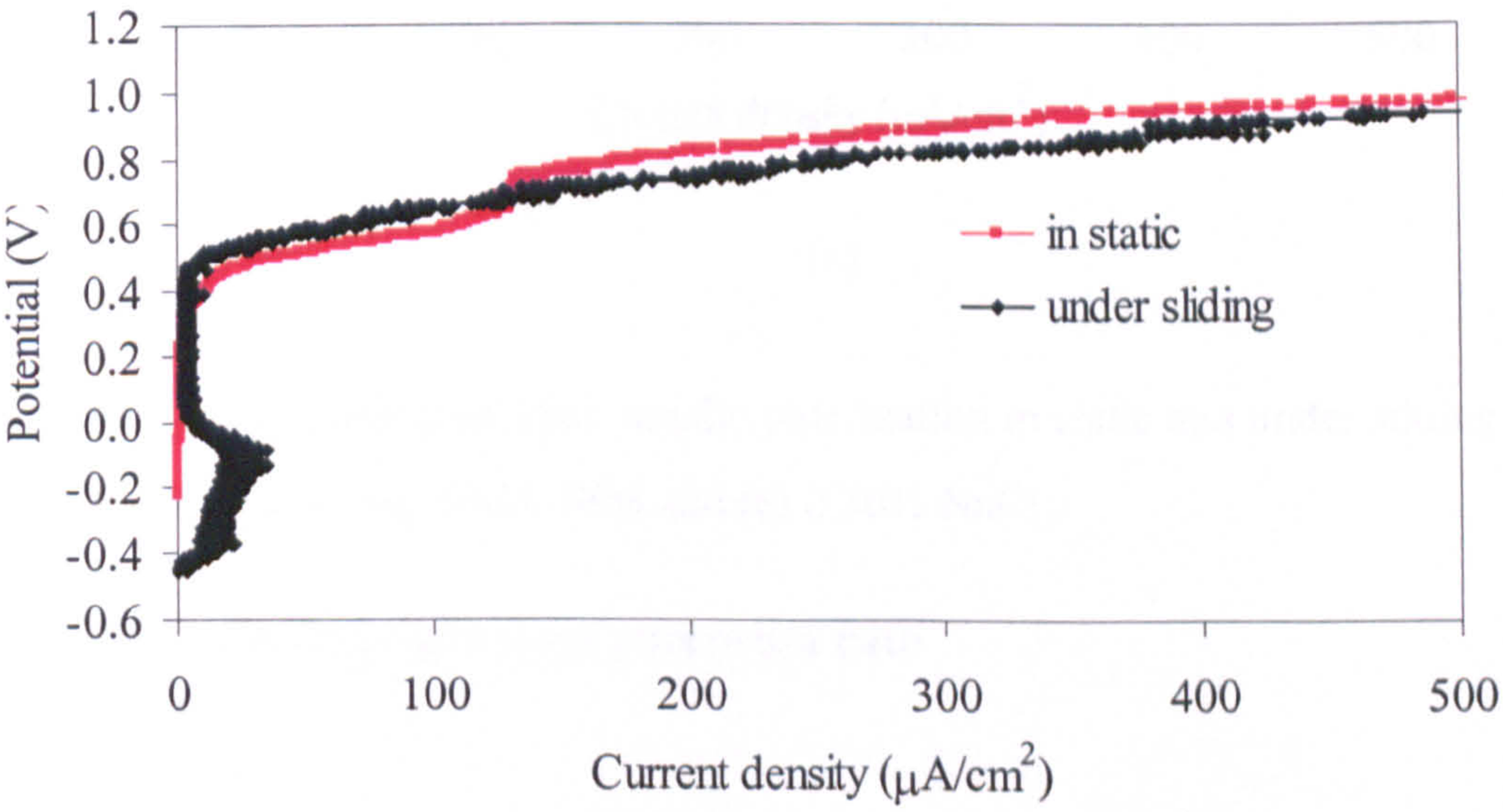

(a)

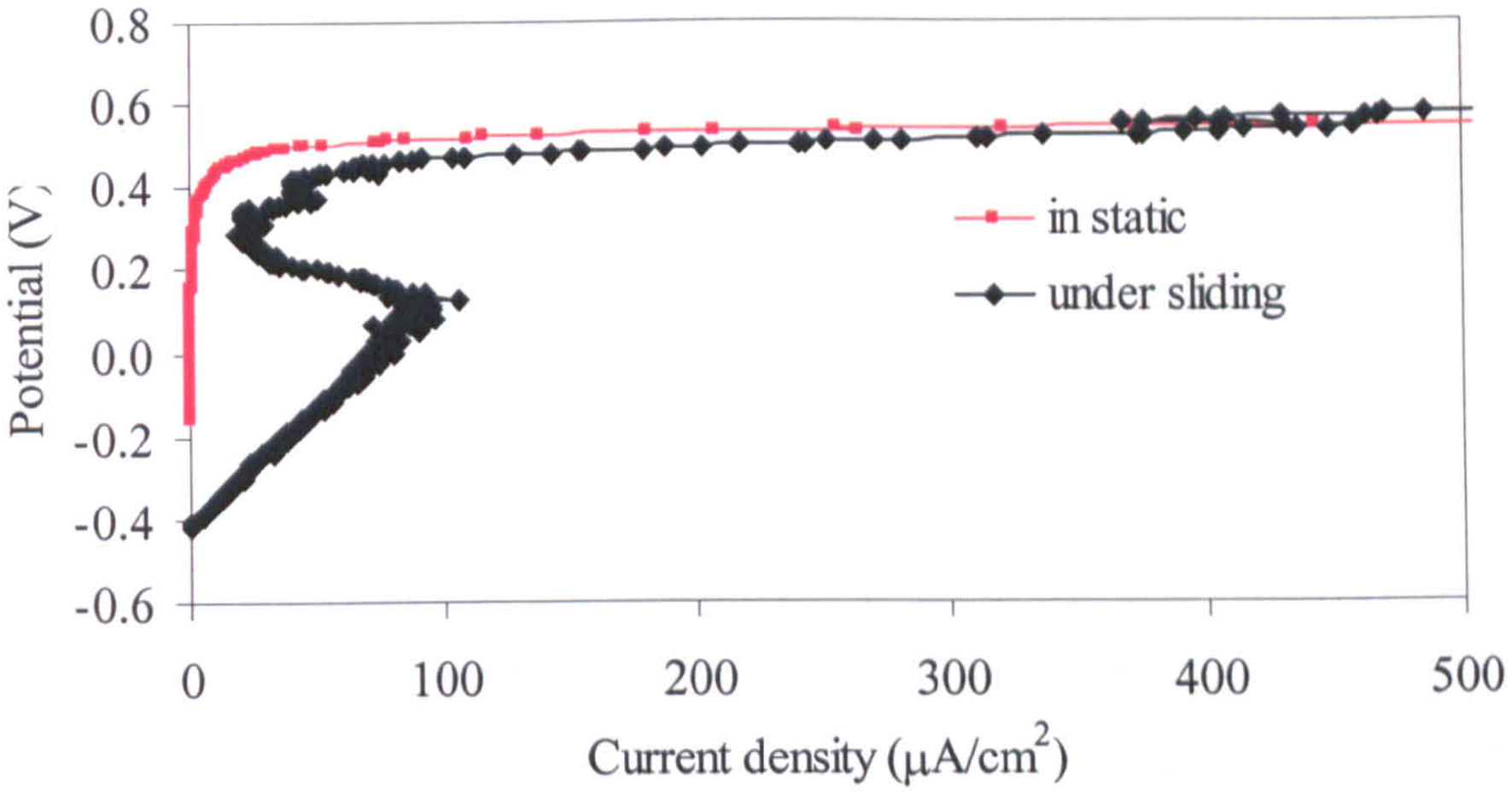

(b)

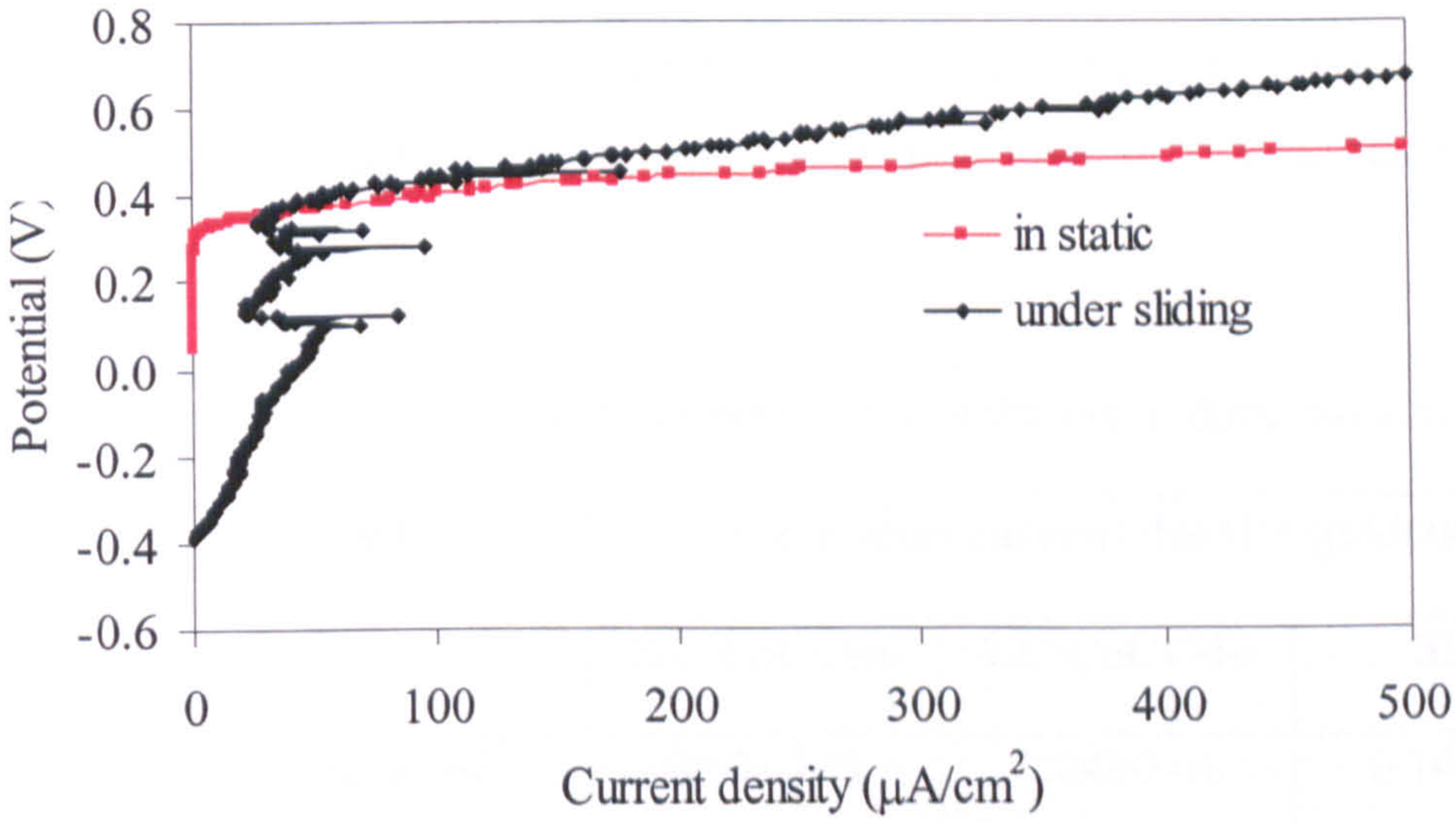

(c)

Figure 6-11 Comparison of 316L anodic polarization in static and under sliding for in (a) 50% serum, (b) DMEM and (c) 0.36% NaCl

6.3.3. The tribology effect on corrosion rate

Table 6-2 compares the corrosion current density for HC CoCrMo in two different conditions: in static and under rubbing. The Tafel extrapolation method

was used to determine the corrosion current density value. Details are discussed in Chapter 2. From Table 6-2, some observations can be obtained:

- Tribological contacts certainly can accelerate the charge transfer and increase the corrosion current density. Due to the fact that the corrosion current density can represent the material degradation caused by corrosion, the current density here can be used to show some extent of the tribology effect on corrosion.
- The corrosion current density is about 15 times greater for HC CoCrMo in 50% serum under rubbing than in static conditions. LC CoCrMo and 316L showed an increase by a factor of 30 under the same conditions.
- 316L had the greatest corrosion current density in all three environments.
- It seems that the extent of wear effect on corrosion is very much material and solution dependent. With proteins involved, the corrosion current density under rubbing is less than in 0.36% NaCl for all materials.

Table 6-2 Results of Corrosion current density for materials in three environments

Solution	**Condition**	**Corrosion current density ($\mu A/cm^2$)**		
		IIC CoCrMo	**LC CoCrMo**	**316L**
50% serum	**In static**	0.04±0.01	0.04±0.01	0.14±0.04
	Under rubbing	0.68±0.03	1.58±0.04	6.10±0.07
DMEM	**In static**	0.03±0.01	0.03±0.01	0.06±0.02
	Under rubbing	0.69±0.03	1.10±0.05	4.20±0.06
0.36% NaCl	**In static**	0.03±0.01	0.03±0.01	0.04±0.01
	Under rubbing	0.69±0.03	1.60±0.04	4.30±0.06

6.3.4. Linear polarization resistance of materials

To assess the corrosion damage alone the polarization resistance, R_p was measured by the linear polarization method. The reference electrode (RE) was placed very close to the working electrode (about 4mm) to reduce the interaction from the different fluids, which also have inherent resistance. This measurement quantifies the pure electrochemical damage and therefore excludes the damage that occurs when corrosion affects wear. Figure 6-12 shows the linear polarization curves for LC CoCrMo in 50% serum. The results are then converted into R_p values and presented in Figure 6-13 for materials in 50% serum. In static conditions, R_p represents the resistance of the passive film to corrosion. In this study, under tribological contacts, R_p is considered from both the wear track and outside the wear. It can be treated as a parallel connection of R_{p1} (wear scar) and R_{p2} (outside the scar).

- As expected the R_p values were consistently higher for HC CoCrMo than for LC CoCrMo and 316L stainless steel.
- For HC CoCrMo, the R_p stabilized after an initial high value period. For LC CoCrMo, R_p increased during the running-in regime and then stabilized.
- An unstable R_p under sliding was observed on 316L in 50% serum, but a general decrease can be seen in the initial period. The observation of R_p oscillation on 316L is consistent with previous findings where an unstable electrochemical response was linked to the instabilities as the passive film was removed and reformed.

Figure 6-14 and Figure 6-15 show the linear polarization resistance for materials in DMEM and 0.36% NaCl. Similar observations can be made:

- HC CoCrMo showed the greatest linear polarization resistance.
- R_p stabilized after an initial period.

- For 316L, the oscillations were smaller than in 50% serum.

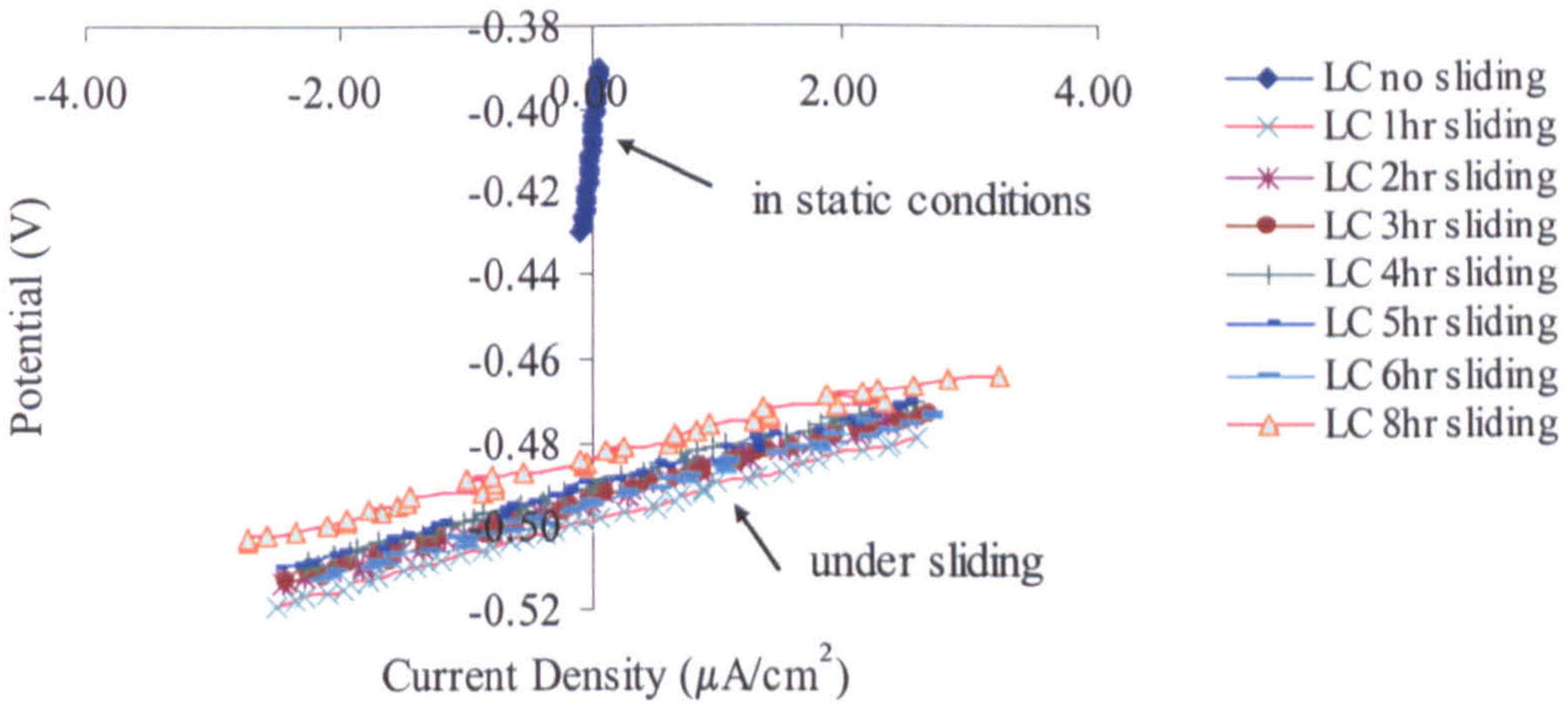

(a)

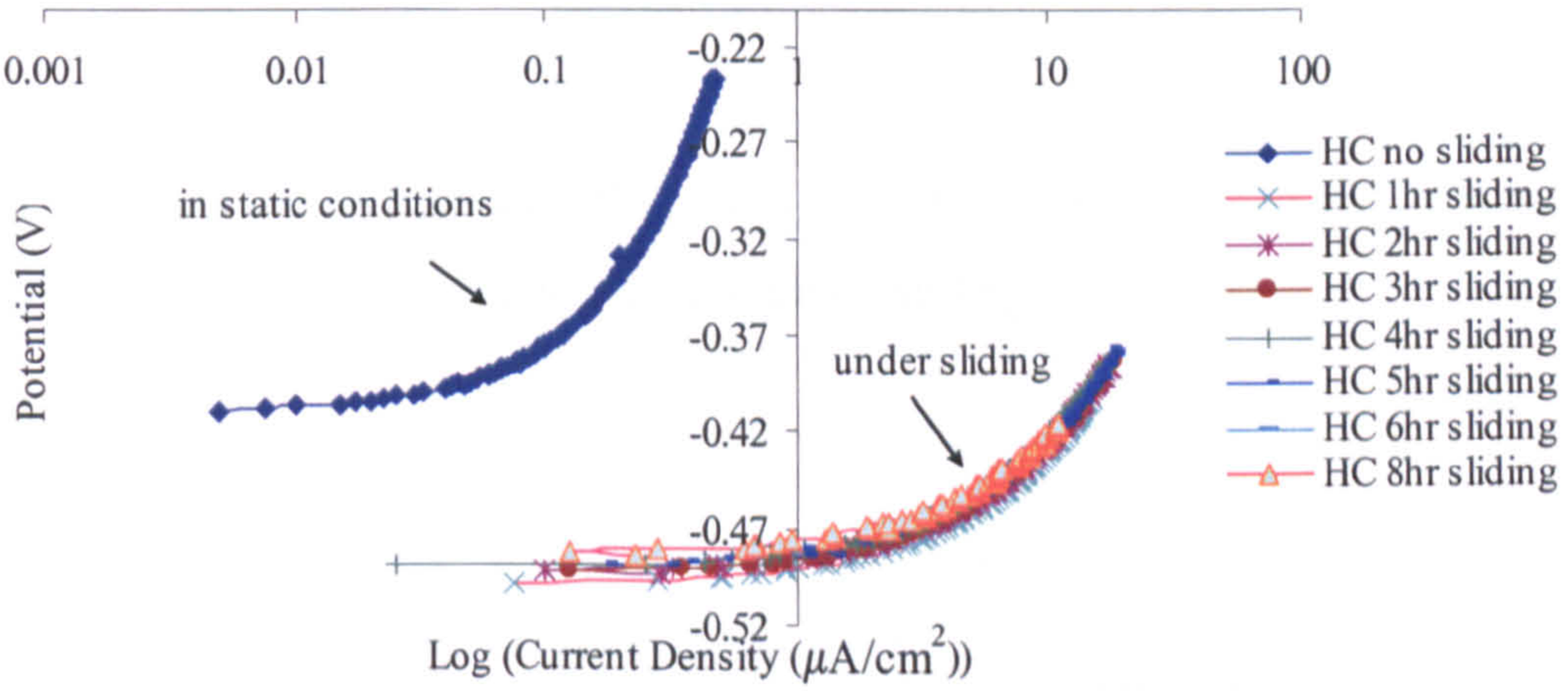

(b)

Figure 6-14 Linear polarization scans for (a) LC CoCrMo (E-i) and (b) HC CoCrMo (E-log(i)) in 50% serum. Measurement was made every hour during rubbing

In static conditions, the linear polarization resistance presents the resistance of a uniform passive film. Normally, the value is over 1 million Ohms/cm^2 [141]. Comparisons are made as below:

- Tribological contacts reduced the polarization resistance by as much as 20 to 120 times depending on material and environment.

- The lowest R_p was observed in 50% serum for all materials both in static and under sliding.

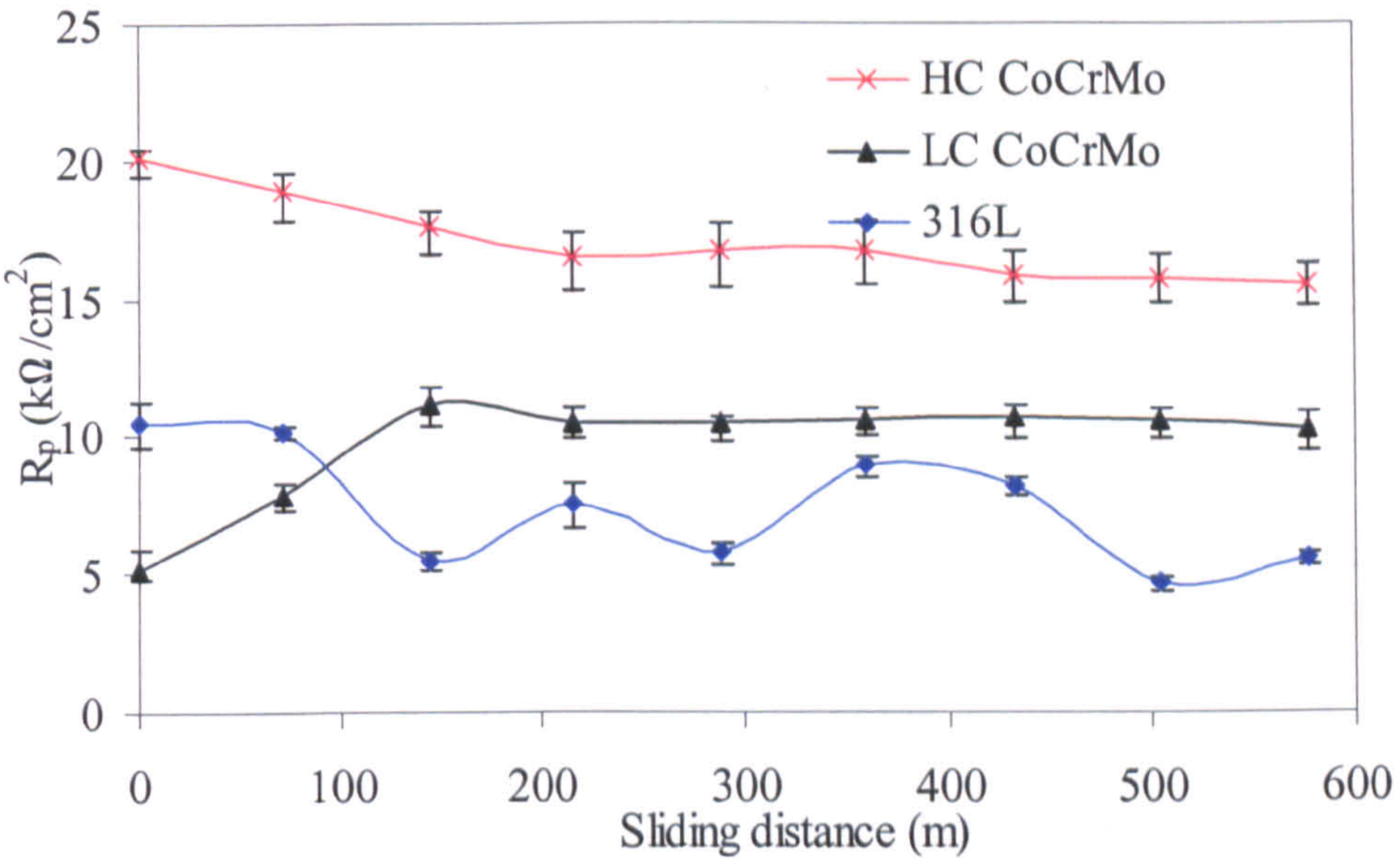

Figure 6-15 Polarization resistance (R_p) for HC CoCrMo, LC CoCrMo and 316L in 50% serum up to 600 metres (8 hours) under sliding

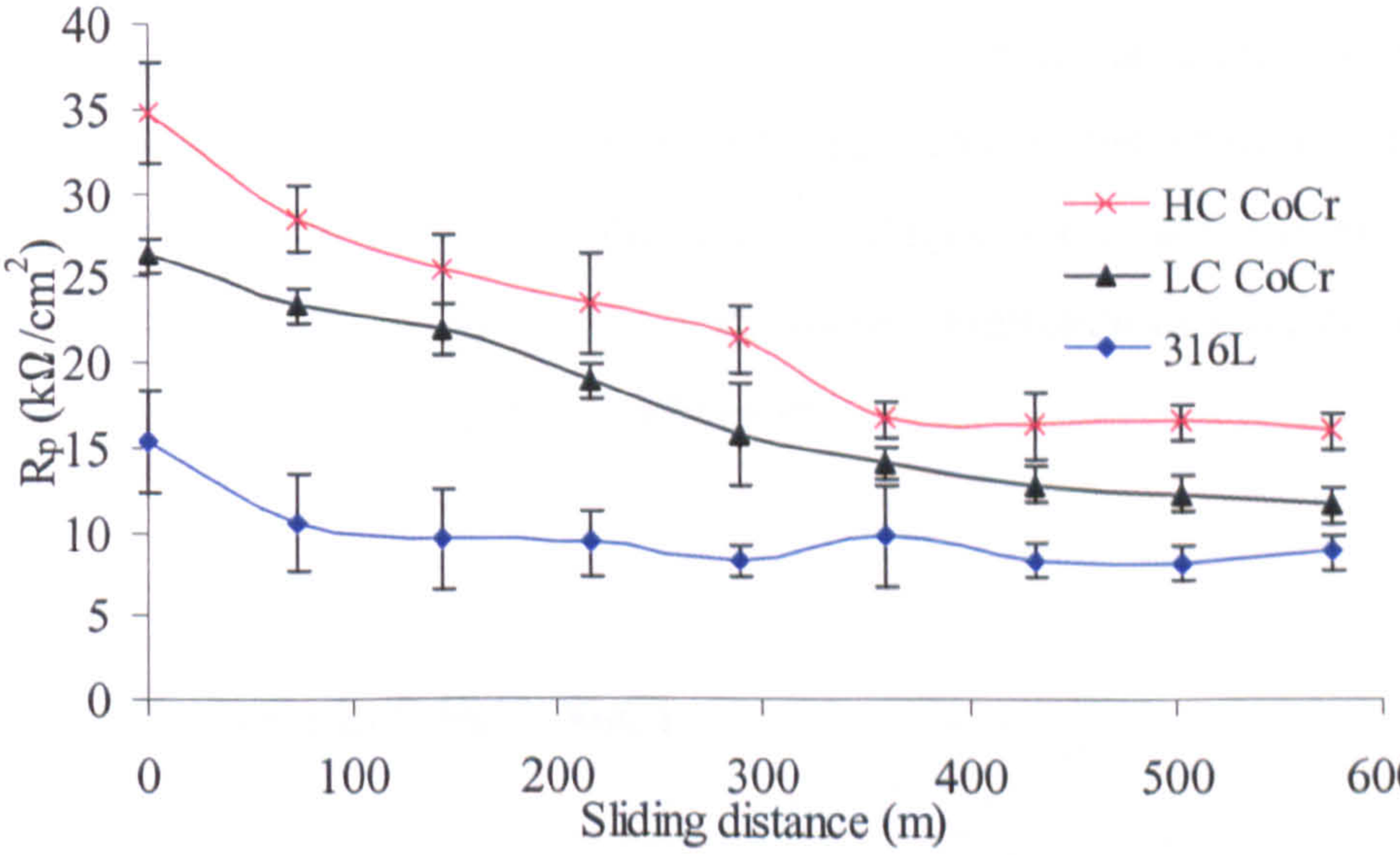

Figure 6-16 Polarization resistance (R_p) for HC CoCrMo, LC CoCrMo and 316L in NaCl up to 600 metres (8 hours) under sliding

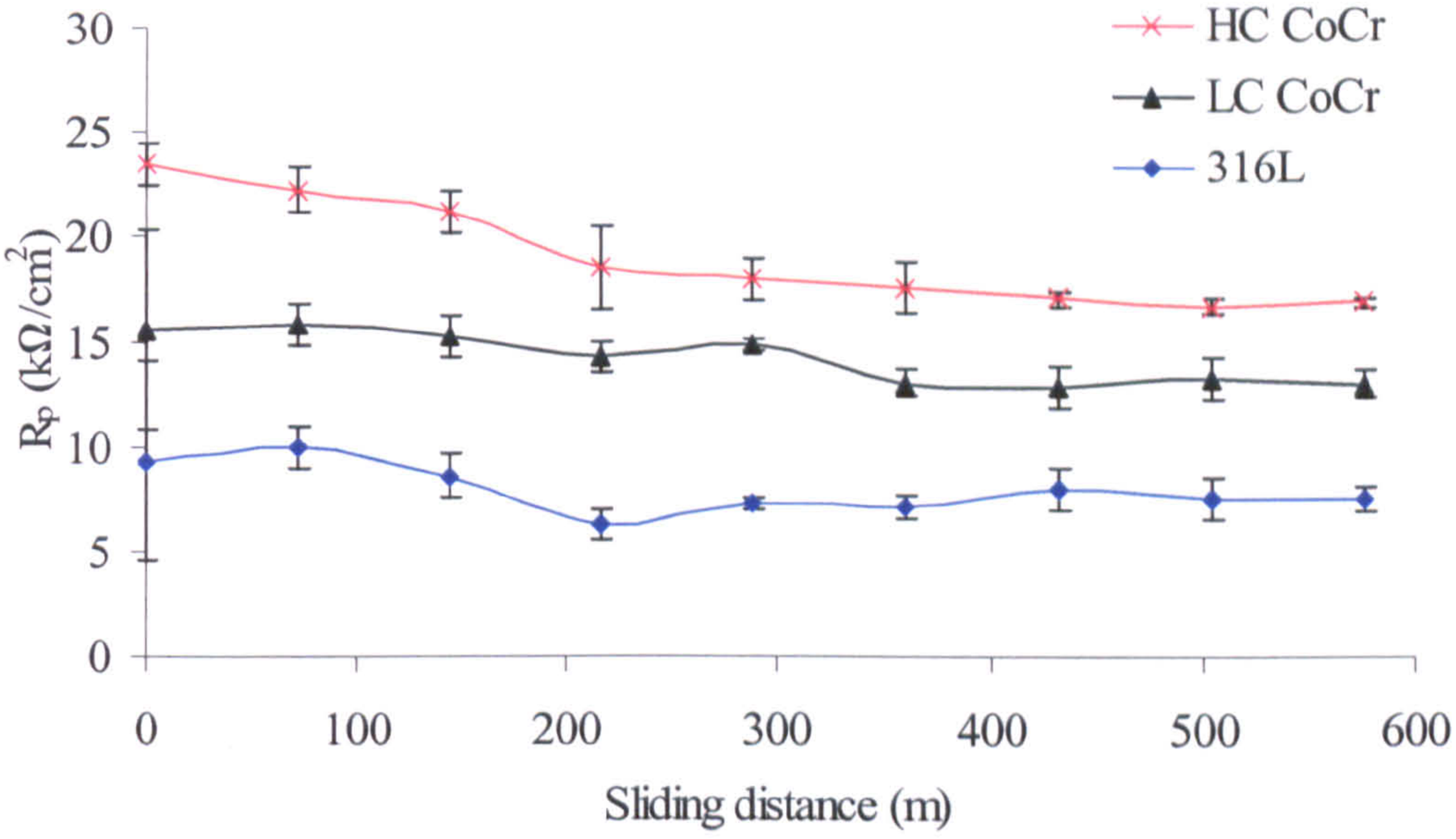

Figure 6-15 Polarization resistance (R_p) for HC CoCrMo, LC CoCrMo and 316L in DMEM up to 600 metres (8hours) under sliding

6.4. The Tribo-film Formation in Different Environments

XPS examinations have been conducted to understand the nature of the near surface film in the wear groove. Due to time constraints, studies were focused in 50% serum which is closer to the real operating conditions for joint replacements. The three different materials show very distinct formation of the tribo-film which is likely to affect wear and friction behaviour.

6.4.1. XPS tests in 0.36% NaCl

The tribofilm inside the wear scar and the area outside the wear scar have been examined after 4 hours sliding tests in 0.36% NaCl. There is no biological species in the solution.

6.4.1.1. Tribo-film on HC CoCrMo

From Table 6-3 and Figure 6-16, some observations are made:

- Co 2p, Cr 2p and Mo 3d content increases as etching progressed.
- C 1s and O 1s decrease. C 1s is mostly involved in Cr and Mo rich carbides and O 1s is believed to be in oxide/hydroxide formations with Co, Cr and Mo (Figure 6-17).

Table 6-3 XPS results for HC CoCrMo in 0.36% NaCl after different etching duration

Etching time (min)	XPS (at%)				
	C 1s	O 1s	Co 2p	Cr 2p	Mo 3d
0	6	34	30	24	6
0.5	5	26	37	25	7
5	5	16	43	27	9

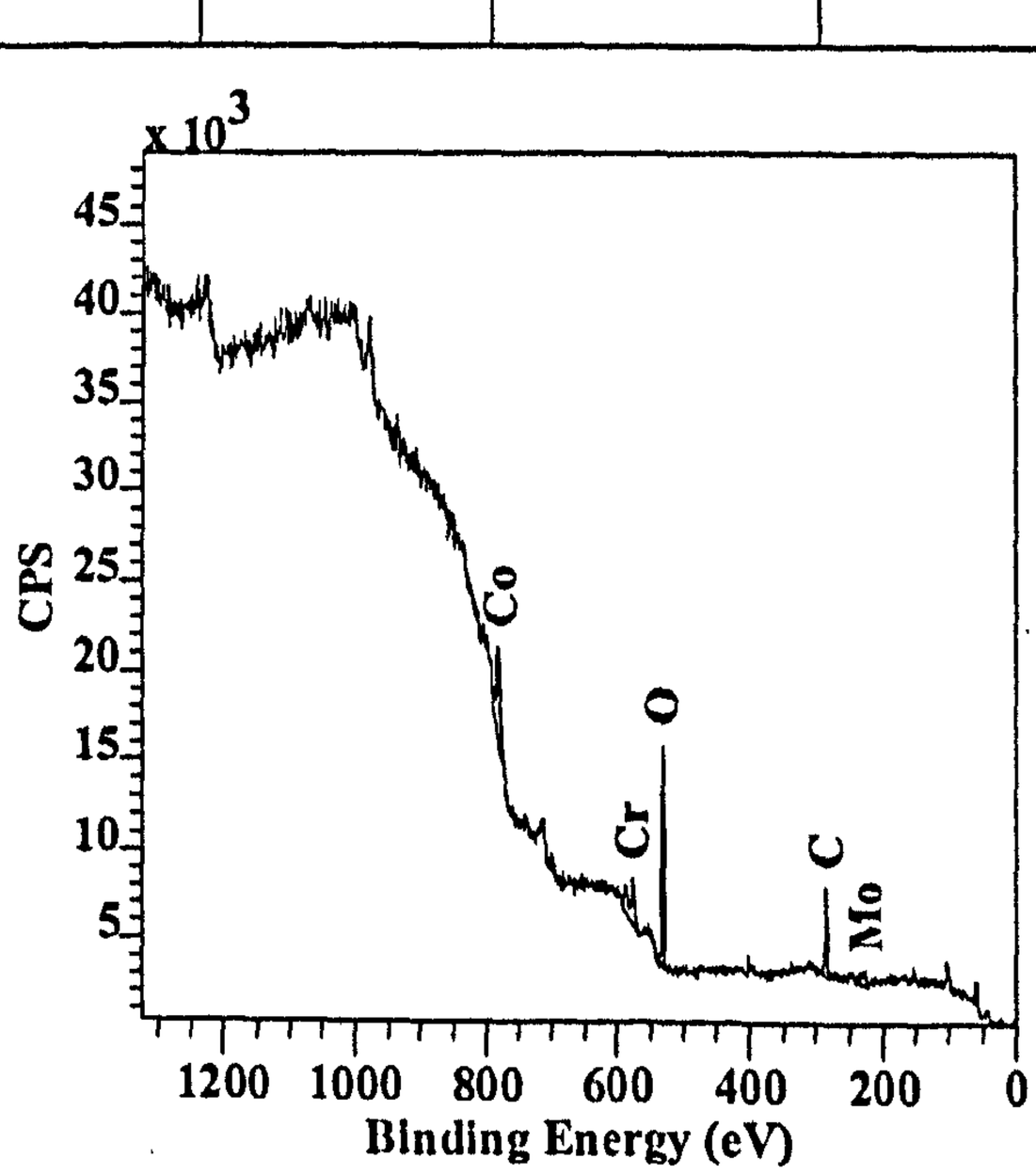

Figure 6-16 Survey scan for the HC CoCrMo wear scar in 0.36% NaCl without etching

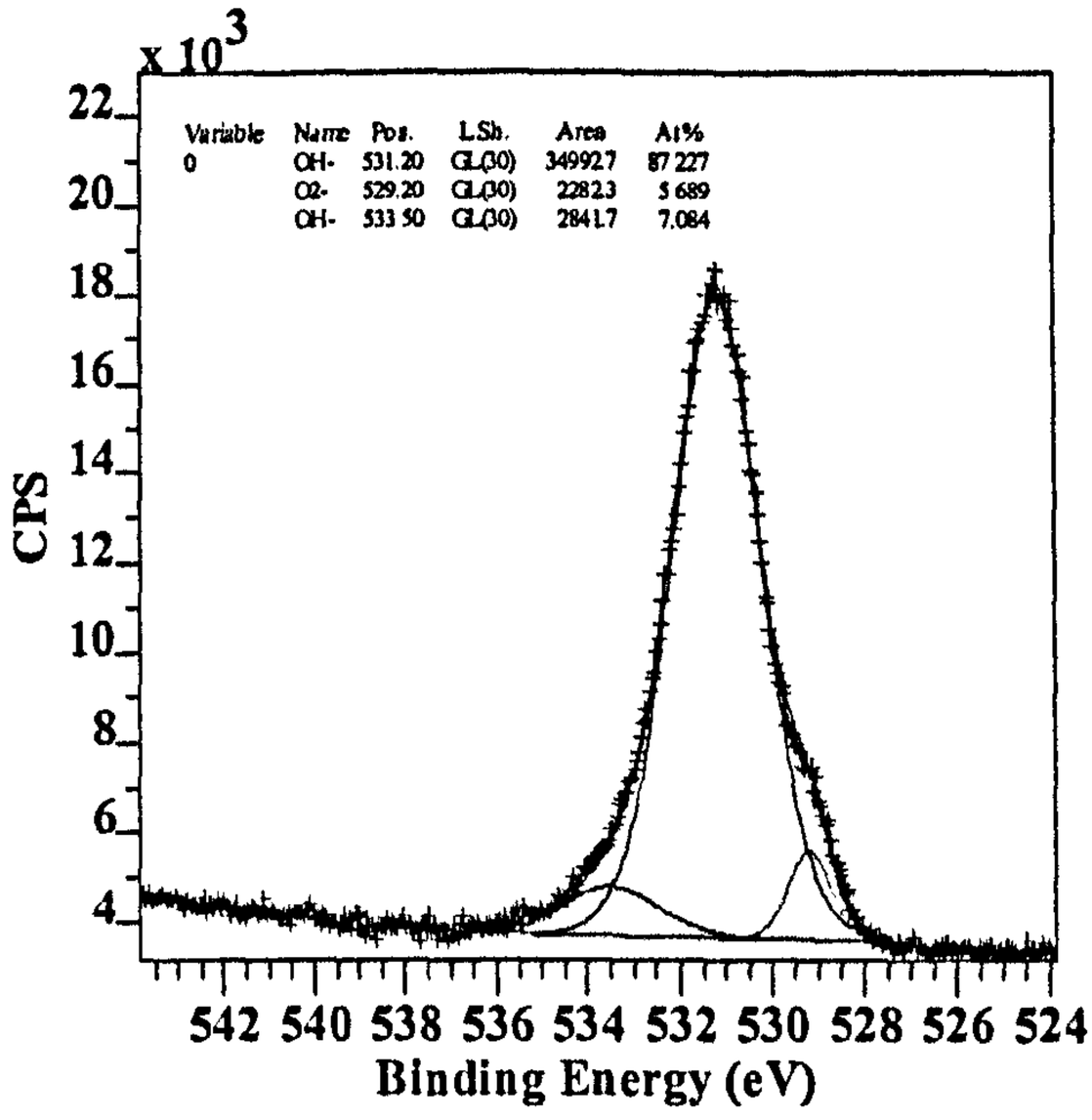

Figure 6-17 Curve fitting for O 1s in HC CoCrMo wear scar without etching

Table 6-4 summarizes the species observed in the tribofilm after different etching duration, it was apparent that

- For Co 2p, more $Co(OH)_2$ was on the top of the passive film. As etching progressed, more Co oxides and Co in the metal form were detected from the inner layer of the passive film and substrate.
- The majority of Cr 2p changed from $Cr(OH)_3$ to Cr_2O_3 on the detection depth of passive film went deeper.
- The main species of Mo 3d was MoO with MoO_2. The ratio between them changed slightly.
- A useful indication of the thickness of the passive film (5-8 nm) outside the wear area and the tribofilm (10-15 nm) in the wear scar can be achieved. It seems that under tribological contact a thickening process of the oxide and hydroxide film occur.

Table 6-4 Species found in HC CoCrMo wear scar under different etching

Etching time (min)	Element	Binding energy	At%	species
0	**Co**	778.5	37	Co_{met}
		780.0	6	$CoO\text{-}Co_2O_3/Co_3O_4$
		782.0	57	$Co(OH)2$
	Cr	574.2	6	Cr carbide
		576.2	30	Cr_2O_3
		577.2	64	$Cr(OH)_3$
	Mo	228.3	89	MoO
		229.5	11	MoO_2
0.5	**Co**	778.5	41	Co_{met}
		780.0	10	$CoO\text{-}Co_2O_3/Co_3O_4$
		782.0	49	$Co(OH)_2$
	Cr	574.2	5	Cr carbide
		576.2	43	Cr_2O_3
		577.2	52	$Cr(OH)_3$
	Mo	228.3	82	MoO
		229.5	18	MoO_2
5	**Co**	778.5	56	Co_{met}
		780.0	29	$CoO\text{-}Co_2O_3/Co_3O_4$
		782.0	15	$Co(OH)_2$
	Cr	574.2	24	Cr carbide
		576.2	73	Cr_2O_3
		577.2	3	$Cr(OH)_3$
	Mo	228.3	80	MoO
		229.7	20	MoO_2

6.4.1.2 Tribo-film on LC CoCrMo

A similar tendency of the tribo-film of LC CoCrMo can be found when compared with HC CoCrMo. The Co 2p, Cr 2p and Mo 3d content increased as

etching progressed (Table 6-5). However, more Co 2p and less Cr 2p and Mo 3d were obtained after 5 minutes etching. After detailed analysis of Co 2p and Cr 2p, the formation of them changed from hydroxides to oxides as etching progressing. Figure 6-18 shows Cr 2p under different etching duration.

Table 6-5 XPS results for LC CoCrMo in 0.36% NaCl after different etching duration

Etching time (min)	**XPS (at%)**				
	C 1s	**O 1s**	**Co 2p**	**Cr 2p**	**Mo 3d**
0	11	48	28	12	1
0.5	8	33	36	21	2
5	5	13	54	25	3

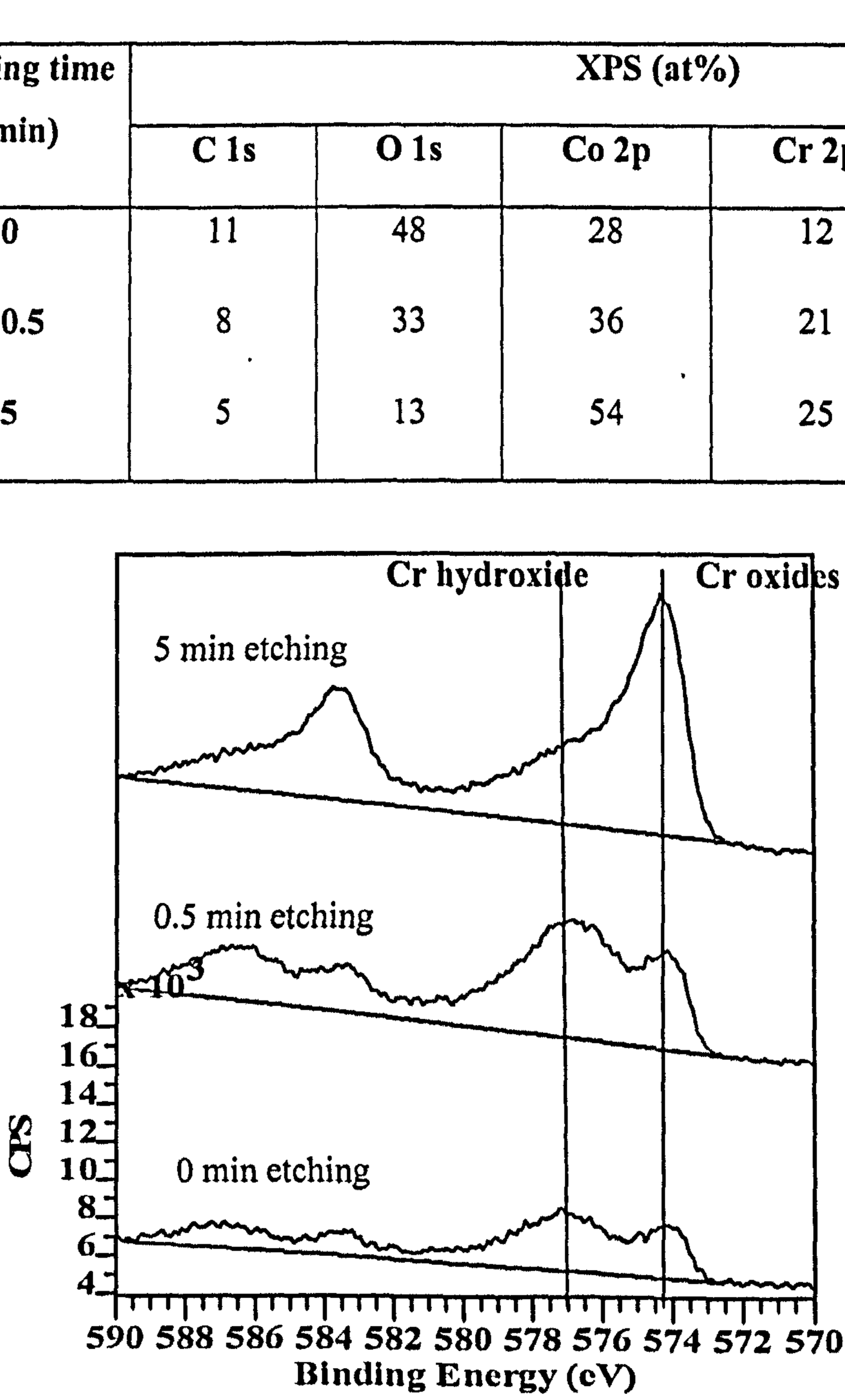

Figure 6-18 Cr 2p under different etching duration for LC CoCrMo

6.4.1.3. Tribo-film on 316L

Table 6-6 Species found in 316L wear scar under different etching

Etching time (min)	Element	Binding energy	At%	species
0	**Fe**	706.9	3	Fe_{met}
		709.3	2	FeO
		710.4	6	Fe_3O_4
		711.4	20	Fe_2O_3
		711.6	69	$Fe(OH)_3$
	Cr	574.4	2	Cr_{met}
		576.2	10	Cr_2O_3
		577.2	80	$Cr(OH)_3$
		579.1	8	CrO_3
	Ni	854.2	46	NiO
		855.8	54	Ni_2O_3
5	**Fe**	706.9	12	Fe
		710.4	11	Fe_3O_4
		711.4	67	Fe_2O_3
		711.6	10	$Fe(OH)_3$
	Cr	574.4	4	Cr_{met}
		576.2	67	Cr_2O_3
		577.2	15	$Cr(OH)_3$
		579.1	14	CrO_3
	Ni	854.2	72	NiO
		855.8	28	Ni_2O_3

For 316L in 0.36% NaCl under tribological contact. The tribo-film contained primarily $Fe(OH)_3$/FeOOH and $Cr(OH)_3$ on the top layer and Fe_2O_3, Cr_2O_3 and NiO in the inner part of the film, which is different from the passive film outside the worn area contained mainly Cr_2O_3 and minor Fe_2O_3 and NiO. Figure 6-19 shows the changes of Fe 2p formation during etching. Table 6-6 gives an overview of the

chemical status of different species inside the tribofilm. The thickness of the tribofilm was 15-18 nm on 316L in 0.36% NaCl.

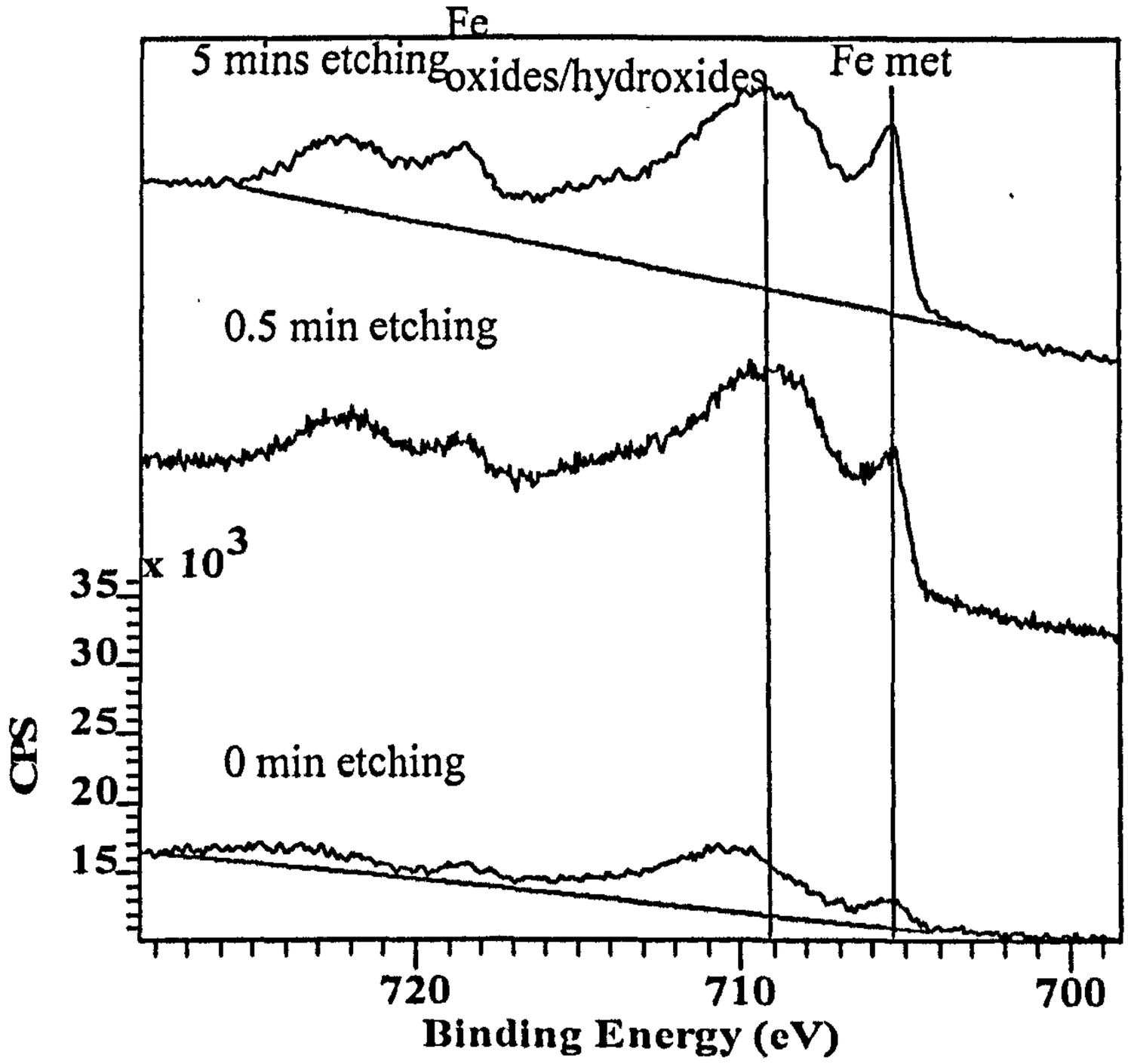

Figure 6-19 Fe 2p under different etching duration for 316L

6.4.2. XPS tests in 50% Serum

With proteins involved, the tribofilm formations are complicated. XPS analysis has been conducted to provide an overall picture of the structure and chemical information about the film inside the wear scar.

6.4.2.1. Tribo-film on HC CoCrMo

Studies have been focused in the wear scar. It is the main contact area when friction and wear (mechanical damage) are evaluated. However, comparison is made with the film formation outside of the scar. Table 6-7 shows the concentration of elements in the wear scar after various etching times. Figure 6-20 compares the survey scans in and out of the wear scar. An apparent difference is that Co 2p was obtained in the top surface of the wear scar. It indicates that Co ions was released but still presented in the tribofilm. It gives the evidence that proteins bind with Co ions in the wear track. Proteins were adsorbed on the sample surface of unworn area, no Co 2p or Cr 2p was found on the top layer of the area outside the wear scar. Figure 6-21 and Figure 6-22 present the C 1s spectra inside and outside of the wear scar. The C 1s spectra observed outside the wear scar is very close to native albumin, which also suggests that an adsorption of proteins has occurred on the unworn surface. Detailed analysis for Co $2p_{2/3}$ is shown in Figure 6-23.

Table 6-7 XPS results for HC CoCrMo in 50% serum after different etching duration

Etching time (min)	**XPS (at%)**					
	C 1s	**O 1s**	**N 1s**	**Co 2p**	**Cr 2p**	**Mo 3d**
0	66	23	8	2	1	
0.5	62	14	8	8	7	1
5	33	11	6	28	18	4

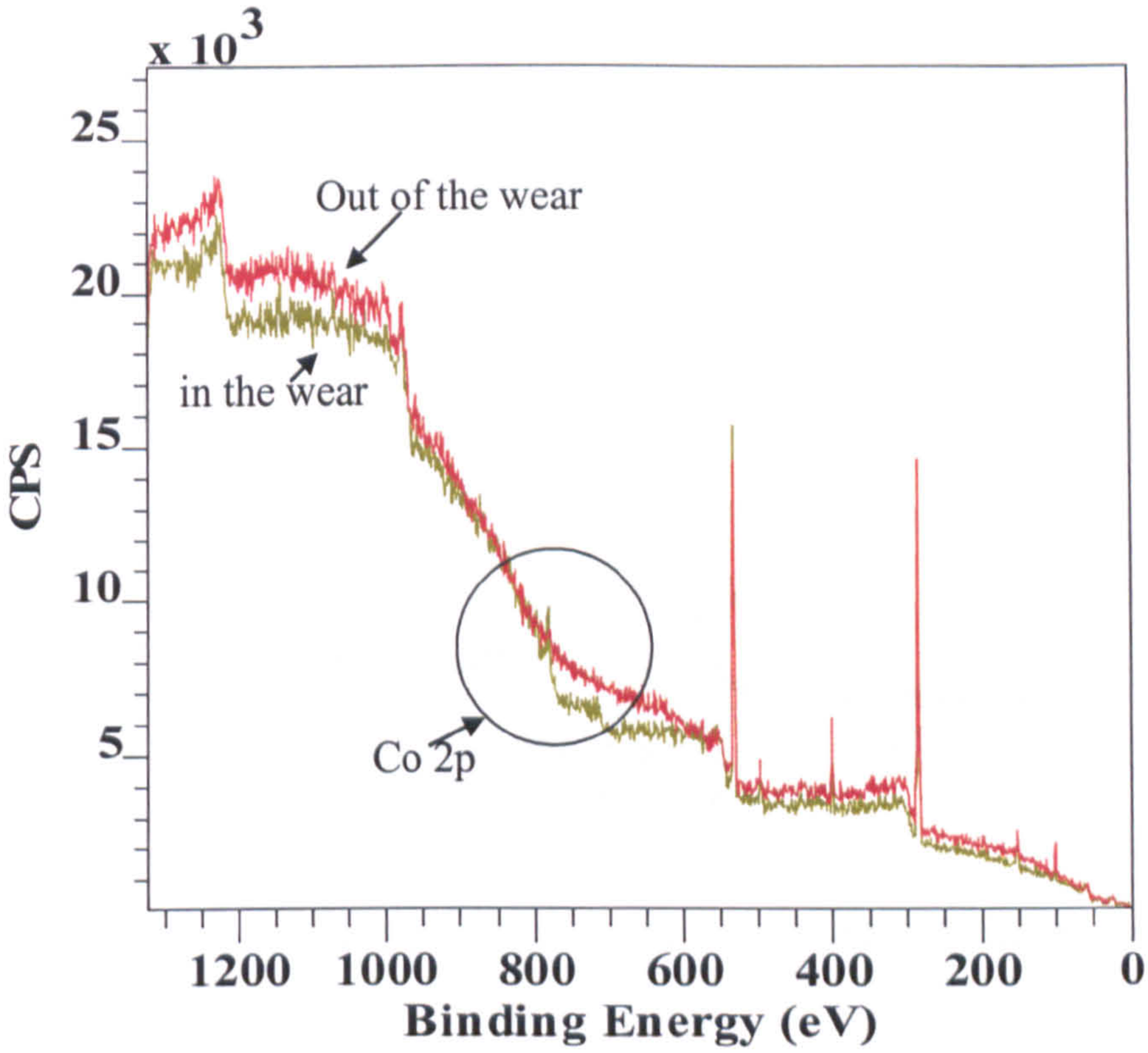

Figure 6-20 Survey scans for HC CoCrMo in 50% serum

Figure 6-21 C 1s spectrum and fitted curves for HC CoCrMo wear scar in 50% serum

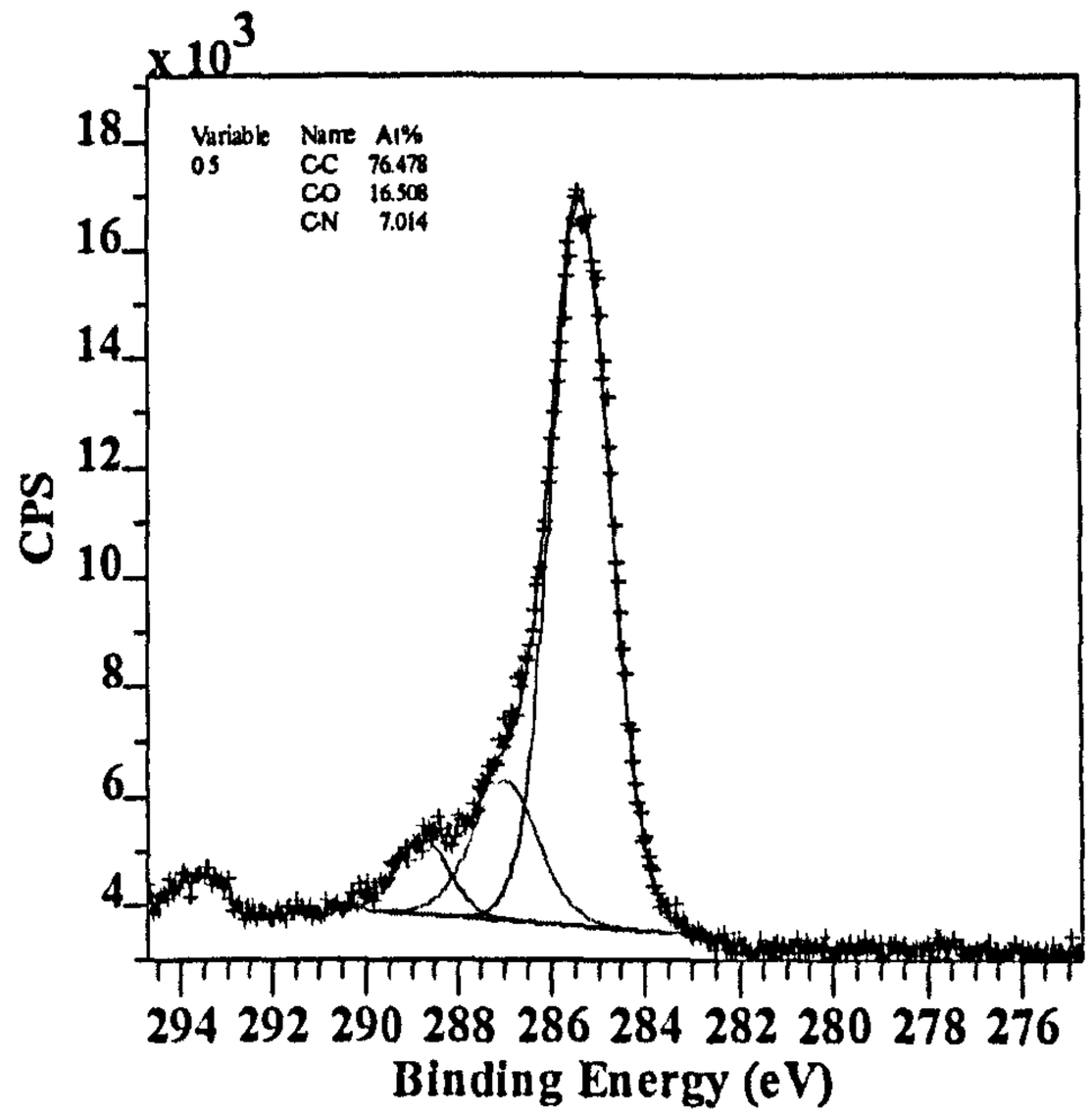

Figure 6-22 C 1s spectrum and fitted curves for out side of HC CoCrMo wear scar in 50% serum

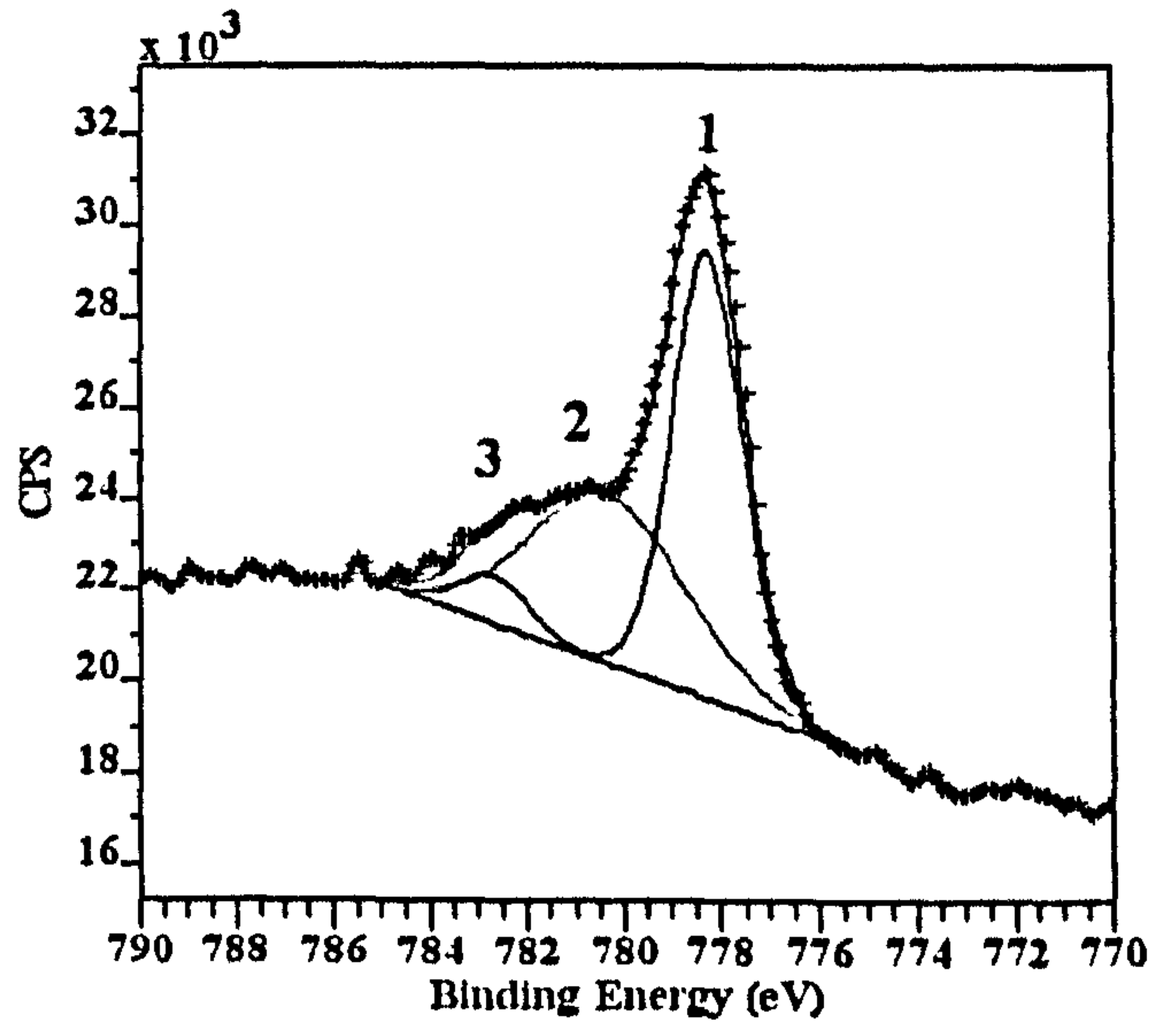

Figure 6-23 Co $2p_{3/2}$ peaks obtained from the wear scar of 4-hour rubbing HC CoCrMo in 50% serum

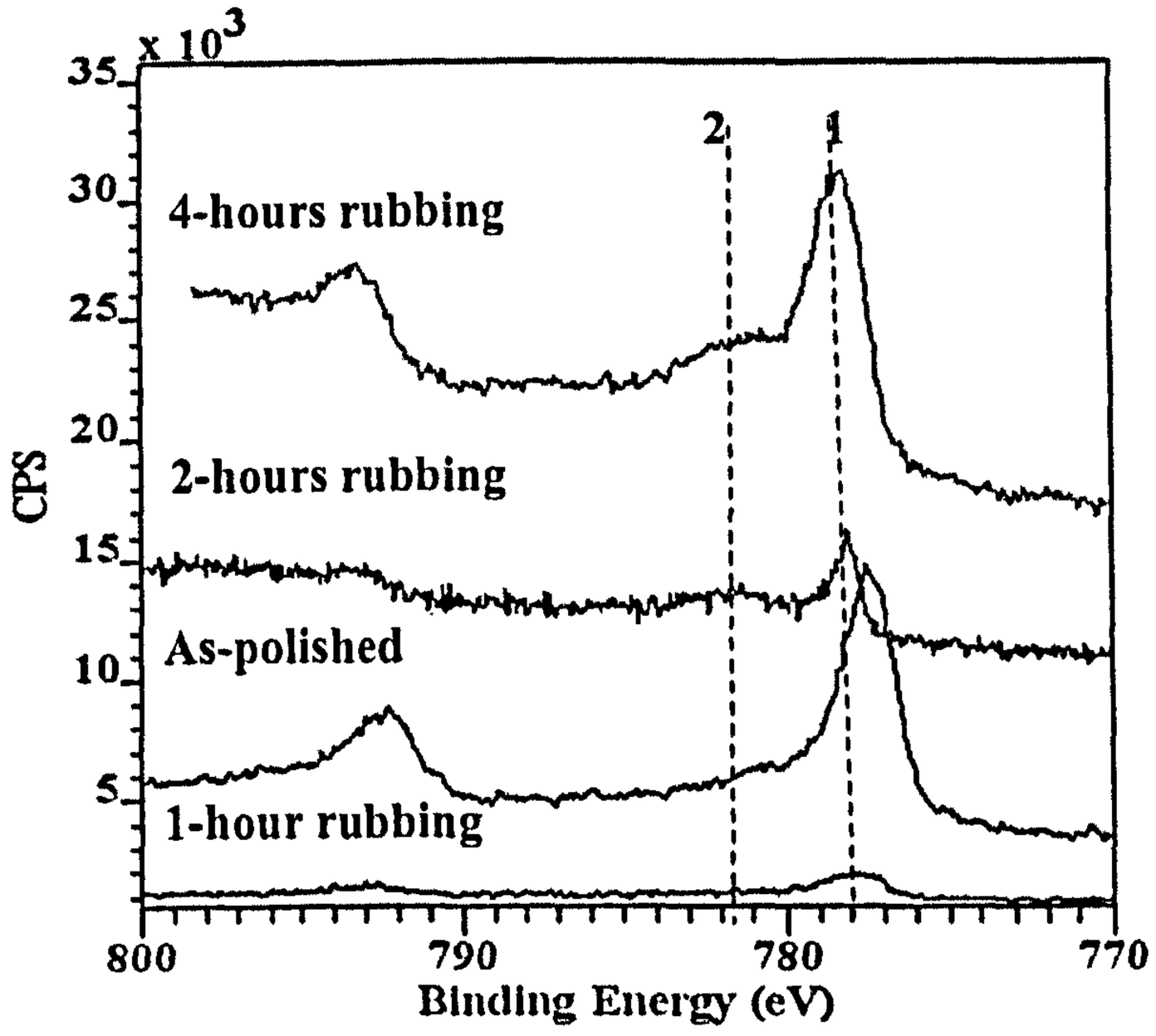

Figure 6-24 The change in the Co 2p spectrum as a function of rubbing time on HC CoCrMo samples

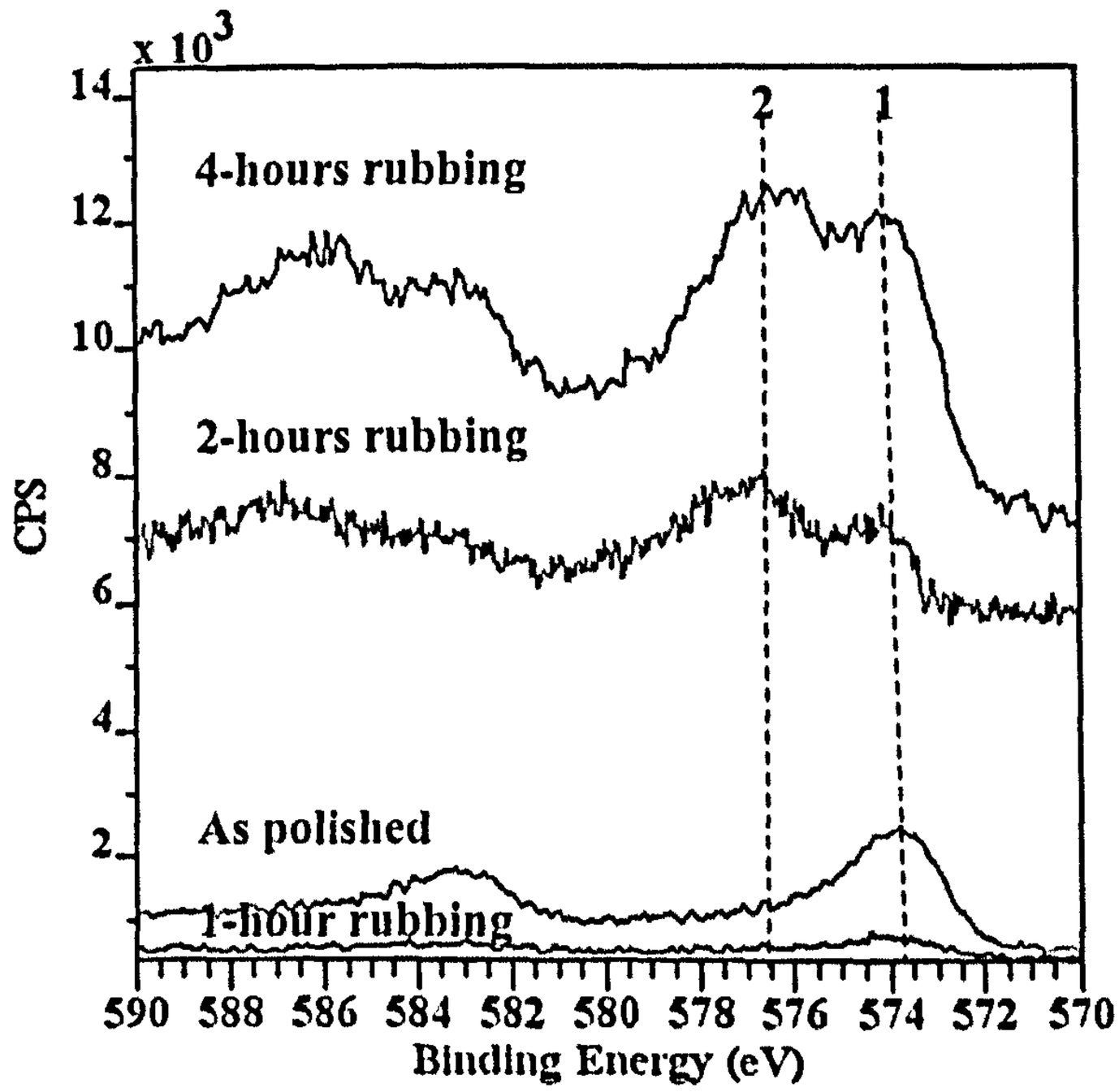

Figure 6-25 The change in the (b) Cr 2p spectrum as a function of rubbing time on HC CoCrMo samples

A thin protein adsorption layer (3-4 nm) was observed on the sample surface for HC CoCrMo after 1, 2 and 4-hours sliding. Three main elements (C, N and O) were observed. All correspond to organic species. The C 1s peaks occur at 285.5, 287.1 and 289.0 eV (Figure 6-21), indicating C bonds like C-C, C-H and C-O C-N, respectively. This can be compared with pure albumin where the range of binding energies for the C 1s peak is between 285.0 eV and 288.2 eV corresponding to various carbon species (aliphatic carbons, protein backbone and peptide carbons). Examining outside the wear scar, C 1s peaks (285.0-284.9 eV) (Figure 6-22) are very consistent with C 1s peaks in the reference albumin. The shift of carbon binding energy and the broadening of carbon spectra in the wear scar are probably due to the denaturation of proteins resulting from the high pressure and instantaneous increase in temperature [9]. The temperature rise in the contact area is defined by

$\Theta = 0.946\frac{\dot{h}a}{K}$ (the Peclet number $P_e = \frac{ua}{2\kappa} << 1$, where $\kappa = \frac{K}{\rho c_p}$) (K=18 W $m^{-1}K^{-1}$ for 316L and 49 W $m^{-1}K^{-1}$ for CoCrMo), where $\dot{h} = \mu p u$. The temperature rise for CoCrMo was 18°C at the very beginning of the test in 50% serum. However, as the tests progressed, in the steady state, the flash temperature was 4°C.

It is noticed that in the wear scar more C-C is observed than outside the wear scar. It may re-establish and result in a reduction of friction. This apparent change in layer structure, compared to the reference albumin is represented in Table 6-8 where the theoretical ratios of C/O and C/N in albumin are 3.2 and 3.7. These can be compared with the experimental results, after sliding, and it is clear the C/O and C/N ratios both increase. However, as sliding time increases, with no etching C/O and C/N ratios decrease and after 4 hours, the ratio of C/O and C/N are close to those of pure albumin. The increase of O 1s might be due to the absorption of water molecules or –OH from the environment.

Table 6-8 Binding energy for C 1s and C/N, C/O ratios

Rubbing time	Etching time	BE for C 1s (eV)[a]	C/N	C/O
Theoretical ratio for albumin	0 min	285.0	3.7	3.2
1-hour	0 min	288.2	5.5	4.0
2-hour	0 min	288.6	5.0	3.9
4-hour	0 min	285.5	4.1	3.4

[a] BE for the main peak

By applying 0.5 minutes argon-ion etching, a passive film containing Cr oxides, Co oxides and Cr hydroxide was detected. It indicates that the protein-rich layer is about 3-4 nm thick. After 4 hours, a dense and thick tribo-film was found underneath the protein adsorption layer. Figure 6-23 shows different Co $2p_{3/2}$ states in the wear scar after 4 hours rubbing. Generally, there are three peaks. Peak 1 (778.4 eV) corresponds to typical Co in the CoCrMo alloy. Peaks 2 and 3 (780.0 eV and 782.8 eV) indicate that Co was present as different oxides (Co_2O_3/CoO) and as an organometallic form. It is well documented that Co, Cr, Fe and Ni can incorporate with Albumin at carboxylate and tyrosine positions or bind with the –SH group of a single cysteine residue [116]. This formation could be responsible for the decrease of friction because of its polymer-like structure.

Figure 6-24 and Figure 6-25 shows the differences of tribo-film for Co 2p and Cr 2p peaks in the tribofilm after 1, 2 and 4 hours sliding compared with the as-polished sample. From Figure 6-24, it is apparent that in 50% serum, Cobalt changed from metallic form in the matrix (as-polished) to Cobalt oxides (Co_2O_3/CoO) and organometallic Co content in the tribo-film (peaks 1 and 2). The formation increased as sliding time increased. The Cr species also changed during tribological contact (Figure 6-24). The Cr 2p spectrum changed from typical Cr formations in CoCrMo

alloys (573.9 eV) to two species dominating the Cr content: peak 1 at 574.4 eV (Cr organometallic form) and peak 2 at 576.4 eV (Cr_2O_3/Cr_2O_4/organometallic). These formations of organometallic Co/Cr and Co/Cr oxides are responsible for the reduction of friction and lower wear rate in the steady state regime. An indication of the thickness of the tribofilm was given, which was more than 25 nm with the thin protein adsorption layer (3-4 nm). Due to the dimension of albumin molecules (3×3×8), the layer seems to be a monolayer of proteins. Calculation of the thickness of the tribofilm was made according to the different rate of argon-ion etching process. For carbon specie, the rate of etching process is about 0.1 nm/s and for Cr_2O_3, the rate is approximately 0.08 nm/s [135-137].

6.4.2.2. Tribo-film on LC CoCrMo

Table 6-9 gives all the elements which can be detected in the wear scar for LC CoCrMo. Abundance of Co 2p was observed after 5 minutes etching. From Figure 6-26, which assesses the Co $2p_{2/3}$ peak in detail, it is clear that the measurement reached the material substrate. Co 2p was in metallic form. However, when just 0.5 minutes etching was applied, a mixture of Co oxides and organometallic material was found (Figure 6-27). Figure 6-28 shows the C 1s peak and I is clear that C-C and C-N were the major binding forms of C 1s. Interestingly, S 2p was detected on LC CoCrMo, which was not seen on HC CoCrMo. Cr oxides were also detected as in the passive film. However, Cr 2p appeared in very deep of the tribo-film only as the etching progressed to more than 5 minutes confirming that it exists deep in the tribofilm. It suggests that the organometallic formation was about 8-10 nm and the oxide layer was about 10-15 nm.

Table 6-9 XPS results for LC CoCrMo in 50% serum after different etching duration

Etching time	XPS (at%)						
	C 1s	**O 1s**	**N 1s**	**Co 2p**	**Cr 2p**	**Mo 3d**	**S 2p**
0	60	31	9				
0.5	58	24	9	7		1	1
5	27	5	5	48	13	1	1

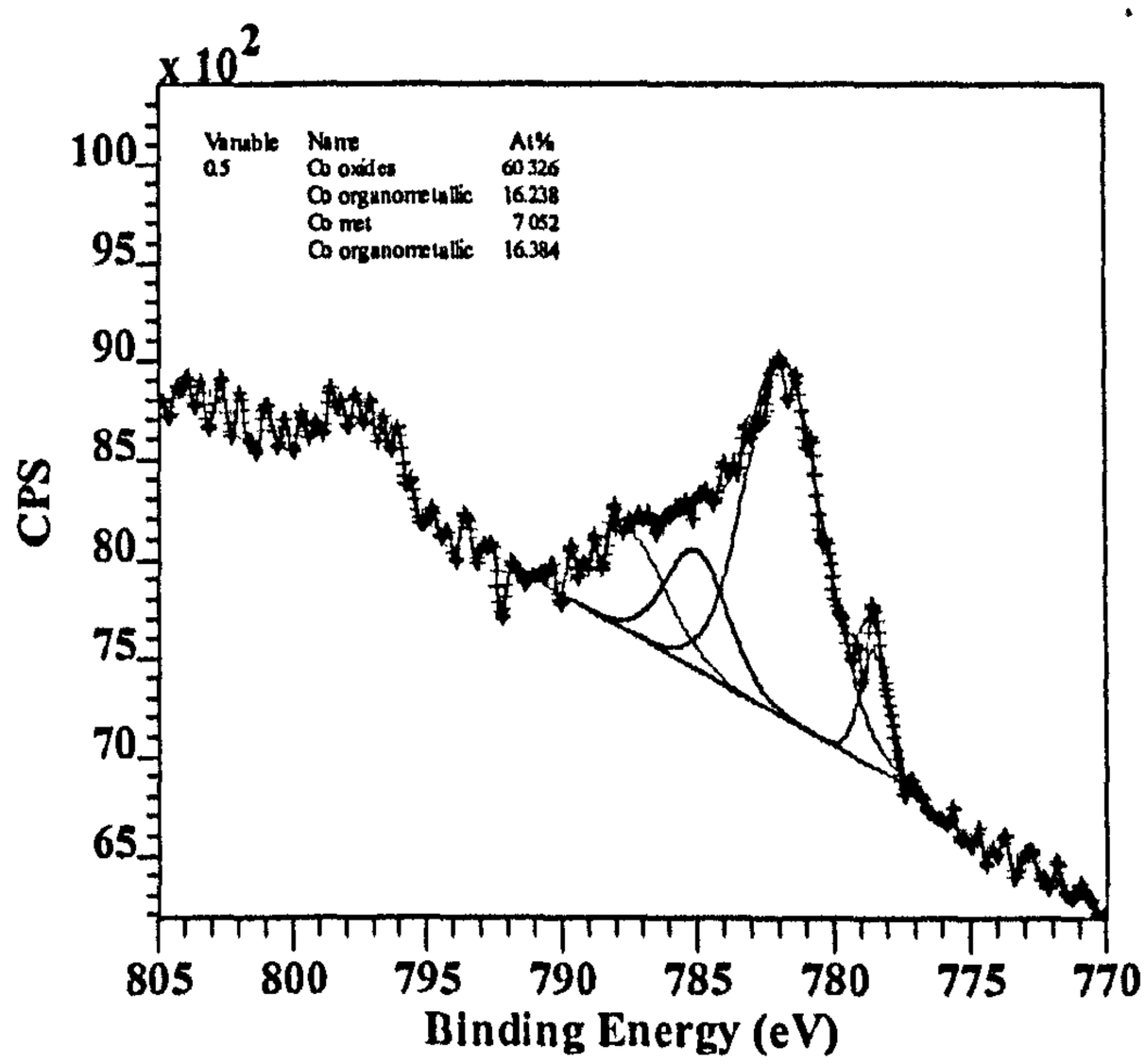

Figure 6-26 Co $2p_{3/2}$ peaks obtained from the wear scar of 4-hour rubbing LC CoCrMo in 50% serum without etching

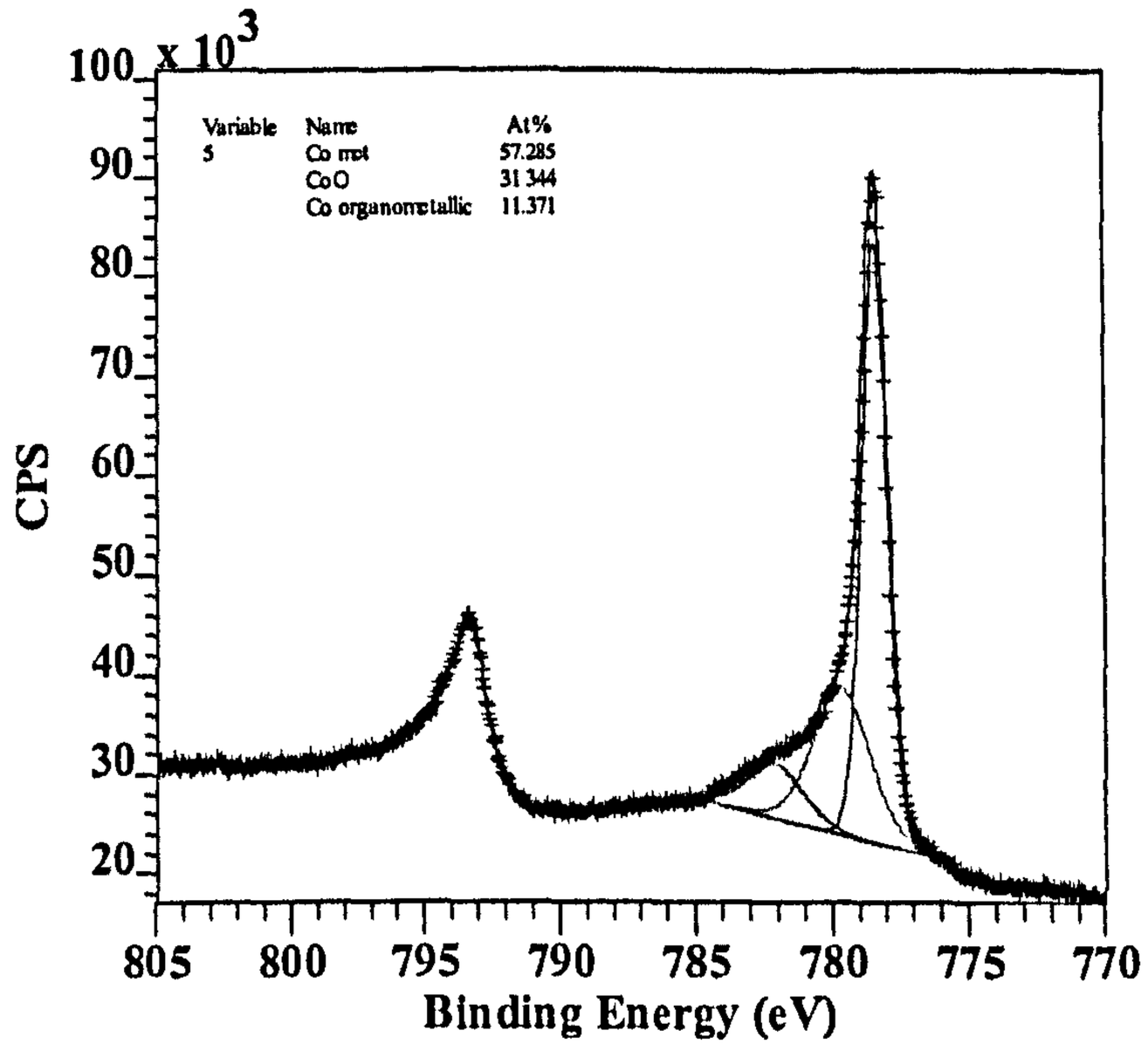

Figure 6-27 Co $2p_{3/2}$ peaks obtained from the wear scar of 4-hour rubbing LC CoCrMo in 50% serum with 5 min etching

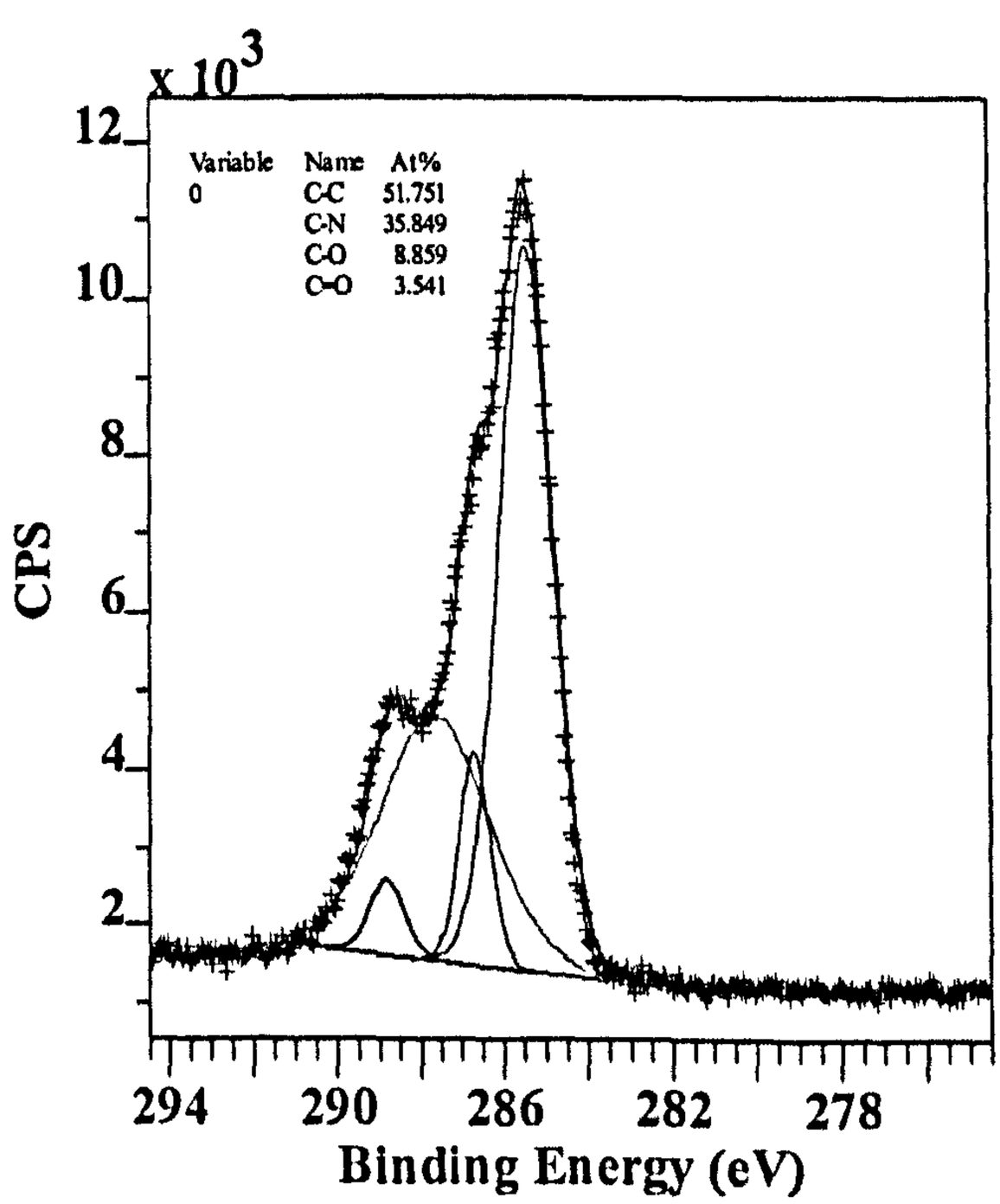

Figure 6-28 C 1s spectrum for LC CoCrMo wear scar in 50% serum without etching

6.4.2.3. Tribo-film on 316L

When 316L was exposed to the same tribological contact in 50% serum, calcium and phosphate were obtained on the surface both inside and outside of the wear scar. Table 6-10 gives all the elements found in the wear scar. Fe 2p was found in the form of oxides and organometallic species as shown in Figure 6-29 and FeS was detected in the wear scar. The main component of Fe oxides was Fe_3O_4. A very complex Cr 2p was observed and Cr_2O_3/Cr_2O_4 (574.4 eV), organometallic Cr (576.4 eV) were the major forms. Ni 2p was found only in oxide form (NiO/NiO_2). Figure 6-30 shows the Fe spectra $2p_{2/3}$ after 5 minutes etching. Increases of Fe metal and oxides and a decreases of Fe organometallic formation can be observed. These components affect 316L tribology behaviour will be discussed later in Chapter 8.

Table 6-10 XPS results for 316L in 50% serum after different etching duration

Etching time (min)	XPS (at%)								
	C 1s	O 1s	N 1s	Fe 2p	Cr 2p	Ni 2p	P 2p	S 2p	Ca 2
0	65	28	4	1			1		1
0.5	33	35	5	12	4	1	5	1	4
5	27	21	2	35	6	5	1	1	3

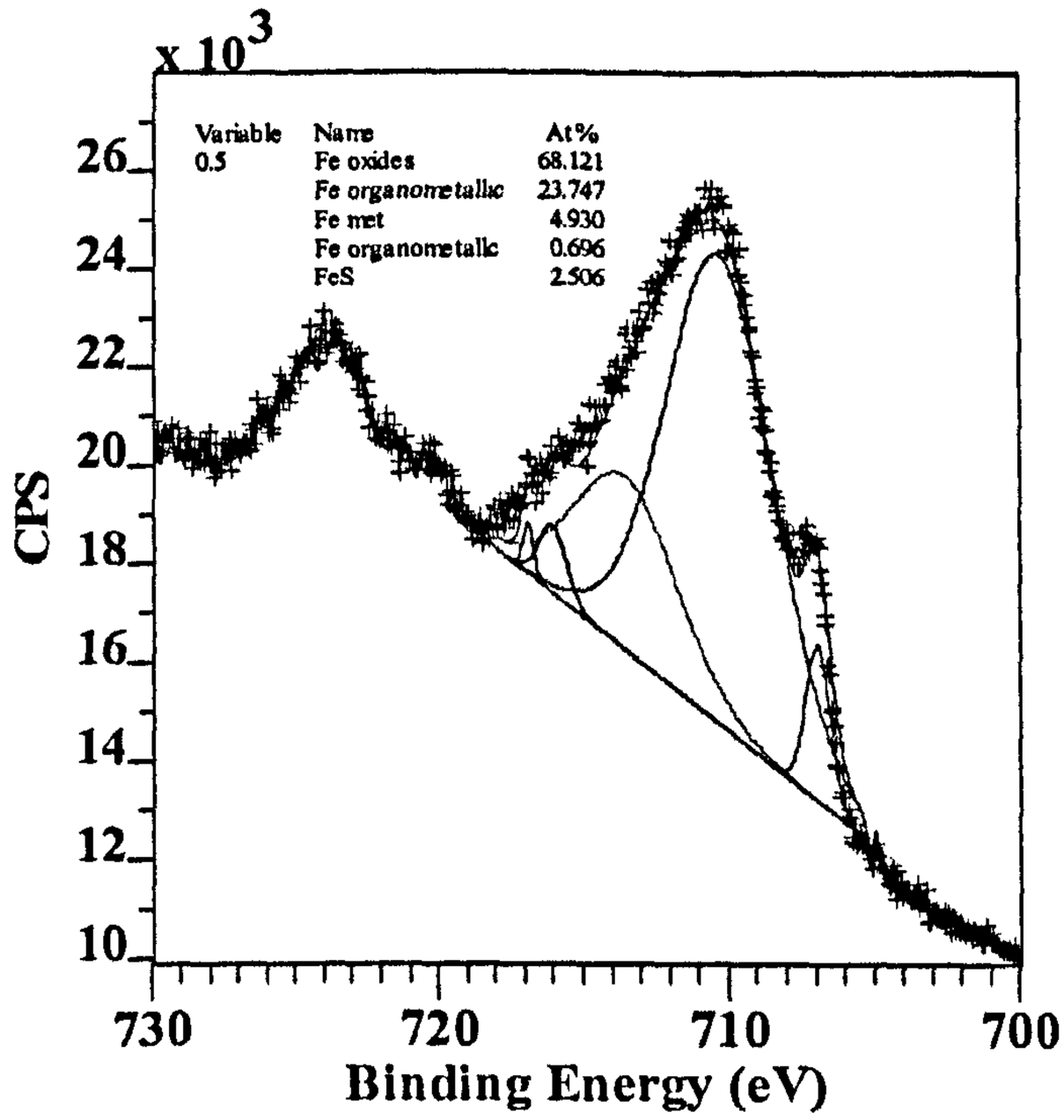

Figure 6-29 Fe $2p_{2/3}$ curve fitting for 316L wear scar in 50% serum without etching

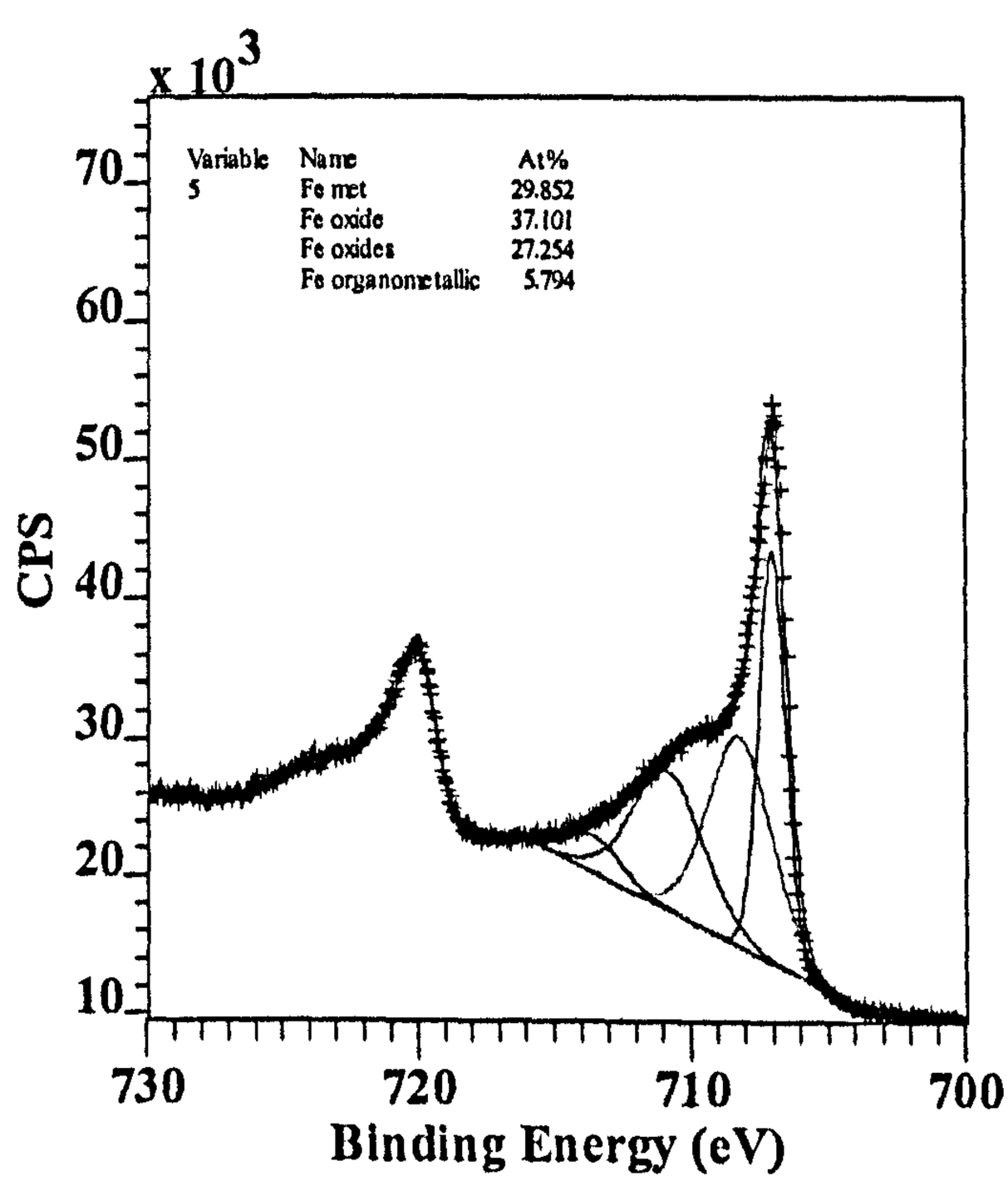

Figure 6-30 Fe $2p_{2/3}$ curve fitting for 316L wear scar in 50% serum with 5 min etching

6.5. Summary

This chapter focuses on the tribological behaviour for materials in three environment and the effect of tribology on metal ion release processes (corrosion).

• Under tribological contact, the contact zone became more active comparing with the unworn area. An increase of corrosion current which was induced by mechanical movement indicated an acceleration of the corrosion rate (metal ion release).

• The electrochemical tests (monitoring E_{corr}) gave a clear indication of the removal and repassivation due to the mechanical force and electrochemical reactions.

• Proteins can act as a lubricant and reduce friction. Amino acids also had some extent of lubrication effect.

• The formation of organometallic complexes (proteins-metal), cobalt sulphide and calcium phosphate during sliding had a tendency to reduce friction. The passive film under tribological rubbing was similar to the spontaneous air-formed passive film but the thickness was greater. For CoCrMo, the passive film contained mainly Cr_2O_3 and minor amounts of CoO/MoO_2. For 316L, Cr_2O_3 and Fe oxides were the major components of passive film.

• HC CoCrMo showed the greatest linear polarization resistance among the tested materials. With organic species (proteins and amino acids), a smaller linear polarization resistance can be observed comparing in 0.36% NaCl.

CHAPTER 7

THE EFFECT OF CORROSION IN TRIBOCORROSION SYSTEMS

7.1. Introduction

In Chapter 6, it was shown clearly that wear has a great influence on corrosion behaviour. In this chapter, integrated tribology-electrochemical tests are performed. Protein effects on wear, friction and tribocorrosion are generally assessed. How corrosion affects the whole tribocorrosion system, wear and friction is analyzed. The link between released ions and friction is studied. By applying a potential on the sample surface, the depassivation and repassivation of materials are studied in detail. The effect of corrosion as a function of time is also under investigation to understand how corrosion behaves and contributes to the entire material degradation processes. Along with the well documented bi-phases of wear behaviour (the running-in and the steady state), corrosion rate also changes as time progresses. The influences of proteins, amino acids and the saline environment on corrosion and tribocorrosion properties are also assessed from experimental results. Figure 7-1 presents a map of the experimental set up and the techniques used in this chapter.

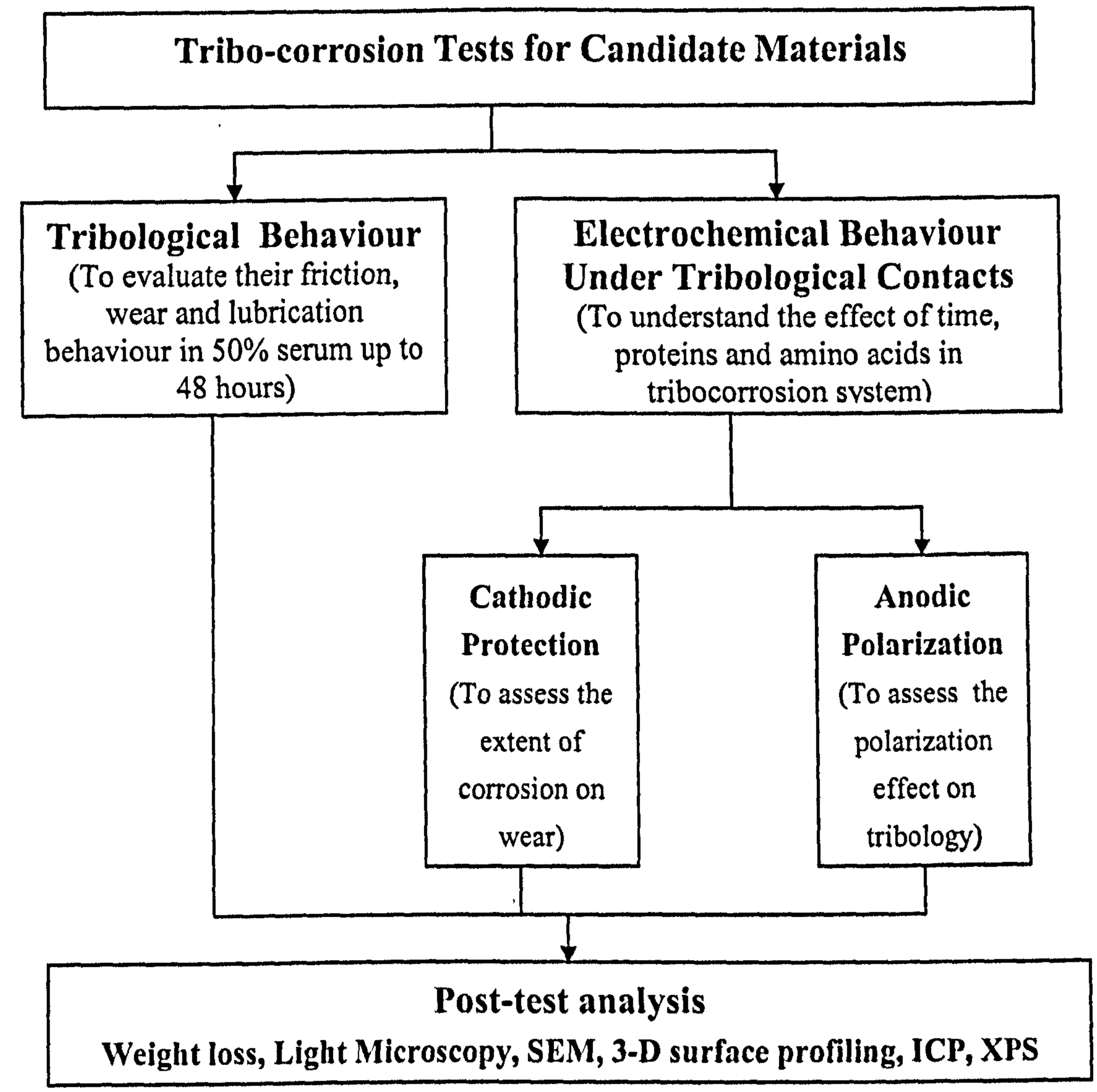

Figure 7-1 Map of the experimental work presented in Chapter 7

7.2. Corrosion Effect on Total Material Degradation

As introduced in Chapter 4, Cathodic Protection (CP), by the impressed current method, is a widely used technique to control corrosion and in this study sliding wear tests under CP have enabled the wear material loss to be determined. Cathodic polarization scans were initially carried out to estimate the protection potential (Figure 7-2). Comparing with the cathodic polarization scan under static conditions, a slight oscillation in current was recorded as shown in Figure 7-2 which

is primarily due to the sliding contact. In addition, the oxygen reduction rate was greater, which can be explained by the reciprocating movement bringing more oxygen to the sample surface and increasing the reaction rate. For CP, the applied potential should be chosen to be more negative than the equilibrium electrode potential for the Co/Co^{2+} reaction yet sufficiently noble to prevent hydrogen-evolution at the surface which would inevitably affect the wear process. Not surprisingly, the hydrogen reaction evolution for the CoCrMo alloys followed the same trend as in static conditions (after -0.8 V).

In this study, the purpose is to prevent corrosion. Pourbaix pH-potential diagrams were also checked [6]. Under these circumstances, -0.8 V was chosen to be the protection potential. ICP tests were conducted after CP tests in 50% serum. Ion concentrations were less than 0.012ppm for Co and 0.04ppm for Fe. It was mainly due to the instrumental error and the ions contained in the natural serum (Table 4-1). Another possible reason is that the produced wear debris in the system also can release ions and have electrochemical reactions at the debris free corrosion potential. Thus, it is shown that the ion release process (*corrosion*) was eventually stopped and wear is the only component to be attributed to the material degradation.

However, a question arises about how CP can affect the protein adsorption. As mentioned in the previous section, proteins carry a net negative charge on carboxyl groups ($-COO^-$) in this environment (pH=7.6), therefore the adsorption process can be inhibited by CP. Discussion of this is extended in Chapter 8.

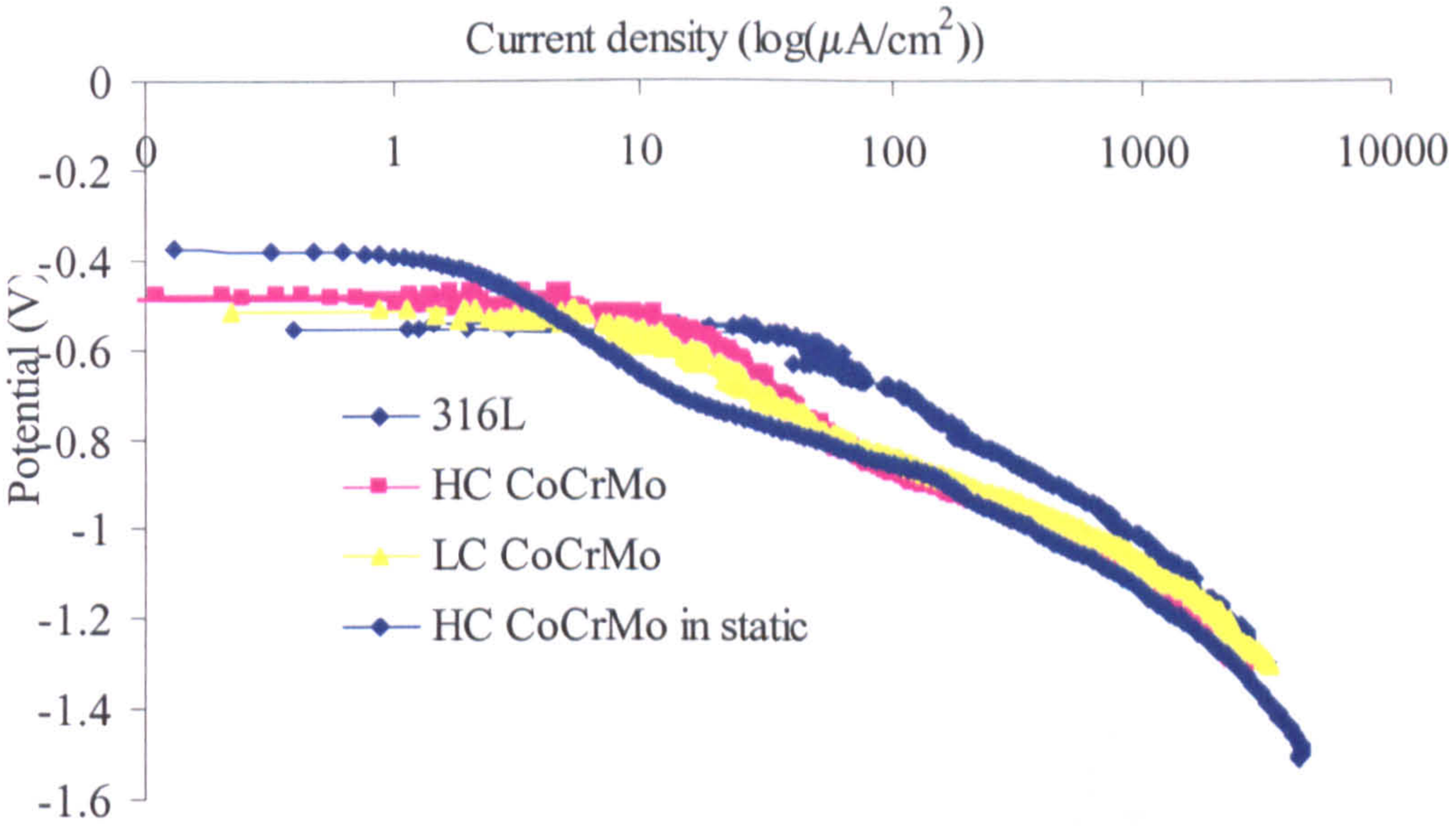

Figure 7-2 Cathodic polarization curves for three materials in 50% serum under tribological contact and a comparison of HC CoCrMo in static

Figure 7-3 reveals several important aspects in relation to the wear and corrosion/wear interactions in sliding wear for these three materials in two solutions.

- Application of Cathodic Protection reduces the total damage (volume loss) in all cases indicating that corrosion or corrosion-related effects (effect of wear on corrosion or corrosion on wear) play an important role in degradation.

- In all solutions HC CoCrMo alloy shows the lowest volume loss followed by LC CoCrMo and the highest volume loss is recorded for the 316L alloy.

- For the LC CoCrMo alloy and 316L the higher total volume loss occurs for 50% serum and the 0.36% NaCl solution leads to the lower degradation. For HC CoCrMo alloy there is little difference between the two solutions.

- For the LC CoCrMo alloy and 316L the highest wear volume loss (by applying CP) occurs for 50% serum. For LC CoCrMo the wear component (pure mechanical damage) is similar for DMEM and 0.36%NaCl. For 316L

the lowest wear was found in 0.36%NaCl. For HC CoCrMo wear volume loss is the lowest in DMEM and in 50% serum and 0.36%NaCl the wear volumes loss was similar.

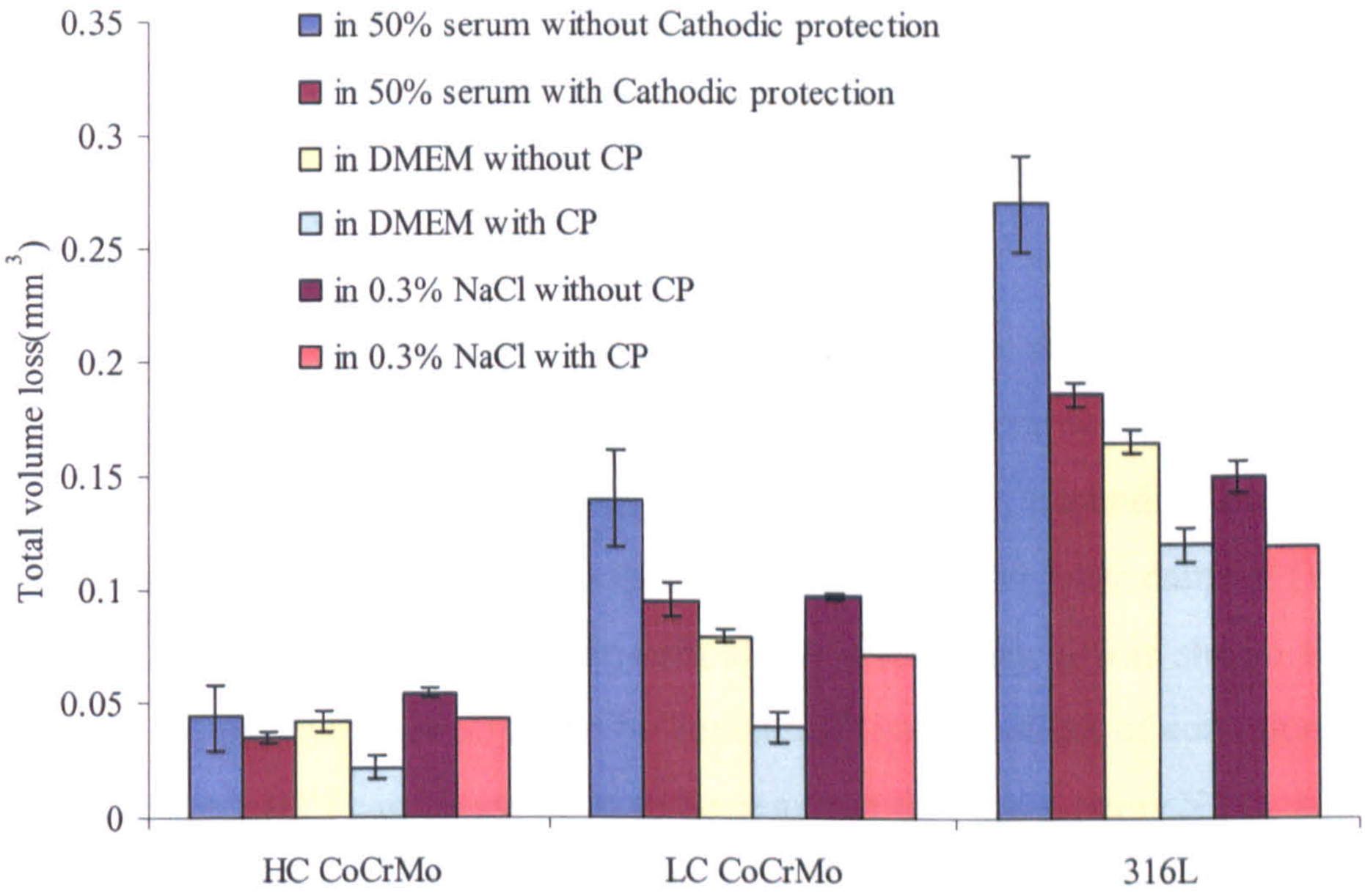

Figure 7-3 Material total volume loss without and with applied CP in three environments

To date, there have been a few studies which attempt to quantify the contributions of material degradation due to corrosion, wear and their interactions in a biotribocorrosion environment where active biological solutions or saline solutions are used [42, 97, 157]. This can be done by considering Eq.7-1 which allows the quantities of corrosion, wear and corrosion-wear to be analyzed.

$$T = W + C' + S \qquad \text{(Eq.7-1)}$$

where W is the material loss in the absence of corrosion, which was measured by applying CP. C' is the material loss due to electrochemial processes (corrosion) in the absence of wear. The synergy S includes two components which are

- the effect of wear on corrosion (C_w) and
- the corrosion effect on wear (W_c).

Corrosion-related damage (C'+S) can therefore be assessed for the three materials as can be seen in Figure 7-4. It should be remembered this is not only the corrosion rate – it is the damage that corrosion processes do when wear-corrosion processes occur in parallel. Hence it is referred to as *corrosion-related damage* rather than corrosion damage.

These results indicate that wear/corrosion interactions were involved and it is clear that in all cases in the present tests, corrosion and corrosion-related damage contributed to between 22% and 50% of the total damage, depending on the alloy and the solution. Figures 7-4 shows the components of total wear damage (W) and corrosion related damage (C'+S) for each alloy. Previously it was shown that the alloys exhibit passivity and so it can be concluded that the effect of corrosion in the absence of wear (C') can be assumed to be zero and that the synergy S (C_w and W_c) is the major corrosion-related component.

Figure 7-5 and Figure 7-6 assist in the understanding of the physical nature of wear/corrosion interactions. For the three alloys in 50% serum the physical differences in:

(i) the extent of wear

(ii) the wear mechanisms

can be observed.

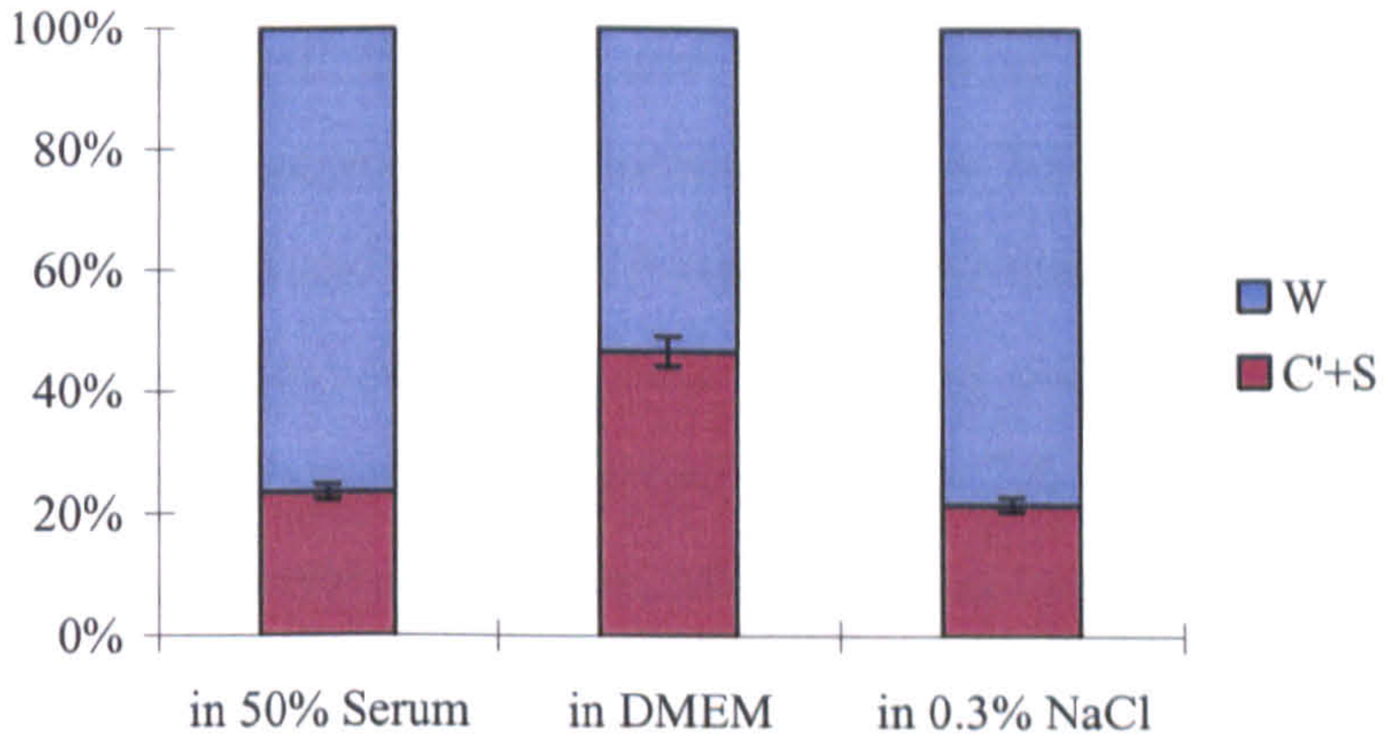

(a)

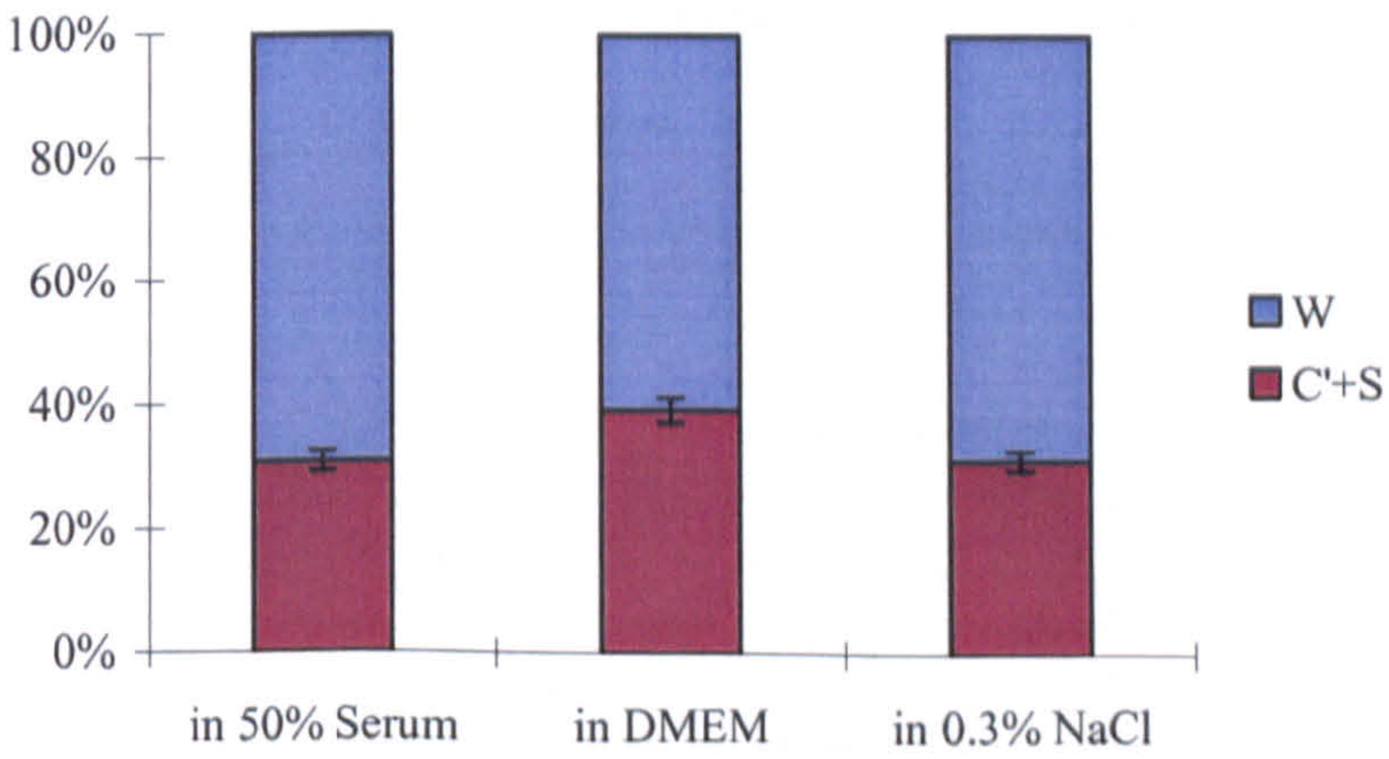

(b)

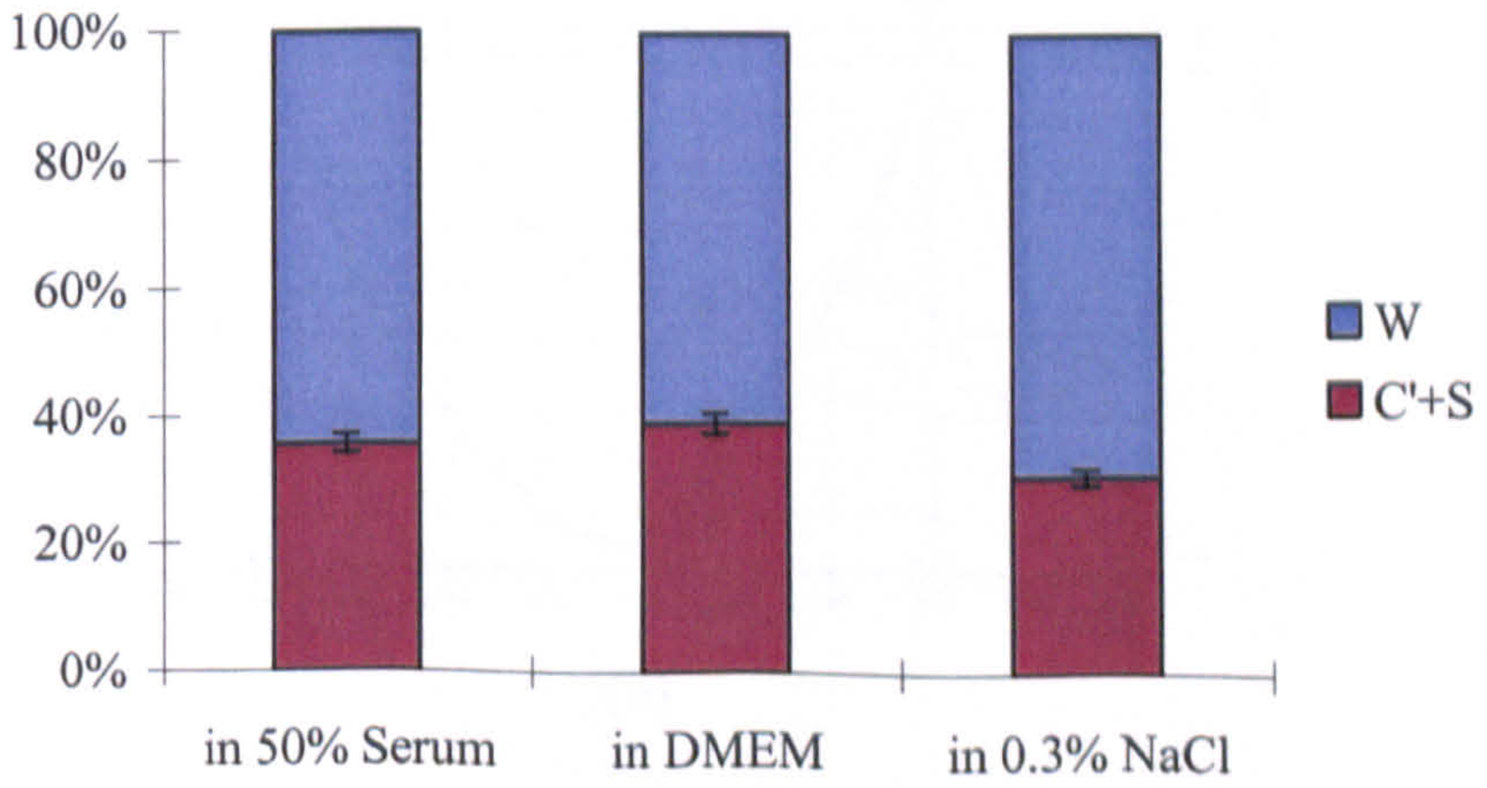

(c)

Figure 7-4 Components of volume loss for (a) HC CoCrMo (b) LC CoCrMo and (c) 316L in 50% serum, DMEM and 0.36% NaCl

From the cross section of the wear scar taken by the interferometer (Figure 7-5), by preventing corrosion, both the width and the depth of the wear scars were decreased in line with the volume loss reduction. Figures 7-6 (c) and (f) show the SEM images from 316L with and without CP and it is clear that when both wear and electrochemical processes occur there is evidence of pitting and gross adhesive wear. With applied CP only smooth grooves can be seen (Figure 7-6 (b) (d) and (f)). It has been reported that in wear-corrosion systems, damage consists of two processes:

(i) mechanical delamination of the passive layer in the wear track

(ii) a progressive electrochemical repassivation of that active wear track area (representing that part of the wear track that temporarily loses its passive character due to the mechanical interaction during sliding).

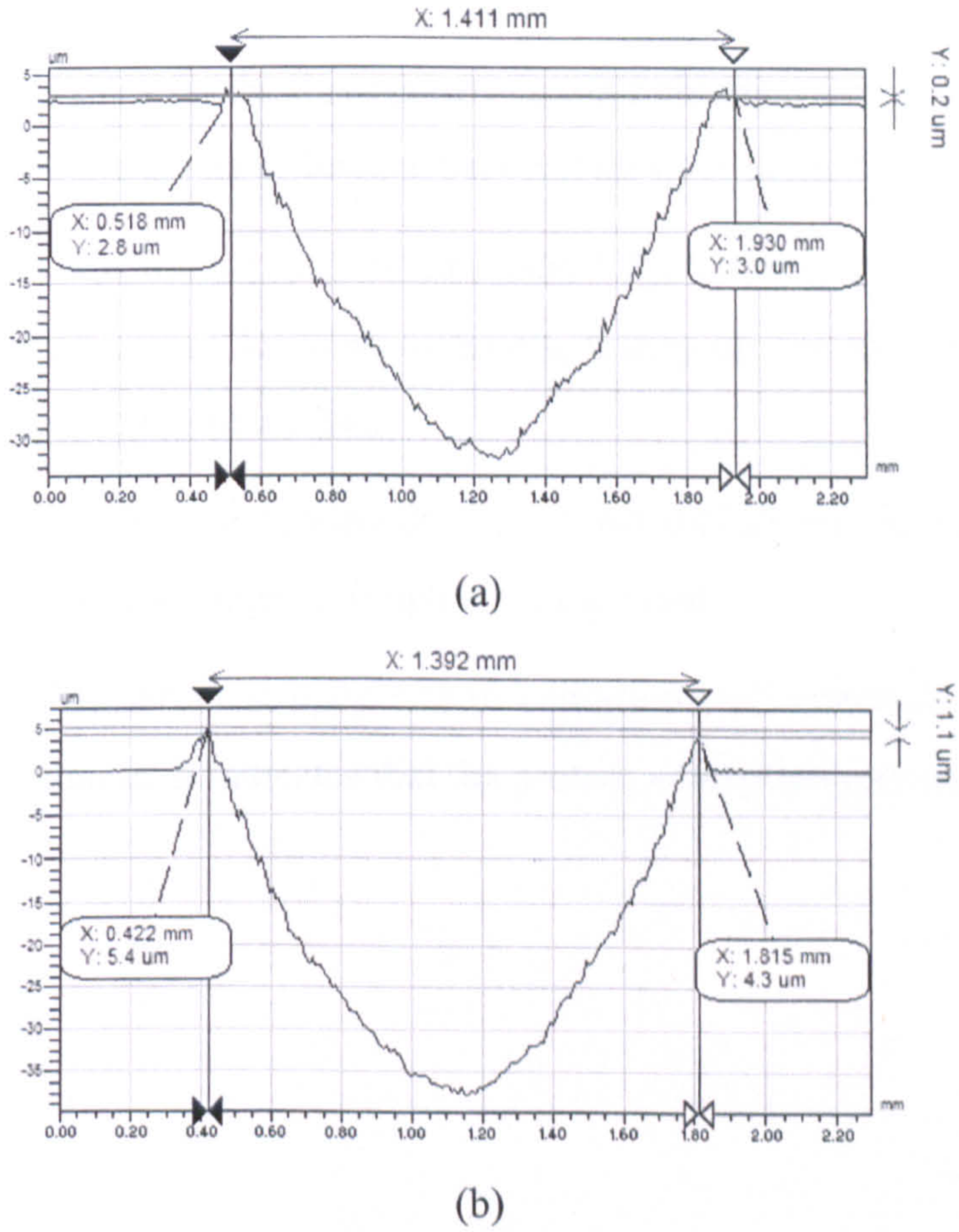

(a)

(b)

Figure 7-5 Typical wear scar image for 316L (a) without applied CP (b) with applied CP obtained by white light interferometry using the Wyko interferometer

By applying CP, it can be seen from Figure 7-6 that delamination is eliminated. No real change in surface structure on the HC CoCrMo alloy is observed – in agreement with the wear coefficient values. Both Cr-rich and Mo-rich carbides can be observed in the wear scar and out of the wear scar on HC CoCrMo. No evidence that carbides had been pulled out can be observed. No evidence of any tribochemical reaction was obtained on the surface of the silicon nitride ball. This could be the low velocity (0.02m/s) and low temperature (37°C) applied in this study and also the high hardness of the silicon nitride ball (three times higher than HC CoCrMo). The ultra smooth surface finish (roughness less than 0.003 microns) and good density by HIPing (Hot Isostatic Pressing) for ball samples in this study can also minimize the possibilities of any tribochemical reaction on the ball surface [143].

Roughness values for the three materials were obtained from the interferometer (Figure 7-7). It compares the difference between samples under CP or at OCP.

- As corrosion was prevented (under CP), the roughness value was lower in 50% serum for three materials. It may be due to less proteins being adsorbed on the surface.
- HC CoCrMo exhibited the smoothest surface among tested materials. 316L had the highest roughness in general.
- In 50% serum at open circuit conditions, all materials showed higher roughness. It indicates that the protein adsorption process presented.

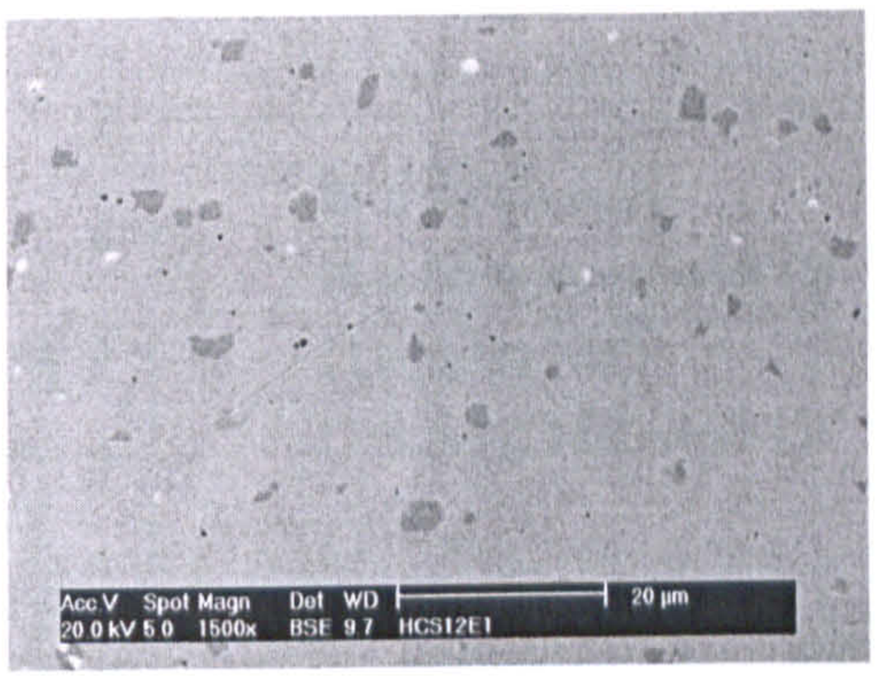

(a)

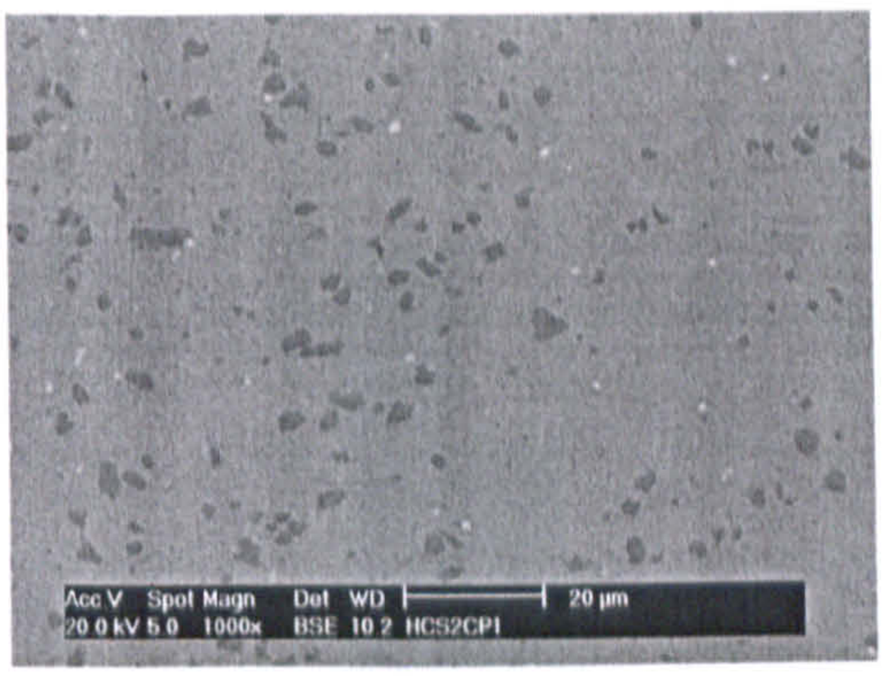

(b)

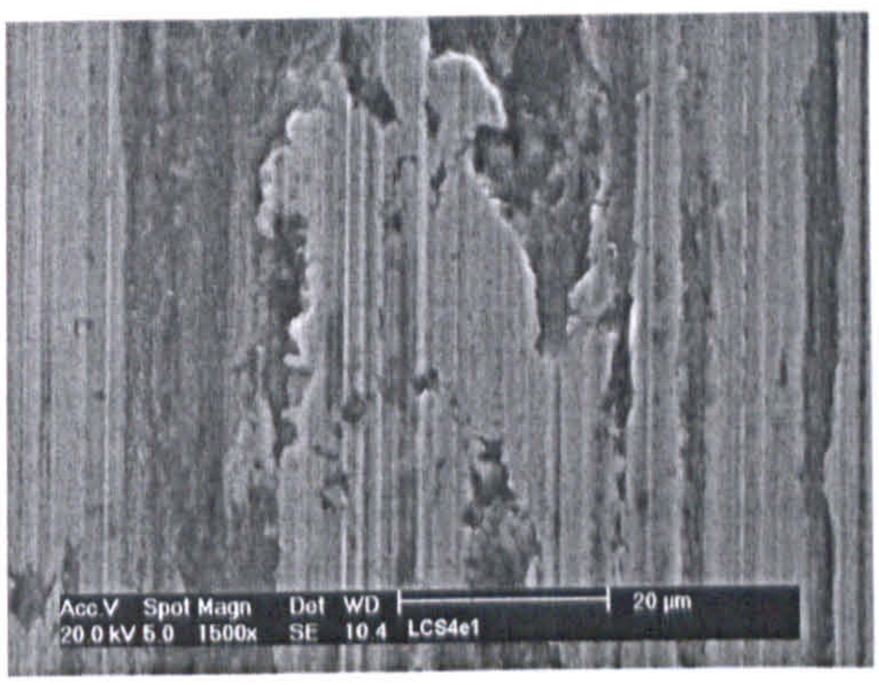

(c)

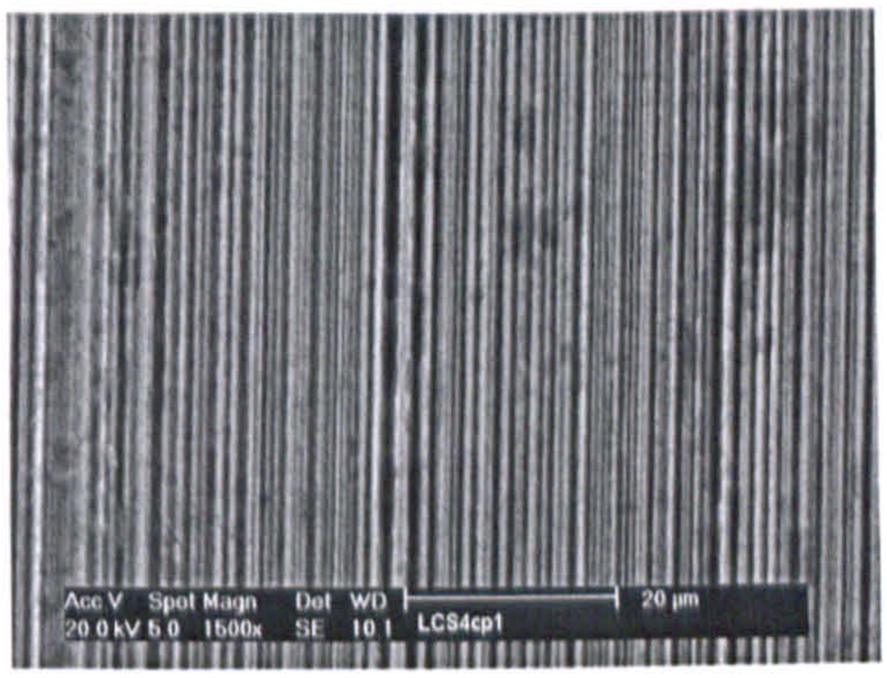

(d)

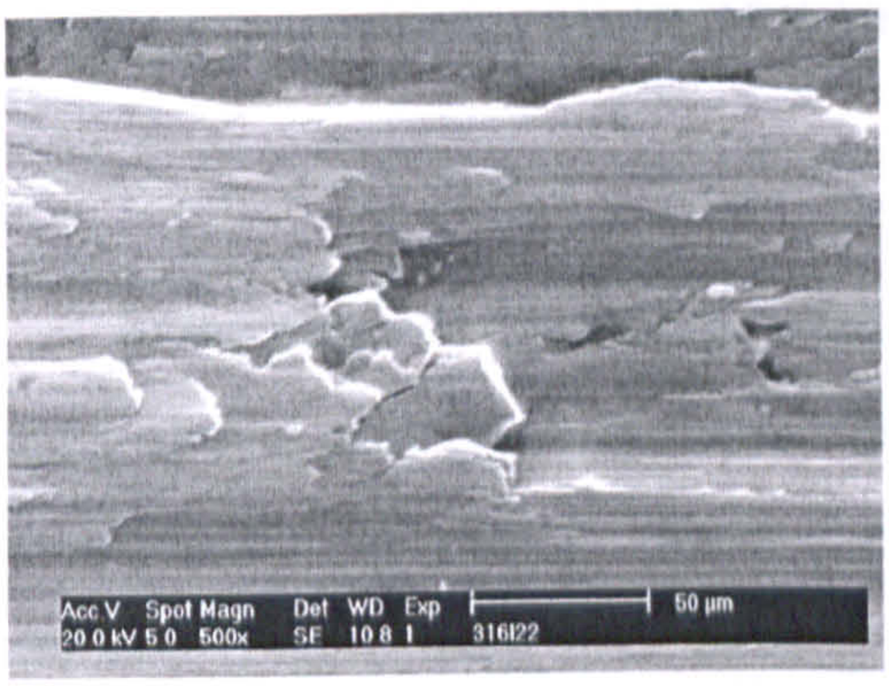

(e)

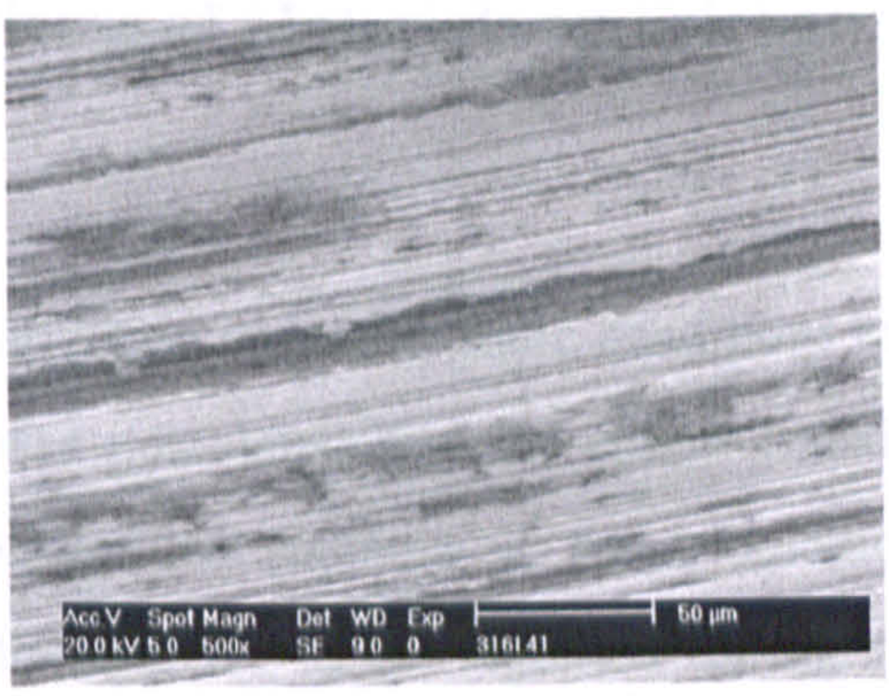

(f)

Figure 7-6 SEM images for (a) HC CoCrMo in 50% serum without Cathodic protection (b) HC CoCrMo in 50% serum with Cathodic protection (c) LC CoCrMo in 50% serum without Cathodic protection (d) LC CoCrMo in 50% serum without Cathodic protection (e) 316L in 50% serum without Cathodic protection (f) 316L in 50% serum with Cathodic protection

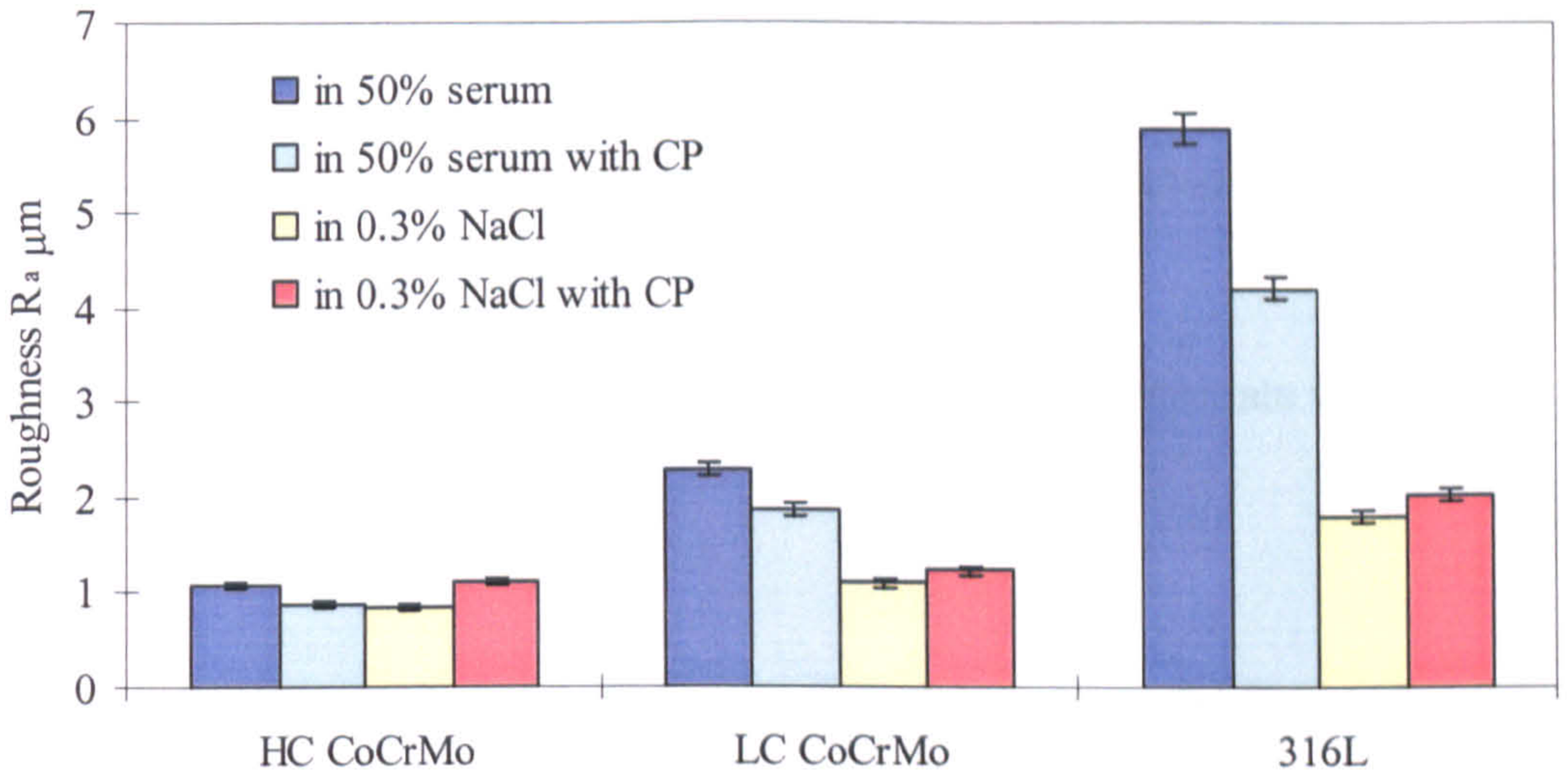

Figure 7-7 Roughness for wear scar of materials after 4 hours sliding tests in 50% serum and 0.36% NaCl with and with applied CP

7.3. Effect of Passivation and Ion Release of Materials on Friction

In the previous Chapter the anodic polarization curves in static conditions and under sliding wear were presented and it was postulated that the charge transfer occurring during sliding affects the adsorption of proteins at the tribological interface (Figure 6-9), thus causing pseudo-passivity to be regained during the polarization curve. In this section the charge transfer and the release of ions have been studied in detail and through linking this to the friction response an understanding of the interfacial processes can be developed.

The released ion concentration has been measured during anodic polarization tests in 50% serum for the three materials. At four potentials during the scan the [Co], [Cr] and [Mo] for LC CoCrMo and HC CoCrMo and [Fe], [Cr] and [Ni] for 316L were recorded respectively and the results are shown in Figure 7-8. The important characteristics of the ion release profiles are:

- An initial rapid release rate as the potential was scanned from E_{corr} to 0V was observed.
- A distinct reduction in release was observed over the potential region between 0 and 0.4V.
- When the potential exceeded 0.4V, the ion release rate was dramatically increased.

Among the detectable metal elements, for both CoCrMo alloys, the main preferentially released ion was [Co] and then [Cr]. However, three times more [Co] ion concentration was obtained from LC CoCrMo than HC CoCrMo. [Fe] was the primary ion which was released from 316L as expected under the anodic polarization scan. This is extremely important when the formation of a pseudo passive layer is considered (from Co or Fe complex formation with proteins) as is discussed in the next section when the anodic polarization response is analysed. Figure 7-9 shows the ion concentration as a function of applied potential during anodic polarization scan in DMEM. Several times of ions were detected for HC CoCrMo in DMEM than in 50% serum. Nevertheless, a reduction of ion release was obtained between 0V and 0.4V, which indicates a charge barrier was formed to cease or slow down the release of ions. It is important to note that no such reduction in [Co] release rate for LC CoCrMo, HC CoCrMo and [Fe] for 316L was measured respectively in the tests performed in 0.36%NaCl as shown in Figure 7-10.

Another fact which should be considered is that for CoCrMo alloys in 50% serum and DMEM, more [Cr] was released than [Mo] and for 316L, more [Cr] was detected than [Ni]. However, in 0.36% NaCl, [Mo] and [Ni] were obtained more than [Cr] for CoCrMo and 316L. It may indicate that apart from [Co] and [Fe] there is a preference binding of [Cr] with protein molecules and amino acids than [Mo] or [Ni].

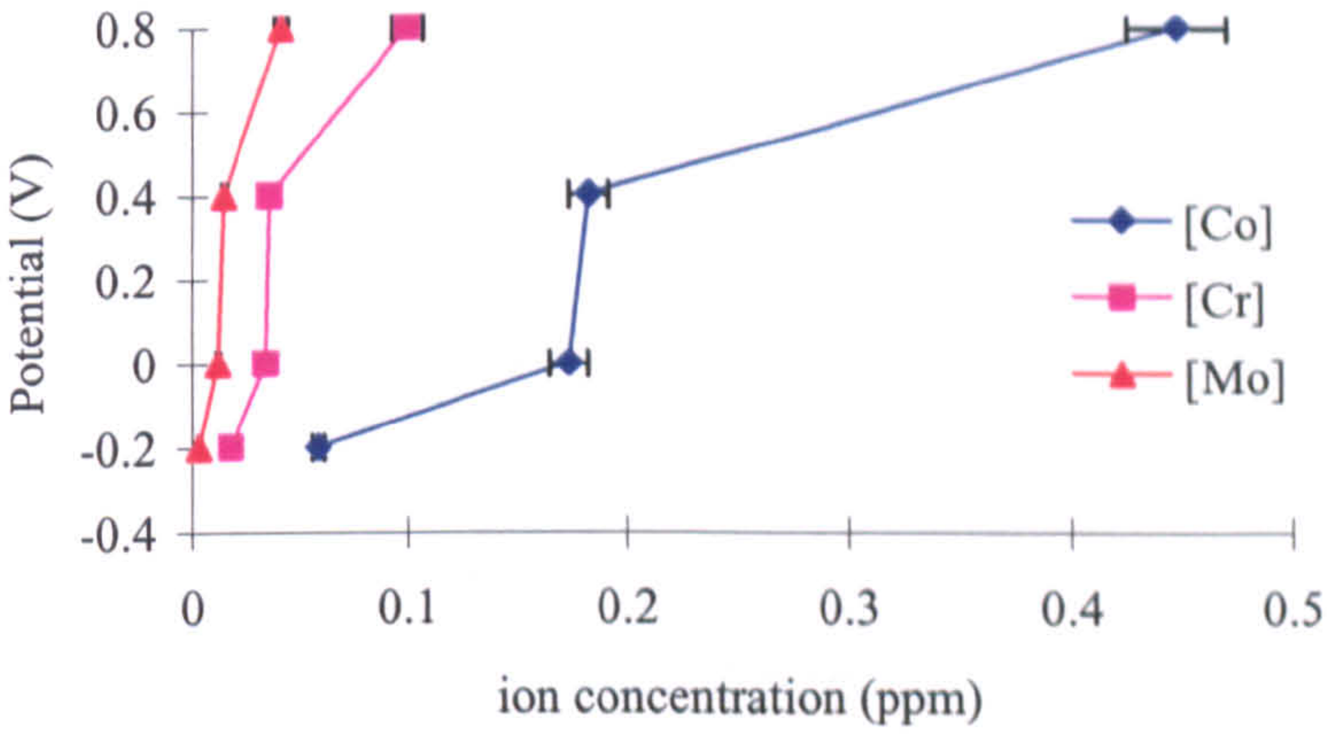

(a)

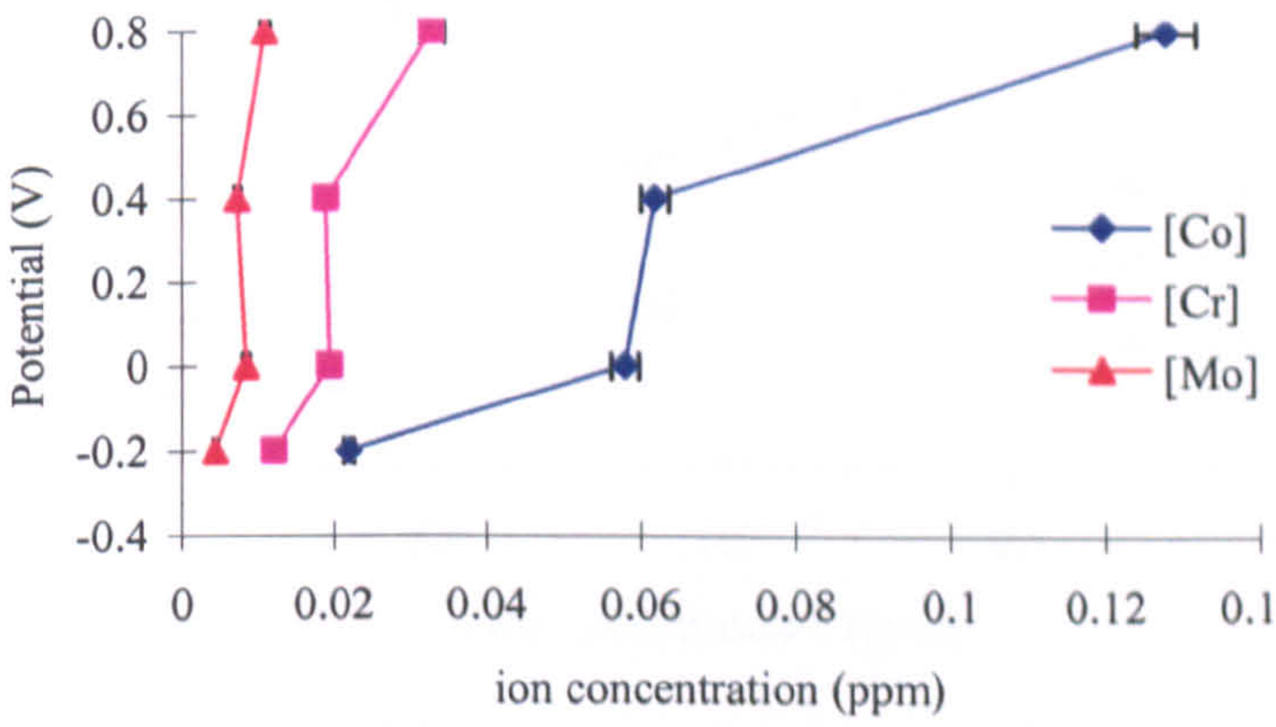

(b)

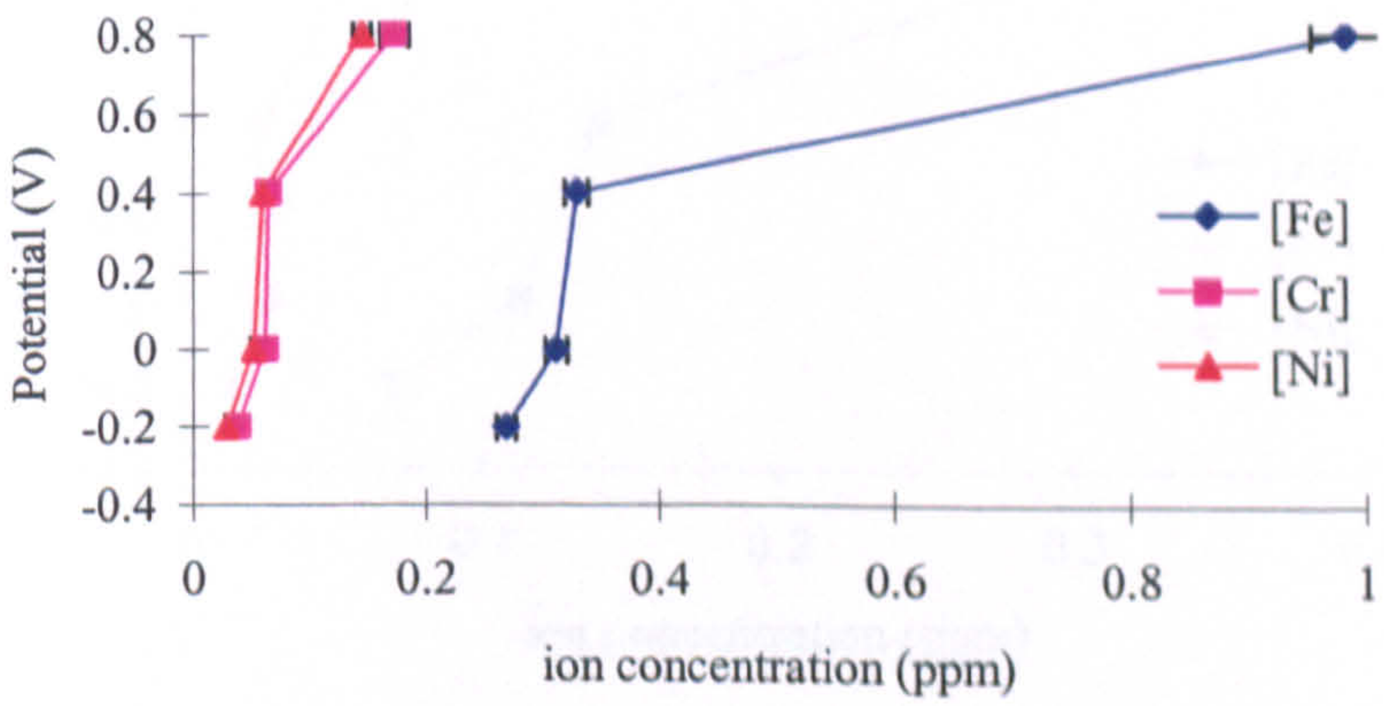

(c)

Figure 7-8 Ion concentration for (a) LC CoCrMo (b) HC CoCrMo (c) 316L in 50% serum by ICP (Inductively Coupled Plasma)

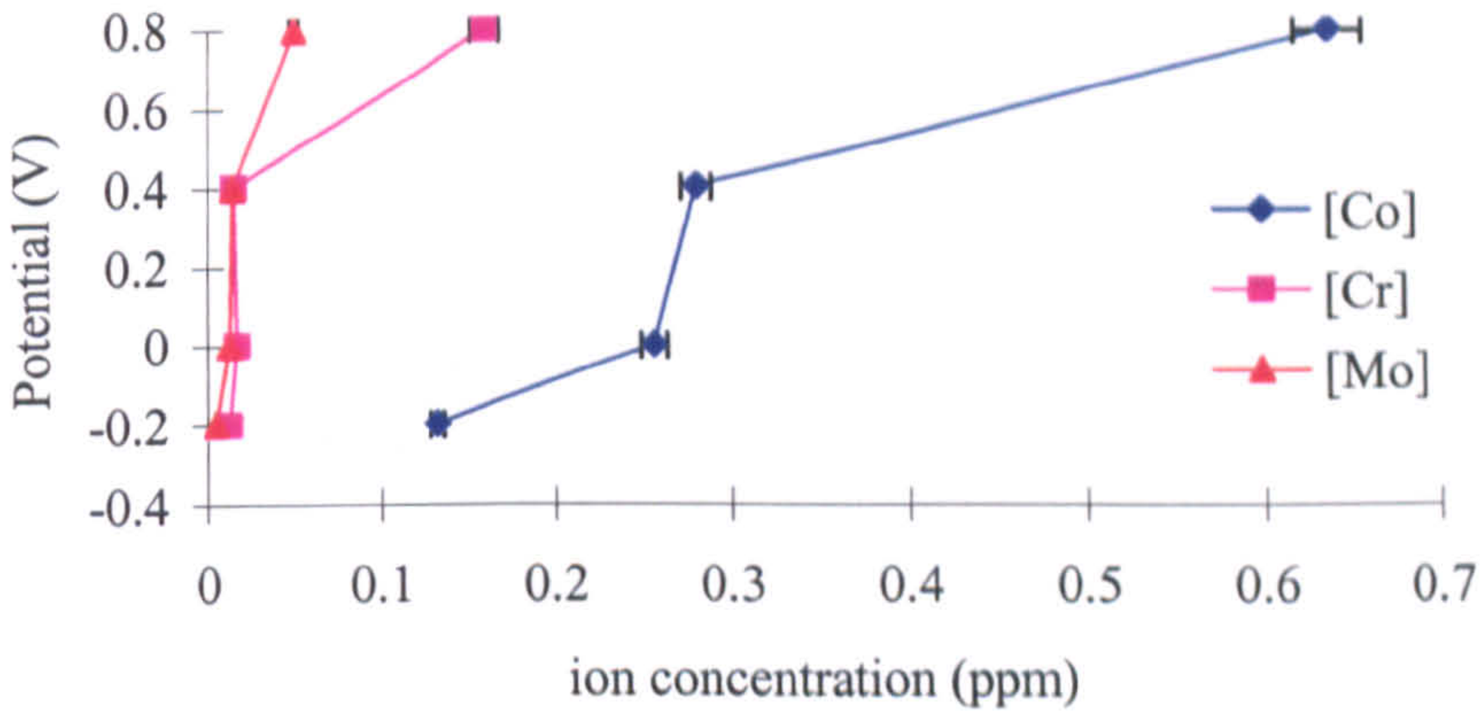

(a)

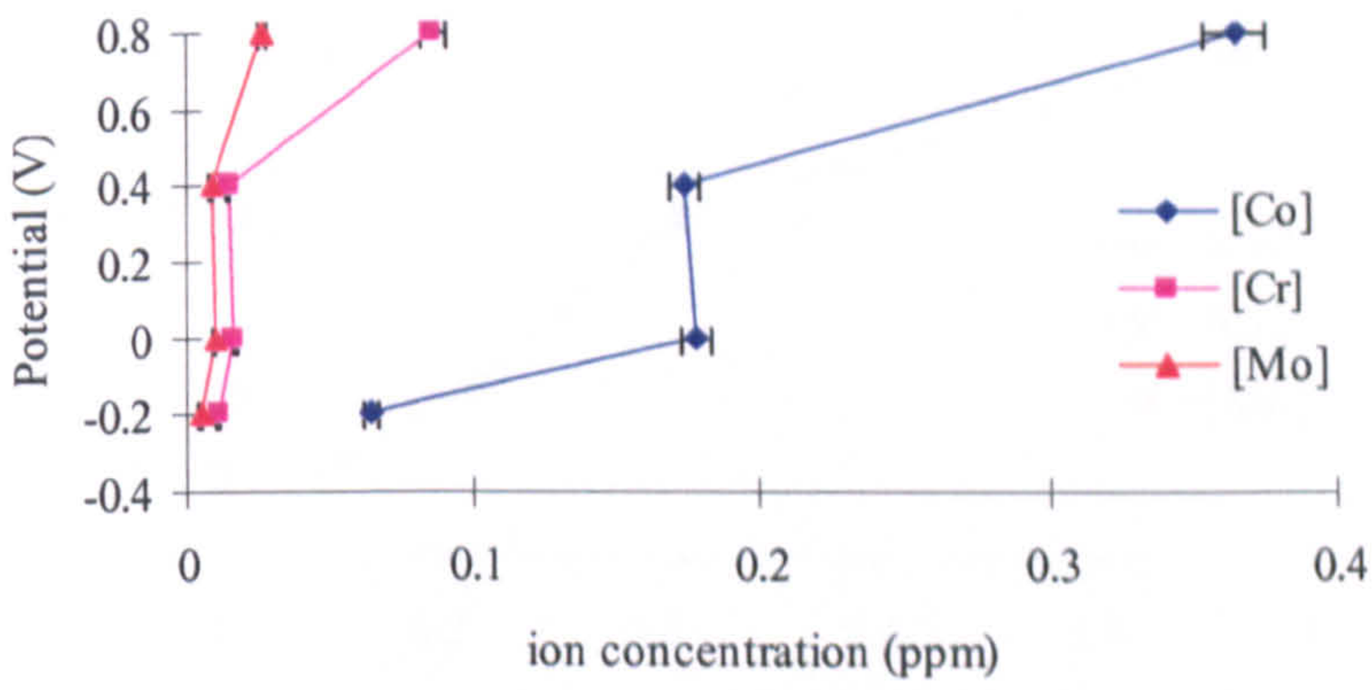

(b)

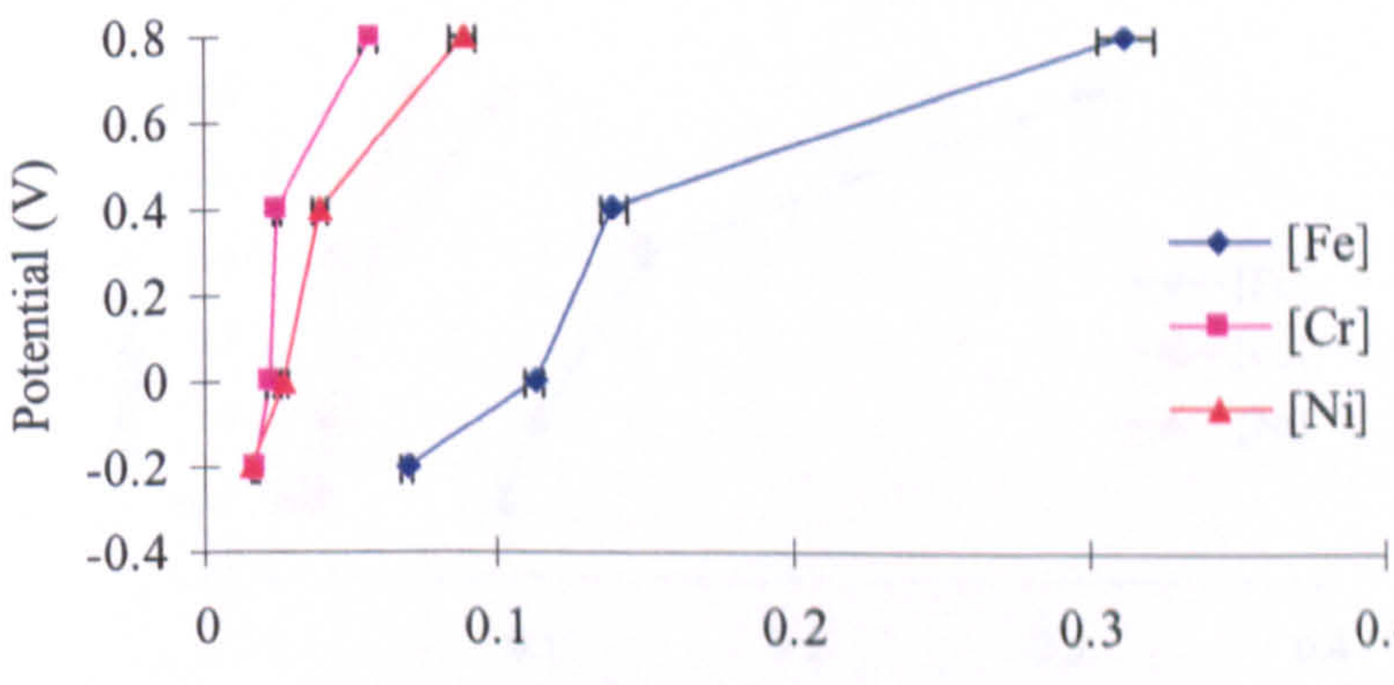

(c)

Figure 7-9 Ion concentration for (a) LC CoCrMo (b) HC CoCrMo (c) 316L in DMEM by ICP (Inductively Coupled Plasma)

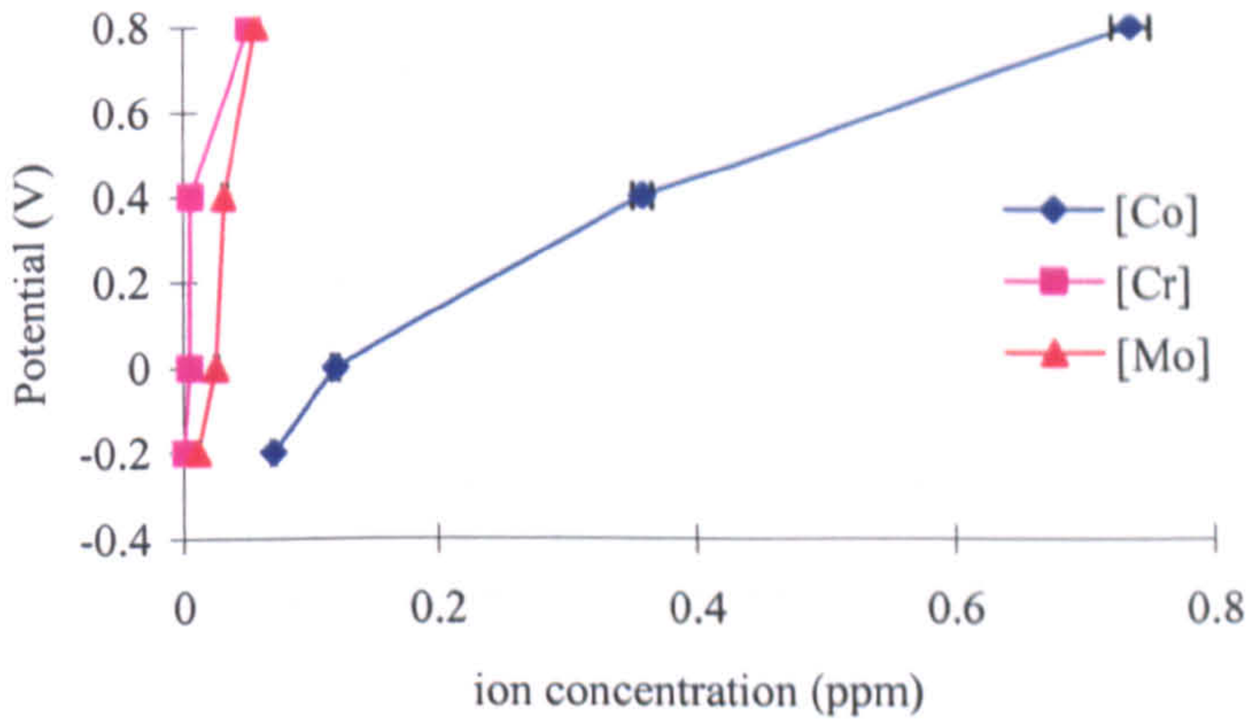

(a)

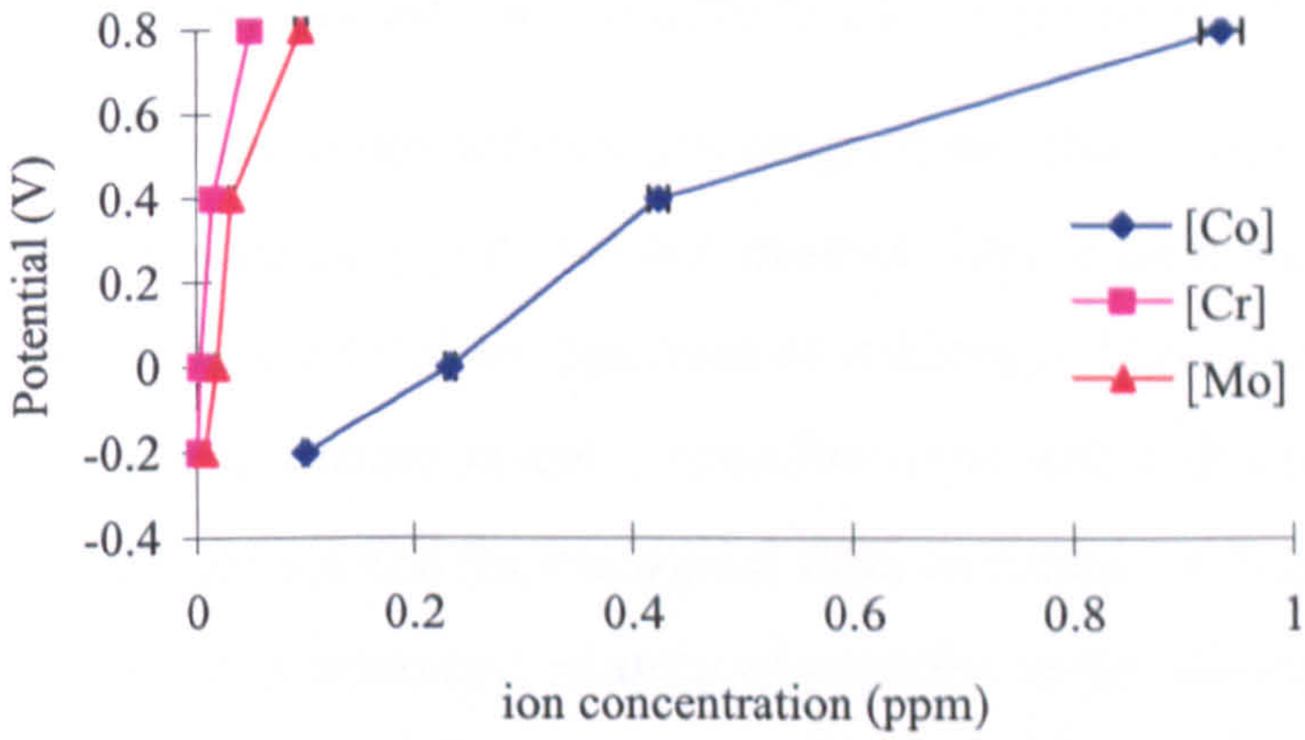

(b)

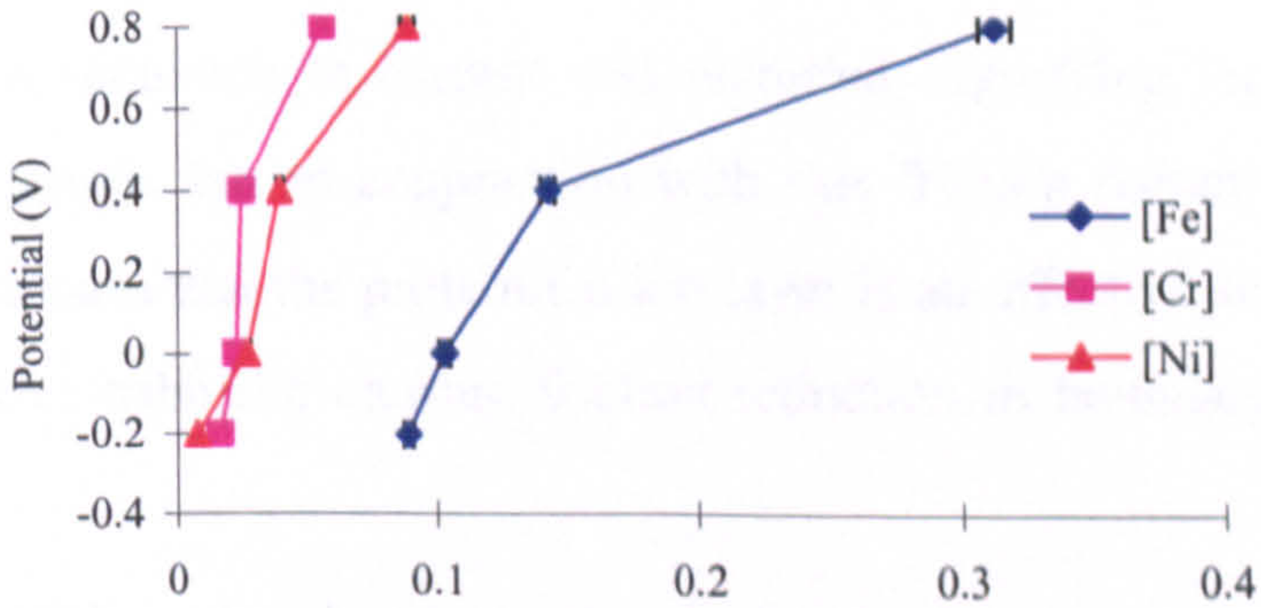

(c)

Figure 7-10 Ion concentration for (a) LC CoCrMo (b) HC CoCrMo (c) 316L in 0.36% NaCl by ICP (Inductively Coupled Plasma)

The question therefore arises – how does the ion release at the interface affect the friction response of the tribo-couple? To assess this the anodic polarization scan results (a plot of potential versus current – where the current is proportional to the ion release) can be compared with the trend in friction coefficient. These results are plotted for the three materials in 50% serum in Figure 7-11. For the first time these results are giving a good indication about the link between ion release, interactions with the biological fluid and the subsequent effect on friction.

The friction coefficient/anodic polarization response can be separated into three clear regions as shown in Figure 7-11. In each region it is possible to explain how the current, ion release and friction coefficient are related as follows:

Region 1 – In this part of the polarization diagram the charge transfer rate was controlled by activation energy given that the passive film, which would act as a charge transfer barrier, is removed by mechanical rubbing. This leads to a rapid release of Co^{2+} ions (and to a lesser extent Cr and Mo ions) and at this point the first interactions between these ions and the biological fluid occurred. It is likely that the release of Co^{2+} ions leads to enhanced binding of proteins under sliding and charge transfer at the metal/solution interface is reduced by forming a corrosion product (crystal), $Co_3(PO_4)_2.2H_2O$ [144] or an organometallic complex [145]. This signalled the start of region 2.

Region 2 – A reduction in current was recorded, signifying formation of a barrier to charge transfer but in conjunction with this friction reduction was also observed. This indicates that the protein/Co ion layer is an effective solid lubricant or forms an effective tribofilm causing friction reduction in boundary lubrication (Figure 7-11).

Region 3 – In this region the electrochemical potential changes lead to pitting of the surface and at this point the protein/Co layer integrity was breached and friction was increased due to a micro-roughening effect.

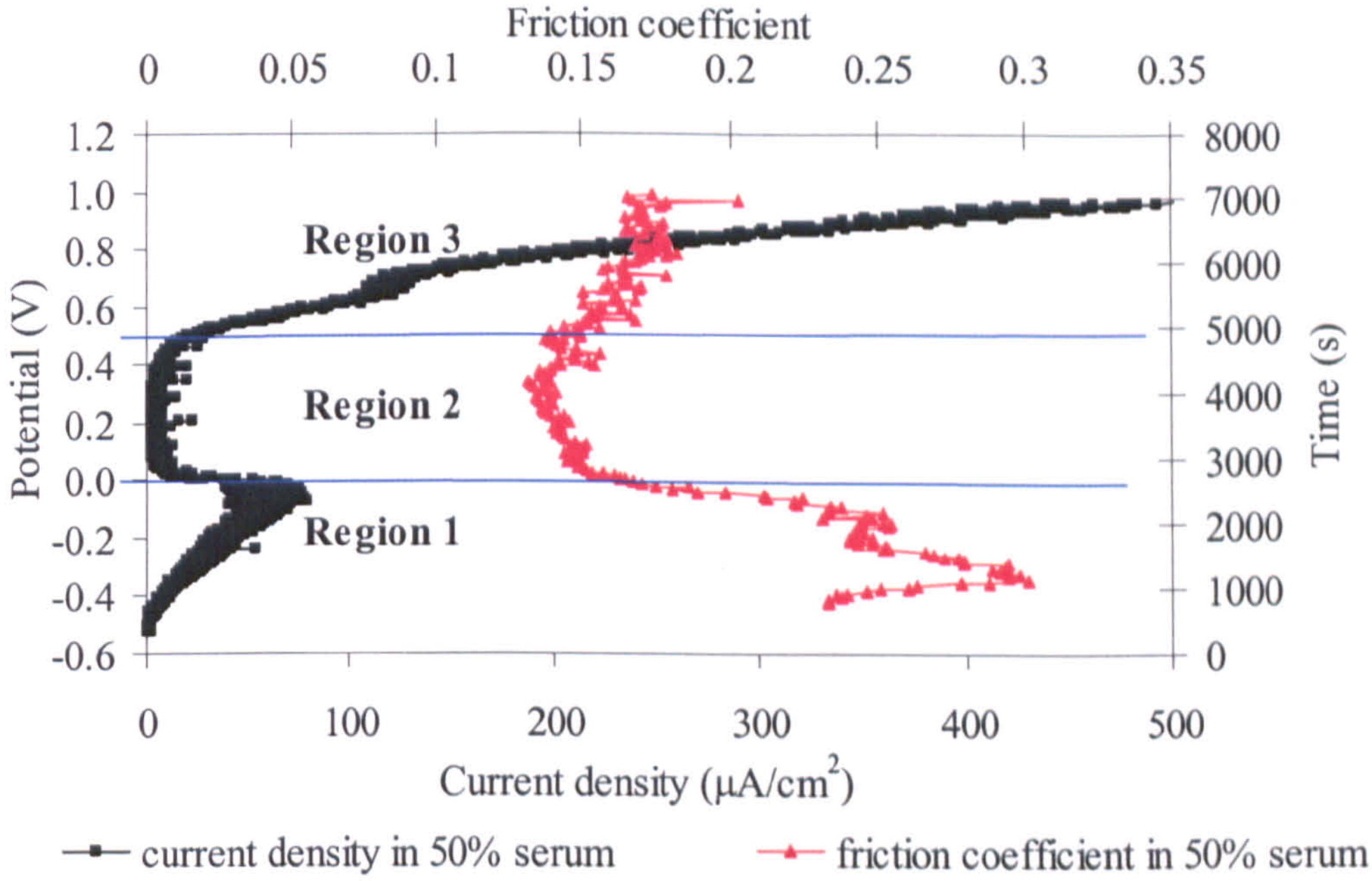
Friction coefficient
0
0.05
0.1
0.15
0.2
0.25
0.3
0.35
Region 3
Region 2
Region 1
Potential (V)
Time (s)
1.2
1.0
0.8
0.6
0.4
0.2
0.0
-0.2
-0.4
-0.6
8000
7000
6000
5000
4000
3000
2000
1000
0
0
100
200
300
400
500
Current density (μA/cm²)
current density in 50% serum
friction coefficient in 50% serum

(a)

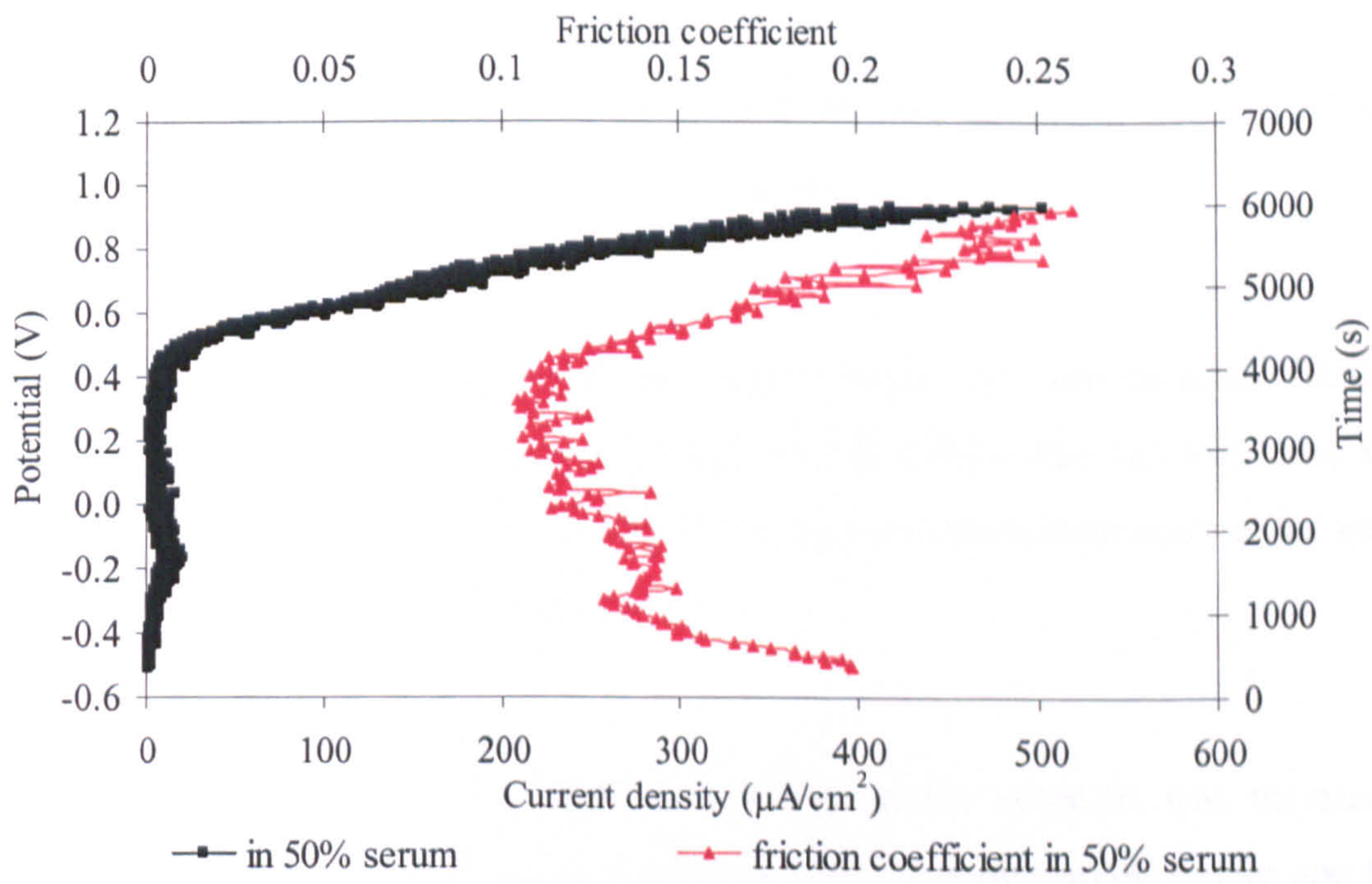
Friction coefficient
0
0.05
0.1
0.15
0.2
0.25
0.3
Potential (V)
Time (s)
1.2
1.0
0.8
0.6
0.4
0.2
0.0
-0.2
-0.4
-0.6
7000
6000
5000
4000
3000
2000
1000
0
0
100
200
300
400
500
600
Current density (μA/cm²)
in 50% serum
friction coefficient in 50% serum

(b)

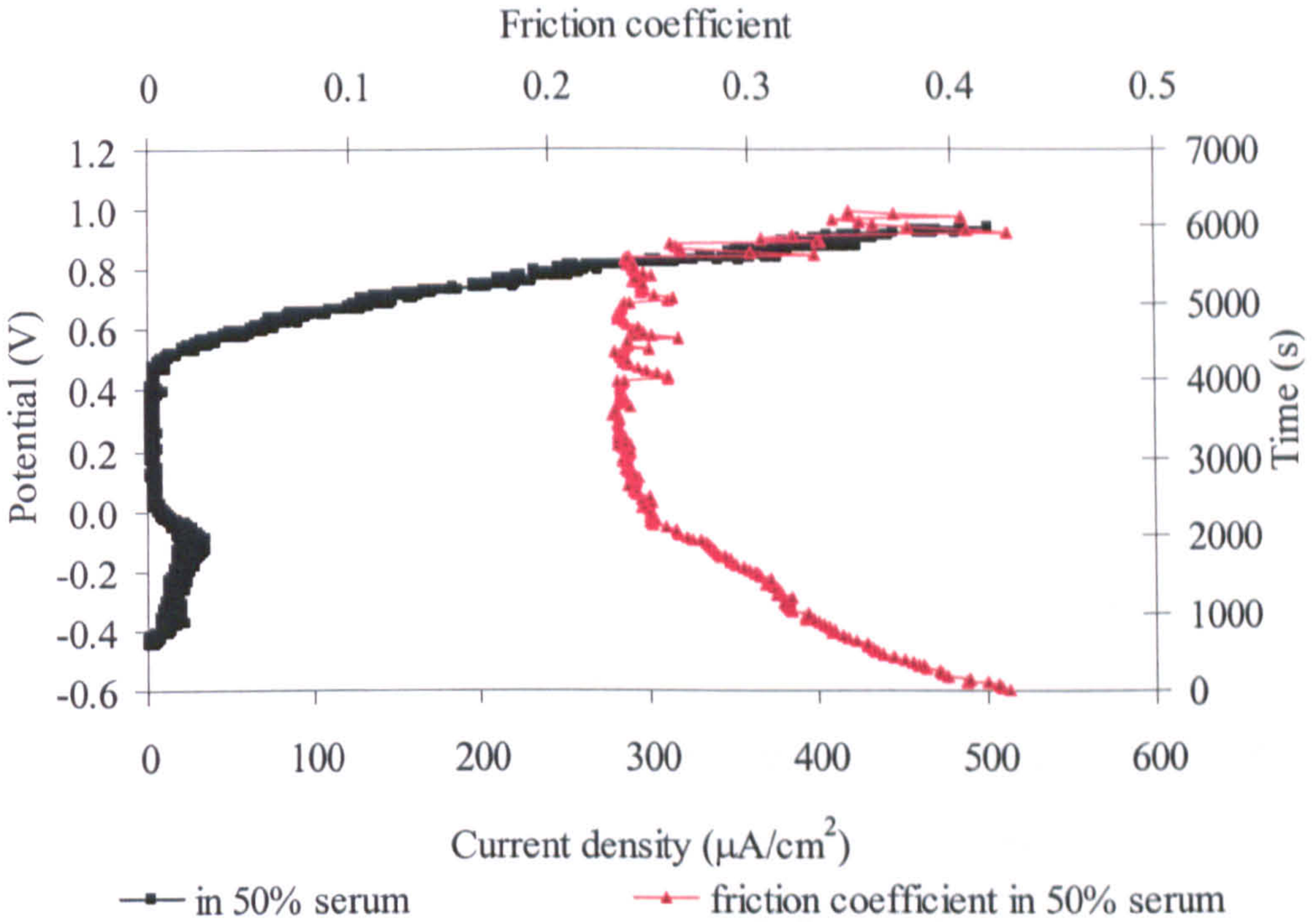

(c)

Figure 7-11 Anodic polarization and friction coefficient curves for (a) LC CoCrMo (b) HC CoCrMo and (c) 316L in 50% serum

Figure 7-12 shows the anodic polarization scans and corresponding friction coefficient traces in DMEM for 316L and HC CoCrMo. For LC CoCrMo, the behaviour is very similar to HC CoCrMo. There are also three clear regions and each region presented distinct performance.

In region 1, current increased dramatically as the potential was increased. Comparing with the same material in 50% serum, the region lasted longer and the current reached a much greater value before a barrier formed. In The friction behaviour was unsteady for CoCrMo alloy.

In region 2, a reduction of both current and friction was monitored. However, this region was much shorter than region 2 in 50% serum. Furthermore, the

minimum current and friction that they reached were greater than in serum, which indicates that the barrier was not as stable and the lubrication effect was not as efficient.

In region 3, the surface broke down in an electrochemical sense and localized corrosion occurred, which led to an increased current and friction coefficient.

From these results it is apparent that the release of Fe^{2+} ions in DMEM and in 0.36%NaCl have little effect on the friction coefficient and a steady high value of 0.6-0.8 is maintained for the 316L alloy during the test. For the HC CoCrMo alloy (and the LC CoCrMo alloy – not shown) there is *some* correlation between ion release and friction but this is not as well defined as it is for the 50% serum. As the release of Co ions progresses in the activation-controlled region of the polarization curve a drop in friction coefficient was recorded to 0.3 and 0.4 in DMEM and 0.36%NaCl respectively suggesting that a tribofilm was formed which modified the frictional characteristics of the interface. This is being examined in detail using XPS and will be shown later but it is sufficient to say here that the amino acids in DMEM have, to some extent, absorption capabilities which can reduce friction. It is however suggested that part of that friction modification is also due to modification of the passive layer by electrochemical processes (non biological) as demonstrated in 0.36% NaCl.

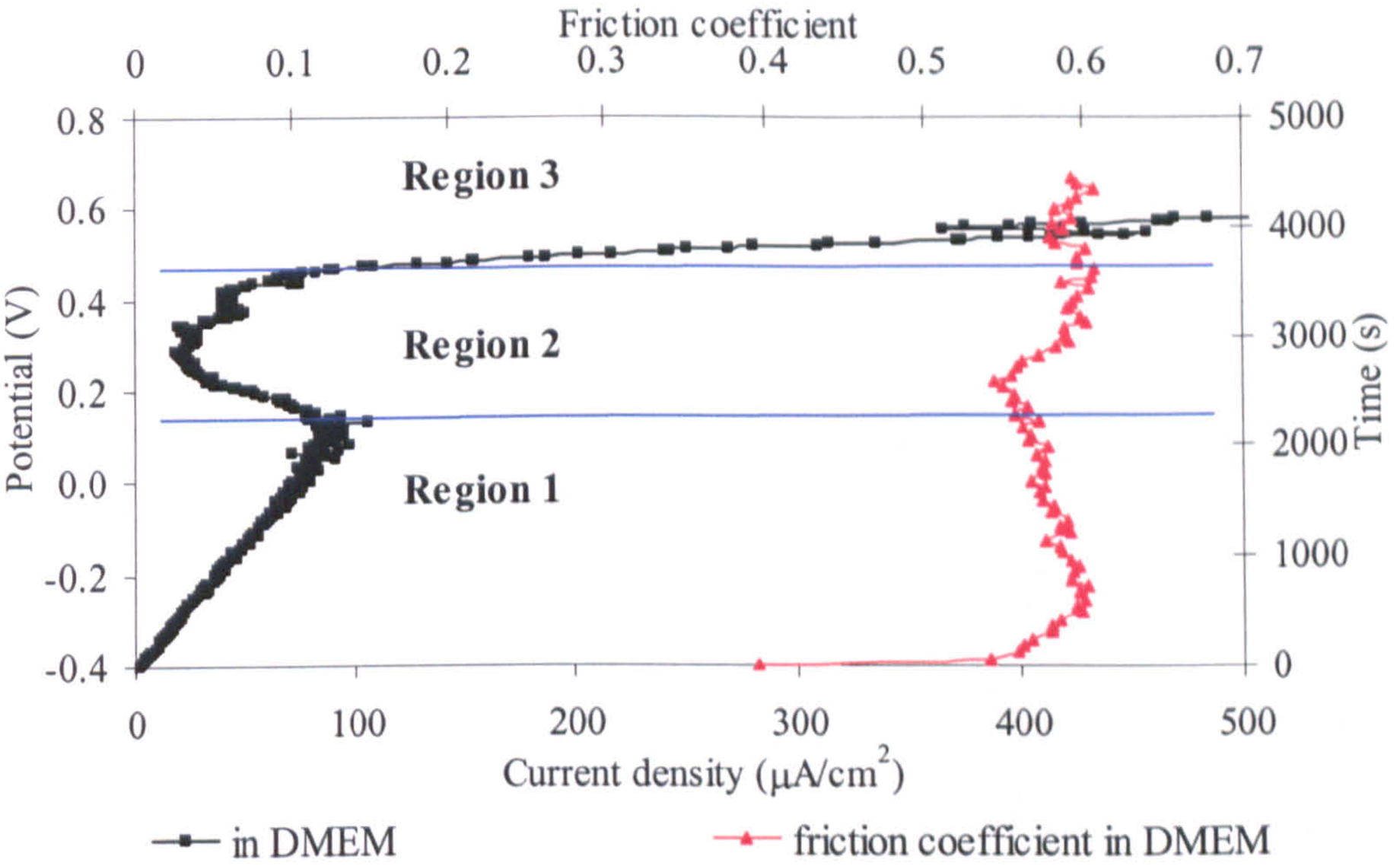

(a)

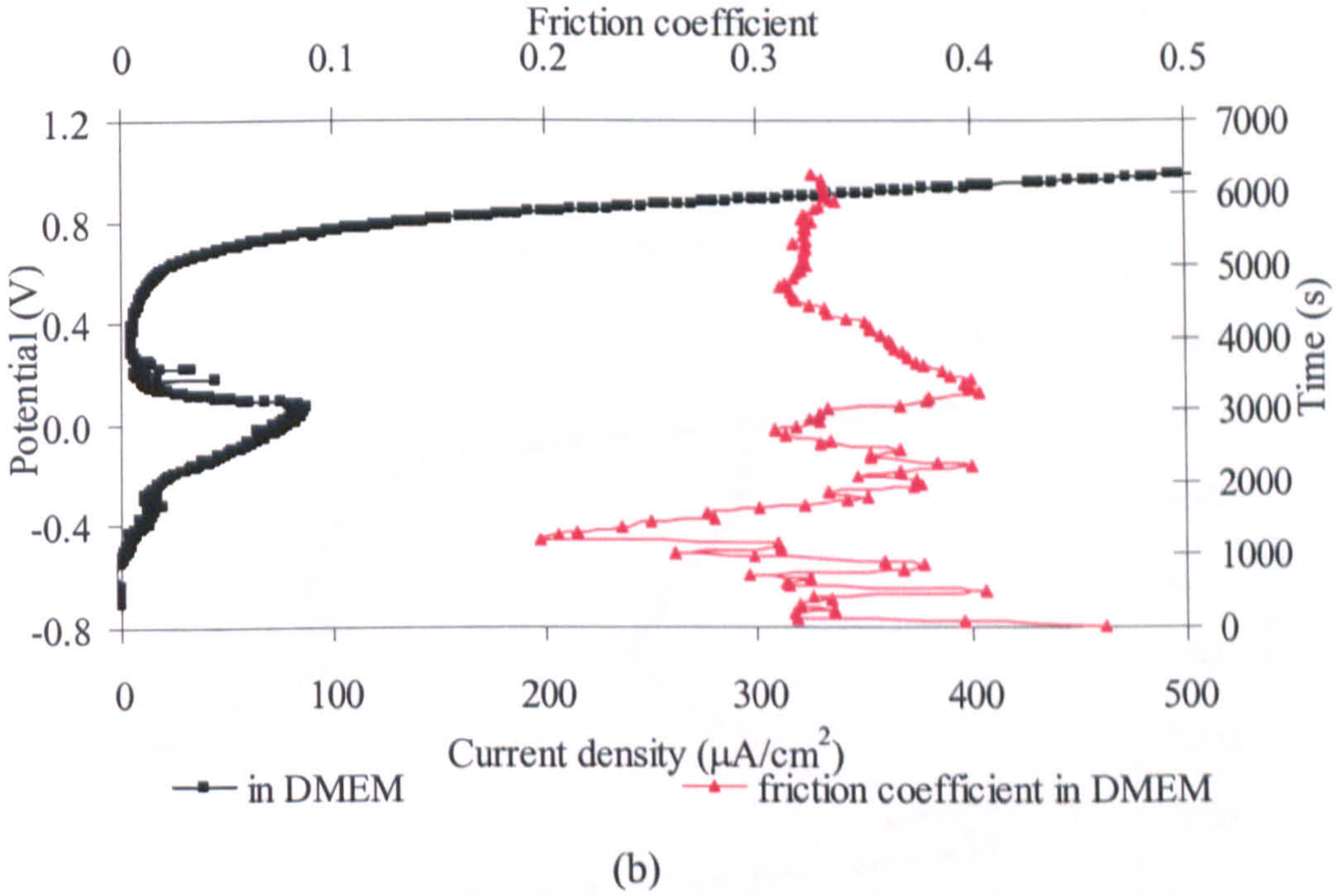

(b)

Figure 7-12 Anodic polarization and friction coefficient curves for (a) 316L and (b) HC CoCrMo in DMEM

Anodic polarization scans were then performed in 0.36% NaCl (Figure 7-13) The behaviour was different when the organic species were involved. A passive film

still managed to form after an activation region. Friction was correspondingly high, which may indicate that the shear force of the removal of the passive film increases the friction.

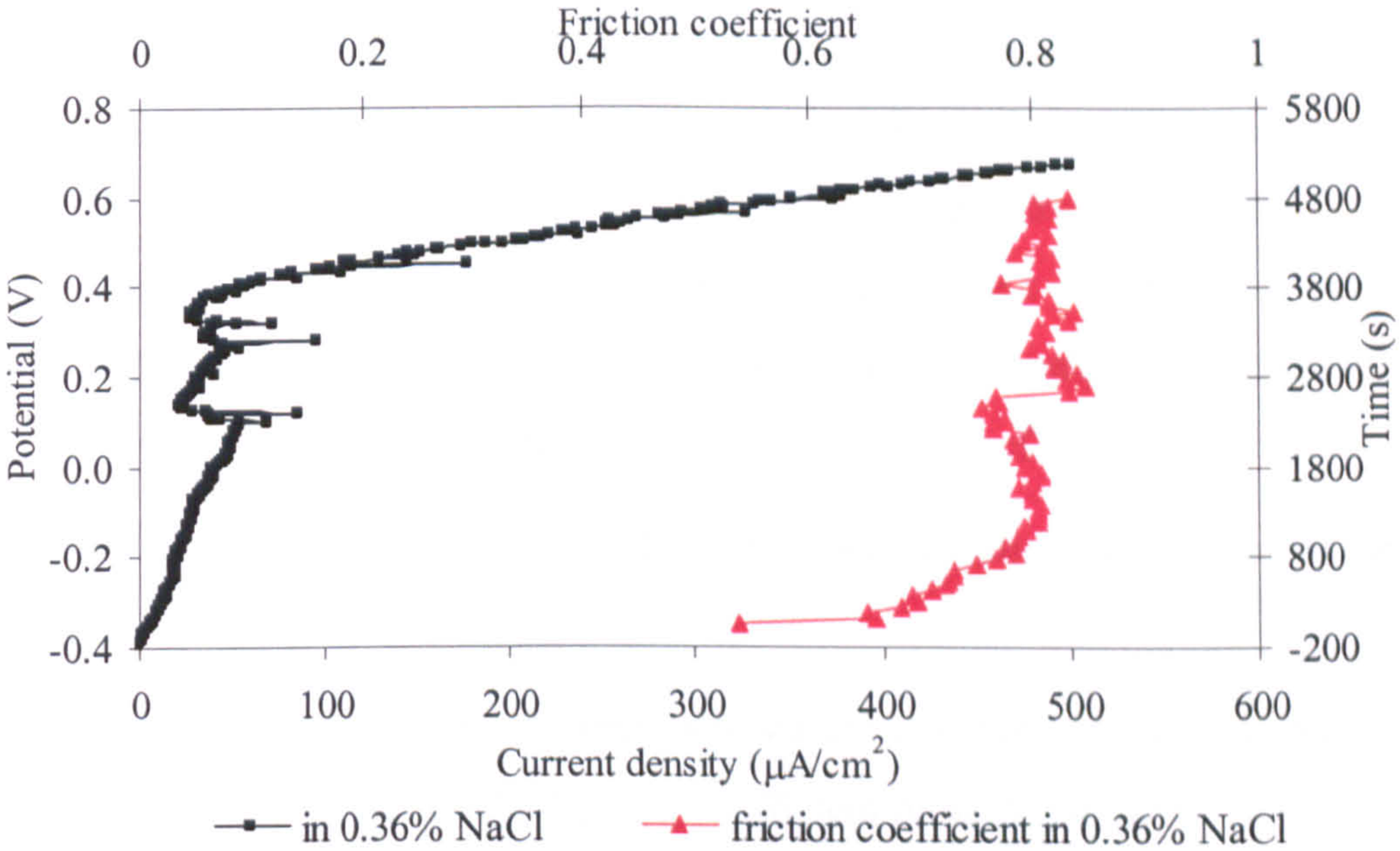

(a)

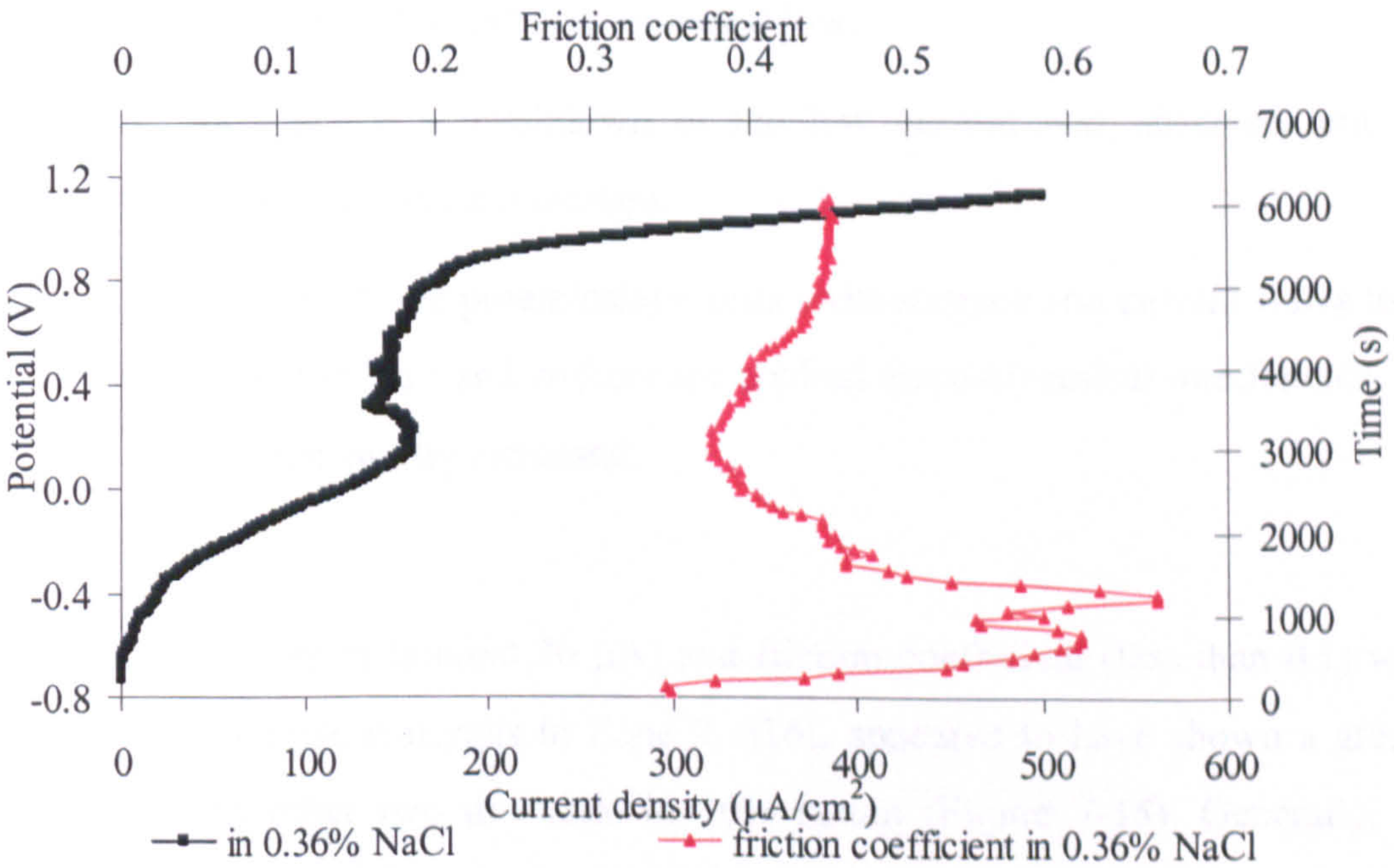

(b)

Figure 7-13 Anodic polarization and friction coefficient curves for (a) 316L and (b) HC CoCrMo in 0.36% NaCl

7.4. Current and Friction Under Potentiostatic Tests

As shown in the previous section, a pseudo-passive like film was obtained during anodic polarization on three materials in 50% serum and DMEM. It slowed down the ion release rate and reduced the friction force. In order to gain a whole picture of this period and this behaviour, potentiostatic tests under tribological contact were carried out. The potential was controlled at 0.2 V, where all materials in this study were in the passive region. Detailed passive, breakdown and behaviour was studied with the changes of friction force and velocity of sample movement.

Figure 7-14 (a) shows HC CoCrMo under potentiostatic test. Four zones can be defined for the friction coefficient.

- In Zone 1, the experiment was started and the current soon reached a steady value and the friction coefficient remained at 0.14.
- In Zone 2, the current rapidly decreased, which caused the drop of friction. The value of current stayed very low (0.02 mA) and the friction coefficient also remained low.
- In Zone 3, a breakdown of the low current was observed and the friction response increased.
- In Zone 4, the potentiostatic tests were stopped (no current flows to or from the WE) and without the applied electrochemical interference, the friction swiftly increased.

Very low current (around 30 μA) and friction coefficient (less than 0.1) were obtained for all three materials in Zone 2. 316L appeared to have shown a greater oscillation than other two materials in 50% serum (Figure 7-15). Generally, the current and friction for 316L were also higher, which is consistent with Figure 6-3 in the previous chapter. Detailed analysis was made in Zone 2 in Figure 7-14 (b). Figure 7-14 (b), Figure 7-15 (b) and (d) show the current in 2 seconds (2 cycles of the reciprocating movement) with the friction force. The velocity of the sliding is not

linear which makes it possible to study the depassivation/rapassivation with the change of velocity. Clear phenomena relating to breakdown by the rubbing and repassivation by electrochemical process were seen.

- The current increased along with the increase of the velocity and the current decreased with the decreased velocity, which indicates that repassivation had taken place after the passive film being rubbed off. In addition, temperature varies across stroke length, which also may contribute to the change of current under sliding. Higher velocity can result in higher temperature then gives a higher current response.
- The friction force was generally uniform. However, while the velocity and the current increased, the friction force has a slightly higher value.
- When the current and the velocity reached the maximum values, the friction force seemed to display the lowest during the cycle.

Tests were also performed in 0.36% NaCl, no clear definition of distinct zones can be noticed (Figure 7-16 and Figure 7-17). Albeit, after the potential (0.2 V) was removed, the materials should firstly depassivated and then built a passive film again, where the friction appeared to decrease. It is consisted with the anodic polarization tests. The locally removal of the passive film by rubbing reinforce the friction coefficient.

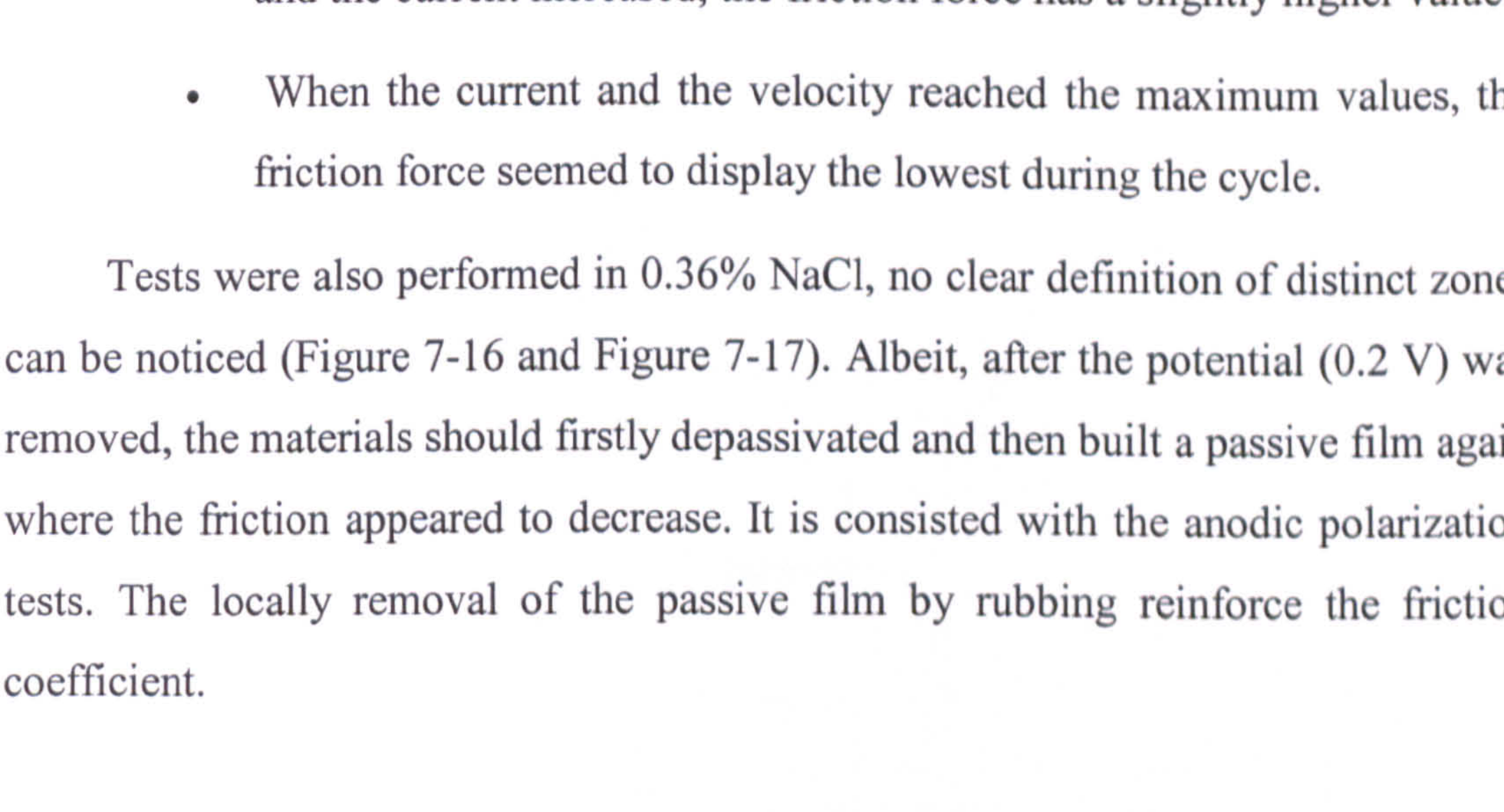

(a)

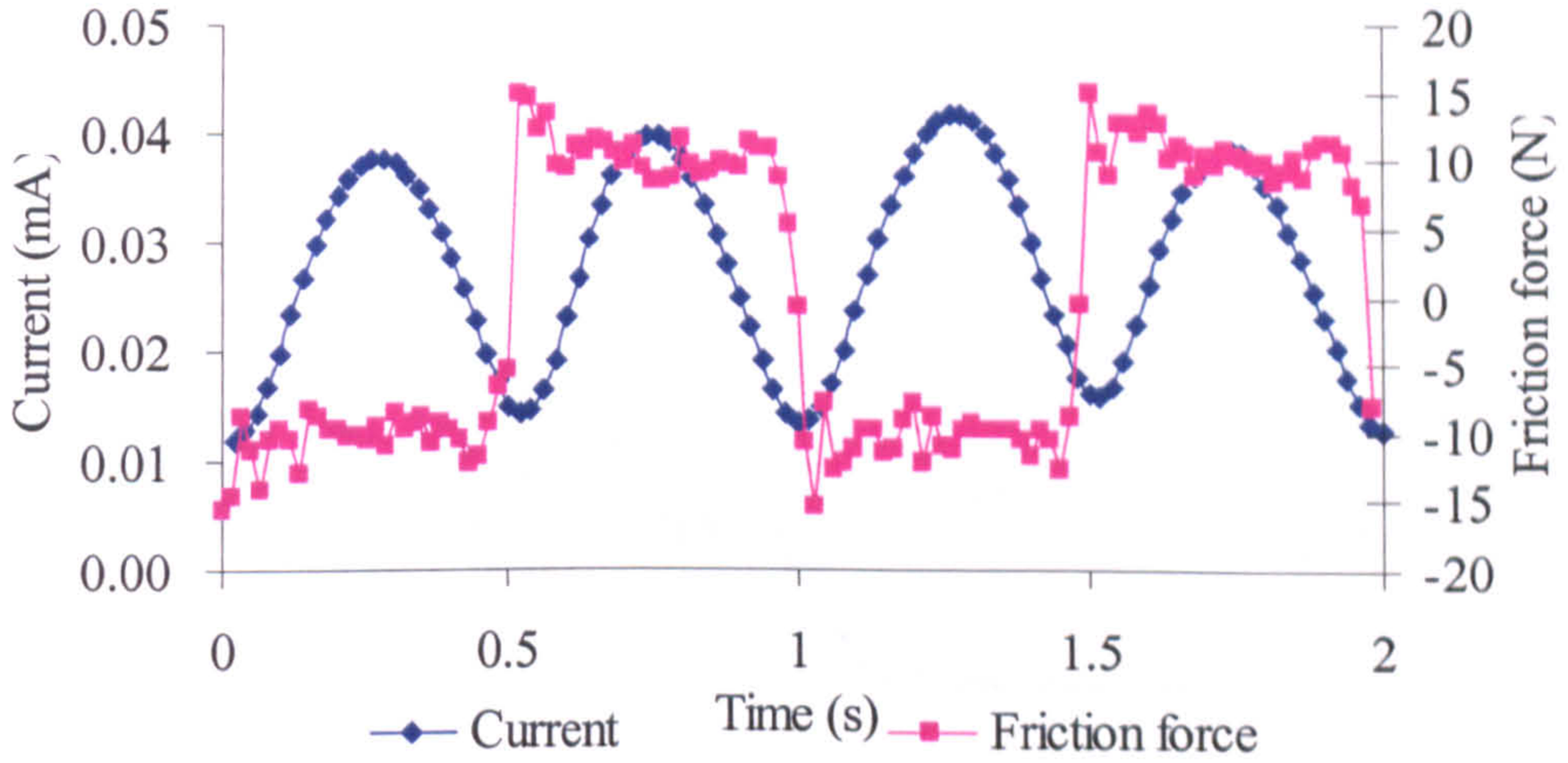

(b)

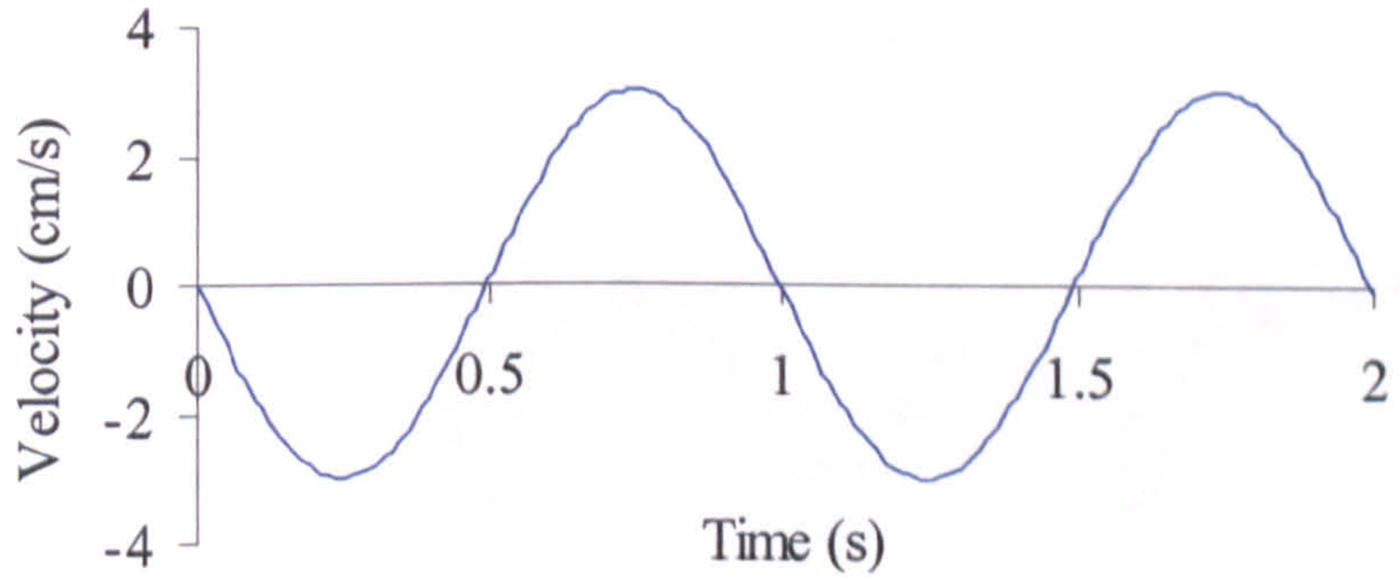

(c)

Figure 7-14 Current and friction curves at 0.2 V applied potential for HC CoCrMo in (a) 4 hours , (b) 2 cycles in the region 2 in 50% serum and the velocity change in 2 cycles is shown in (c)

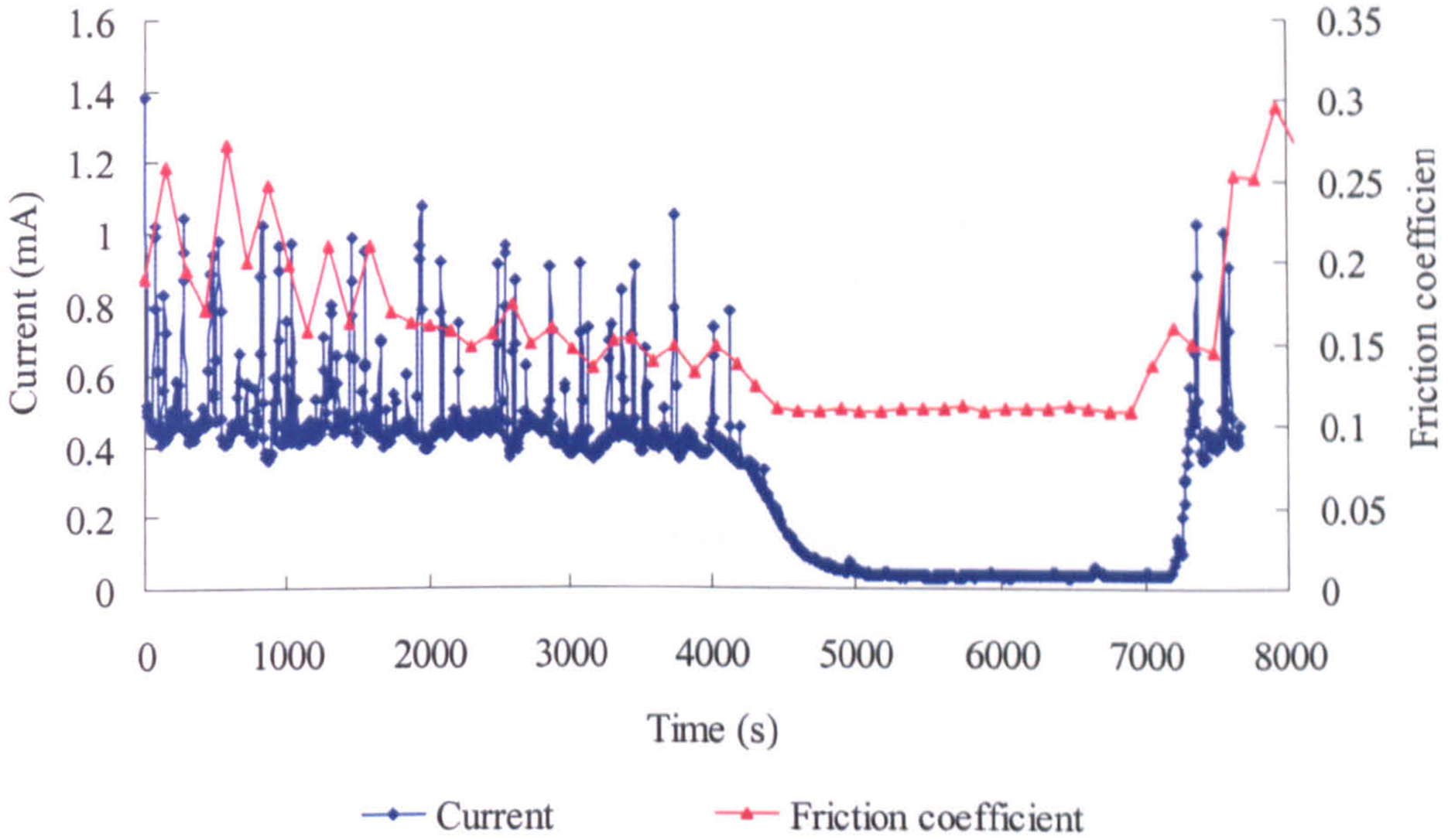
Current (mA)
Friction coefficien
Time (s)
Current
Friction coefficient

(a)

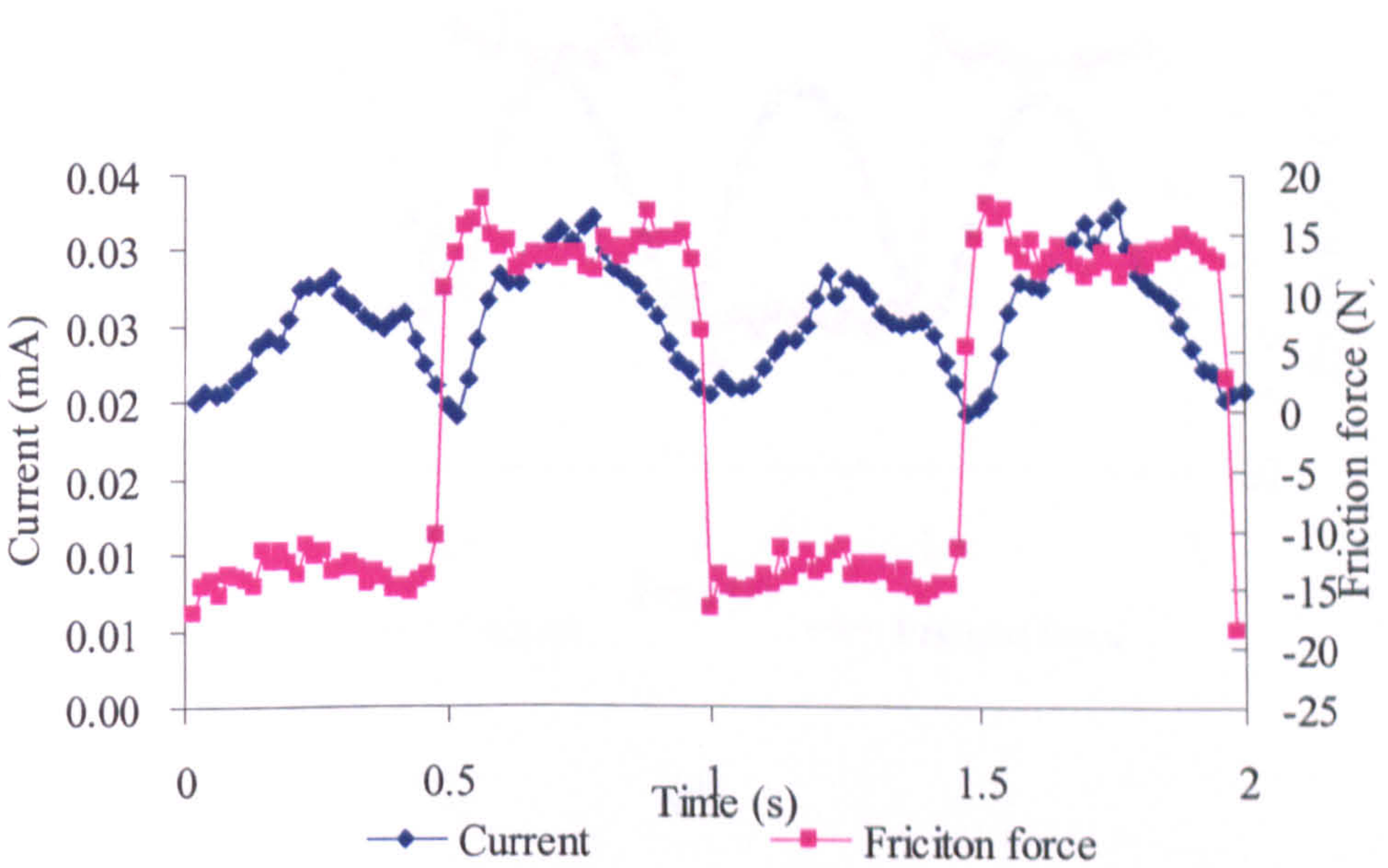
Current (mA)
Friction force (N
Time (s)
Current
Friciton force

(b)

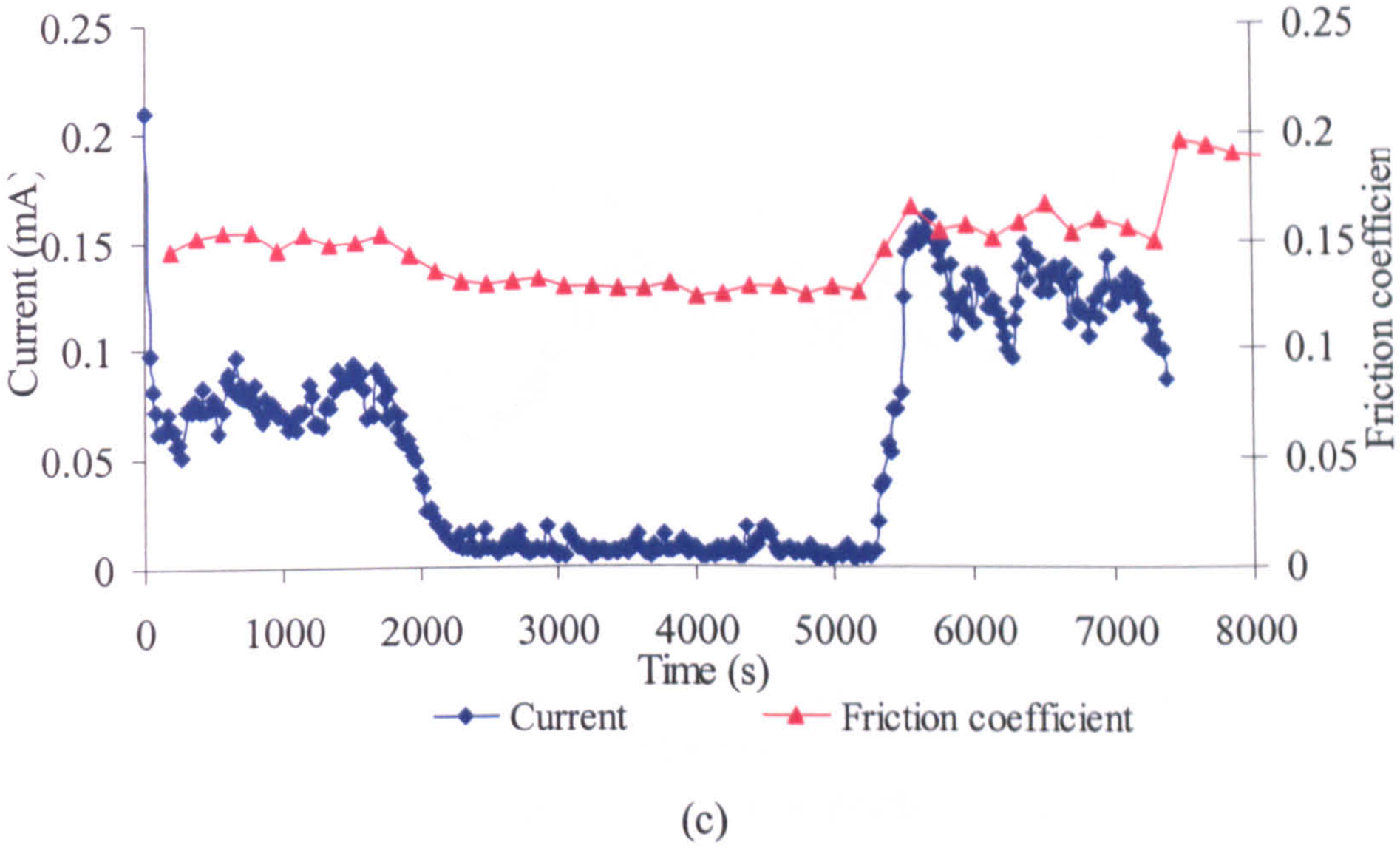

(c)

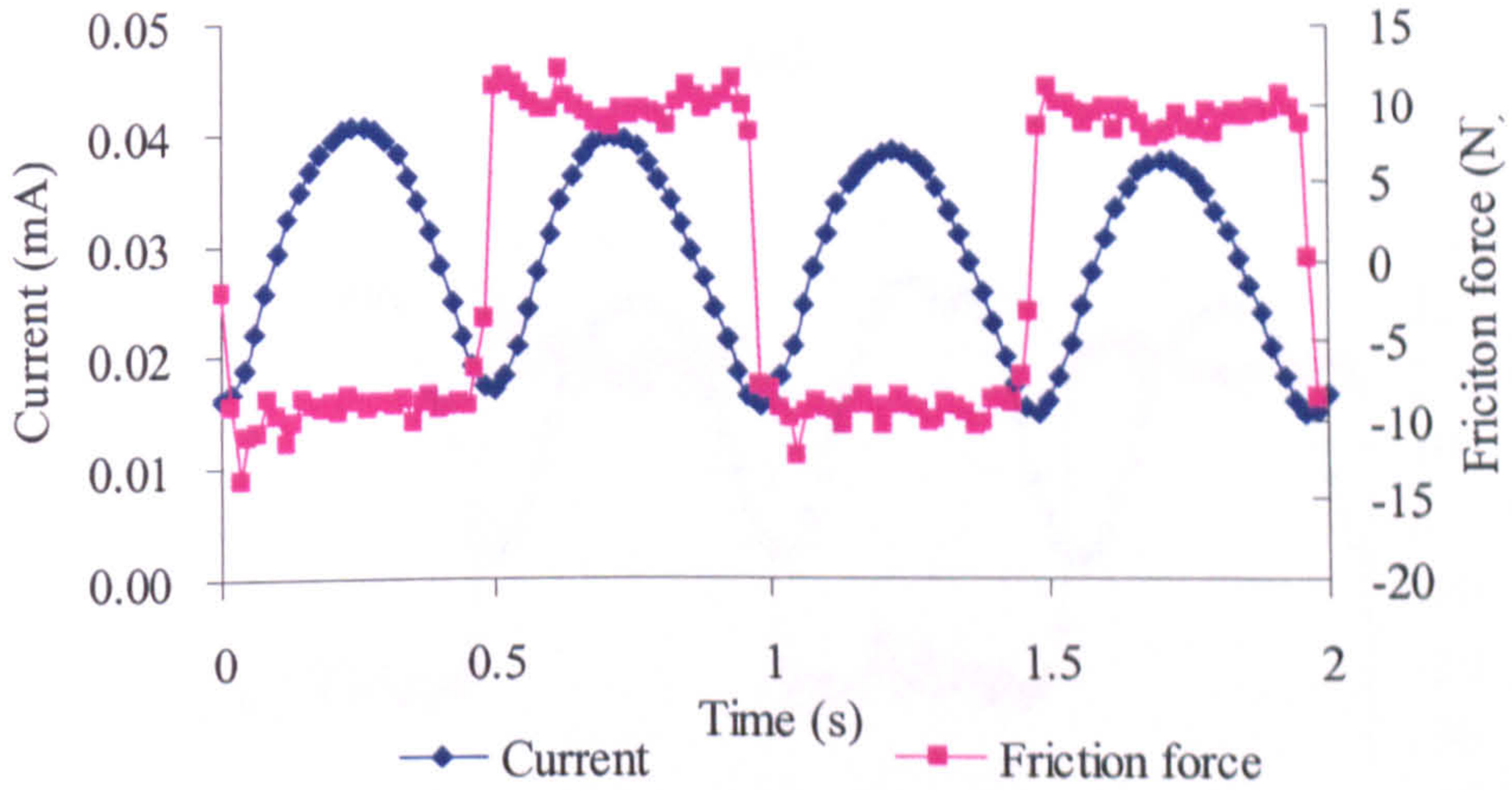

(d)

Figure 7-15 Current and friction curves at 0.2 V applied potential for 316L in (a) 4 hours , (b) 2 cycles in the region 2 and LC CoCrMo in (c) 4 hours and (d) 2 cycles in the region 2 in 50% serum

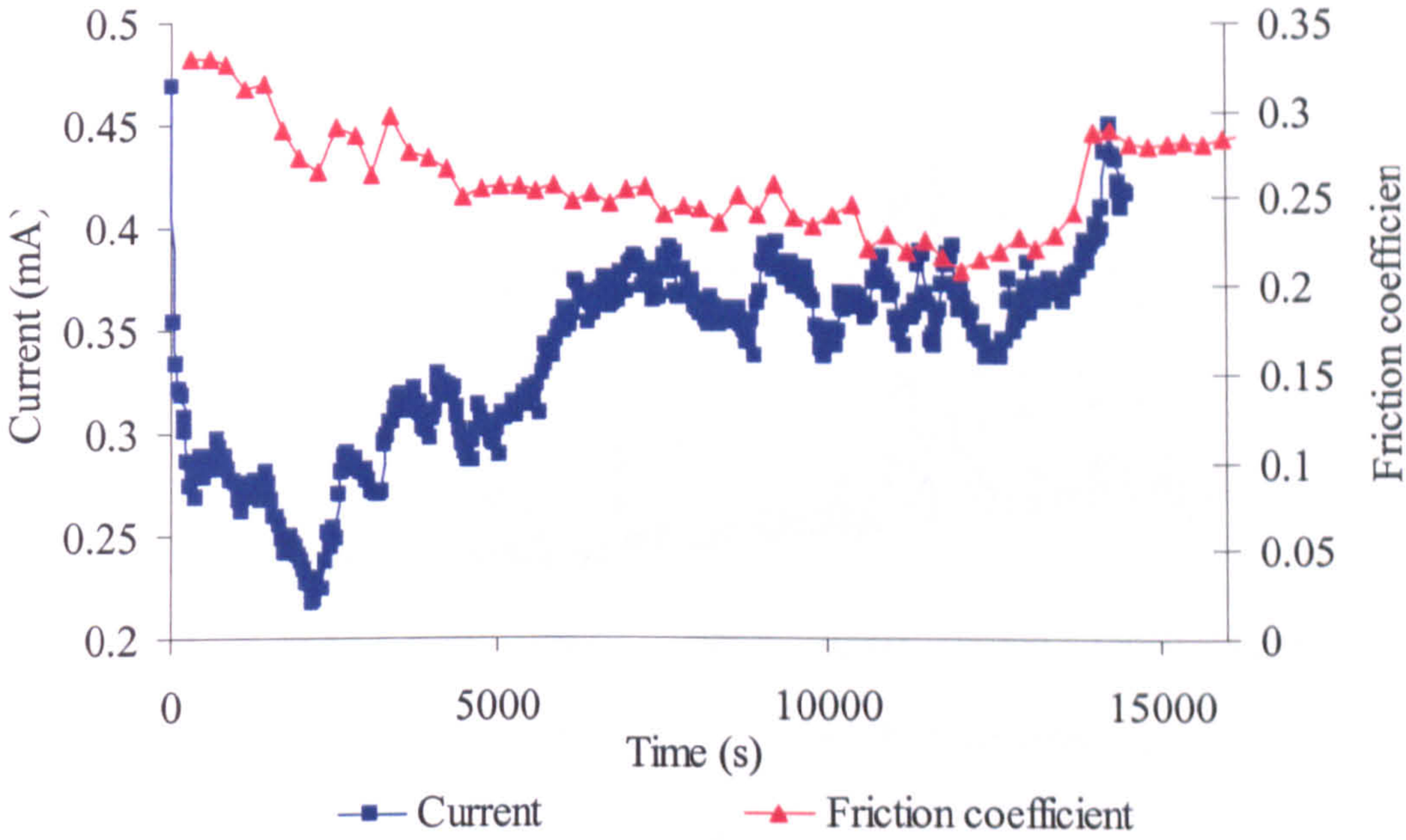

(a)

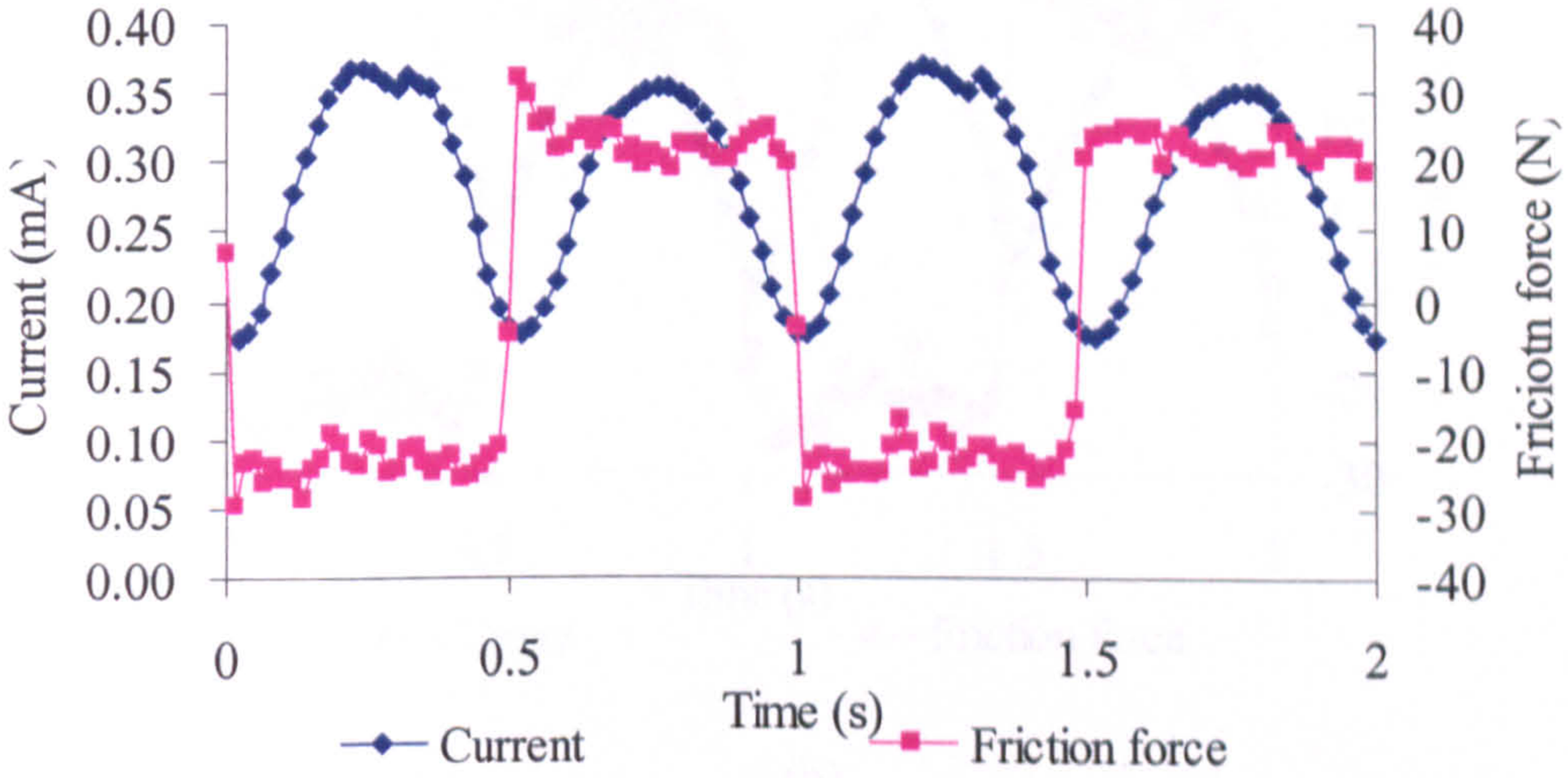

(b)

Figure 7-16 Current and friction curves at 0.2 V applied potential for HC CoCrMo in (a) 4 hours , (b) 2 cycles in the region 2 in 0.36% NaCl

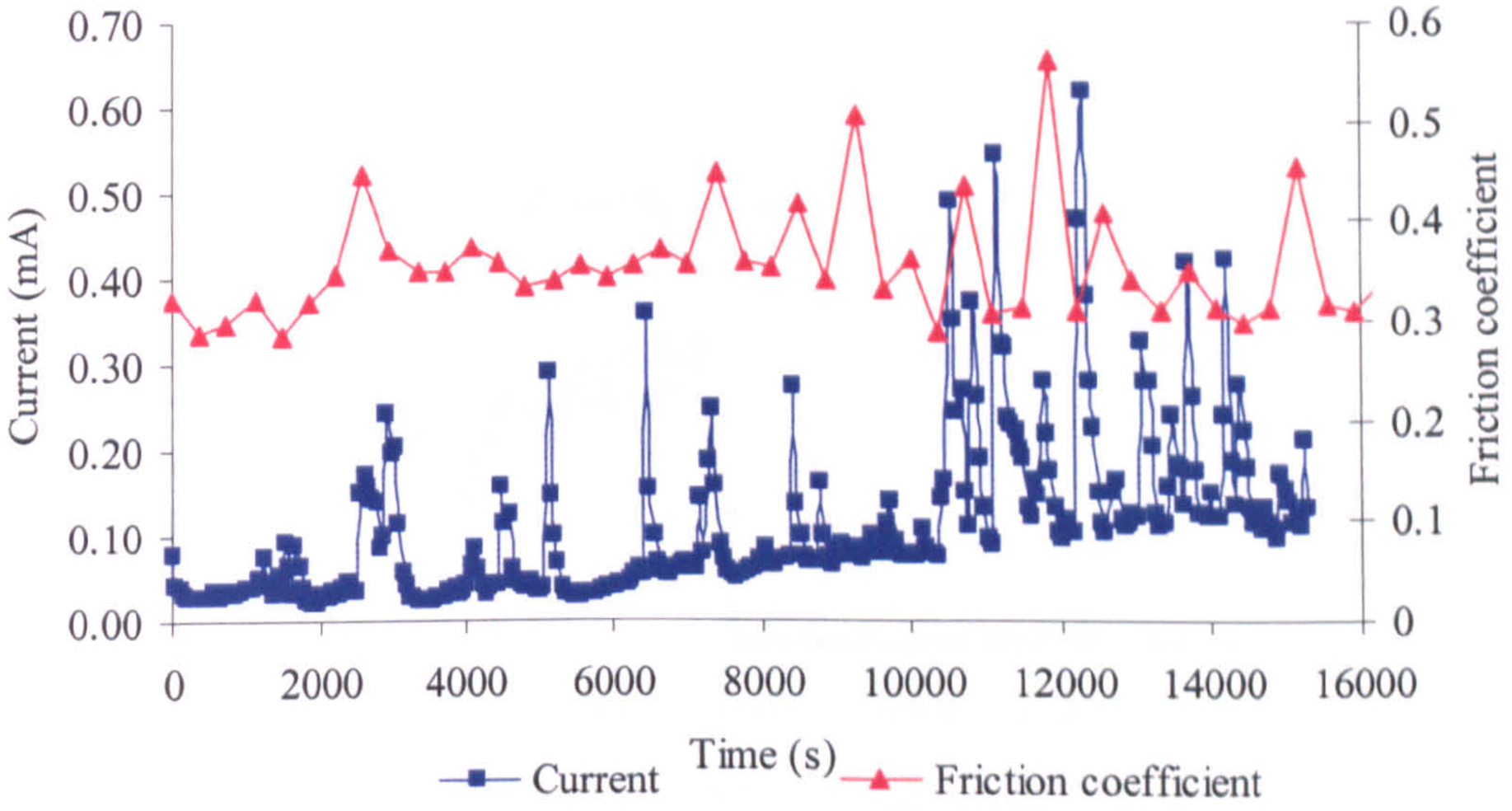

(a)

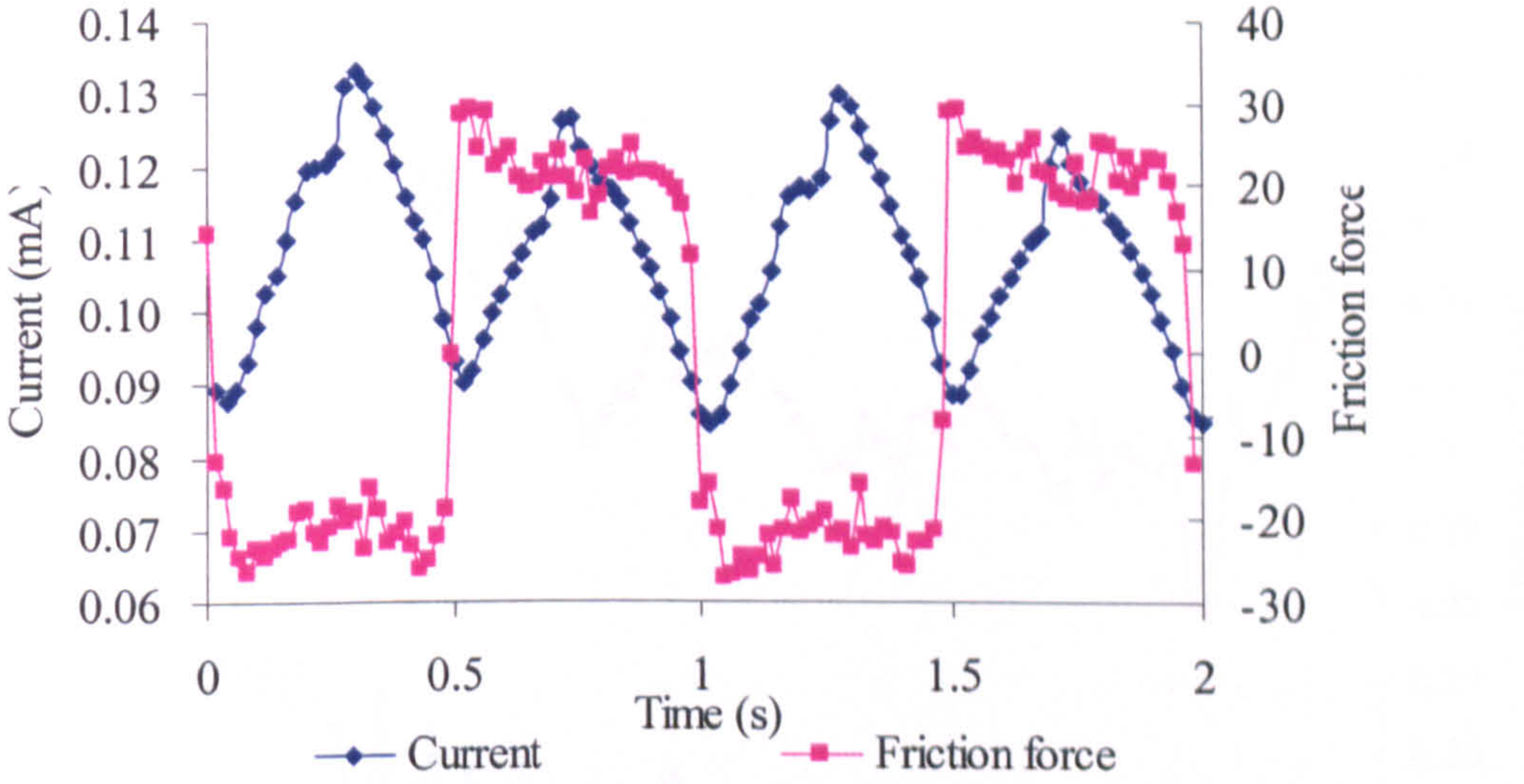

(b)

Figure 7-17 Current and friction curves at 0.2 V applied potential for 316L in (a) 4 hours , (b) 2 cycles in the region 2 in 0.36% NaCl

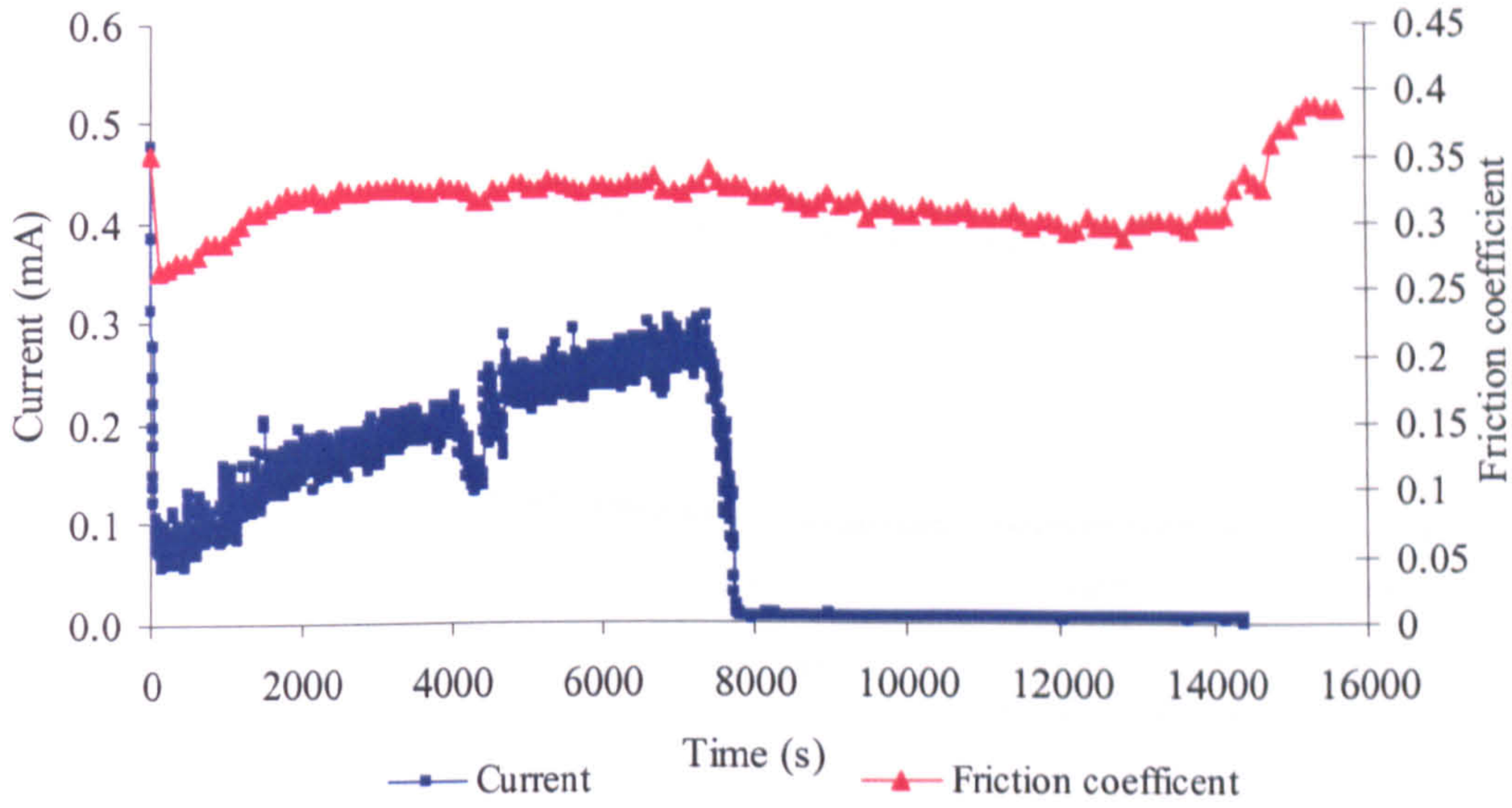
Current (mA)
Friction coefficient
Time (s)
Current
Friction coefficent

(a)

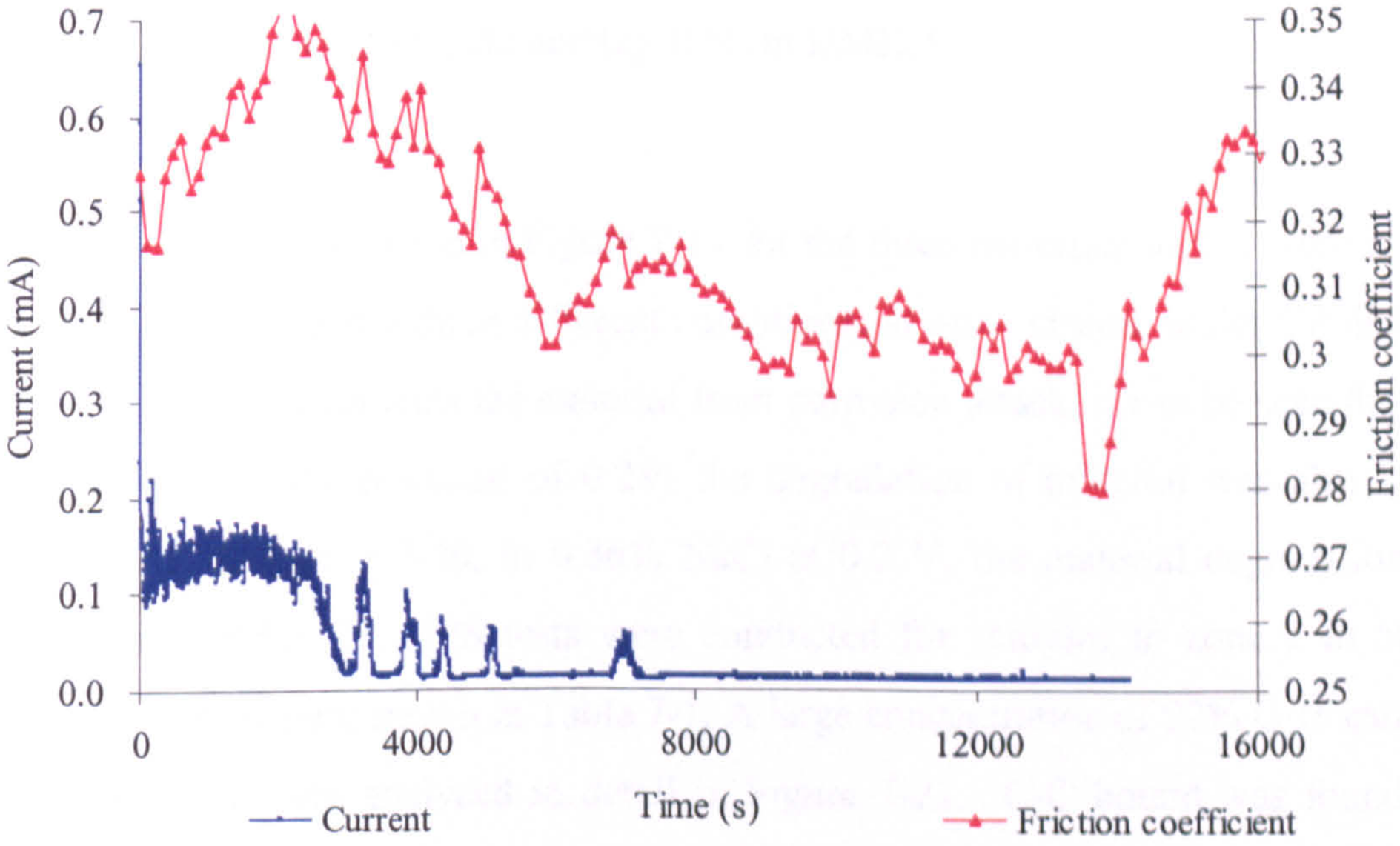
Current (mA)
Friction coefficient
Time (s)
Current
Friction coefficient

(b)

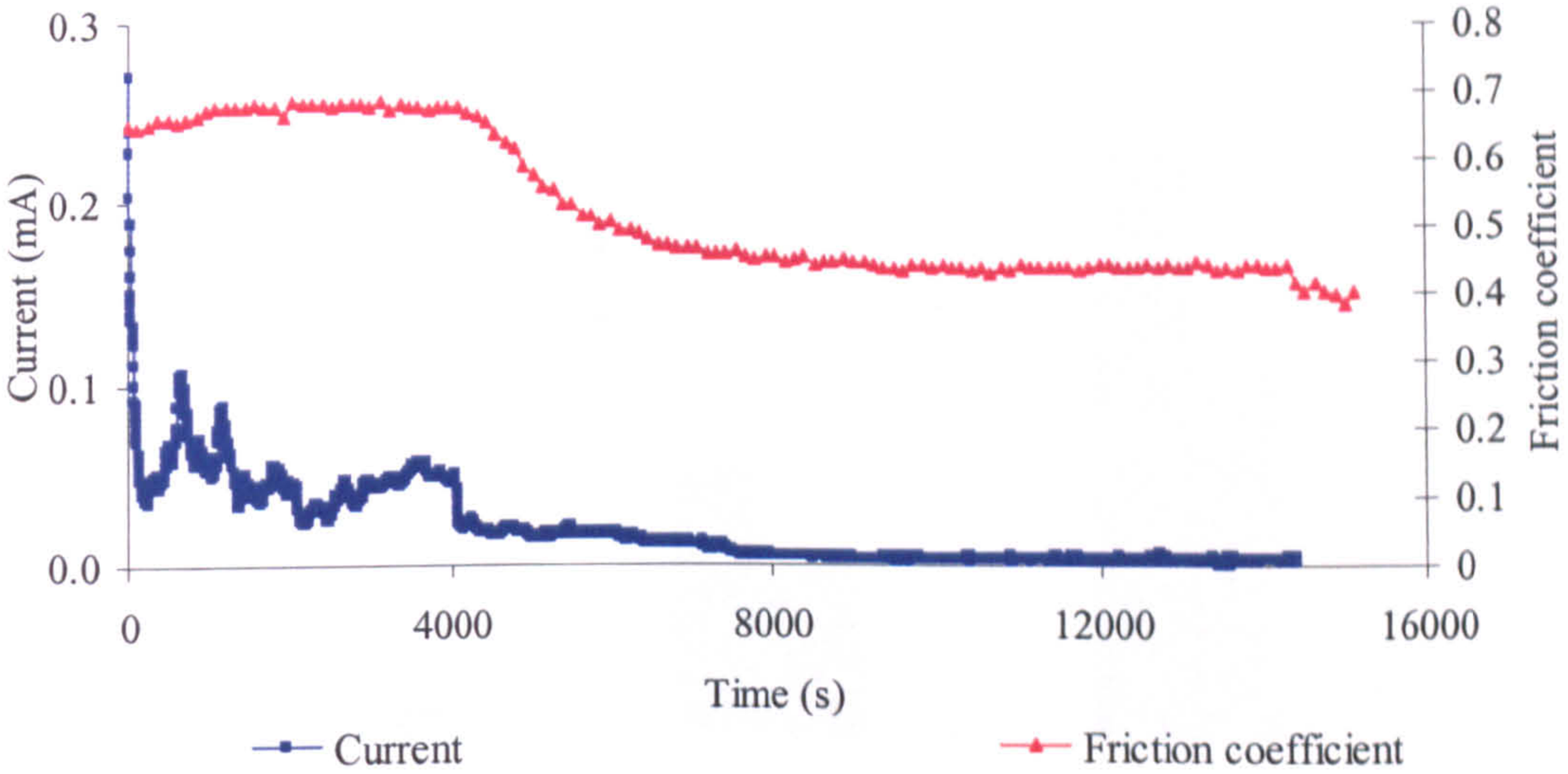

(c)

Figure 7-18 Current and friction curves at 0.2 V applied potential for (a) HC CoCrMo (b) LC CoCrMo and (c) 316L in DMEM

Material loss is shown in Figure 7-19 for the three materials in 50% serum for the same duration under three different conditions: at open circuit, under CP and at 0.2V. Although CP protects the material from corrosion attack, it can be seen that at a controlled positive potential of 0.2V, the degradation of material was also less. However, from Figure 7-20, in 0.36% NaCl at 0.2 V, the material degradation is greater than under CP. XPS tests were conducted for samples in zone 2 in 50% serum. The results are shown in Table 7-1. A large concentration of 92% C 1s can be quantified. C 1s was analyzed in detail in Figure 7-21. C-C bound was found to contribute 51.5% with the C-H bound accounting for a lower amount. The applied potential certainly affected the formation of the film and displayed an interesting lubrication effect. After 5 minutes argon ion etching, some Co 2p and Cr 2p (4.3% and 2.3%) were obtained.

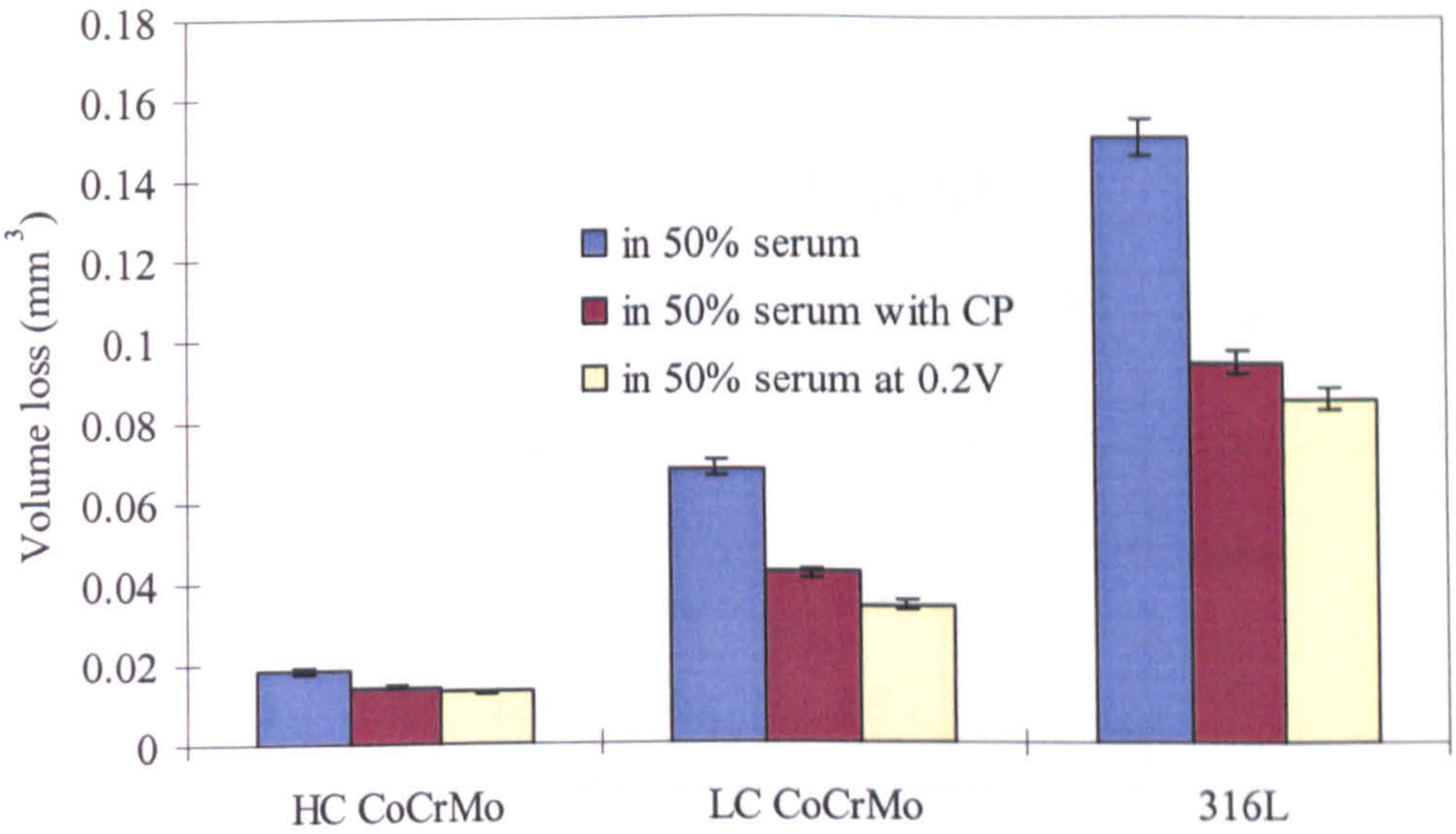

Figure 7-19 Material volume loss in open circuit, under CP at -0.8V and at 0.2V in 50% serum

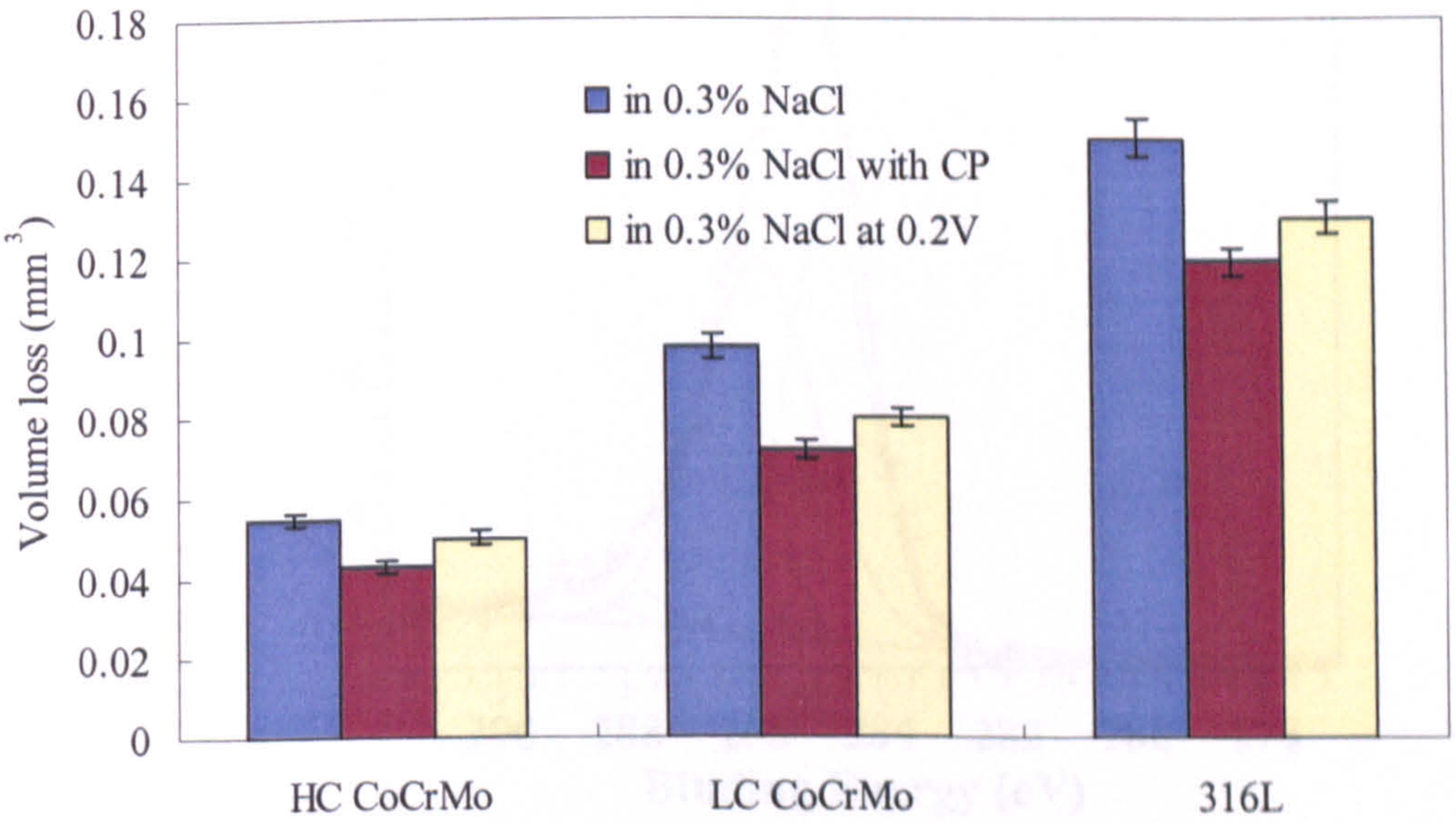

Figure 7-20 Material volume loss in open circuit, under CP at -0.8V and at 0.2V in 0.36% NaCl

Table 7-1 XPS survey analysis for HC CoCrMo in zone 2 in 50% serum at 0.2V

Etching time (min)	XPS (at%)								
	C 1s	O 1s	N 1s	Co 2p	Cr 2p	Mo 3d	P 2p	S 2p	Ca 2p
0	92	4.5	3.2						
0.5	84	7.6	4.9	2.1	1.4				
5	78.6	7.6	6.3	4.2	2.3				

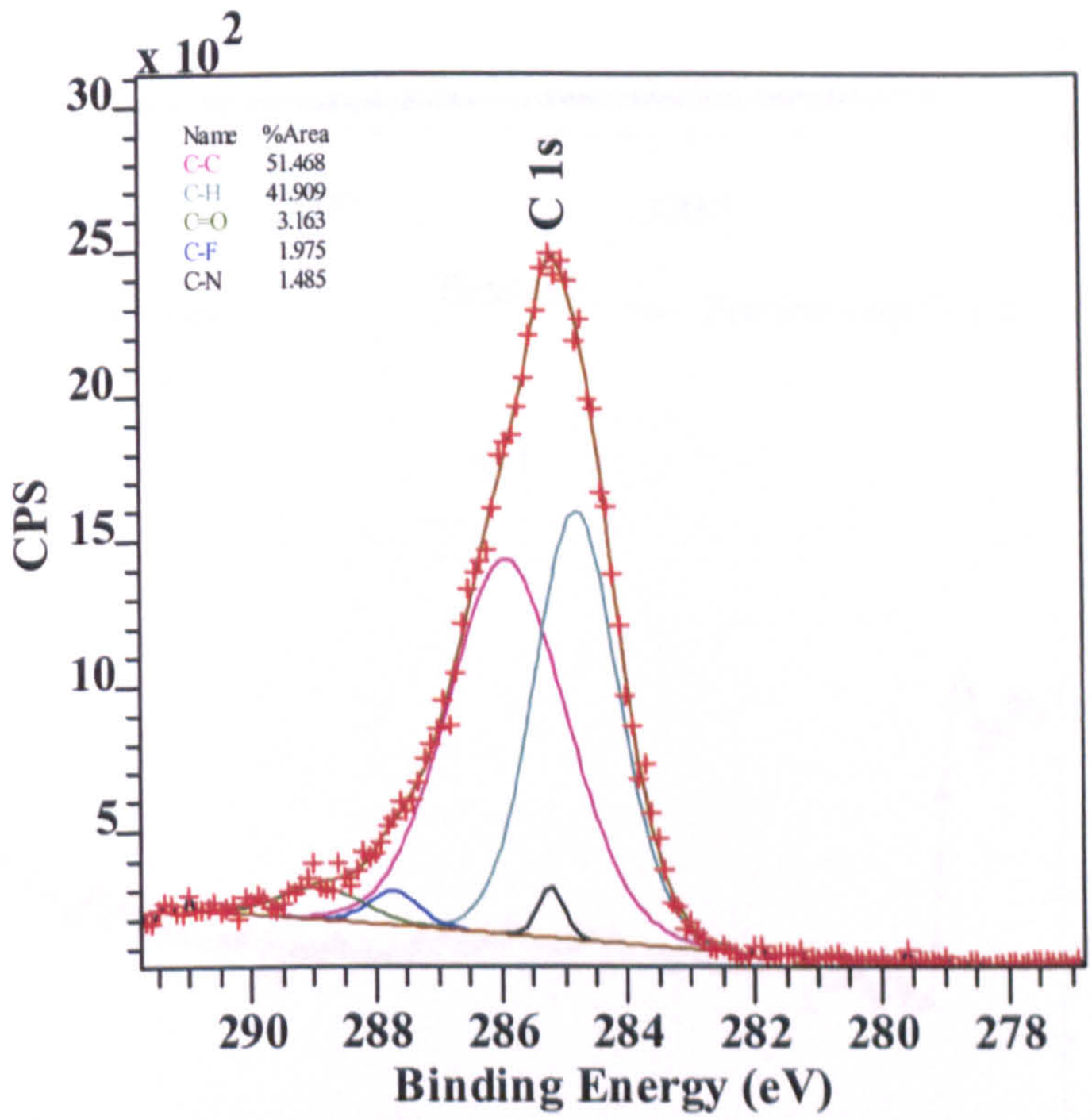

Figure 7-21 C 1s spectra for HC CoCrMo in zone 2 at 0.2 V in 50% serum

Potentiostatic tests were also conducted at 0.4V for materials in 50% serum (Figure 7-22). Due to the binding of proteins and released metal ions from the AP test, the current dropped rapidly after tests started for all materials and the current value remained very low (<20μA). Correspondingly, a lower friction coefficient was

recorded than at 0.2V (Figure 7-14 and Figure 7-16). For 316L (Figure 7-22 (c)), an unstable current was obtained and pitting corrosion was observed outside of the wear scar. The friction coefficient remained stable. Both lower friction coefficients and lower currents were recorded than for materials at 0.2V in 50% serum which is consistent with the AP results (Figure 7-11).

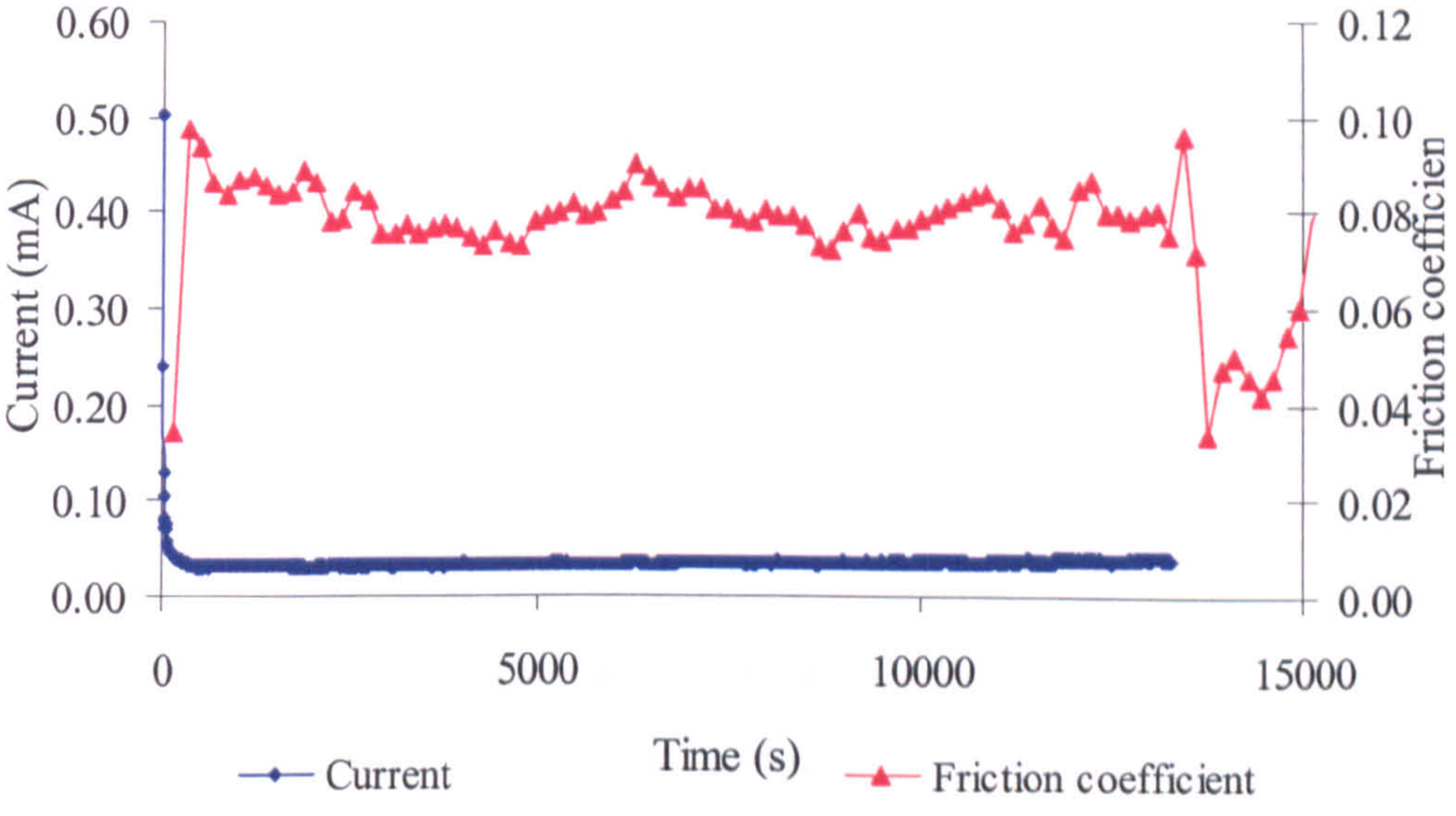

(a)

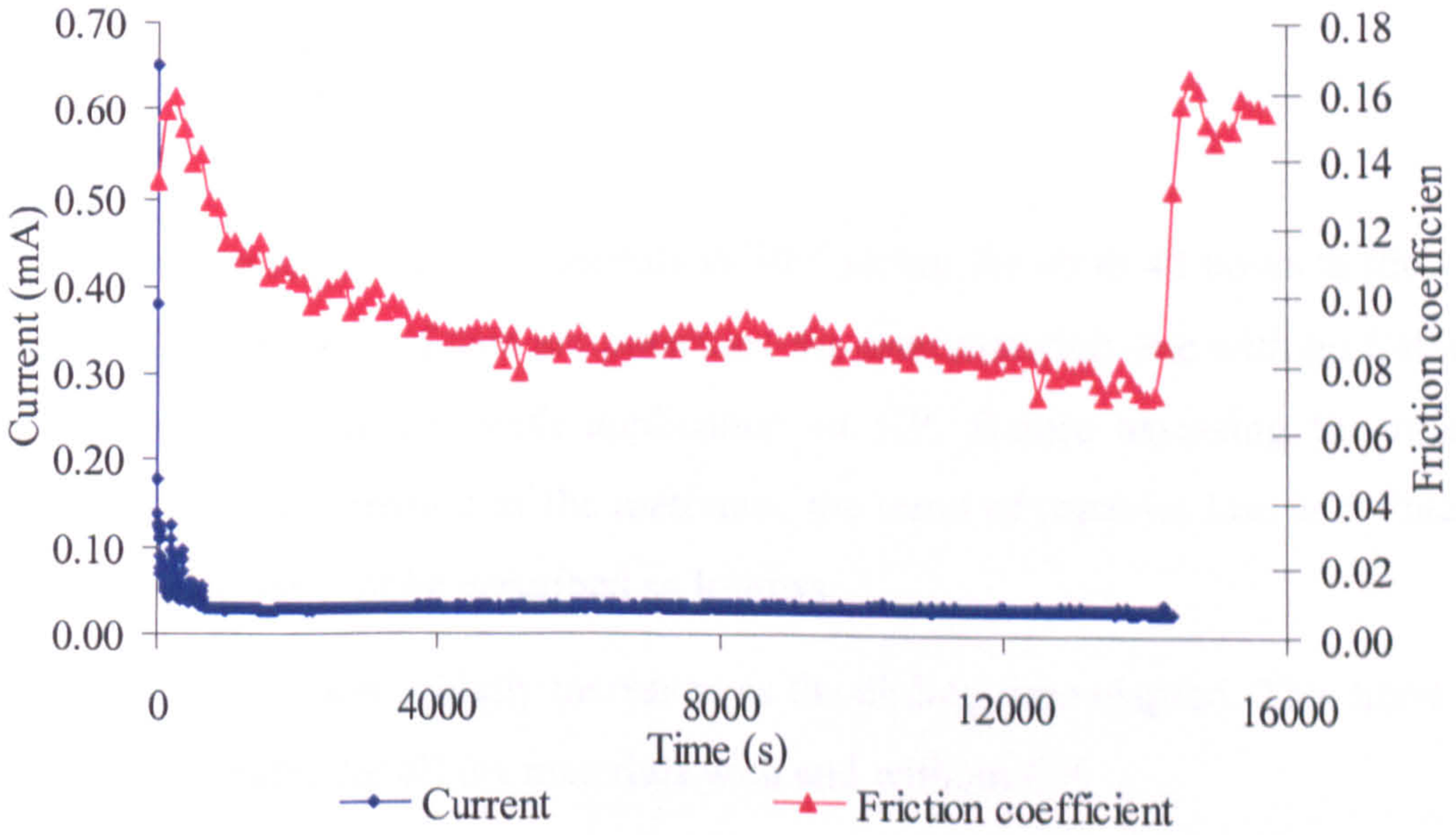

(b)

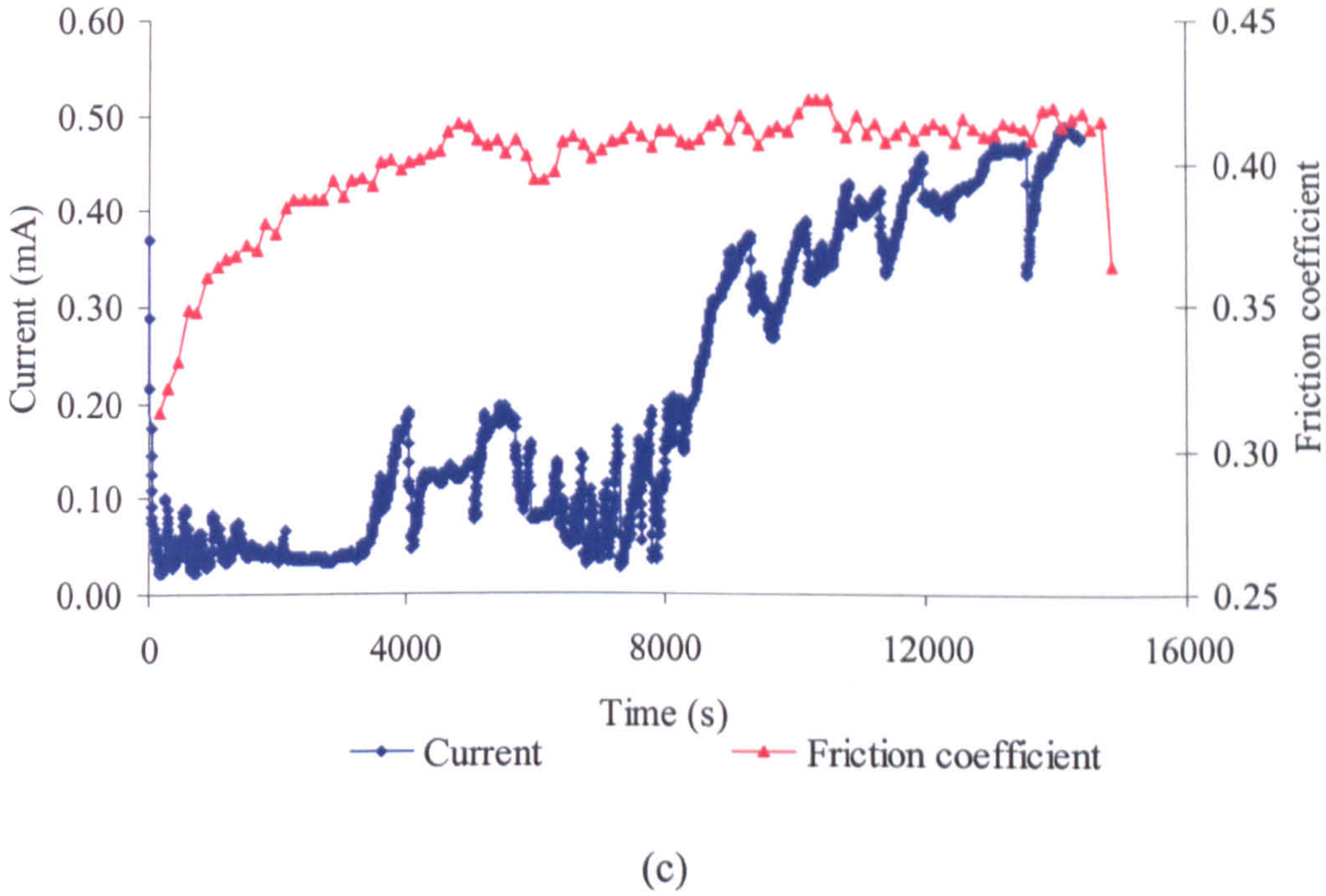

(c)

Figure 7-22 Current and friction coefficient curves at 0.4 V in 50% serum for (a) HC CoCrMo (b) LC CoCrMo and (c) 316L

7.5. Effect of Proteins on The Time Duration of Wear and Corrosion

The volume loss for all materials in 50% serum for up to 48 hours is shown in Figure 7-23. Two sets of data are presented for each material: one with no Cathodic Protection (CP) and one with application of CP. Before assessing the relative resistance to tribocorrosion of the materials, the trend of material loss as a function of sliding distance will be described as follows:

- The volume loss initially increased as the sliding time elapsed. This trend was comparable for all the materials with and without CP.
- It is clear that after around 4 hours, or a sliding distance of 300 metres, all materials reached a steady-state in terms of their overall material loss.

- The durability of HC CoCrMo was significantly better (with or without CP) than LC CoCrMo and both materials performed substantially better than 316L.

For the first 300 metres, all materials showed a higher wear rate and then the wear rate decreased and remained very stable. The penetration rate or the wear rate gradually decreased for 316L and LC CoCrMo after the initial running-in. A 52% decrease of volumetric wear rate in the steady-state can be observed for 316L and 42% for LC CoCrMo. Interestingly, HC CoCrMo had a very steady and low wear rate. The distinction of two phases (running-in and steady state) is not that clear with an approximate 10% decrease in wear rate in the steady state regime compared with the running-in regime.

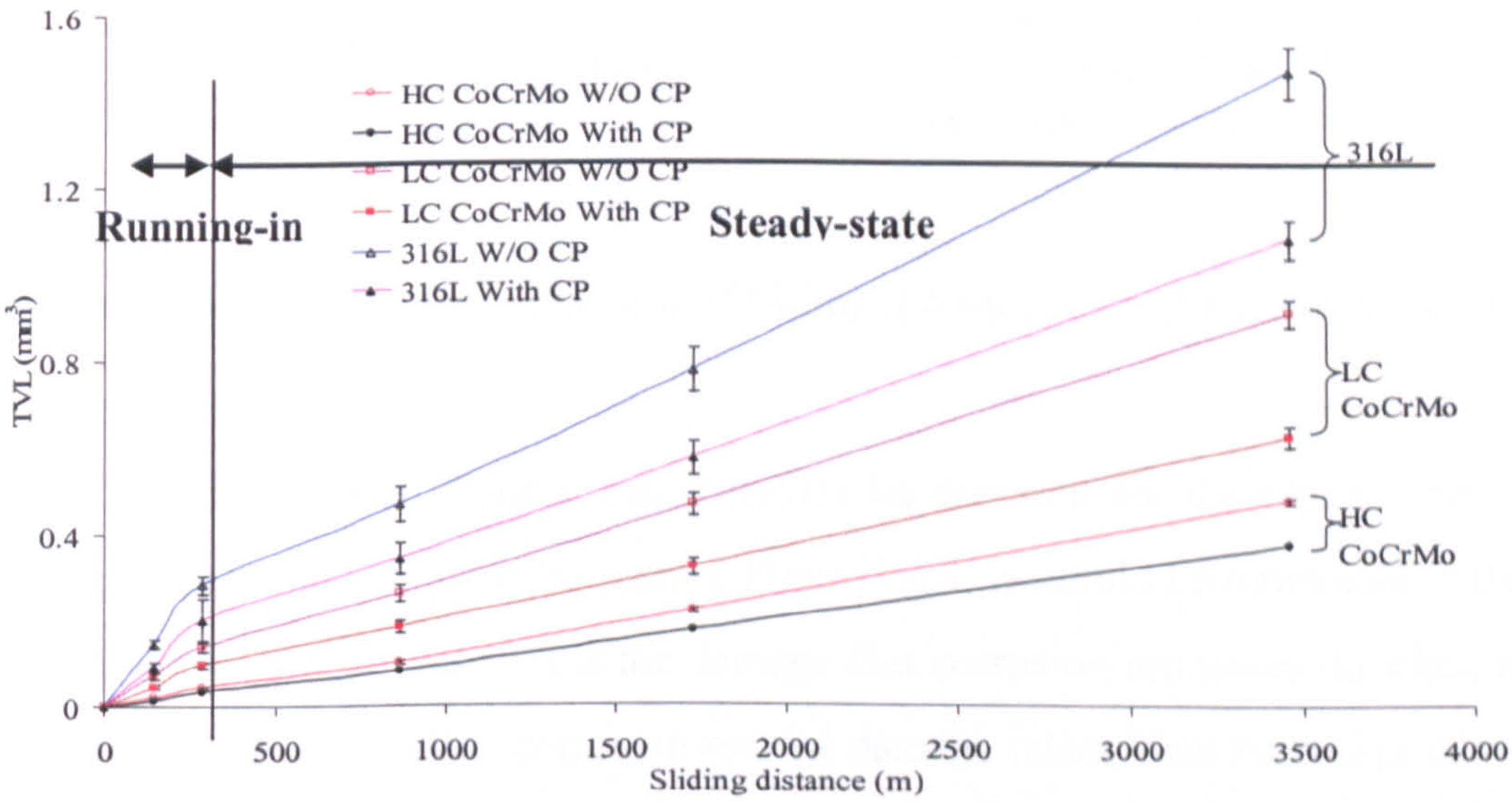

Figure 7-23 Total volume losses (TVL) for three materials (HC CoCrMo, LC CoCrMo and 316L) in 50% serum up to 3500 metres (48hours)

In order to have a full understanding of the biphasic behaviour, their roughness was firstly evaluated and the results are presented in Figure 7-24. After the first 4 hours roughening, the roughness kept stable as time progress, which may be due to the corrosion effect and on the other hand corrosion may be attributed the steady roughness and furthermore the steady wear rate. As in the previous chapter, the linear polarization resistance remained constant after the initial running in period (Figure 6-13).

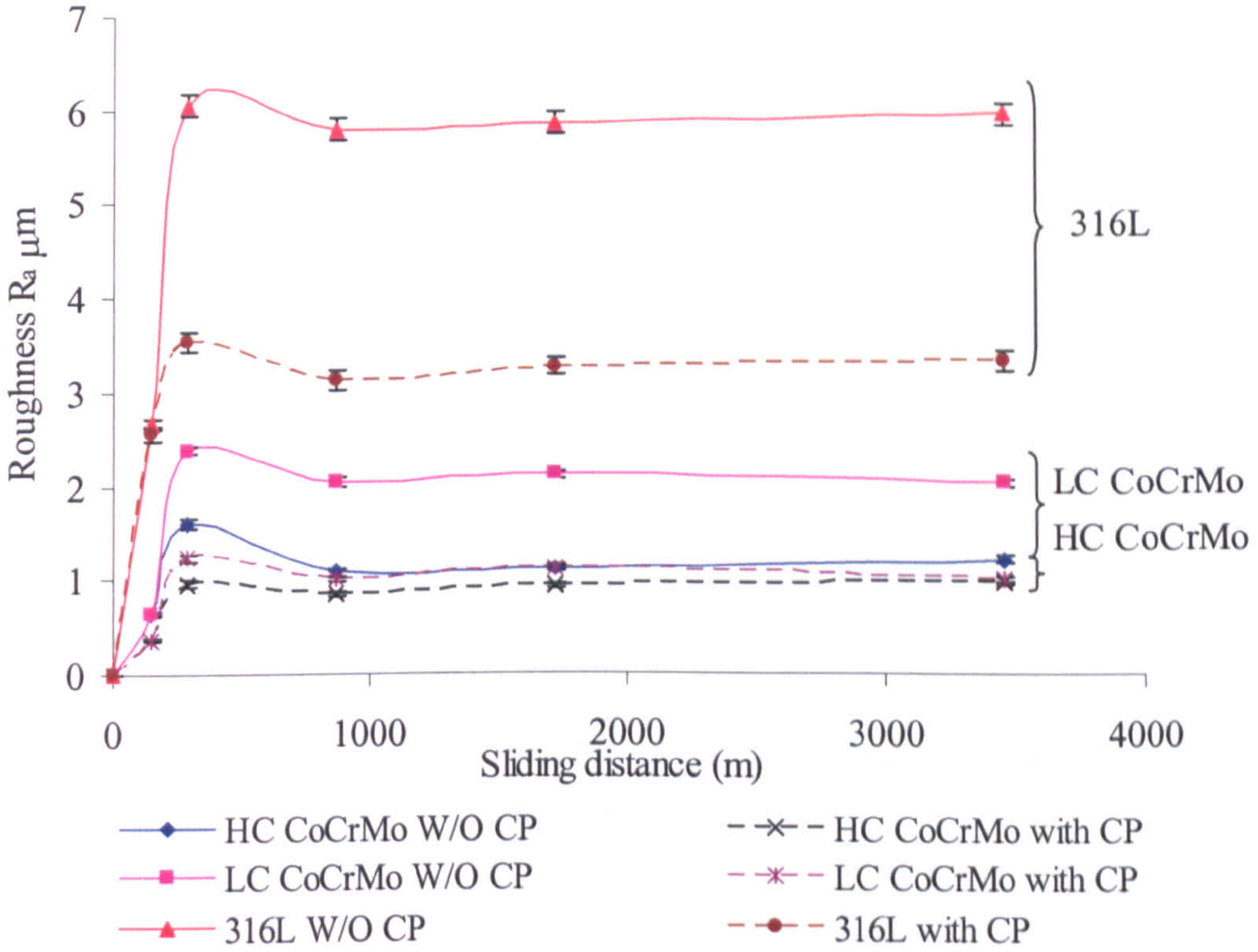

Figure 7-24 Roughness as a function of sliding distance for materials in 50% serum

Corrosion-related damage can therefore be assessed for the two regimes and for the three materials as can be seen in Figure 7-25. It should be remembered this is not only the corrosion rate – it is the damage that corrosion processes do when wear is affected and so is called corrosion-related damage rather than corrosion damage. The corrosion–related damage for both LC CoCrMo alloy and 316L decreased dramatically in moving from the running-in regime to the steady state regime. The lower wear rate in the steady-state regime can therefore be partly attributed to a reduction in corrosion–related damage.

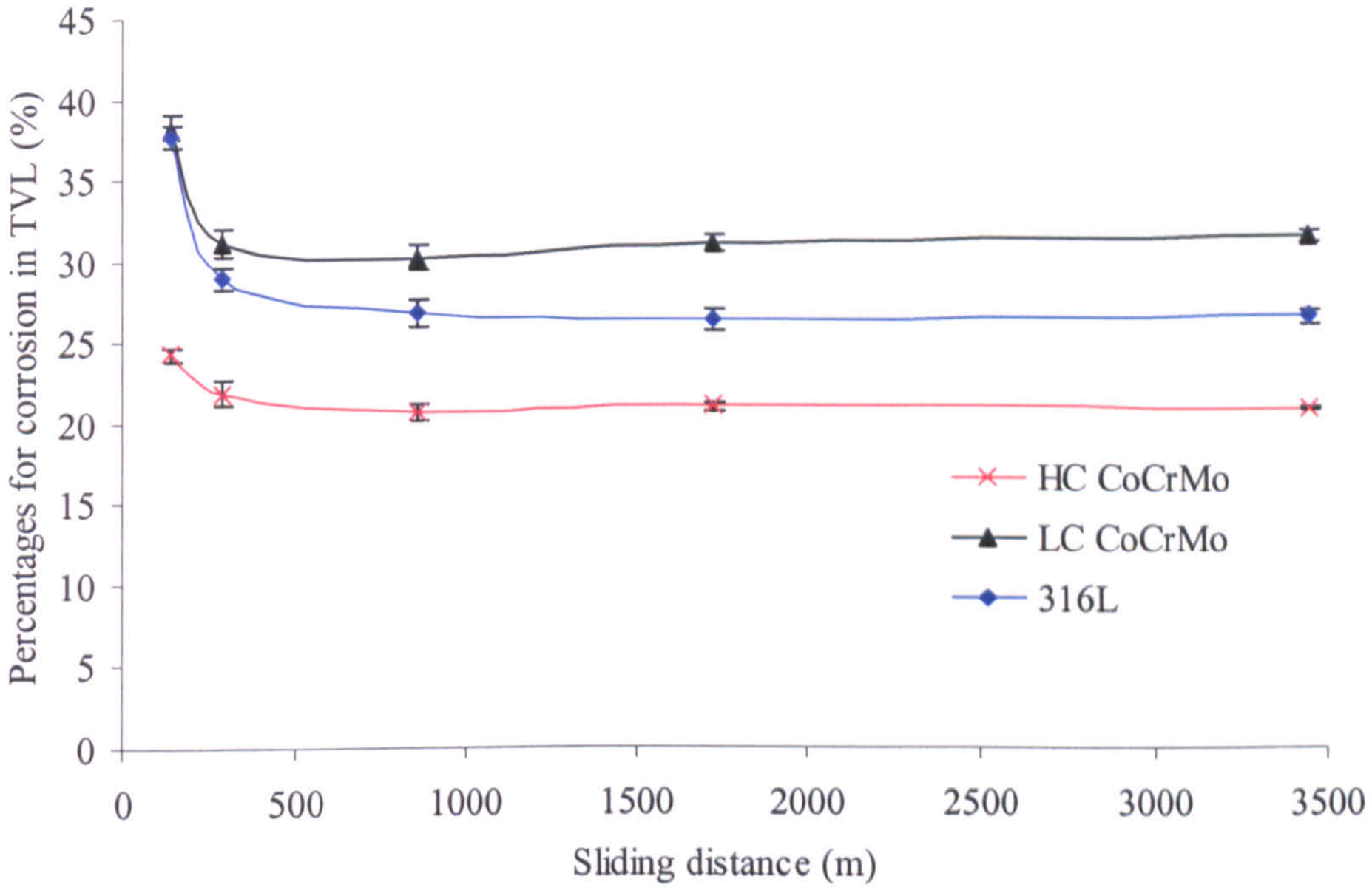

Figure 7-25 Percentages of corrosion in Total volume loss (TVL) for three materials in 50% serum up to 3500 metres (48hours)

In contrast to static corrosion resistance which relies on a stable spontaneous passive film, the tribocorrosion behaviour depends on the depassivation of the passive film and formation of a tribo-film (include adsorbed proteins and passive-like film). HC CoCrMo shows the lowest mechanical wear damage (Figure 7-21) and a very stable corrosion resistance (Figure 7-25), therefore it exhibits the best tribocorrosion performance. However, even in the steady-state regime, over 20% of the material degradation could be attributed to corrosion. This points to the fact that there is still potential for development of better corrosion resistant materials to be able to resist degradation under the combined effects of corrosion and wear. Of course, the challenge is to preserve the good wear resistance in the development of improved corrosion resistant alloys.

The wear factor was calculated from equation Eq. 7-2 and the results are shown in Figure 7-26.

$$k = \frac{\text{Wear volume}}{\text{Applied load} \times \text{sliding distance}} \ (mm^3/Nm) \qquad \text{Eq. 7-2}$$

A lower k was observed in steady-state. Figure 7-27 shows the mean friction coefficient for the three materials in the two regimes. Compared with the other two materials, HC CoCrMo showed the lowest friction coefficient for the entire test. All of the materials in this study exhibited a lower friction coefficient in the steady-state regime than in the running-in regime. It indicates that more effective lubricating conditions exist in this regime which is invariably linked to the nature of the lubrication interface. Details of the tribofilm have been discussed in Chapter. The free corrosion potential is represented in Figure 7-28. Both 316L and LC CoCrMo appeared to have a more negative (active) shift of the potential. Meanwhile, HC CoCrMo had a very slight shift in a the noble direction. However, the difference of potential is rather small (around 50mV) and so the change of the passive film is not very apparent.

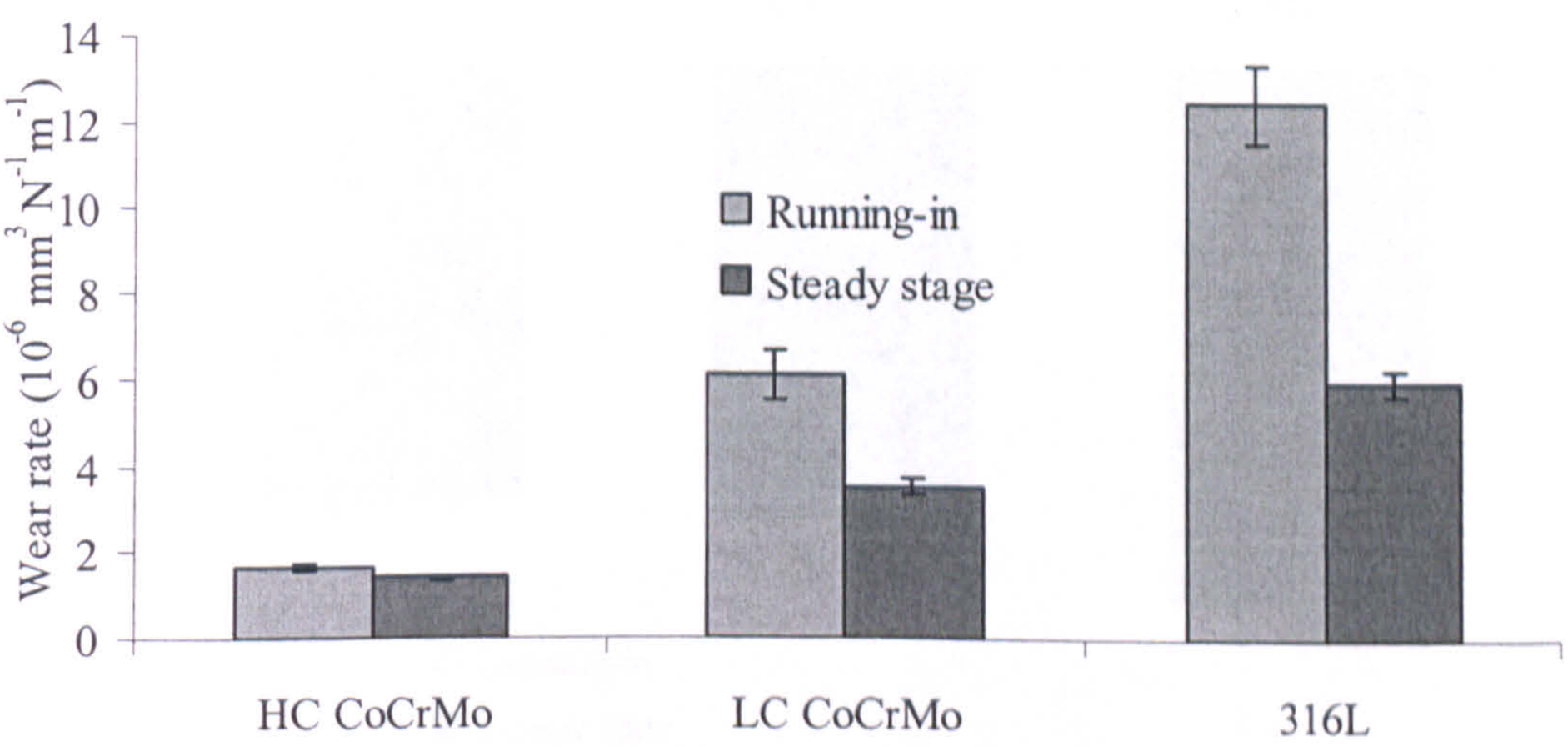

Figure 7-26 Wear rate of two phases (running-in and steady state) for three materials (HC CoCrMo, LC CoCrMo and 316L) in 50% serum up to 3500 metres (48hours)

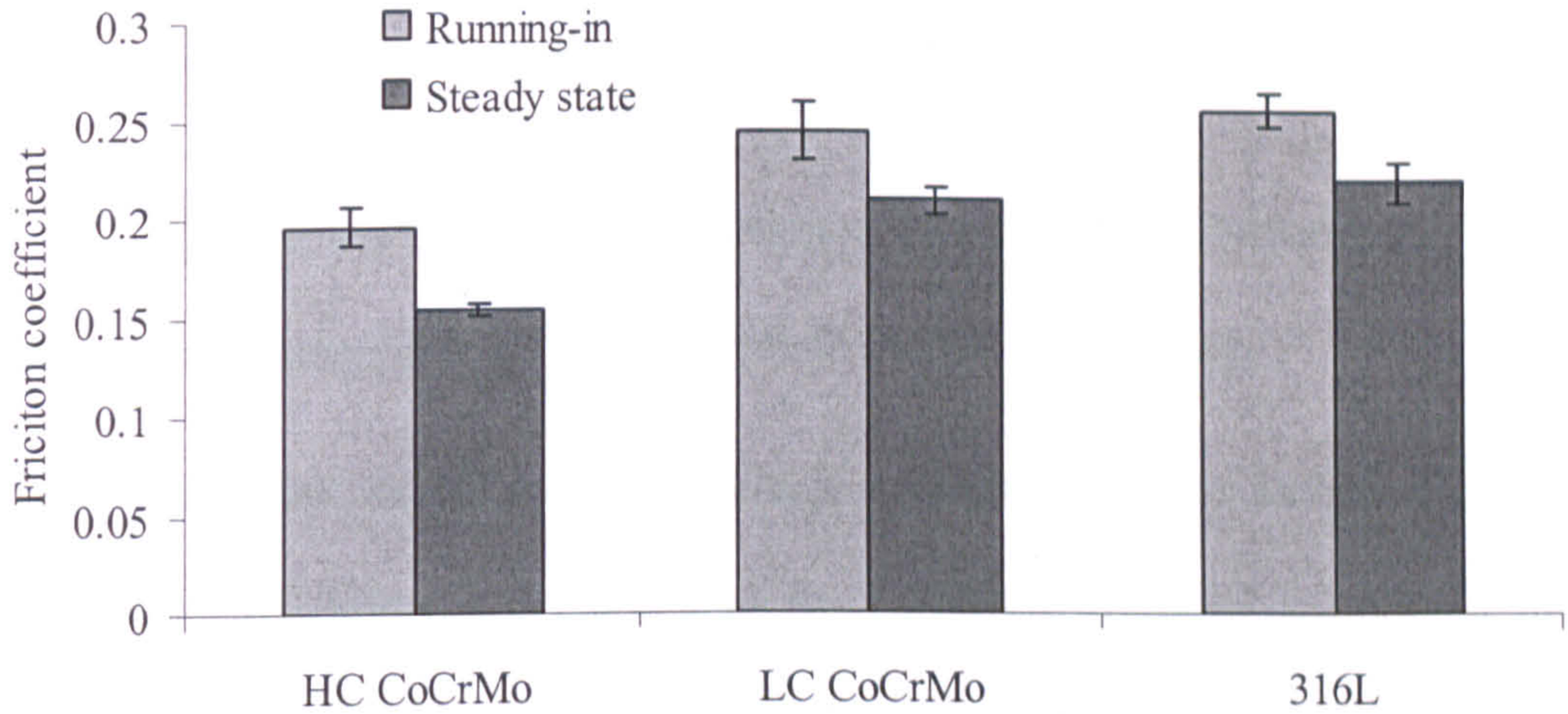

Figure 7-27 Friction coefficient in two phases (running-in and steady state) for three materials (HC CoCrMo, LC CoCrMo and 316L) in 50% serum up to 3500 metres(48hours)

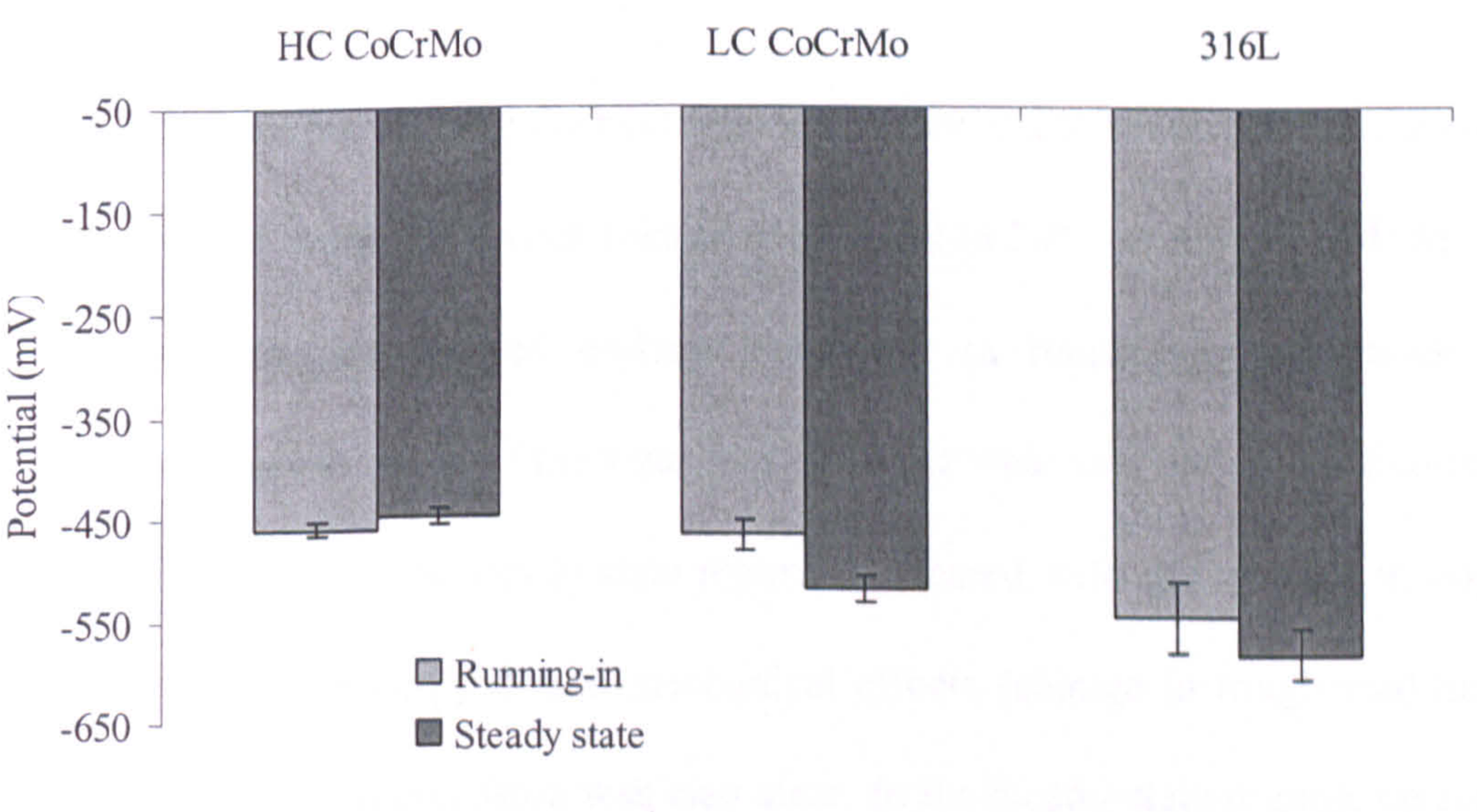

Figure 7-28 Free corrosion potential (E_{corr}) in two phases (running-in and steady state) for three materials (HC CoCrMo, LC CoCrMo and 316L) in 50% serum up to 3500 meters (48hours)

7.6. Summary

In this chapter, the effect of corrosion on wear and the tribocorrosion behaviour were generally analyzed. Some major points can be summarized:

- Corrosion played an important role and affected wear extensively. For the reciprocating wear tests and the materials/solutions considered in this study, corrosion accounted for between 21-49% of the total volume loss, the remainder being attributable to mechanical wear.
- Co^{2+} and Fe^{2+} were the most ions to be released in the solutions from CoCrMo alloys or 316L. However, they can bind with proteins and form complexes to reduce friction and become a barrier to cease further metal ion release.
- HC CoCrMo showed the best wear resistance and tribocorrosion resistance. It also exhibited lowest friction coefficient in 50% serum and DMEM.
- All materials showed biphase behaviour (a running-in and steady-state regime) in terms of the wear rate. A lower wear rate and lower fiction was observed in the steady-state regime compared with the running-in regime. This is primarily due to mechanical effects (change in roughness) but the influence of corrosion was also clear. In the steady-state regime, corrosion-related damage contributed20%-30% of the total material loss.

CHAPTER 8

DISCUSSION

8.1. Introduction

In Chapter 3, a general review of current literature in orthopaedic implant materials and tribocorrosion was presented. What emerges from that review is that a clear understanding between the materials (especially metallic materials) and biotribocorrosion does not exist. Released metal ions and metallic debris have been found exclusively in patients with artificial joint replacement. Although there is not enough evidence to prove that released metal ions are certainly carcinogenic, concerns still exist in relation to the released metal debris/ions with the surrounding biological environment.

In previous chapters of this thesis results from an experimental study are presented. The corrosion behaviour in static conditions, the effect of tribology on corrosion and vice versa, as well as chemical characterization of tribofilms have been presented. This chapter brings together these results and the main findings and discusses their relevance to other published literature and in relation to the key contribution made by this thesis.

Firstly, the effect of organic species on tribology, corrosion and tribocorrosion properties are reviewed. The tribofilm characterization is linked to materials performance. Then, the interaction between tribology and corrosion and how it affects the system are discussed carefully. The metal ion release mechanisms are related to the tribological contact. Finally, the time dependence of these combined effects is analyzed.

8.2. Organic Species Effect on Tribological Properties

8.2.1. Friction

The calculated lambda ratios for the tribological system in this study were shown in Table 6-1. Due to the higher pressure viscosity of 50% serum, the minimum film thickness was greater in such environment than in DMEM or in 0.36% NaCl. Comparison of the starting lambda ratio with the friction coefficient is given in Figure 8-1. A general trend of decrease of friction coefficient with the increase of the starting λ can be seen. It may be because the greater minimum film thickness can result in less number of asperities in the contact interface and then the reduction of friction. Figure 8-2 shows the Stribeck curve. All tests were performed in the boundary lubrication regime, where at the lower λ (<1), an enhancement of friction is displayed.

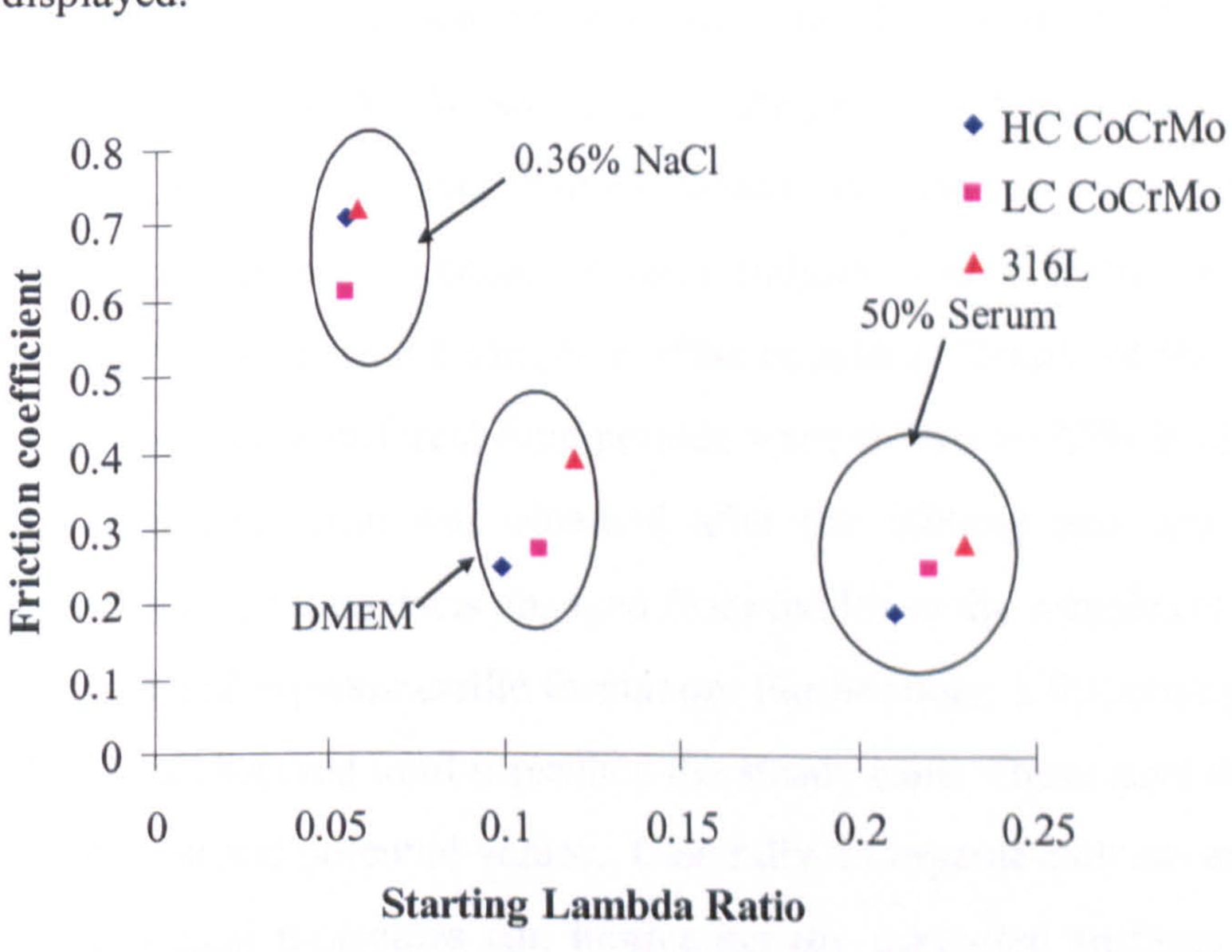

Figure 8-1 The relation of lambda ratio and friction coefficient

As time progresses, the wear scar became wider and deeper (Figure 7-6), which means that the contact area increases and the contact pressure decreases. Meanwhile, the roughness experienced an initial increase in the running-in process and a polishing effect in the steady-state (Figure 7-24). They are attributed to the decrease of friction (Figure 7-27).

Results showed an initial friction increase in 0.36% NaCl for all materials and a decrease of friction followed by an increase in 50% Serum (Figure 8-3). For 0.36% NaCl, the initial running-in process raised the friction in the beginning until it reached a relatively smooth mechanical depassivation and electrochemical repassivation phase which gave a stable friction and potential response (Figure 6-9). Proteins in 50% serum under tribological contact, were involved in the tribochemical processes, which resulted in lowering the friction for the initial period followed by an equilibrium (Figure 6-3). The response of potential also showed a corresponding behaviour. An transient shift to more negative direction was observed. When the equilibrium of friction was reached, the potential tended to be stable. The trend of friction coefficient changes and the responses of the potential were shown. A stable potential indicates the passive layer formed, which also can influence the friction behaviour. The friction and potential changes indicate that a initial reaction of proteins and amino acids with the sample surface occurred. Details of the tribofilm formation in 50% serum at different time periods were shown by XPS tests. The re-establishment of passive film was obtained after the rubbing was applied. The tribofilm under tribological contacts changed from oxides to the complexes of metal oxides, hydroxides and organometallic formation. Furthermore, a thickening process of the tribofilm was observed until it reached the steady state. These gave the output as changes of friction and potential values. Generally, in organic-rich environments, the adsorbed biological molecules can lubricating the contacted surfaces. In 50% serum and DMEM, the friction coefficients were smaller than in 0.36% NaCl.

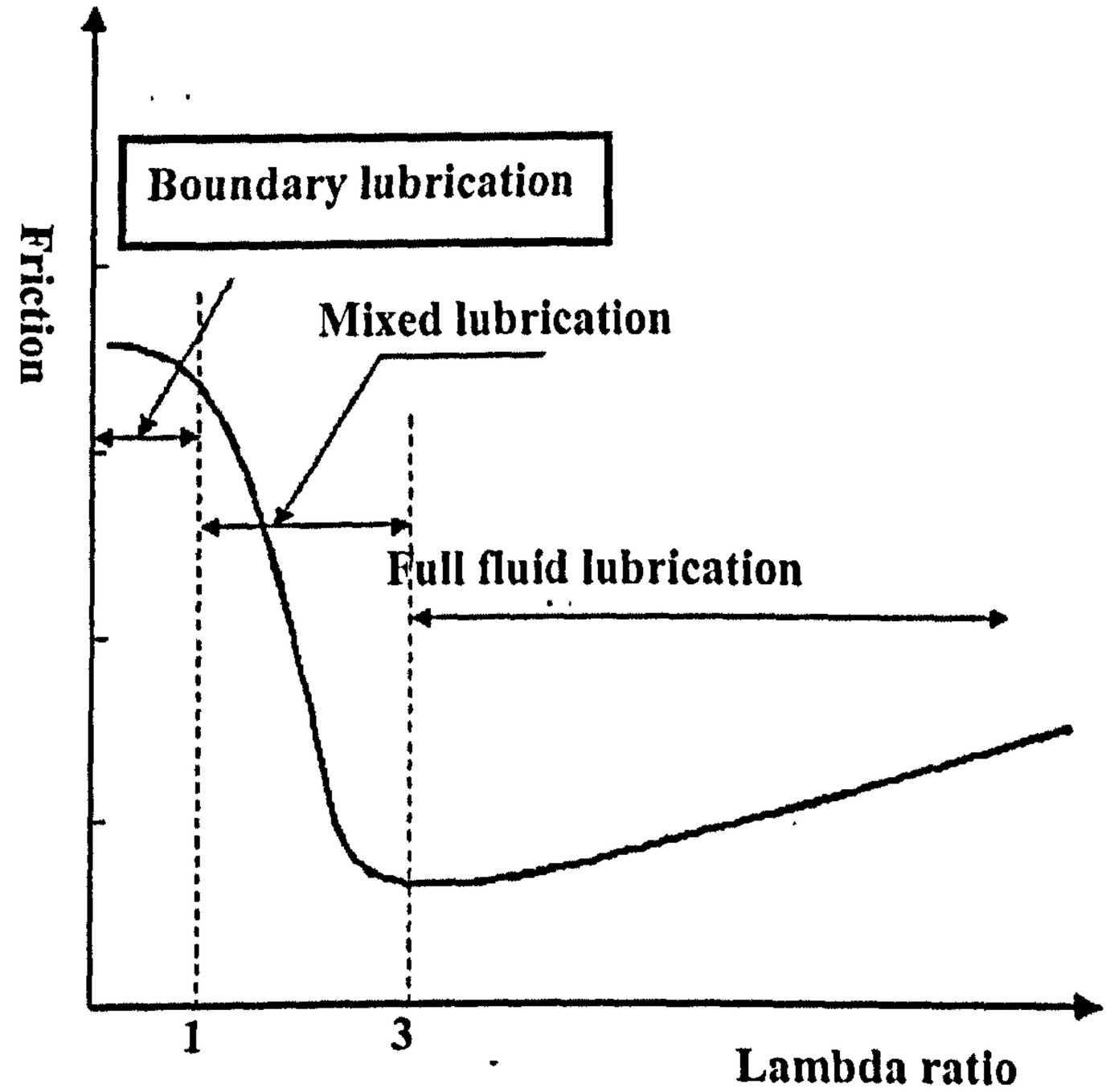

Figure 8-2 Stribeck curve [10]

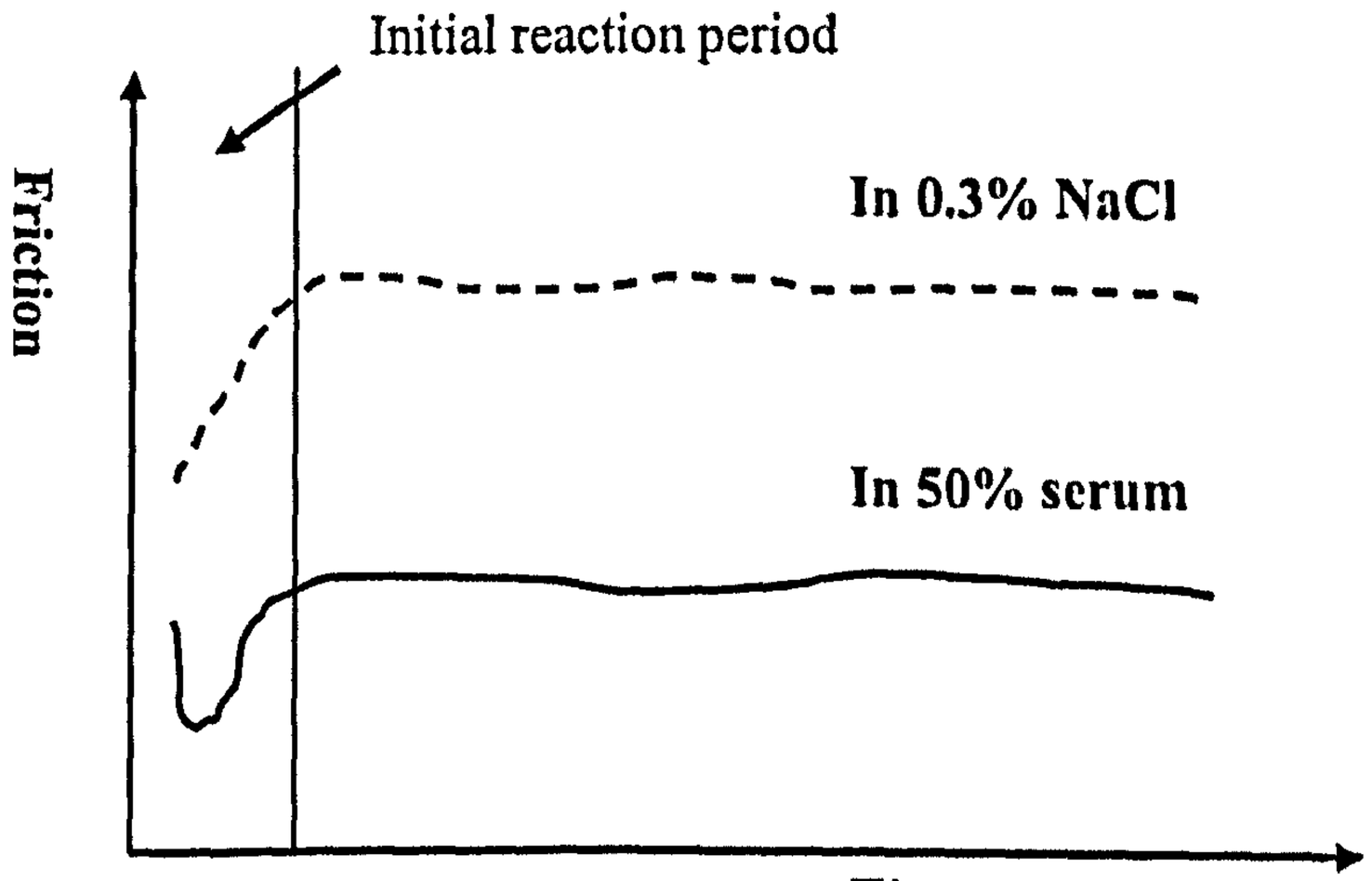

Figure 8-3 Schematic representation of friction coefficient in 50% serum and 0.36% NaCl

8.2.2. Wear

The friction coefficient as a function of total volume loss for materials in three environments is shown in Figure 8-4. In this part, wear refers to the total material loss. HC CoCrMo showed very similar values of material loss in three solutions while 316L exhibited a lower friction coefficient when a higher wear rate was recorded. It can be explained by their different wear mechanisms. Detailed discussion will be made later in this chapter with their effect on corrosion as well. However, some points can be given.

From Figure 6-6 (c) and Figure 7-6 (e), evidence has been shown that 316L suffered severe adhesive wear in 50% serum and slight adhesive wear in 0.36% NaCl. For CoCrMo, abrasive wear was the main mechanism. However, the SEM image suggested that LC CoCrMo also had some negligible adhesive wear (Figure 6-6 (b)). It is in line with the observation from the revised MoM or MoP hip replacements. Abrasive and adhesive wear have been seen in artificial joint repayments [23, 25]. In addition, they may cause the failure of TJR [31, 38]. A large number of debris was produced in 50% serum from 316L, which may result in a third body effect. Debris was rolling between two counterparts and may reduce the friction. Nevertheless, the lubrication effect from proteins and amino acids and the difference on film formation on the surface were the main reasons for the recorded lower friction. According to the contact measurements (Figure 5-18), 316L had the least surface energy, therefore the adsorption of biological species on the surface was less than the two CoCrMo alloys. It is also a possible reason that the wear mechanism for 316L was different to the CoCrMo alloys. $Ca_3(PO_4)_2$ was obtained only on 316L in this study. The formation also can interrupt the adsorption process and increase the friction coefficient and wear. The details of tribofilm on the contact area and their behaviour to the tribocorrosion system are discussed below.

0.1% sodium azide was added in 50% serum in order to prevent the initiation and growth of bacteria. However, as discussed in previous sections and some suggestions in the literature [7], material wear (mechanical and electrochemical) resistance shows a very strong relationship with its passive film (tribo-film under tribological contacts) formation. During sliding in this work, the passive film was removed by the mechanical interference. The repassivation or the re-formation of the protective film becomes very important. Sodium azide is an oxygen scavenger, which consumes oxygen and reduces the oxygen content to 1/3 in the tested solutions [133]. The repassivation process needs oxygen to support to form stable oxides/hydroxides. With less oxygen in 50% serum than in DMEM and 0.36% NaCl, the repassivation process was inhibited, which results in an increase of material degradation (wear). However, due to the lubrication effect of protein adsorption on sample surface, the friction coefficient showed lowest value among tested environments. Comparing with wear and friction coefficient in DMEM and 0.36% NaCl, a corresponding relation of a lower friction coefficient with a lower wear can be observed in DMEM.

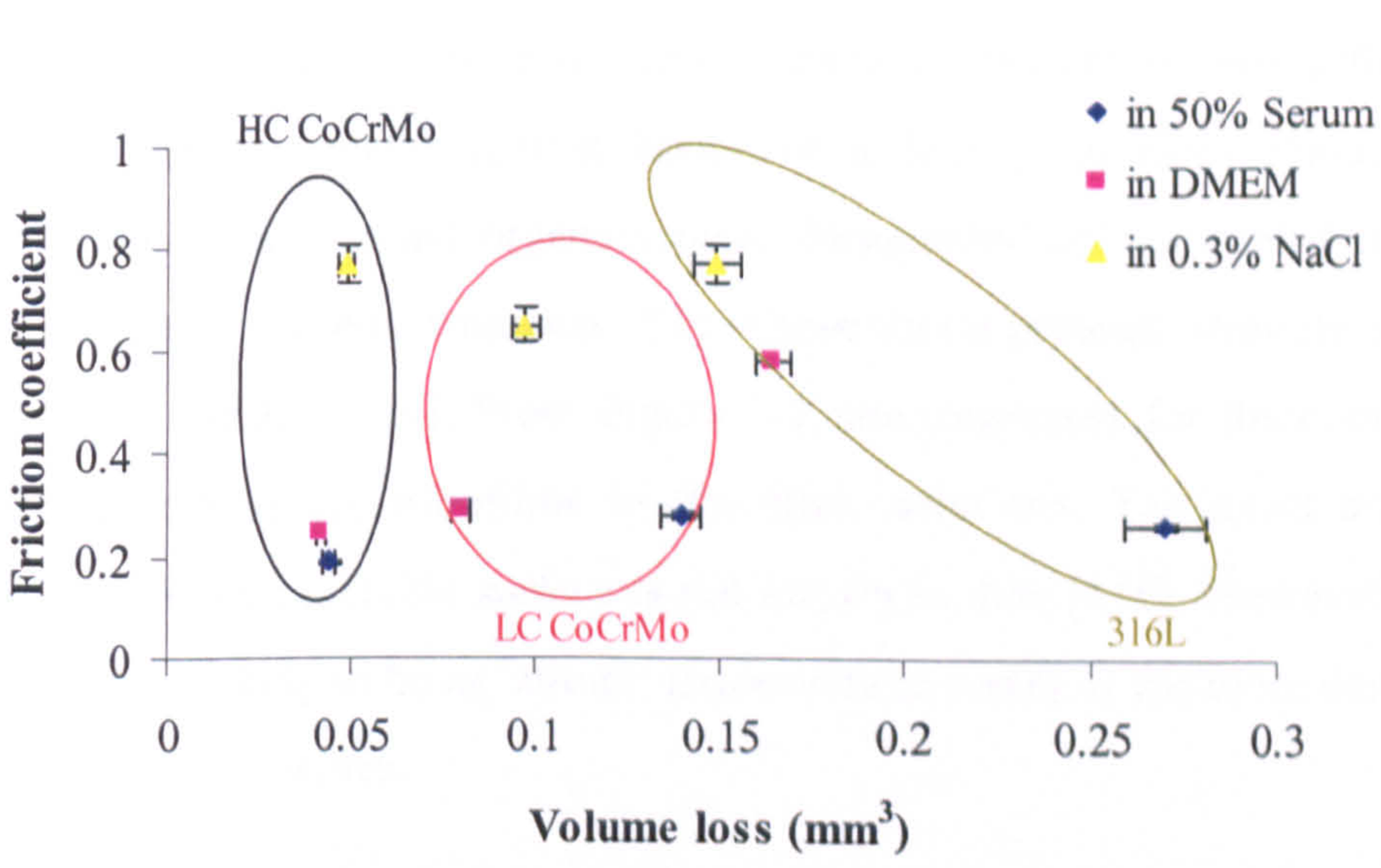

Figure 8-4 Friction coefficient linked with total volume loss

As shown in Chapter 3, many authors have been trying to give models to link wear with surface roughness [83, 84]. An attempt is presented here (Eq. 8-1) to give

an indication of the wear rate as a function of surface roughness. It is summarized from data presented in Figure 7-23 and Figure 7-24.

$$w = w_l w_e w_m (R_a)^c \qquad \text{(Eq.8-1)}$$

The wear rate is shown as w. The lubrication factor is w_l (hydrodynamic lubrication w_l=0, boundary lubrication w_l=1, mixed lubrication $0<w_l<1$). The environmental factor is w_e. The material factor is w_m. R_a is the surface roughness. A factor c is given between 0.3-0.6 [85, 86]

8.2.3. Link of the tribofilms and tribological performance

8.2.3.1. 50% serum

With biological molecules involved, organometallic complexes were found in the tribofilms for all three materials. Organometallic formations are defined as compounds containing metal-element bonds of a largely covalent character. A number of studies have found organometallic formations from corroded metallic implants in protein-rich environments [53]. Those metal-proteins strongly interact with the sample surface [114]. From Figure 7-7, the roughness for the complexed film was higher than the tribofilms in the other solutions. The exact adhesion strength of proteins on metallic surface is not known to date [116]. However, those formations are not likely to be as 'strong' (resistance to wear) as the more dense and compact native metal oxides.

No calcium, phosphorous or sulphur was detected up to 4 hours rubbing either in the wear scar or outside of the wear scar for HC CoCrMo. One explanation might be that calcium phosphates will form after 4 hours, because from some literature, calcium phosphate was obtained on the CoCrMo alloy surface. However, the specific chemical composition (contains high carbon or low carbon) of those alloys was not given. Another reason may be that the HC CoCrMo surface and the

reactions at the interface are not favourable for the formation of calcium phosphates due to its certain value of surface energy. Ti alloys and 316 stainless steel surfaces were found to favour the deposition/formation of calcium phosphate [19]. Nevertheless, they were found on LC CoCrMo and 316L sample surfaces.

Sulphur was observed as a sulphide form (peak 1 in Figure 8-5 (a)) on LC CoCrMo. The binding energy is 778.4 eV in Figure 8-5 (b), and indicates that a possible CoS_2 (S 2p 162.5 eV) formed during sliding. CoS_2 is similar to MoS_2, which due to its weak interlamellar bonds, reduces friction. Peaks 2, 3 and 4 show S in amine (169.4 eV), amino acids (163.2 eV) and organometallic forms (163.8 eV). They are possible S-S and S-H or S=O bonds which can be explained by the theory of denaturation/desorption of proteins [114]. When proteins adsorb on certain surfaces, they tend to denature or unfold by breaking S-S bonds [115], then the bind with free Co^{2+} for LC CoCrMo or Fe^{2+} for 316L is possible.

With a very thin protein adsorption layer and a sulphide film (iron sulphide), an additional formation of calcium (hydrogen) phosphate/diphosphate was seen on 316L as shown in Figure 7-6, after 4 hours rubbing. Peaks 1 and 2 (133.7 eV- 133.9 eV) correspond to phosphate or hydrogen phosphate (Figure 8-6 (a)). Peak 1 (347.6 eV), peak 2 (348.1 eV) and peak 3 (349.1 eV) to calcium phosphate, calcium hydroxide and calcium diphosphate. They are likely to form as a result of the tribo-chemical reactions. Some authors have stated that in the steady-state, this can contribute to reduced friction [146] by acting like a solid lubricant. In contrast, some studies have shown that the formation of calcium phosphate can prevent a very important fluid film on the sample surface [147]. One possible reason is that under tribological contacts, the condition favours formation of calcium phosphate and with different surface energies, HC CoCrMo is not. Another hypothesis is that the released Fe ions can accentuate the non-soluble calcium phosphate to deposit on sample surface [13]. Due to relative movements of counterfaces, they were carried to be under the protein adsorption layer. Cr oxide (Cr_2O_3) and Fe oxides were detected under the calcium phosphate layer.

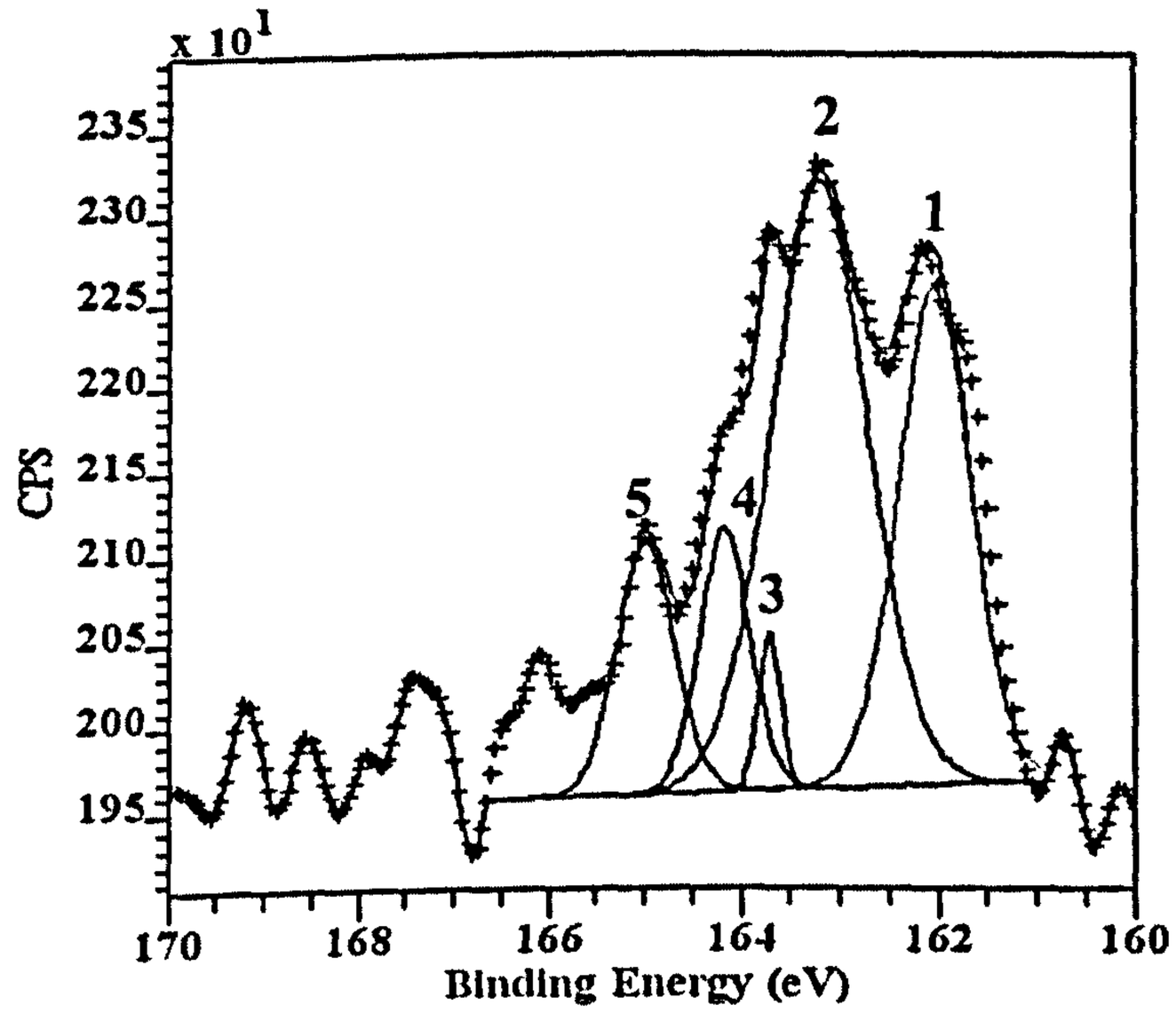

(a)

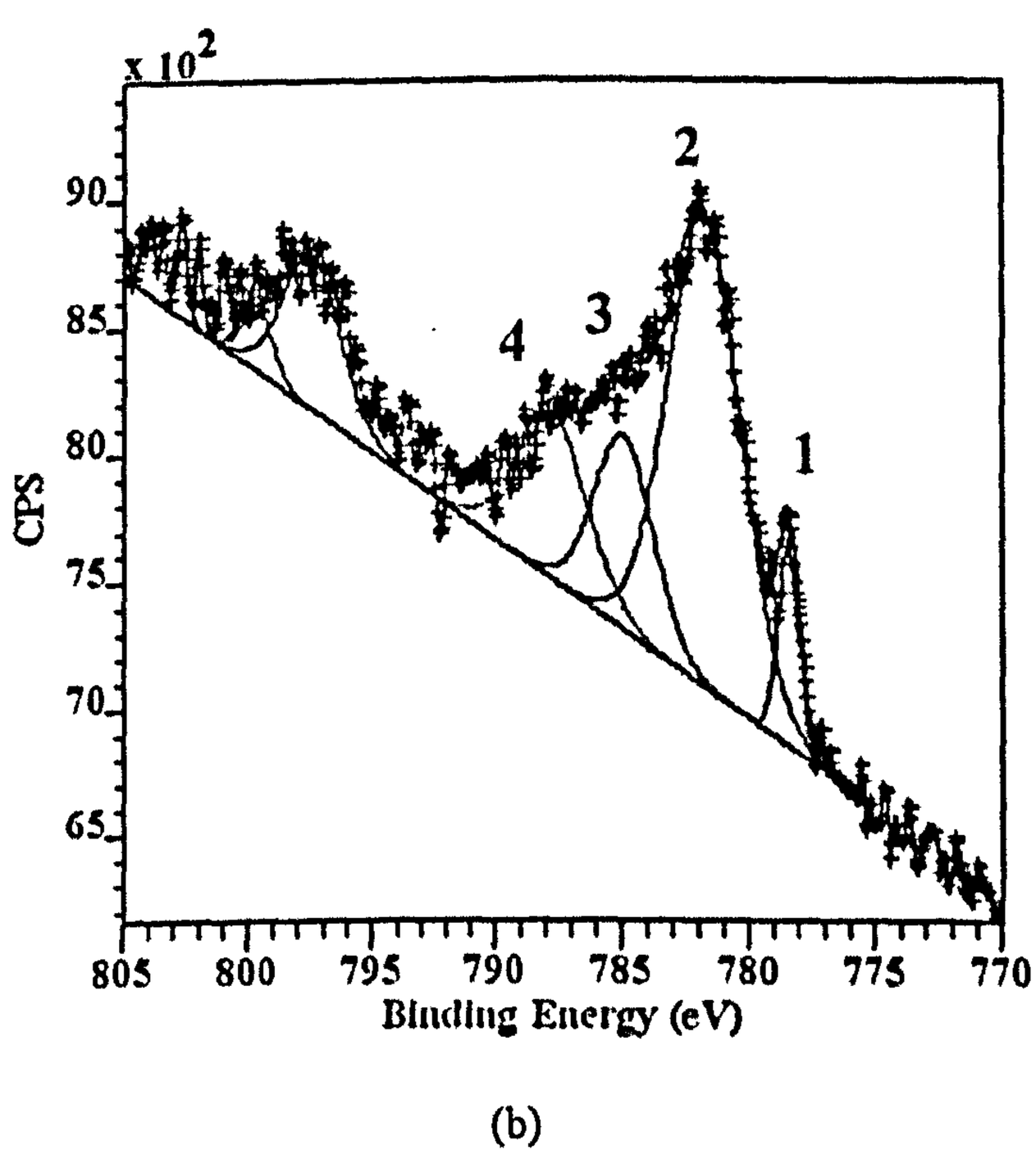

(b)

Figure 8-5 Curve fitted (a) S 2p and (b) Co 2p XPS spectra recorded in the wear scar after 4 hours sliding on LC CoCrMo

For both CoCrMo alloys, the complexes were mostly Co-bounded proteins from XPS tests. Fe in 316L was the main element to combine with the organic molecules. From Table 6-9, on the top of the wear track for HC CoCrMo, Co and Cr were found. The possible structures of the multi-layer on materials in the wear scars are schematically shown in Figure 8-7. After 5 minutes argon ion etching, Cr oxide can still be detected on the sample surface for HC CoCrMo, but for 316L, Fe metal (Fe $2p_{3/2}$ 706.9 eV) was obtained. It indicates that the multi-layer was removed by argon ions and the substrate of 316L was reached. Information from different etching times gives an indication of the relative thicknesses for the multi-layered structures, which are presented in Figure 8-7. Based on XPS tests, the thickness of tribofilm on HC CoCrMo is 10-15 nm in 0.36% NaCl and 20-25 nm in 50% serum. For 316L, the tribofilm with the protein adsorption layer is 12-18 nm. The boundaries for different layers in reality are not as clearly defined but the schematic representation gives a good indication of the overall structure. The layers tend to interact with each other. Also, spatial variations should be taken into account. The 'layer' may not cover the whole sample surface. Outside the wear scar, a very thin protein film and passive layer (mainly Co and Cr oxides for CoCrMo and Fe/Cr oxides for 316L) can be detected for all materials. It indicates that sulphide, calcium phosphate and organometallic species are primarily as a result of tribo-chemical reactions.

Studies have been suggested that for fatty acids, when pressure reached $10^9 N/m^2$, the adsorbed molecules were not removed from a steel surface [149]. The absorbed molecules on CoCrMo and 316L may resist the high pressure and lubricate the counterparts.

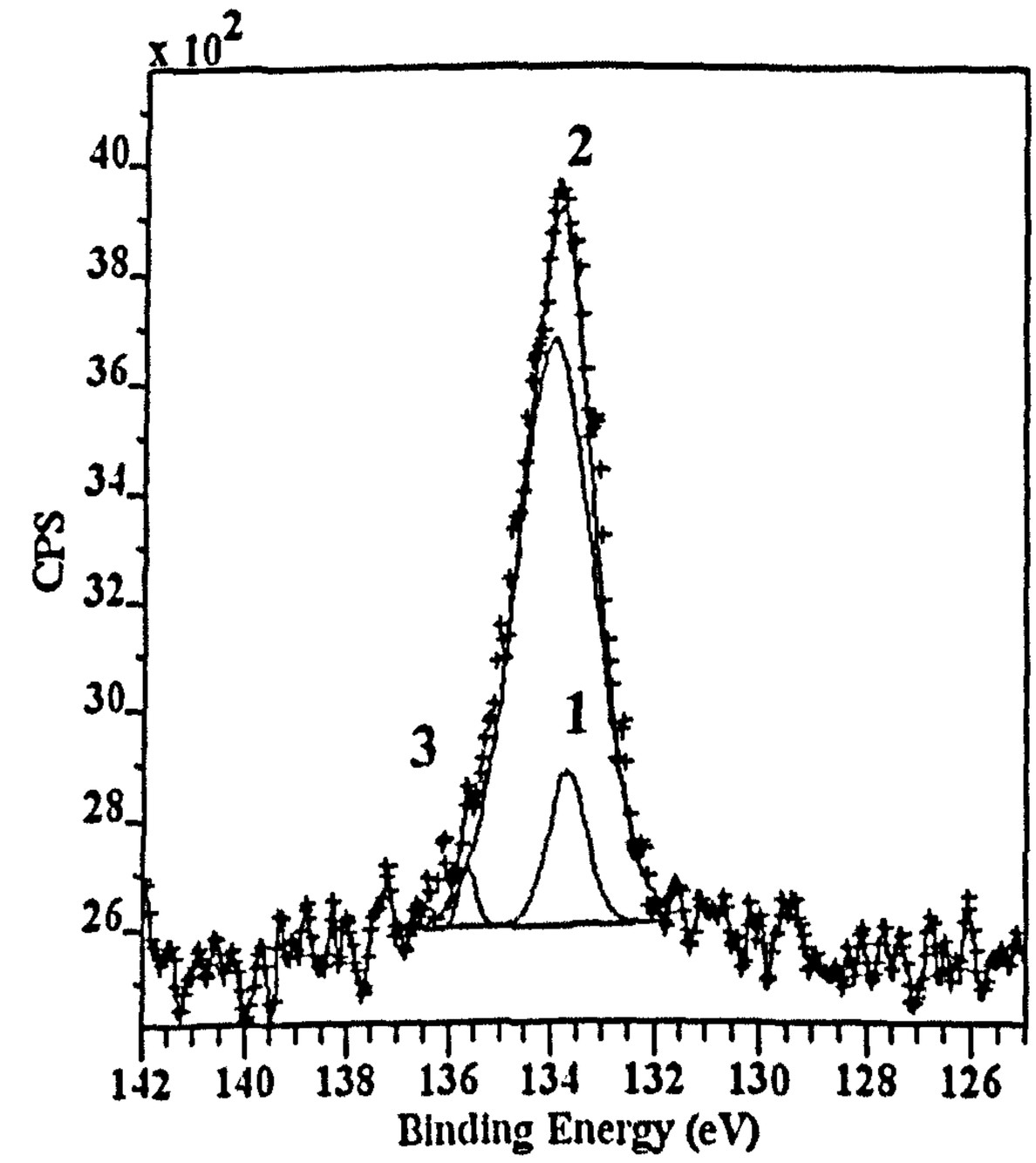

(a)

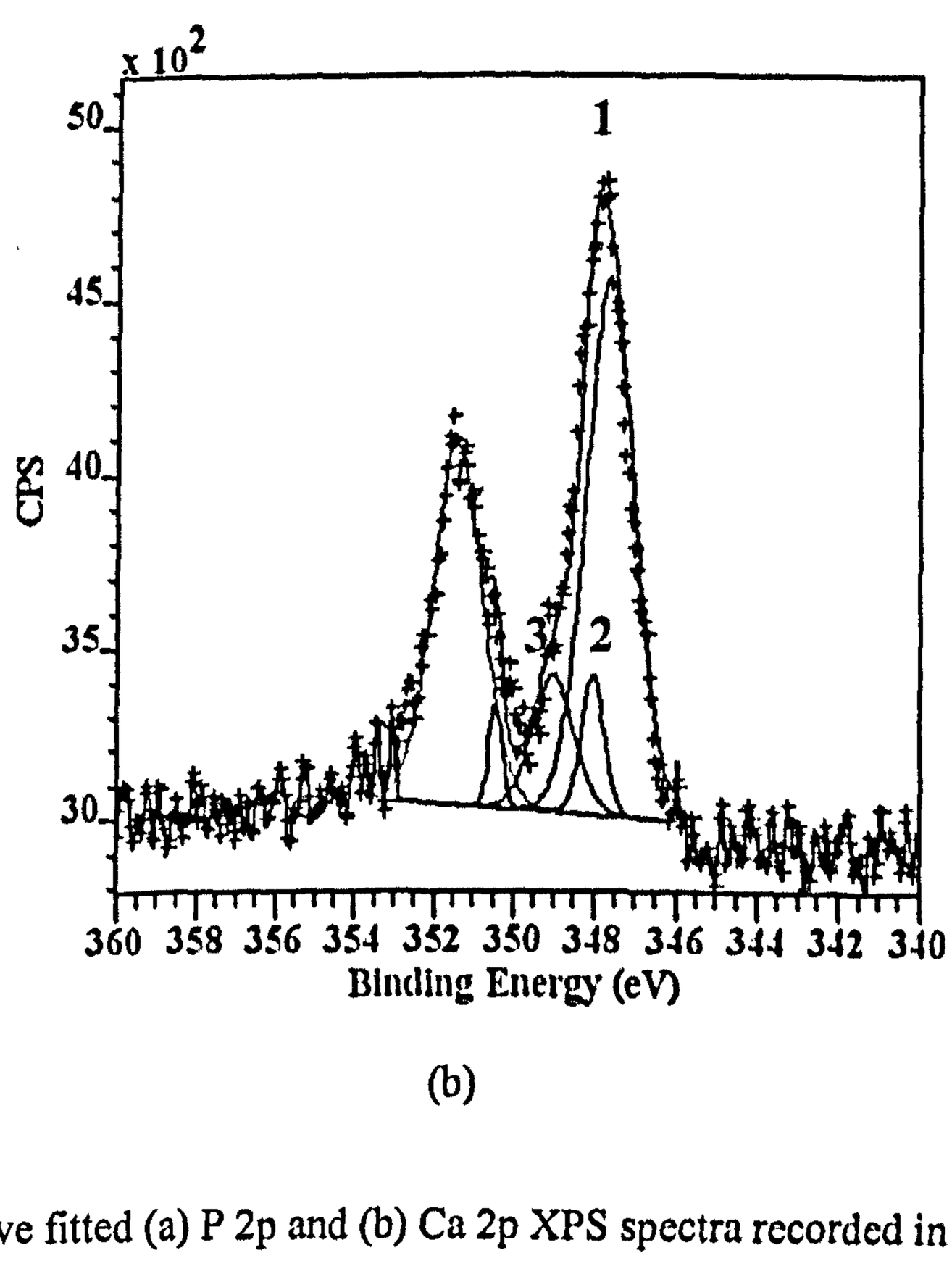

(b)

Figure 8-6 Curve fitted (a) P 2p and (b) Ca 2p XPS spectra recorded in the wear scar after 4 hours sliding on 316L

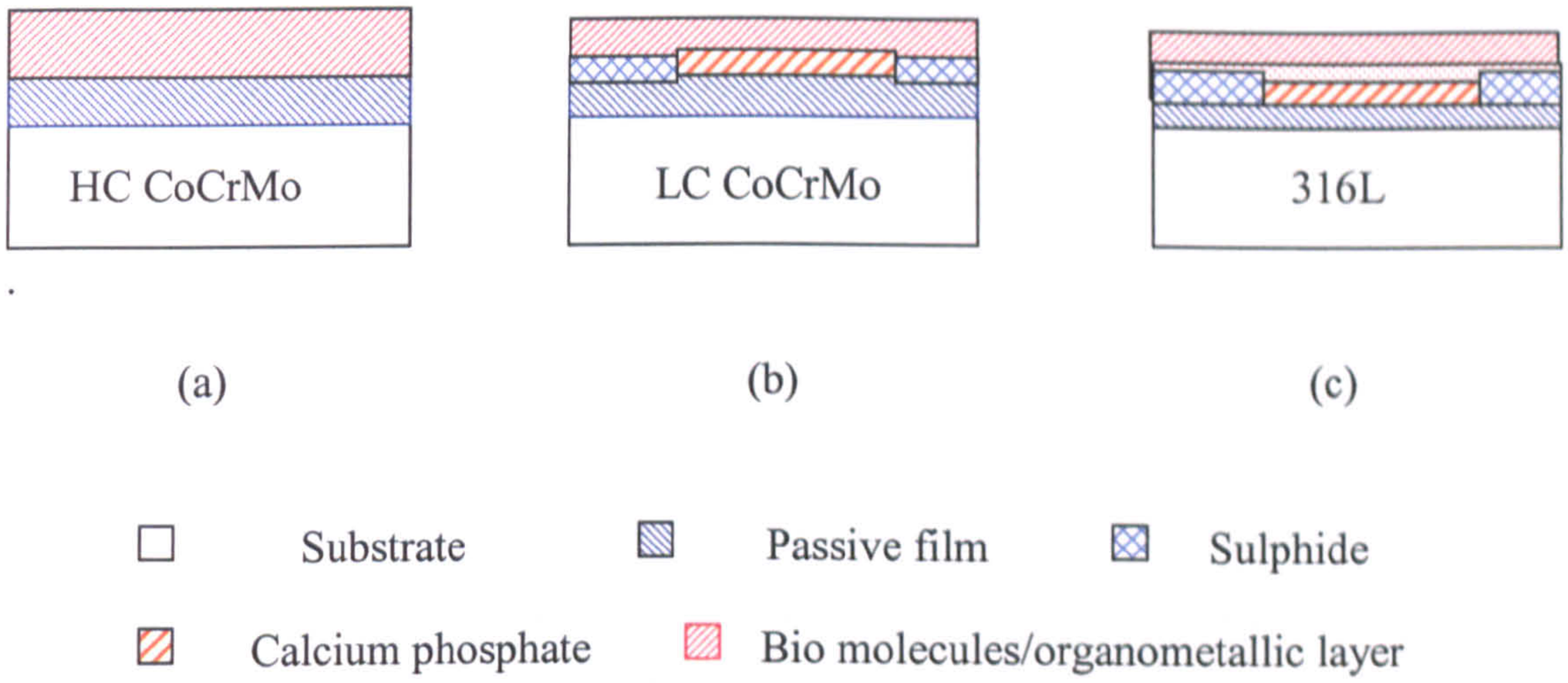

Figure 8-7 Schematic structures of wear scars on (a) HC CoCrMo, (b) LC CoCrMo and (c) 316L after 4hour rubbing in 50% serum

8.2.3.2. 0.36% NaCl

The friction force is dependent upon the shear strength of the contact material (softer). Therefore, the type of oxide may play an important role as solid lubricant in the sliding contact of the contact pair. It is known that the rhombohedral oxide Fe_2O_3 is less effective as a lubricant than the spinel oxide Fe_3O_4. [13]. In this study, samples were at low speed, therefore, adhesive wear may happen for 316L. Different from the spontaneously formed passive film (oxides) in air, the established tribofilm on 316L contained Fe-rich hydroxides/oxides with Cr hydroxides/oxides, which is in line with the finding from Hanawa [19]. It is mainly caused by the tribochemical processes and the reconstruction of passive film under tribological contacts. The formation of Fe(III) hydroxides/oxides changed the contacted mechanisms and gave a different tribology and corrosion response compared with tests in 50% serum. For HC CoCrMo, Co and Cr oxides/hydroxides with minor Mo oxides were found in the contact zone. Additionally, Cr and Mo carbides were also detected. Under sliding motion, these carbides may contact with the Silicon Nitride ball. Due to the higher hardness than the matrix, it may result in a greater friction and less wear.

Results from Chapter 5 suggested that organic species could influence the passive formation and breakdown in static conditions. Additionally, evidence has shown that the tribo-film for materials was affected by the organic molecules as well.

One important issue should be mentioned is that no silicon trace was obtained in the wear scar in any of the tests. It indicates that there is no transfer material from the counterbody (silicon nitride ball). However, the analysis of the Si_3N_4 is not under study here. Future research will be against material typically used in TJR- either metal (CoCrMo or other ceramic, such as alumina). This material was chosen to be an electrochemically inactive material for what is the first study of tribochemical/triboelectrochemical materials in this environment. From visual observations, no severe mechanical damage (some shallow scratches) occurred.

8.3. Tribocorrosion Behaviour- The Interaction Between Wear and Corrosion

In Chapter 6 and Chapter 7, the effects of tribology and corrosion on each other were presented. It is certain that corrosion plays a very important role in this system. Its effect is not only on the entire material degradation process but also on the friction and wear mechanisms.

8.3.1 Effect on material degradation

From Figure 7-3 and Figure 7-4, the proportion of corrosion-related damage was shown. However, based on Eq. 8-1 questions remain as to whether the corrosion effect on wear (W_C) is more serious than the effect of wear on corrosion (C_W).

$$T = W + C + S \qquad \text{Eq.8-1}$$

where

$$S = W_C + C_W \qquad \text{Eq.8-2}$$

so

$$T = W + C + W_C + C_W \qquad \text{Eq.8-3}$$

T is the total material loss in tribocorrosion systems. W is the damage caused by pure mechanical process (in absence of corrosion), which was obtained by applying CP in this study.

Table 6-3 displayed the corrosion current density (i_{corr}) determined by Tafel extrapolation from anodic polarization (AP) curves. Faraday's second law (Eq.8-4) is used to calculate the material loss from the current density.

$$V = \frac{ItM_{at}}{nF\rho} \qquad \text{Eq.8-4}$$

so Eq.8-3 can be written as

$$T - W = \frac{ItM_{at}}{nF\rho} + W_c \qquad \text{Eq.8-5}$$

where, V is the material loss in volume. M_{at} is material's atomic weight. F is the Faraday constant (96500 sA/mol), ρ is the density of material and I is the current which is determined by

$$I = i_{corr}A \qquad \text{Eq.8-6}$$

The sample in this study was under reciprocating sliding. A wear scar (a more active area) can be observed. As shown in Figure 8-8, A_1 is the real contact area (wear scar). A_2 is the area which was not under rubbing and remained passive. A_1+A_2 are the whole sample surface area.

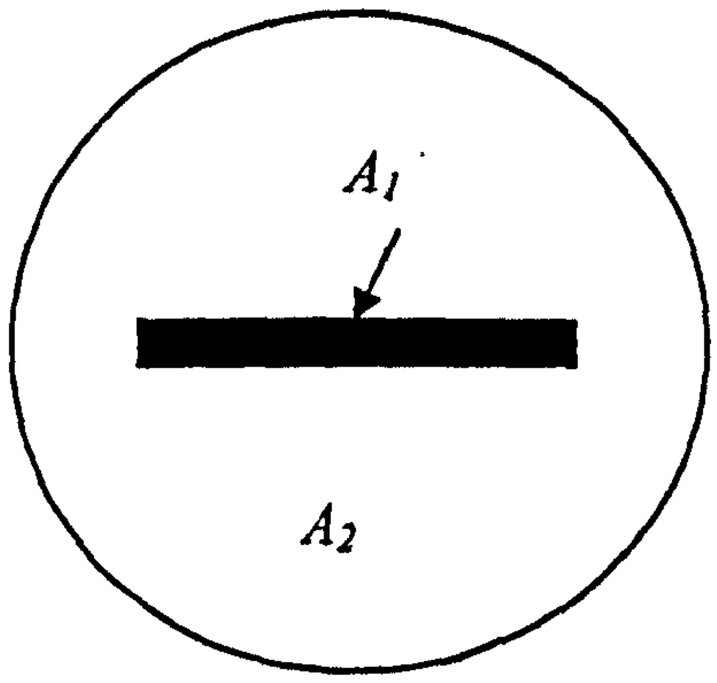

Figure 8-8 Schematic representation of the sample surface after sliding

Thus due to the nature of the electrochemical measurement, the current density in Table 6-2 is the sum of the current density from the active area and the rest of the surface. So Eq. 8-6 should be modified as Eq. for this study.

$$I = i_{corr1} A_1 + i_{corr2} A_2 \qquad \text{Eq. 8-7}$$

Because apart from the active area (wear scar), the rest of the surface is uniformly established by a protective passive film. The material loss from this area can be assumed to be negligible. Based on Eq. 8-3 and the passive current for materials in static conditions, less than 1% of the total material degradation was contributed from outside the wear track area. Based on Eq. 8-4 and Eq.8-7 and Table 6-3, the contributions from tribology, corrosion and the effect of wear and corrosion to each other are shown in Figure 8-9, Figure 8-10 and Figure 8-11.

For all materials in three environments, mechanical damage is the major cause of the material loss (more than 50%). However, the synergy effect clearly contributes to the degradation. For HC CoCrMo, the effect of wear on corrosion is about 2% to 3%, which is similar as LC CoCrMo (2% to 3%). It indicates that due to their good corrosion resistance, the mechanical damage did not affect the electrochemical processes massively. For 316L, 4% to 6% damage was from the wear effect on corrosion. The corrosion effect on wear is by far the largest component of damage

accounting for corrosion/wear interactions (S) in the tribocorrosion system. Corrosion affects the surface properties then will influence the wear mechanisms abundantly. A detailed discussion is presented. However, an increase in error for W_c which results from combined data W and C_w can be gained. The errors for the combined data have been considered and the range of components for the material degradation processes is shown in Figure 8-9.

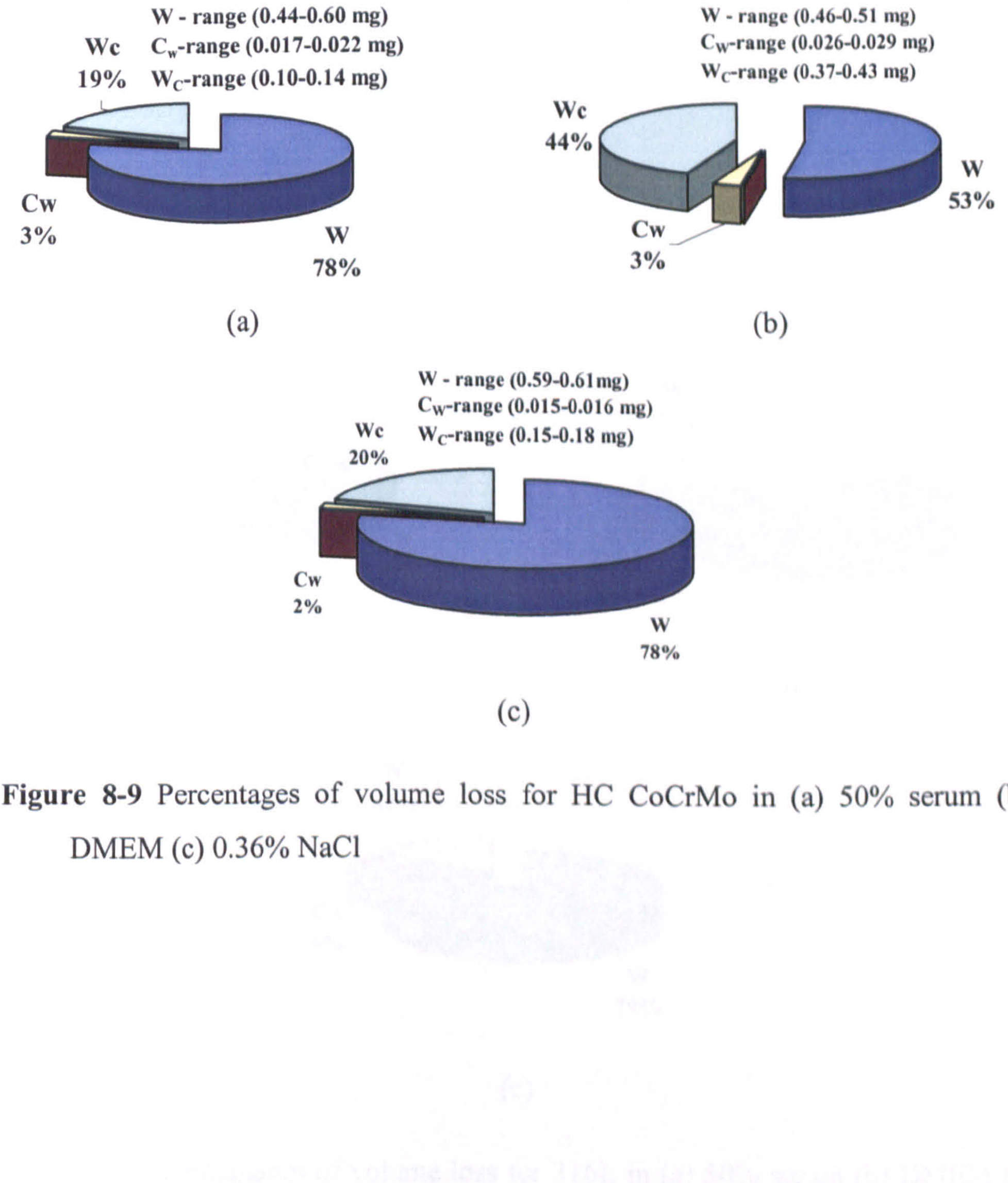

Figure 8-9 Percentages of volume loss for HC CoCrMo in (a) 50% serum (b) DMEM (c) 0.36% NaCl

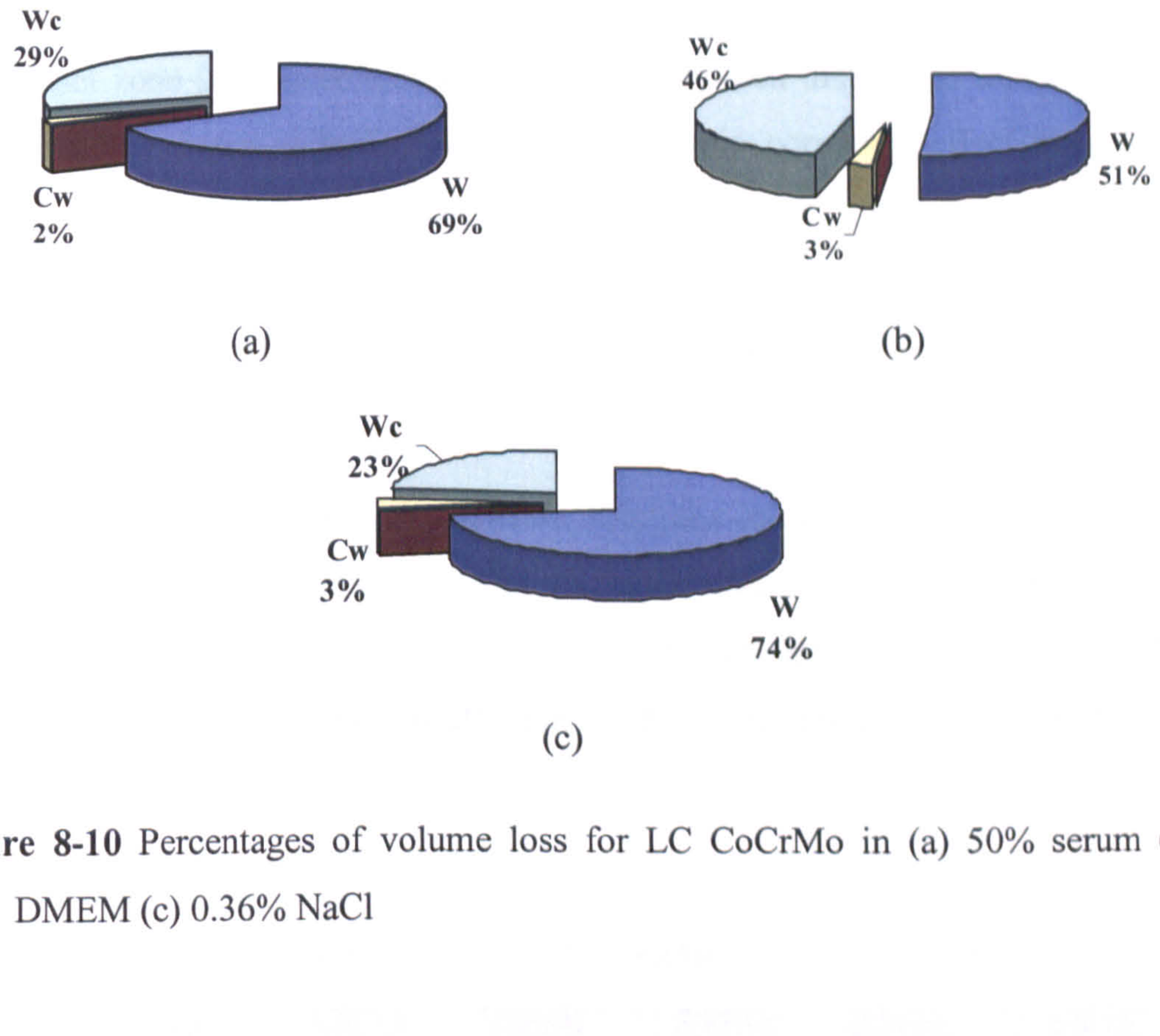

Figure 8-10 Percentages of volume loss for LC CoCrMo in (a) 50% serum (b) DMEM (c) 0.36% NaCl

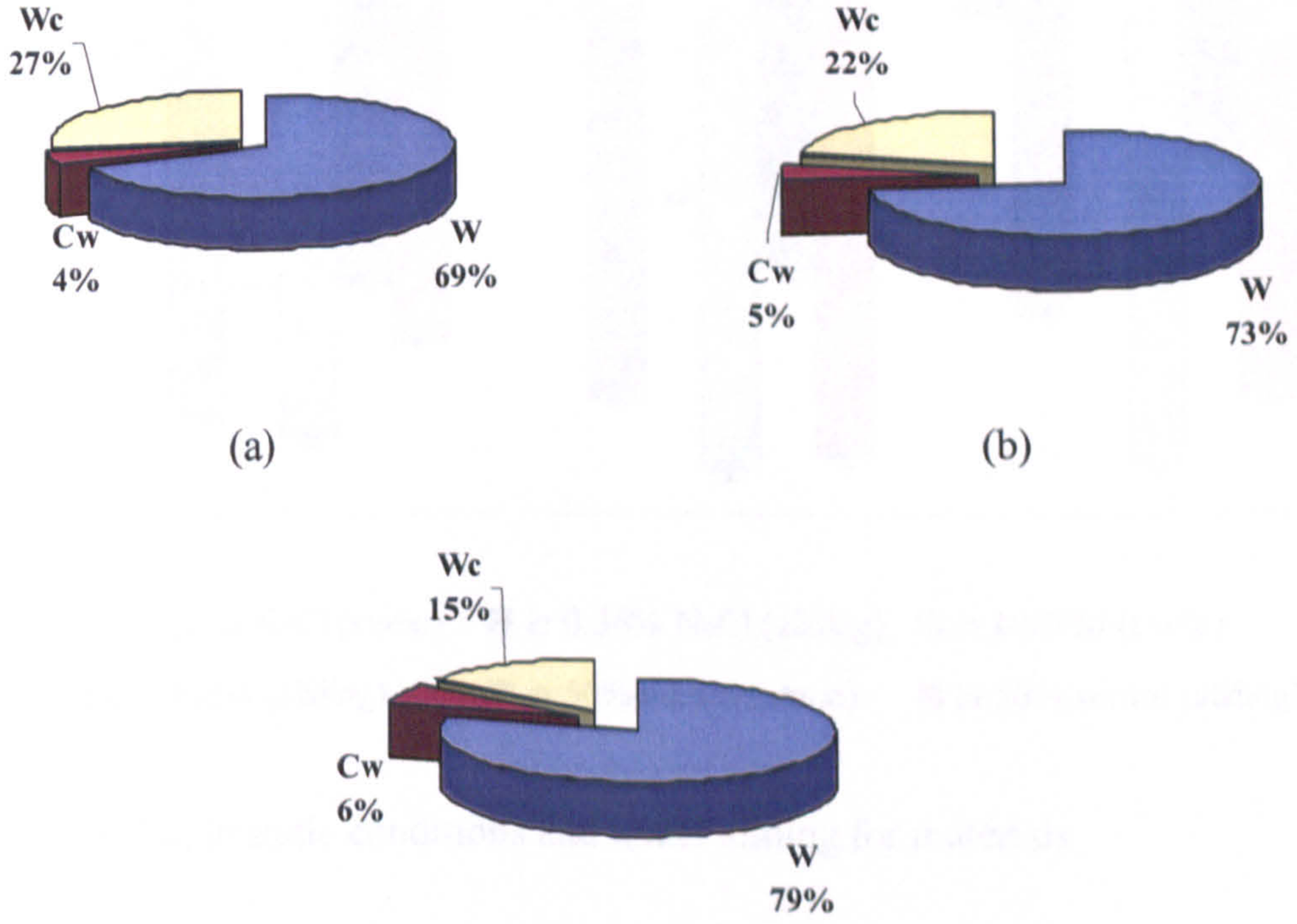

Figure 8-11 Percentages of volume loss for 316L in (a) 50% serum (b) DMEM (c) 0.36% NaCl

Another issue relating to the wear effect on corrosion is that due to the sliding, the contact zone (A_1) became more active (anodic) then the rest of sample surface (A_2) turned to more cathodic. A possible galvanic corrosion effect may occur resulting in an accelerated ion release rate from the wear scar, which accentuated the material degradation even more. The ratio of the anodic/cathodic reaction and quantification of the effect of it in tribocorrosion systems was not studied here.

Figure 8-12 shows E_{corr} in different solutions in static conditions and under sliding. Clearly, the potential moved to more negative when the material in tribological contacts. The shift is due to the activated area (A_1— wear scar). The uniformed passive film was locally removed, which resulted in a decrease of potential.

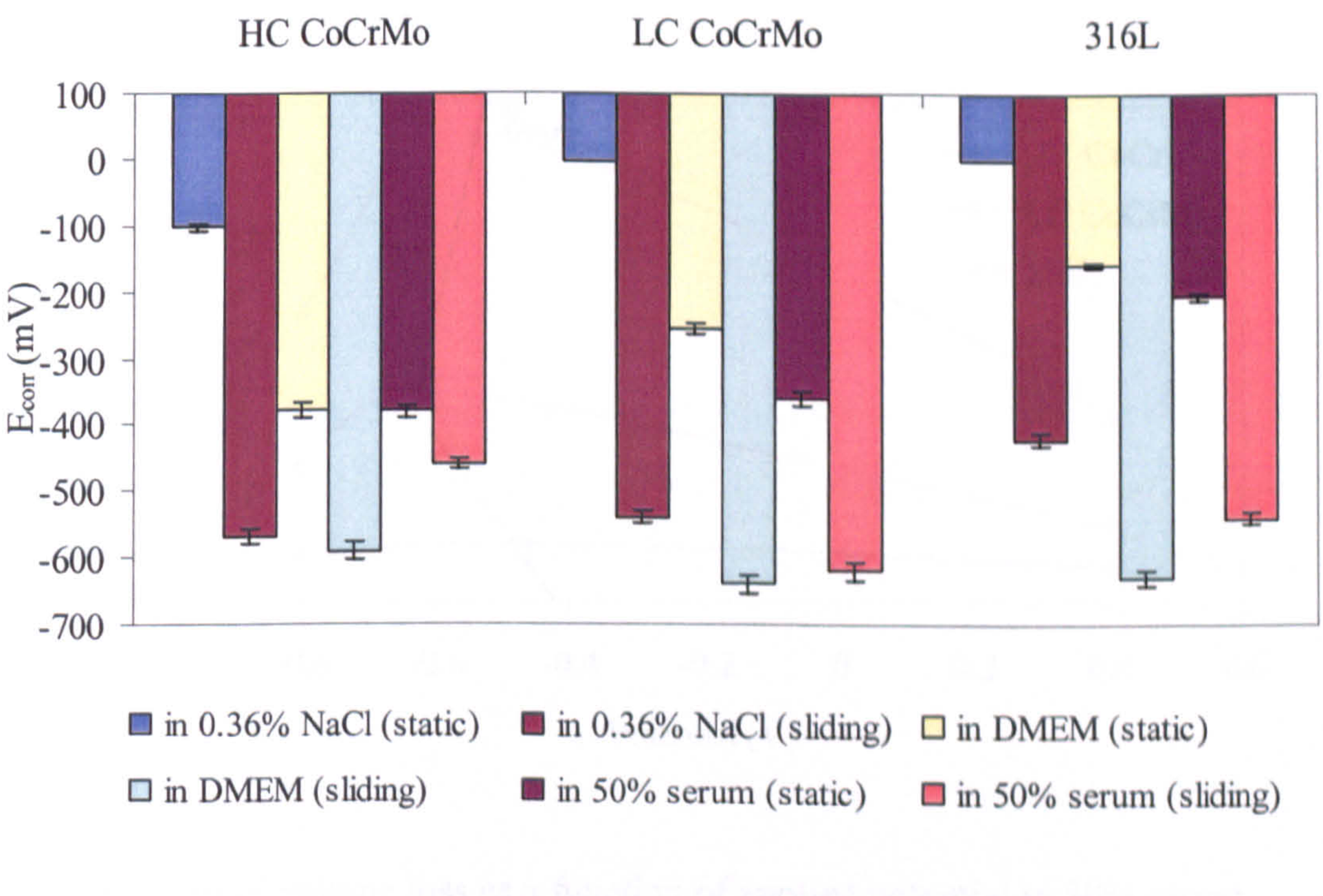

Figure 8-12 E_{corr} in static conditions and under sliding for materials

Experiments show a different extent of material loss under different potential and open circuit. Figure 8-13 summarizes the relationship between total wear and applied potential in 50% serum. In this study, -0.8 V is the CP potential. At both 0.2 V and 0.4 V, materials are in the passive region. It shows that both a negative

potential (-0.8 V) and positive potentials (0.2 V and 0.4 V) reduce the material degradation. However, the mechanisms are different. Under CP, corrosion was prevented by an impressed current. No metal ions were released in the bulk solution. The material loss was totally controlled by mechanical factors. At 0.2 V and 0.4 V, a passive film with organometllic layer was forced to form. Due to its protective behaviour, the release of metal ions (corrosion) was minimized. Therefore, the mechanism of material degradation was influenced by both mechanical factors and electrochemical behaviour of individual material. It clearly proves that by forcing the passive film and organometllic complexes to form can improve wear, corrosion and tribocorrosion resistance of materials.

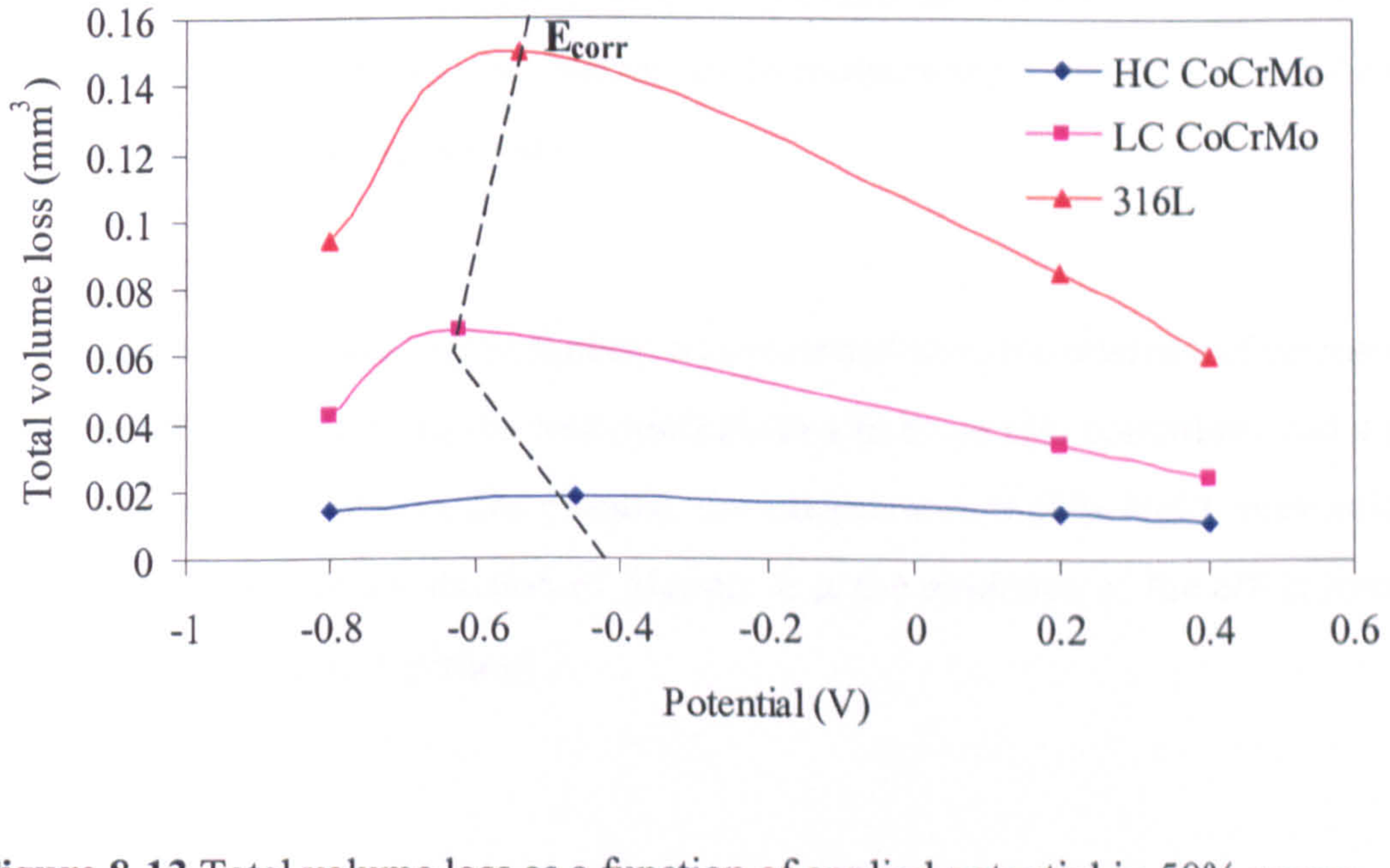

Figure 8-13 Total volume loss as a function of applied potential in 50% serum

8.3.2. Effect of corrosion on friction

The effect of corrosion on friction (Figure 8-14) is primarily related to how the surface properties change as electrochemical reactions proceed. CoCrMo alloys and stainless steel suffer pitting corrosion in aggressive/corrosive environments. Those micro-pits can change the surface roughness and increase friction if materials are in contact. Nevertheless, the formation of passive film can also change the friction behaviour as discussed earlier. Figure 7-7 showed the roughness differences in three solutions after 4 hours rubbing for all materials. With the application of CP, corrosion was prevented and the friction response differed. No relationship between the roughness and friction coefficient in 50% serum or DMEM was established. Because that the soft organic complexes were attached to the sample surface, the measured roughness can not present the real substrate surface property. However, due to the limitation of this study, details of proteins adsorption can not be measured. The friction measurement, the contact angle measurement and the electrochemical tests are all macro-measurements.

However, slightly higher friction was recorded with the absence of corrosion in 50% serum. It is related to the wear mechanisms in these two conditions and will be discussed in detail later in this chapter. For materials in 0.36% NaCl, prevention of corrosion resulted in a reduction of friction. It is the evidence of the effect from the localized corrosion (i.e. pitting).

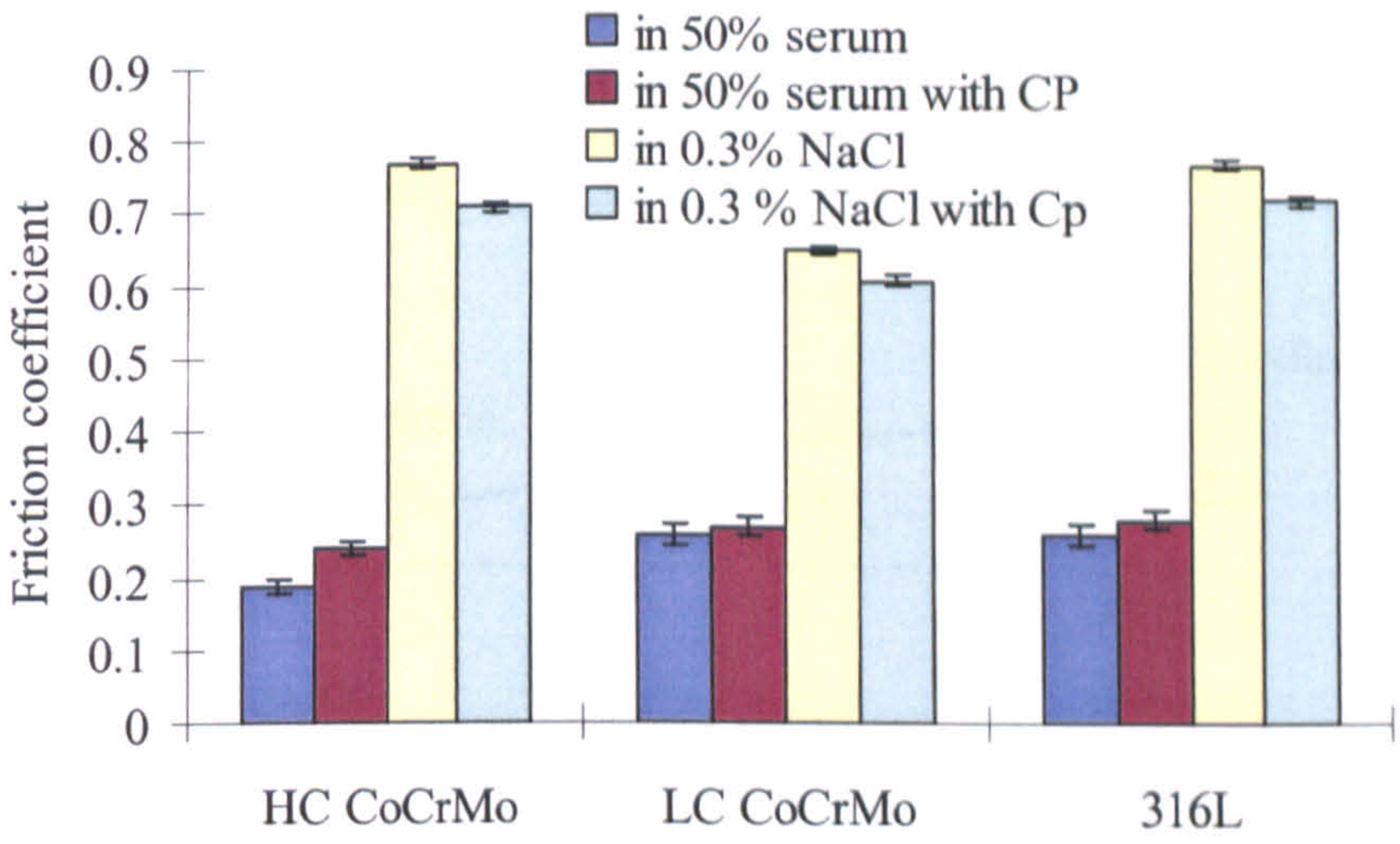

Figure 8-14 Corrosion effect on friction coefficient for all materials in 50% serum and 0.36% NaCl

Figure 7-11 presented the anodic polarization with the corresponding friction coefficient for materials in 50% serum. It is the first attempt ever to evaluate materials friction and electrochemical behaviour together in a biological environment. The accelerated electrochemical tests brought materials from an electrochemically active state to a passive state and then to an active state again. The friction coefficient showed a corresponded behaviour. To analyze the friction behaviour under passive or active regime of materials under tribological contact can give us an indication how friction and ion release processes can affect each other. The friction coefficient and anodic polarization curves are schematically drawn in Figure 8-15 (a). For all materials, the friction coefficient decreased in region 2. In 50% serum, an interesting pseudo-repassivation regime can be seen in region 1. This pseudo-passive film can act like a solid lubricant and reduce the friction. In region 3, companied by the pseudo-passive film breakdown, the friction increased and oscillations can be observed in region 2 and region 3. LC CoCrMo showed the same tendency. The explanation for the changes of friction with potential is illustrated in Figure 8-15 (b) for region 2 and Figure 8-15 (c) for region 3. In region 2, a film formed and ions releasing processes slowed down. The silicon nitride ball was damaging the pseudo-passive layer but can hardly reach the substrate. In region 3,

electrochemical breakdown occurred due to high potential. The film started being electrochemical dissolved especially in the stroke, and the ball can reach the bare metal surface, which resulted in an increase of the friction.

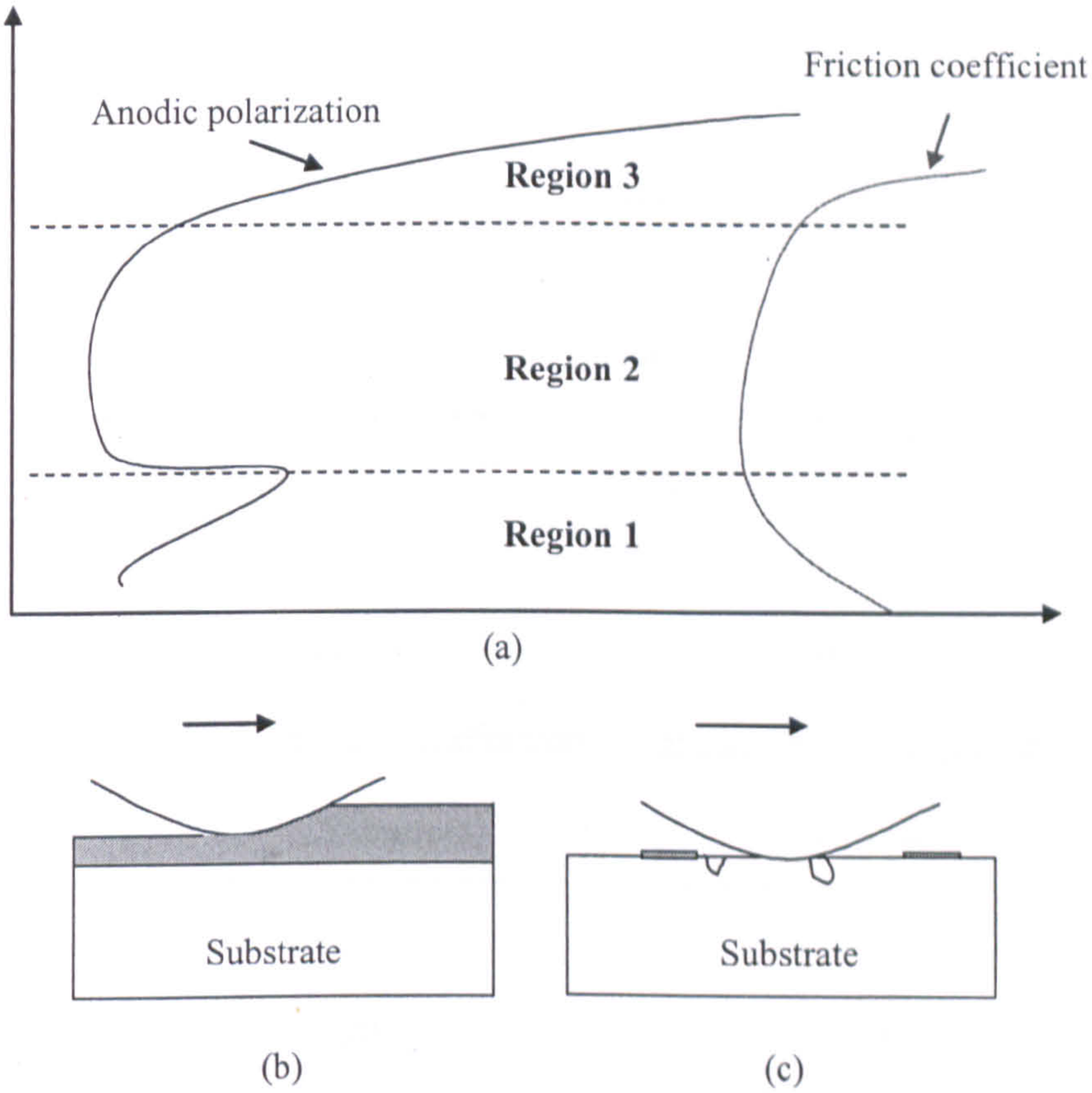

Figure 8-15 (a) Schematic representation of the anodic polarization curve and friction coefficient response for materials in 50% serum (b) cross section schematic profile of the tribofilm in region 2 (c) cross section schematic profile of the interface in region 3

For HC CoCrMo, in region 2 of both solutions (0.36% NaCl and DMEM), the initial tendency of friction is similar with 316L (Figure 8-16). After the sample reached region 2, the current decreased and the corresponding friction decreased. HC CoCrMo has a harder surface may be responsible for the different behaviour on friction. LC CoCrMo had the same phenomena as HC CoCrMo.

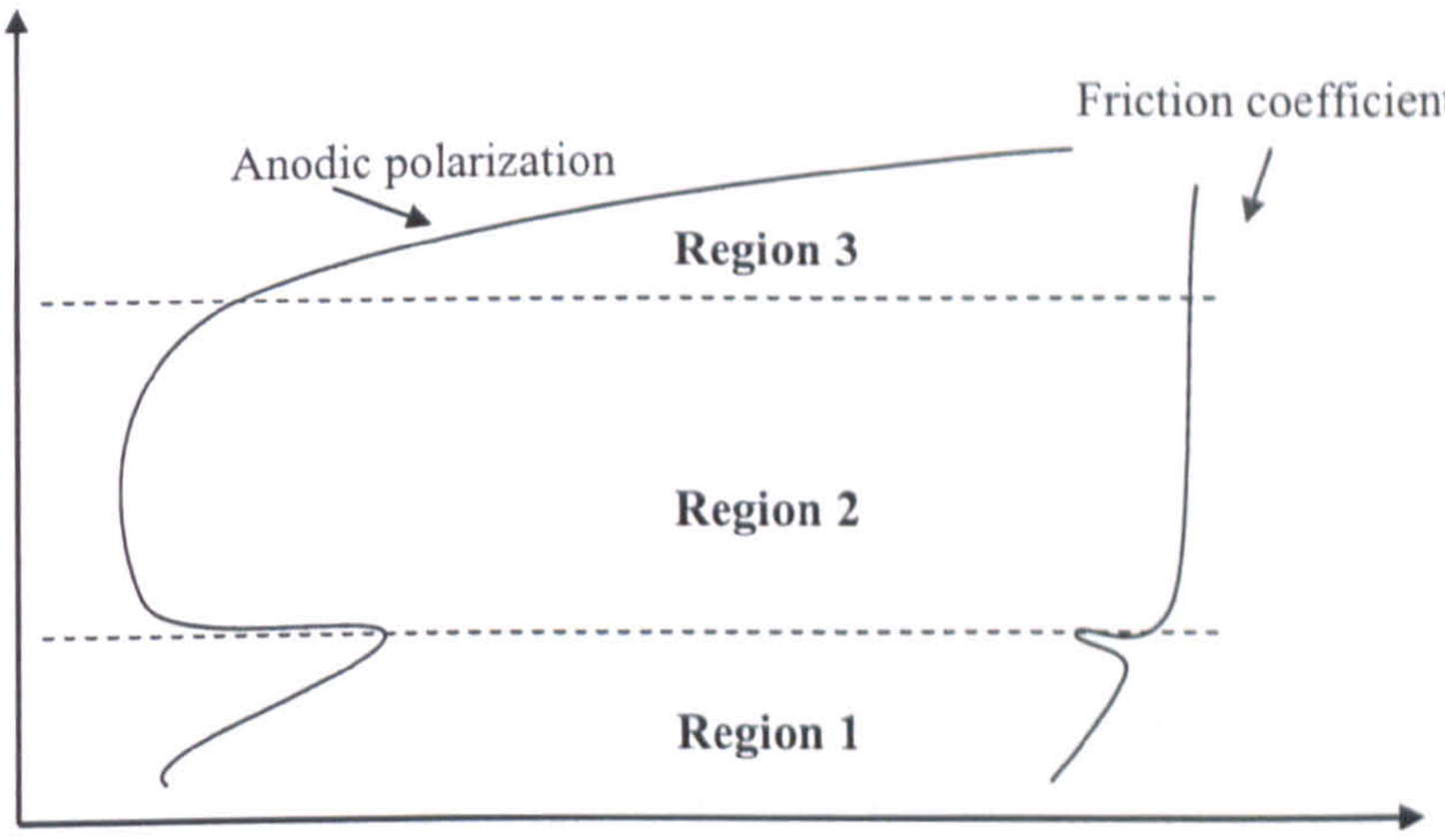

(a)

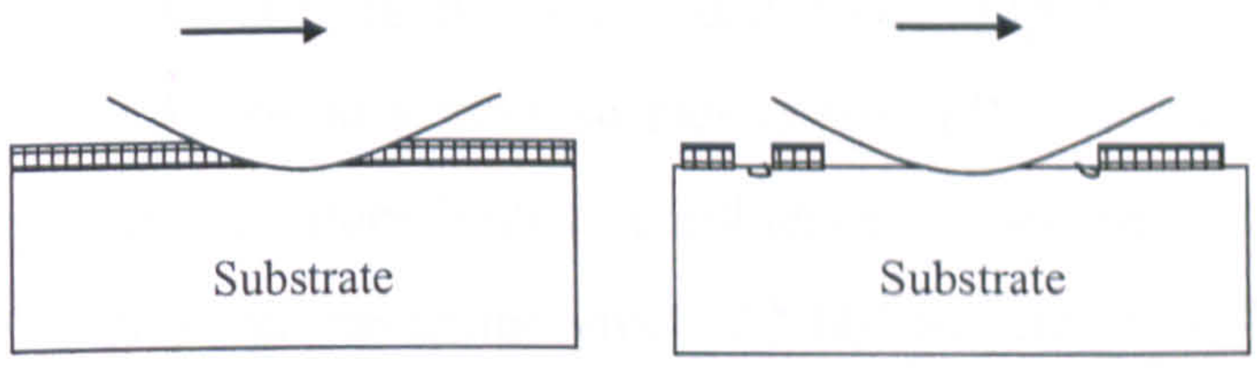

(b) (c)

Figure 8-16 Schematic drawing for 316L in 0.36% NaCl and in DMEM (a) friction coefficient during anodic polarization scan (b) cross section schematic profile in region 2 (c) cross section schematic profile in region 3

From these results it is apparent that the release of Fe^{2+} ions in DMEM and in 0.36%NaCl have little effect on the friction coefficient and a steady high value of 0.6-0.8 is maintained for the 316L alloy during the test. For the HC CoCrMo alloy (and the LC CoCrMo alloy – not shown) there is *some* correlation between ion release and friction but this is not as well defined as it is for the 50% serum. As the release of Co ions progresses in the activation-controlled region of the polarization curve a drop in friction coefficient was recorded to 0.3 and 0.4 in DMEM and 0.36%NaCl respectively suggesting that a tribofilm was formed which modified the frictional characteristics of the interface. It is however suggested that part of that

friction modification is also due to modification of the passive layer by electrochemical processes (non biological) as demonstrated in 0.36%NaCl.

8.3.3. Cathodic protection effect on protein adsorption

An important issue for this study is if CP can change the protein adsorption mechanism. Due to the fact that CP is performed by an impressed current to the sample surface to stop metal ions being released, the entire sample surface carries a negative charge, which is different from open circuit condition. In open circuit condition, metallic sample surfaces have a different anodic and cathodic potential map. Under CP, the sample surface may attract different groups of protein molecules. The adsorption of proteins on to sample surface is controlled by many factors [96, 97]. Surface energy and pH values both can influence the adsorption process. The carboxyl group (-COOH) and the amine group ($-NH_2$) in protein molecule are the major groups to interact with solid surfaces [151]. During the application of CP, the pH value near the sample surface increases. The carboxyl group intends to loss H and becomes $-COO^-$. Therefore, according to the electrostatic principles, the adsorption is less. However, from Figure 8-14, the friction did not change dramatically in two different conditions (with CP and without CP) in 50% serum. It indicates that the lubrication effect of adsorbed biological species is similar for the two conditions. Moreover, contact angle measurements confirm that the surface energy of sample surfaces under CP and open circuit in 50% serum differs by just 3%.

8.3.4. Metal ions release and metal-protein binding

The release of metal ions into the bulk solution is driven directly by electrochemical processes. However, mechanical processes can also contribute to the release in two ways.

- The effect of wear on corrosion processes.
- The production of wear debris which can also be corroded resulting in release of metal ions.

Therefore, the quantification of metal ions in the solution (Q_S) can be concluded as

$$Q_S = Q_R + Q_D \qquad \text{Eq. 8-8}$$

where

Q_R is the charge from material surface and Q_D is the total charge released from wear debris.

Anodic polarization tests for all materials give the relationship of the increased potential with the transferred electrons (current). The total charge (Q_{AP}) can be calculated by integrating the recorded current.

$$Q_{AP} = \int Idt = \int iAdt \qquad \text{Eq. 8-9}$$

A is the sample surface area and i is the current density. Figure 8-17 gives an example of the results calculated from Eq. 8-9. A very slow increase of charge transfer for HC CoCrMo can be seen in the middle of the curve which corresponds to the protective pseudo-passive film being established in 50% serum.

Released metal ions in the solution were detected by ICP and results were shown in Figure 7-8. Therefore the mass of release metal ions in the cell is:

$$C = M_s V_s \rho_s \qquad \text{Eq.8-10}$$

where

M_S is the concentration which was measured by ICP. V_s is the liquid solution volume. ρ_s is the density of the solution. By combining Eq. 8-10 and Eq. 3-10

($Q_S = \frac{CFn}{M_{at}}$), Eq. 8-11 is obtained to calculate the charge produced from metal atoms to metal ions processes.

$$Q_S = \frac{M_S V_S \rho_S N_A E_e n}{M_{at}} \qquad \text{Eq.8-11}$$

Where, N_A is the Avogadro's number (6.02×10^{23}). Therefore, E_e is the electric charge constant which a single electron carries 1.6×10^{-19} coulombs ($F=N_A E_e$). Eq. 8-10 presents the charge which were released from the metal atoms to metal ions processes in the solution.

In this discussion, although wear debris participated in the total ion release, the amount may be neglectable comparing with the ions which were produced by tribocorrosion processes due to the short testing time (1 hour for AP test). However, metal ions from wear debris are believed to be an important and key source to the total released ions in long term for metallic bearing implants. In the accelerated electrochemical tests, wear debris was produced but in a comparable small amount. Therefore, it is not included in the calculation (assume Q_D=0).

Interestingly but not surprisingly, a difference can be obtained between the charge in the solution and the charge released from the material in 50% serum and DMEM. A chart is shown in Figure 8-18 for LC CoCrMo in 50% serum. It is evident that released Co^{2+} from the tribocorrosion processes did not manage to travel to the bulk solution. Instead, a number of them bound with biological molecules and formed complexes and attached in the wear scar. The amount of charge from bounded metal ions is Q_f. Therefore,

$$Q_f = Q_{AP} - Q_S \qquad \text{Eq. 8-12}$$

If the charge from wear debris was taken into account, the value of Q_f can be even greater. Both in 50% serum and DMEM, metal ions were found to be bound with biological molecules.

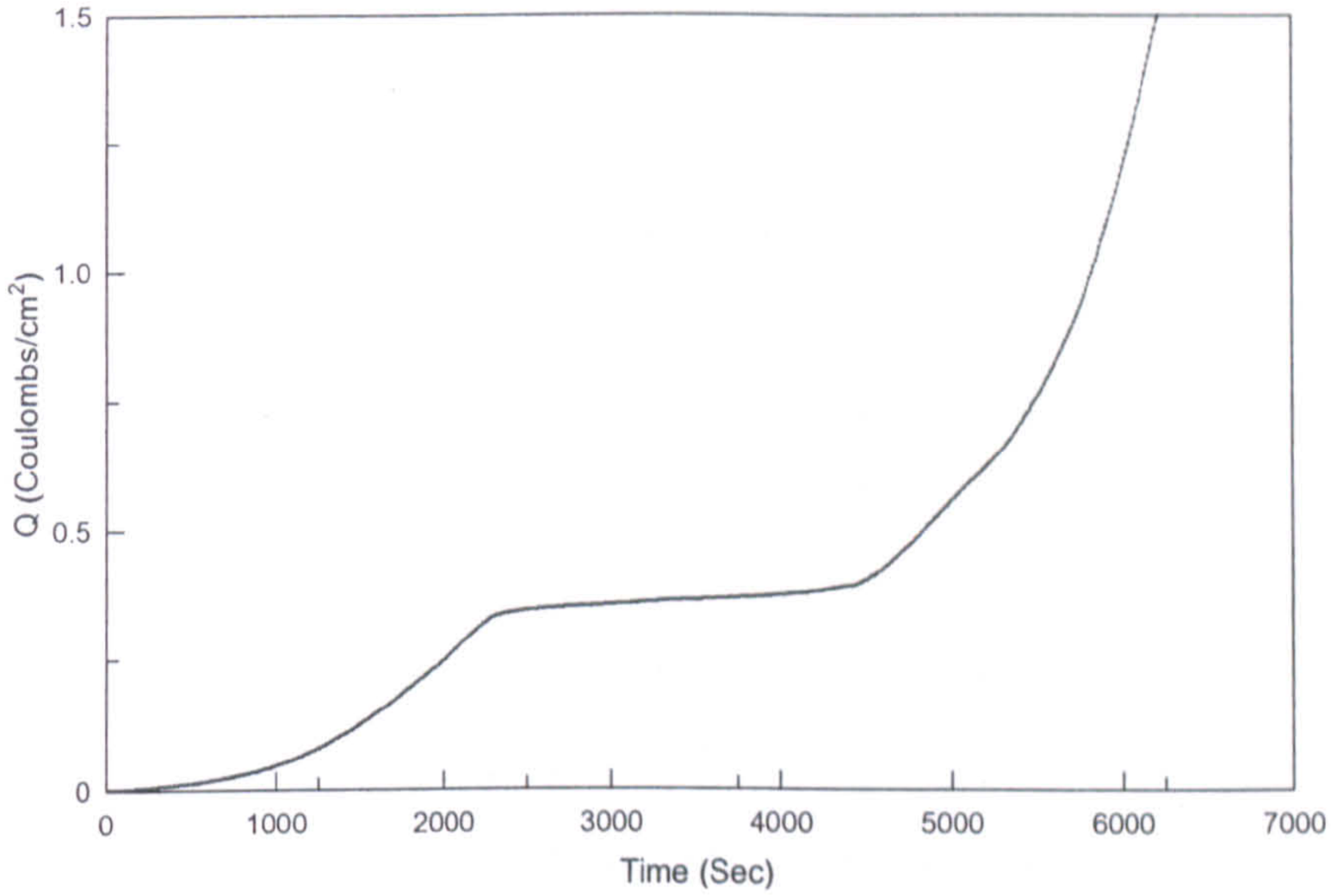

Figure 8-17 Charge as a function of time by integrating current from anodic polarization tests

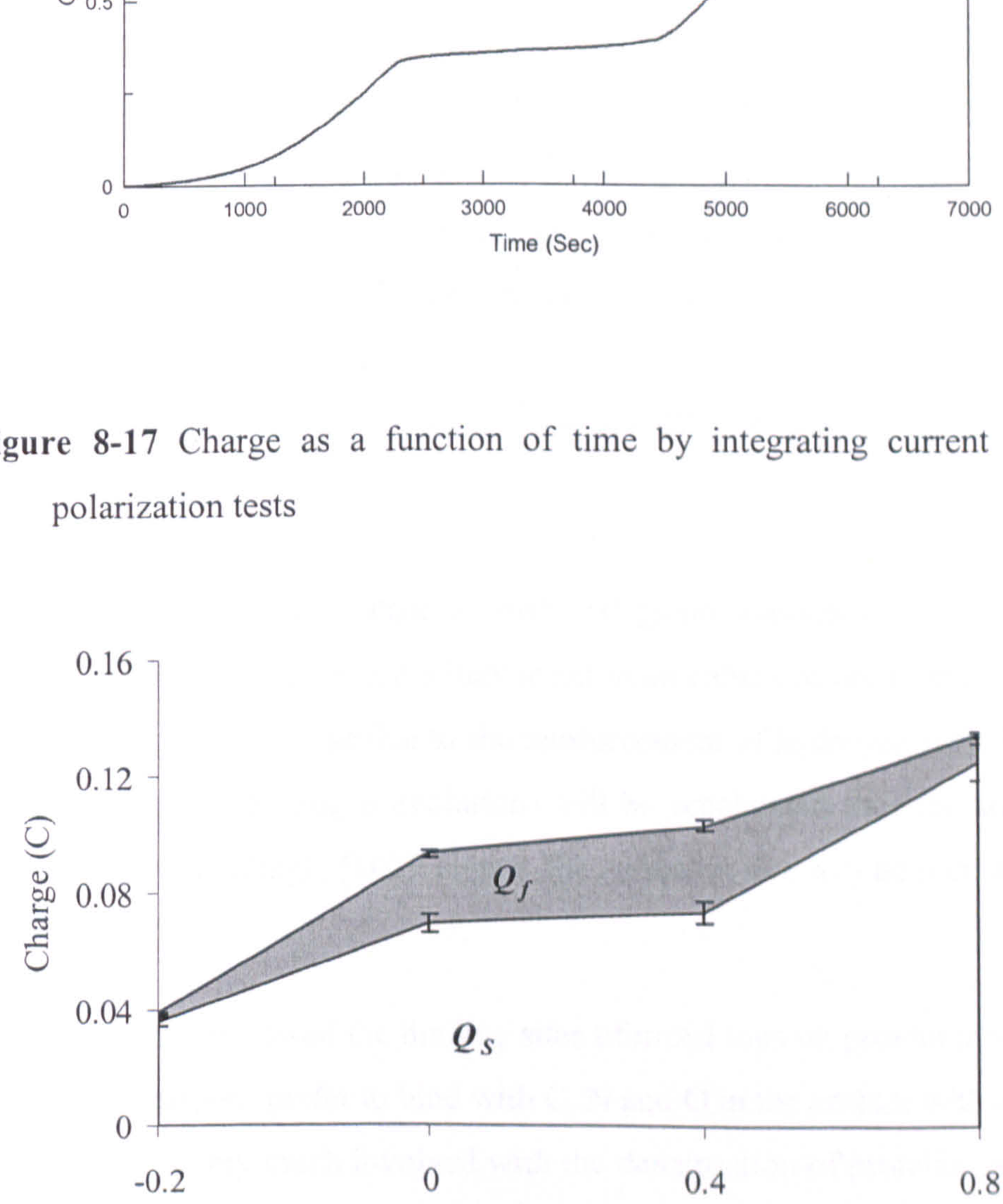

Figure 8-18 The relation of Q_f, Q_S and Q_{AP} (Q_f+ Q_S)

8.3.5. The reactions of proteins and metal ions

As mentioned in previous chapters, in the anodic reaction on the test materials the metal element loses electrons. The major cathodic reactions are the oxygen-reduction and hydrogen-evolution reactions. However, in 50% serum, the complexity of proteins makes the reactions complicated. Some suggestions will be discussed here as the possibilities of the reactions. The anodic reaction is still straight forward, although proteins seem to attract metal ions strongly and accelerate the ions release rate but they lead to a drop in charge in the pseudo-passive region due to the bind with the released metal ions. ·Hallab [152] studied the thribochemistry of carboxylic acids, which is the main component for Albumin protein. The whole process can be concluded as the following.

$$R-CH_2-CH_2-\overset{O}{\overset{\|}{C}}-OH + e^- \rightarrow R-CH=CH-\overset{O}{\overset{\|}{C}}-O^- + 2H$$

Under tribological contact, the carboxyl group receives an electron and releases two hydrogen ions. This process may result in an enhanced corrosion process. Firstly, the pH value will decrease due to the reinforcement of hydrogen ions. Secondly, the cathodic reaction (hydrogen evolution) will be accelerated thus the anodic reaction will increase accordingly [102]. Hence, the corrosion rate will be increased.

Chapter 3 reviewed the binding sites of metal ions on protein molecules. From research, metal ions prefer to bind with C, N and O in the protein with a ligand bond. The process is very much involved with the denaturation of proteins. Albumin tends to degrade though the break of –SH binding and also the N-terminal. Figure 8-19 shows a model which was suggested by Chan [153]. An example of Co[II] binding with N-terminal is presented in Figure 8-20. If the N-terminal degraded in the tribocorrosion system, Co ions can still strongly attach with molecules and than become a ligament of separate amino acid branches. This formation may carry some responsibility for the reduction of friction. Also, binding with released Co, Cr, and

Fe ion can accelerate the denaturation of normal folded proteins [113,114]. Peak 1, 2 and 3 in Figure 8-21 along with the Co, C and O spectra (Figure 6-22 and Figure 6-23). A possible formula for the complex in the wear scar on HC CoCrMo is suggested [137].

$$[Co(NH\text{-}CH\text{-}C_6H_3(O)\text{-}NO_2)(NH_3)_4](NO_3)_2$$

Even though Co ions were the metal ions which were preferentially released in the biological environments from studied CoCrMo alloys and bound with the proteins, Cr ions also presented in both the bulk solution and as metal-protein complexes on sample surface. An exchange process of Co to Cr can occur. It may happen in the pseudo-passive film breakdown process (region 3 in Figure 7-11) and more Co were released from the organometallic complexes and recorded in Figure 7-8. Based on ICP tests, in 50% serum the released Cr ions in the bulk solution were less than in 0.36% NaCl.

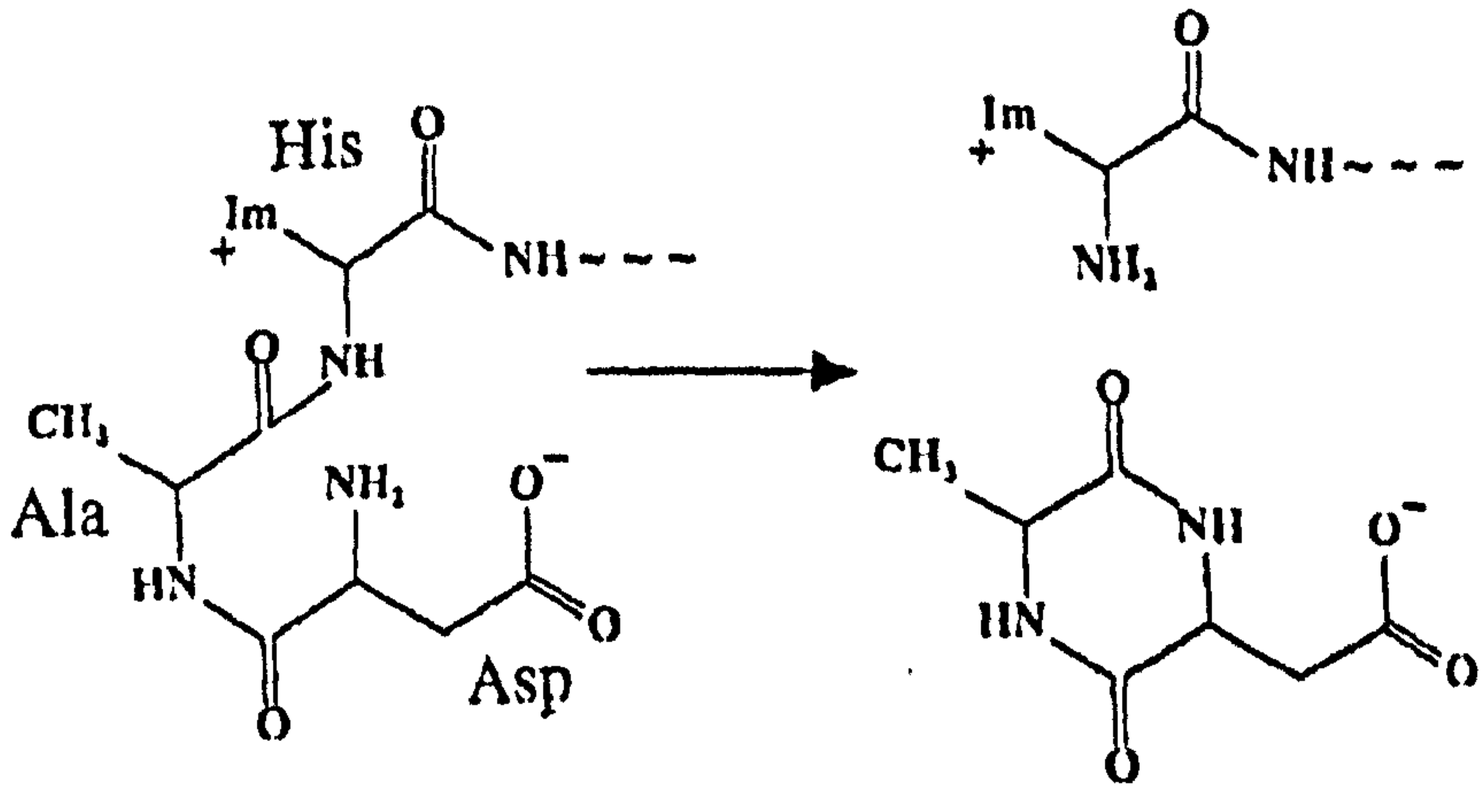

Figure 8-19 Models for N-terminal degradation [154]

$$(NH_3)_5Co-O-\overset{O}{\overset{\|}{C}}-R^{n+} + Cr^{2+} \rightarrow$$

$$Co^{2+} + 5NH_3 + (H_2O)_5Cr-O-\overset{O}{\overset{\|}{C}}-R^{n+}$$

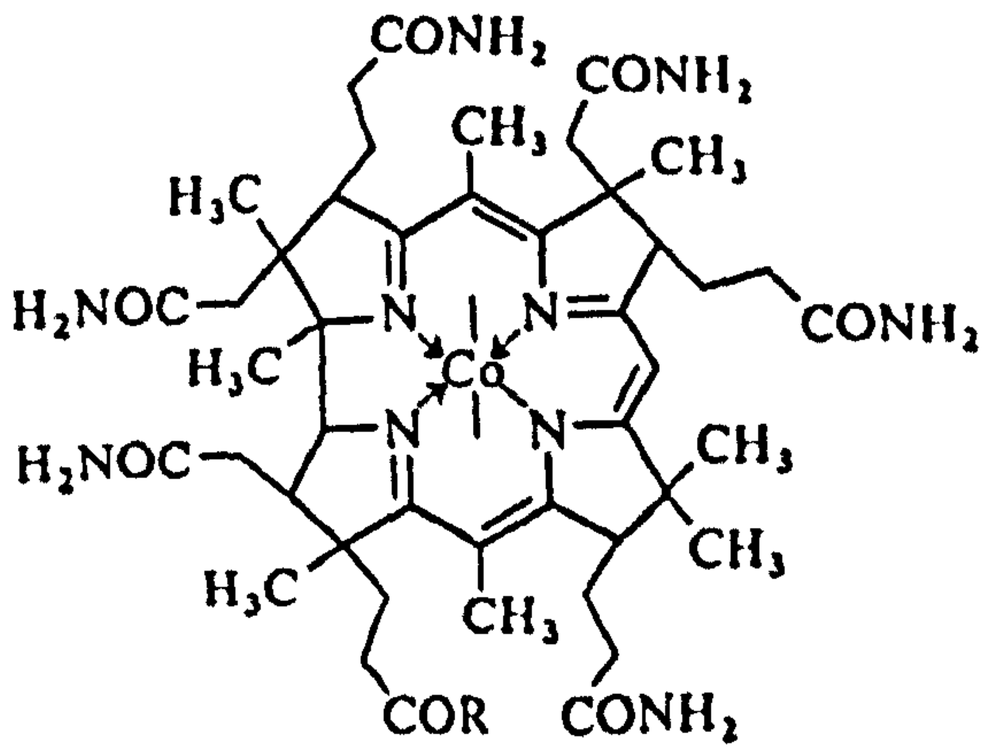

Figure 8-20 [Co] binding with N-terminal of a bio molecule

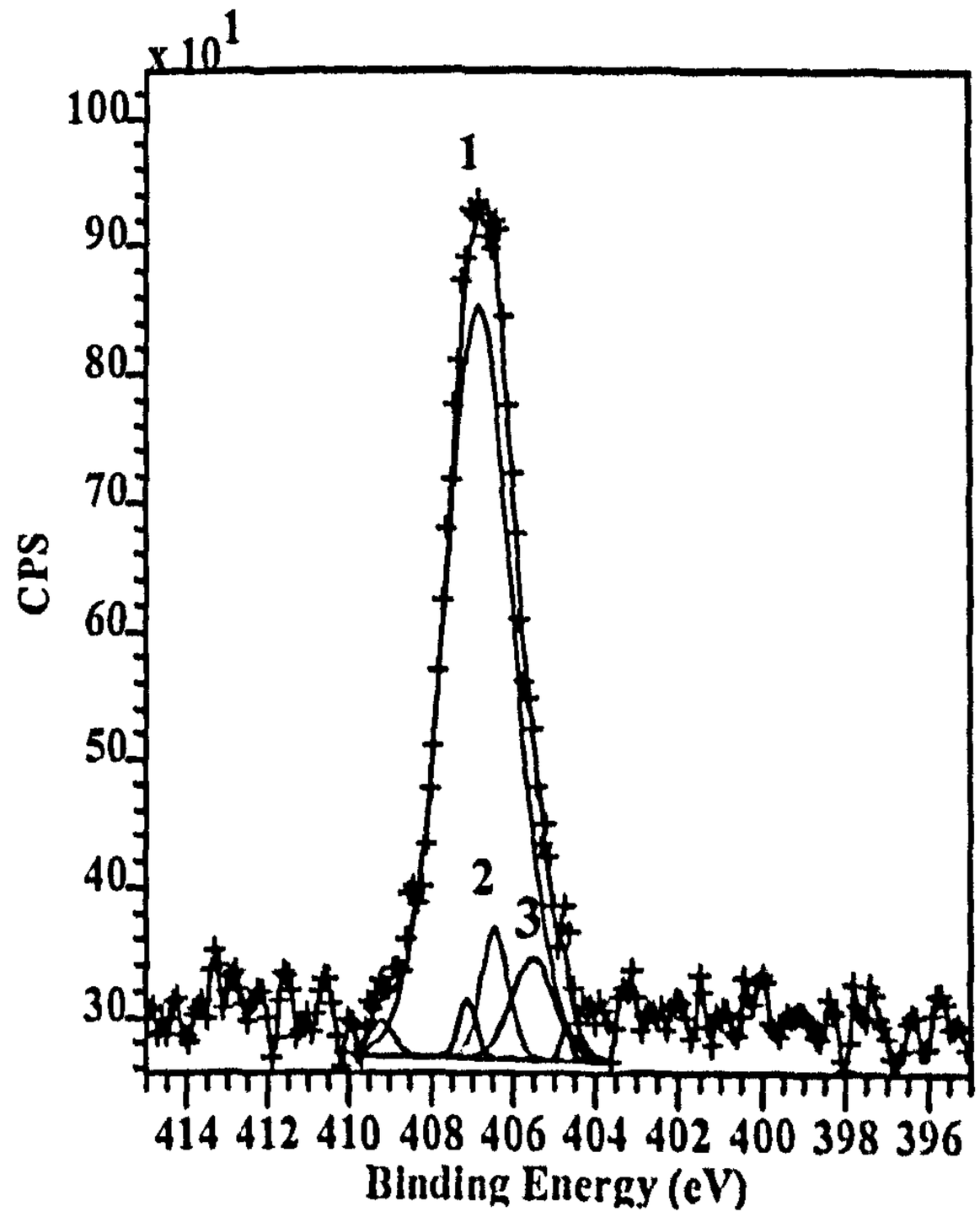

Figure 8-21 N 1s spectrum for HC CoCrMo in 50% serum

8.3.6. Mechanical depassivation and electrochemical repassivation

Under open circuit conditions, the passive film is removed by the mechanical movement from the counter body (depassivation process). For most implant materials, such as Co-based alloys and stainless steel 316L in this study, they tend to re-establish the passive film, which is driven by the electrochemical force (energy). This is called a repassivation process. The ability of a metallic material to repassivate is rather an important issue to evaluate the materials' tribocorrosion behaviour. In static conditions, 316L appeared no repassivation potential in 50% serum and it indicates that it is difficult for it to re build the protective film if localized corrosion occurs and propagates. CoCrMo alloys showed a decrease in repassivation capacity. One possible explanation is that proteins can block access of oxygen to the sample surface and then there is not enough oxygen to form oxides. Another reason is due to the set up of the experiments. In order to prevent the growth of bacteria in the biological environment, 0.01% sodium azide was added. It is an oxygen scavenger, which results in a decrease of oxygen content in the solution.

From Figure 6-9, the potential was monitored as the sliding progressed. It gives a good indication of the depassivation/repassivation transformation. In Figure 7-14, materials were under applied active potential. It is much clear and uniform. It is shown that in 50% serum the maximum current appeared when the motion reached highest speed. The current increased as the increase of the velocity (8-18). It is a competition between the removal of the passive film and the recovery.

For 316L, a similar trend was also observed. Probably, it is due to adhesive wear. Higher current was recorded in 0.36% NaCl than in 50% serum. Comparing the material loss, because a protective film formed (rich of Carbon) in 50% serum and in 0.36% NaCl, the potential brought sample to an active stage, materials in 50% serum had a lower degradation result than under CP. Oxygen was needed to form the passive film. Therefore, oxygen may be 'rubbed' from the proteins molecules and to

recruit the lack of free oxygen in the solution and left a carbon rich layer which was very efficient to the reduction of friction. The film was brokedown until no possible oxygen was received.

One the other hand, a reduced material loss compared to open circuit conditions and an enhanced loss than under CP was noticed. It is because that passive film was forced to form and it did have some benefits on the wear reduction but corrosion still took place on the sample surface. For 316L, the oscillations and spikes of current and corresponding friction is again due to the abrasive wear in the groove.

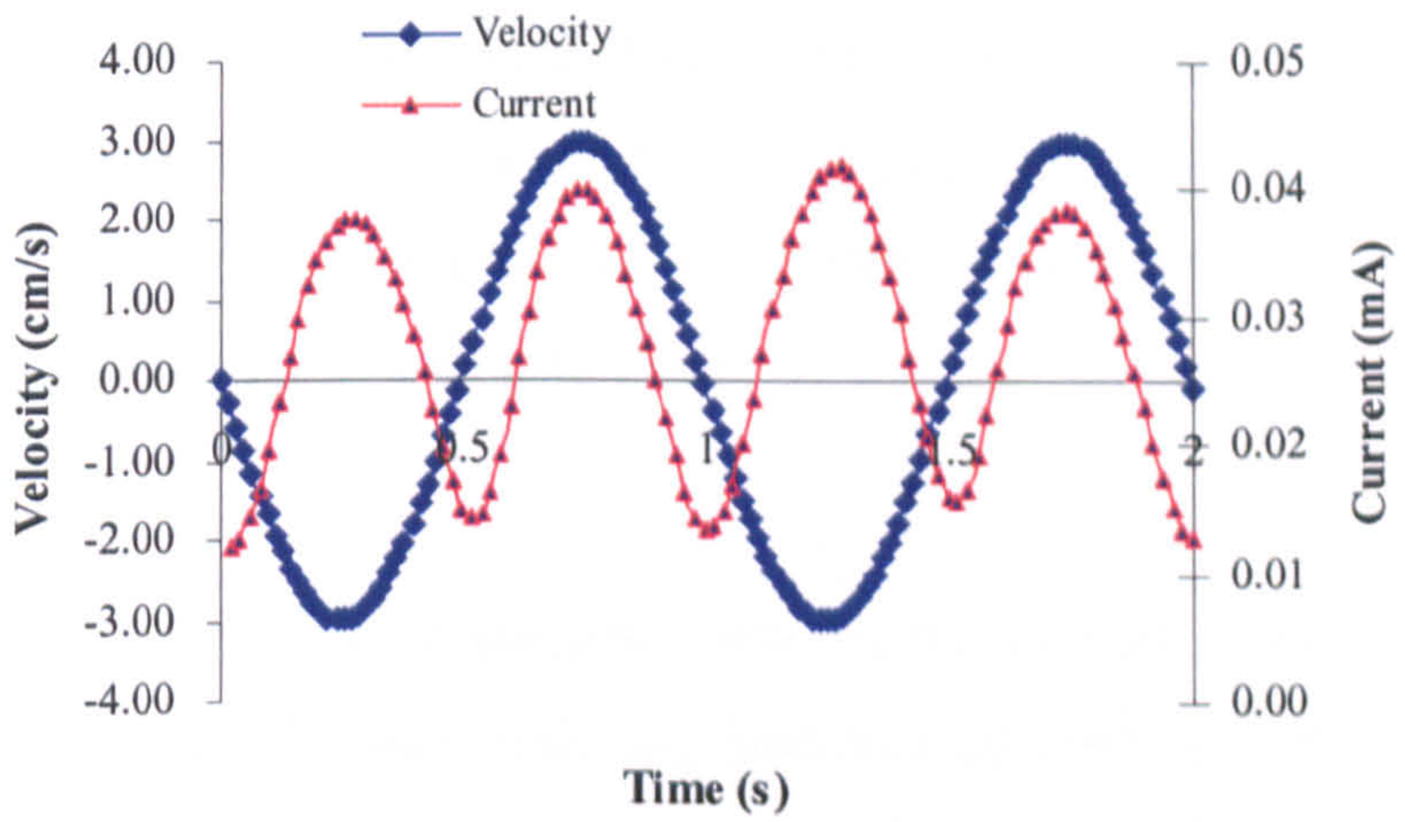

Figure 8-22 Current with change of velocity of reciprocating movement in two cycles for HC CoCrMo in 50% serum

8.4. Microstructure and Chemical Composition Effect on Tribology and Corrosion

The effect of hardness on wear resistance is of interest to many researchers. In this study, with the lowest hardness, 316L appeared to have the greatest material loss in all conditions. However, hardness is not the only factor to influence materials' tribological properties and the role is in much debate. The microstructures and

elemental compositions are more important on the effect of their wear behaviour. For HC CoCrMo and LC CoCrMo, in terms of micro hardness, they do not show big difference (Table 5-1), but they exhibited very distinguishable phenomena under tribocorrosion systems.

The only difference between HC CoCrMo and LC CoCrMo is the carbon content. Although the difference is from 0.05% to 0.19%, it makes a great distinction on materials microstructures and hence their behaviours in surrounding environments. In Chapter 5, the static corrosion behaviour for two of them is quite similar in terms of current density and breakdown potential. Sometimes, LC CoCrMo showed better corrosion resistance, probably due to the fact that no Cr is tightened with carbon and form hard phase carbides, which leave more Cr and Mo in the matrix to produce a continuous protective passive barrier to ion release. The main effort from higher carbon content is noticed in their tribology behaviour, furthermore, their tribocorrosion behaviour.

Figure 8-23 shows the relationship between the carbide volume fractions with the material loss. In all cases, with the presence of corrosion or the absence of corrosion, a higher carbide fraction corresponded to lower wear/corrosion-wear damage. It can be concluded that carbides can improve the wear/corrosion-wear resistance for CoCrMo alloys. However, the optimal carbides fraction is still not studied. If the fraction is too high, carbides may became overcrowded in the matrix and can not stabilize the matrix to resist wear damage. Moreover, they may be easier to be plucked off from the matrix.

Figure 8-24 shows friction changes with the carbide fraction. In general, friction does not appear to be affected much by different proportions of carbides. The reason is for samples in 50% serum and DMEM, they have greater values of minimum film thickness and adsorbed organic molecules than in 0.36% NaCl. However, in 0.36% NaCl, due to a thinner maximum film (Table 6-1), carbides may contact the counterpart and increase the friction.

The stabilization of the matrix by carbides also helps to reduce the plastic deformation. From Figure 6-8, HC CoCrMo did not show any deformation on the edge of the wear track. However, LC CoCrMo had slight deformation. The deformation can transfer to debris during the tribological contact. Therefore, the reduction of it can indicate less wear particles and less wear.

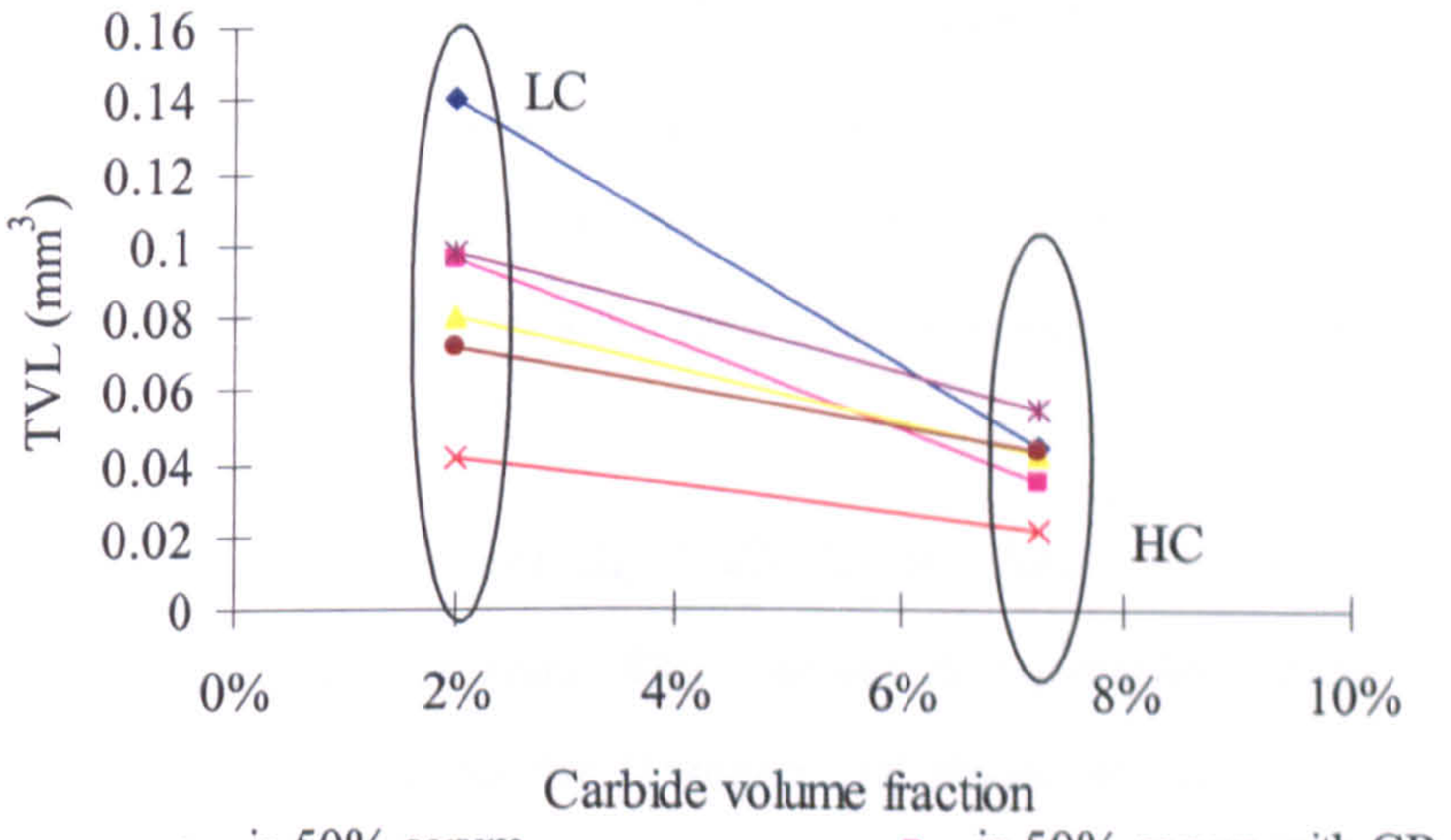

Figure 8-23 The relation of carbide volume fraction and material volume loss

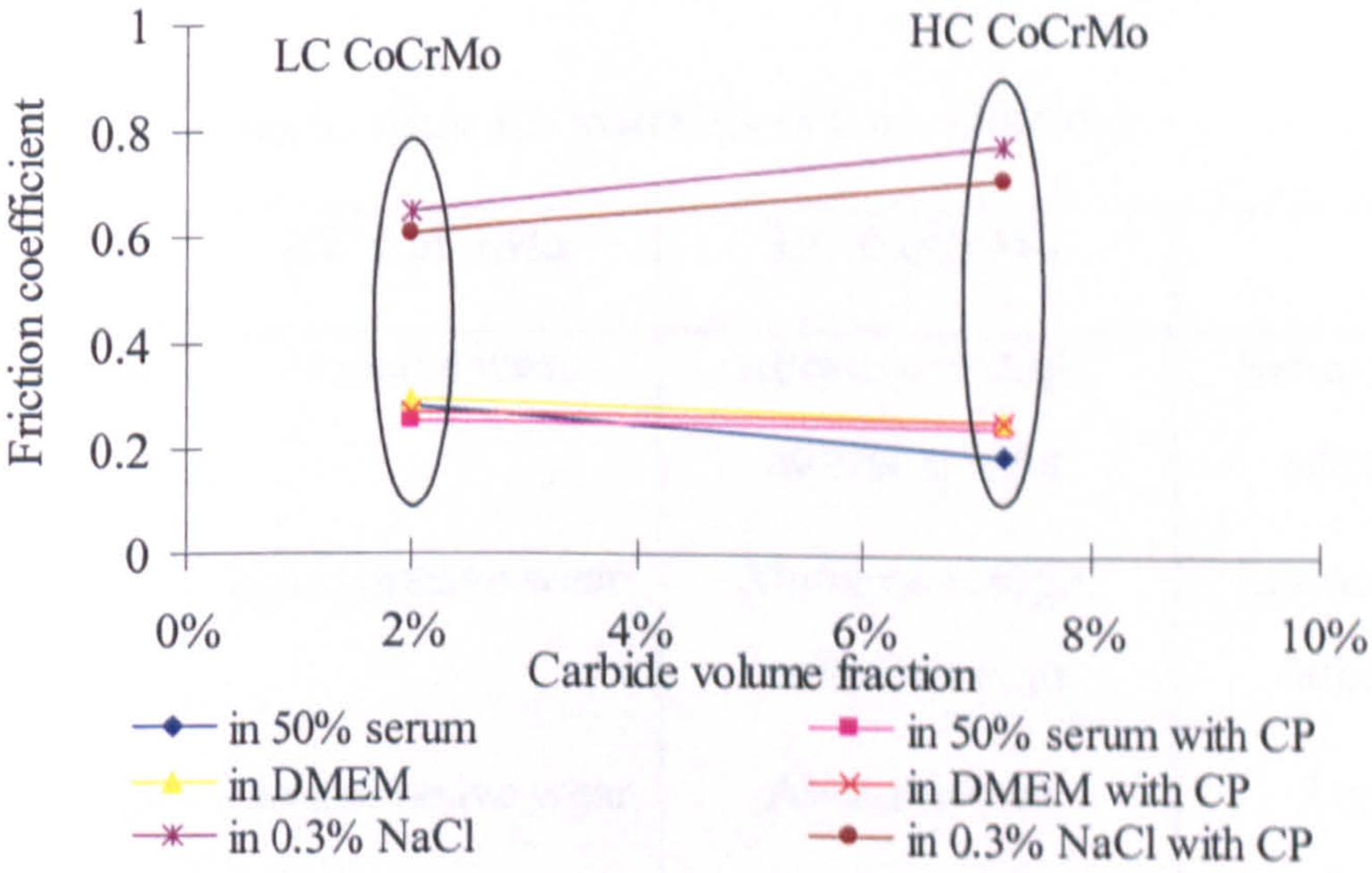

Figure 8-24 The relation of carbide volume fraction and friction coefficient

8.5. Wear Mechanisms and Corrosion Effect on Wear Mechanisms

The discussion of wear mechanisms is important to have a better understanding of the material degradation process and how corrosion affects it. Results have shown in Figure 6-6 and Figure 7-6. Delamination, removal of materials and scratches were all found on 316L. For HC CoCrMo, slight scratches were observed and for LC CoCrMo, few attached debris were found on the surface. Therefore, the wear mechanisms for three materials were concluded in Table 8-1. The wear mechanisms for HC CoCrMo and 316L in 50% serum were schematically shown in Figure 8-25 and Figure 8-22.

As mentioned earlier, for HC CoCrMo, the debris can act like a third body and can roll between two materials. This caused the scratches in the contact area. For 316L, adhesive wear led to the 'transfer' of material, not only to the counterpart (very few), but also to another position of the wear scar. The development and process is shown in Figure 8-27. The transferred material is more brittle than the substrate/passive film, so the propagation of cracks can be expected on both the passive film and also transferred debris. Less adhesive wear in 0.36% NaCl may be due to no organic species effect on the passive film and the adhesive strength was required higher than in 50% serum. Ploughing on 316L may cause the delamination of materials.

Table 8-1 Wear mechanisms for materials in three solutions

	HC CoCrMo	**LC CoCrMo**	**316L**
50% serum	Abrasive wear	Abrasive + slight adhesive wear	Serious abrasive + adhesive wear
DMEM	Less abrasive wear	Abrasive + slight adhesive wear	Serious abrasive + adhesive wear
0.36% NaCl	Least abrasive wear	Abrasive wear	Abrasive and adhesive wear

After debris was produced, the bare surface was left which accelerated the ions released to the solution. Also, cracks on the surface created possible sites for corrosion to propagate (Figure 8-27). On the other hand, when pitting corrosion occurred the material was much easier to be removed by the counterpart (Figure8-28).

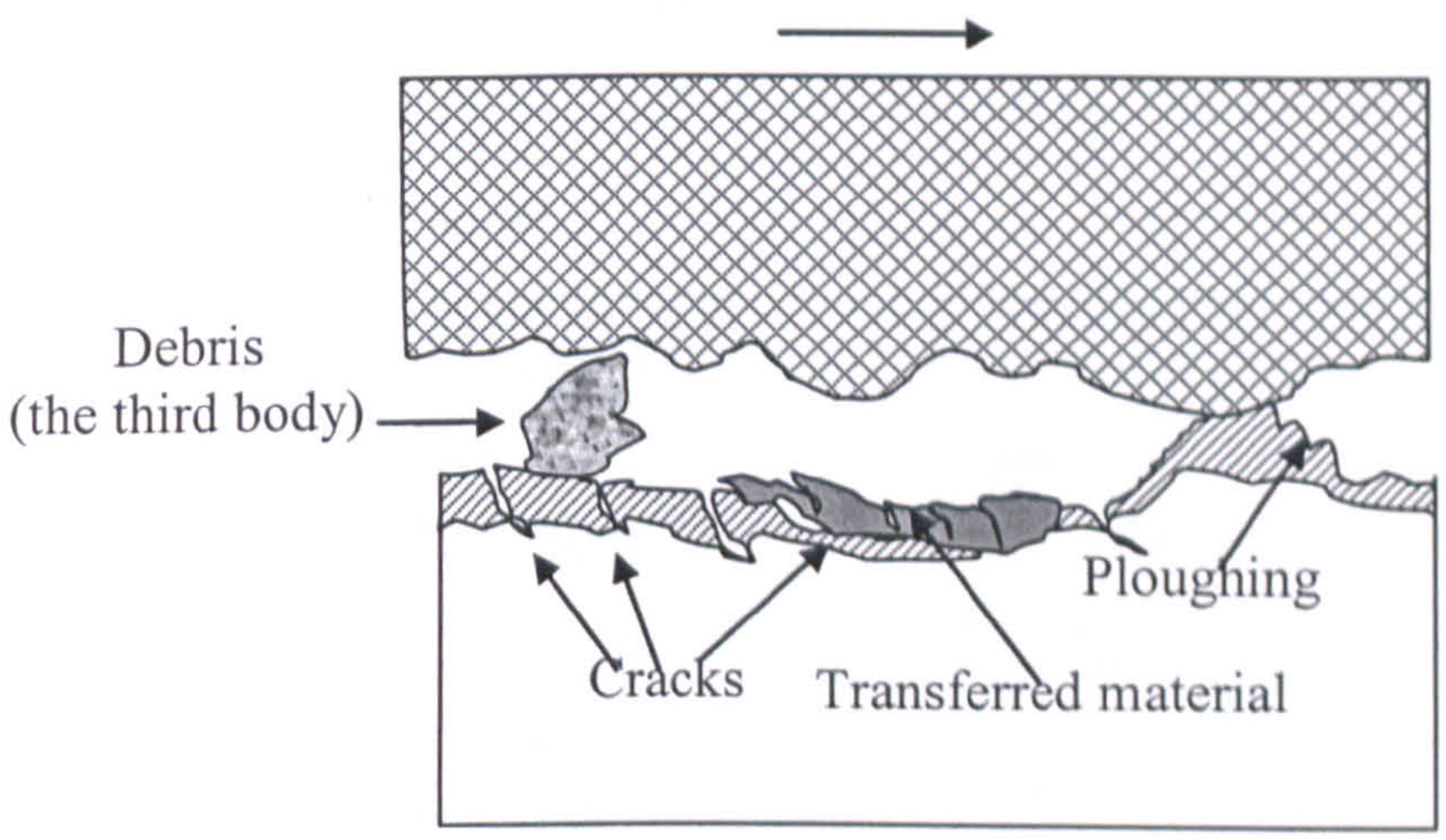

Figure 8-25 Schematic wear mechanisms for 316L

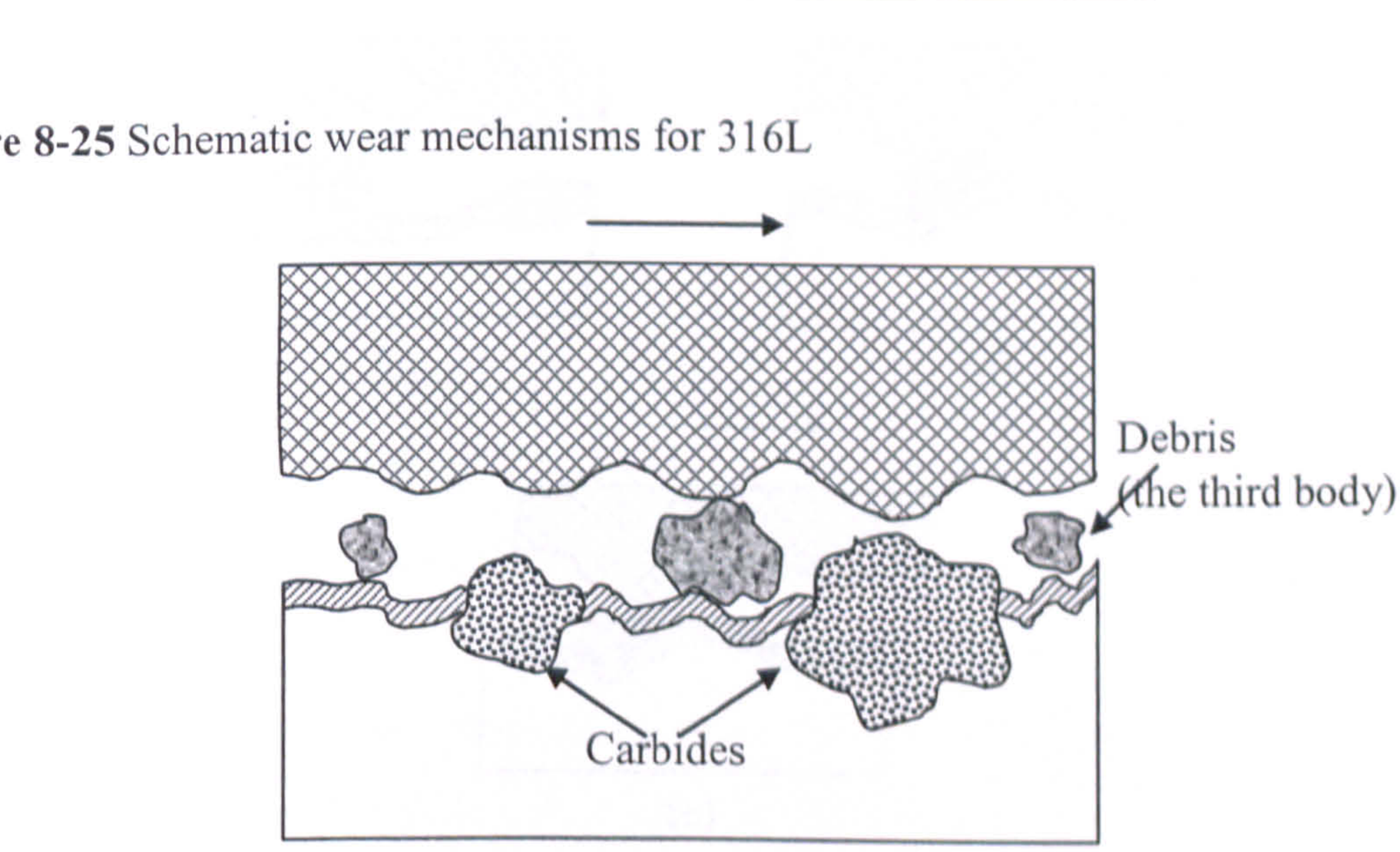

Figure 8-26 Schematic wear mechanisms for HC CoCrMo

Evidence was also observed from Figure 6-3, Figure 7-11 and Figure 7-15, in the presence of oscillations and spikes of potential, current and friction. The adhesive wear removed materials from sample surface very quickly which left serious damage on the surface. It reflects the increase of the current and decrease of the potential. Because of the rubbing effect, the friction had a transient increase. Then the recovery of the area where the material had been lost took place. Passive film re-formed and a decrease of current and friction coefficient can be recorded.

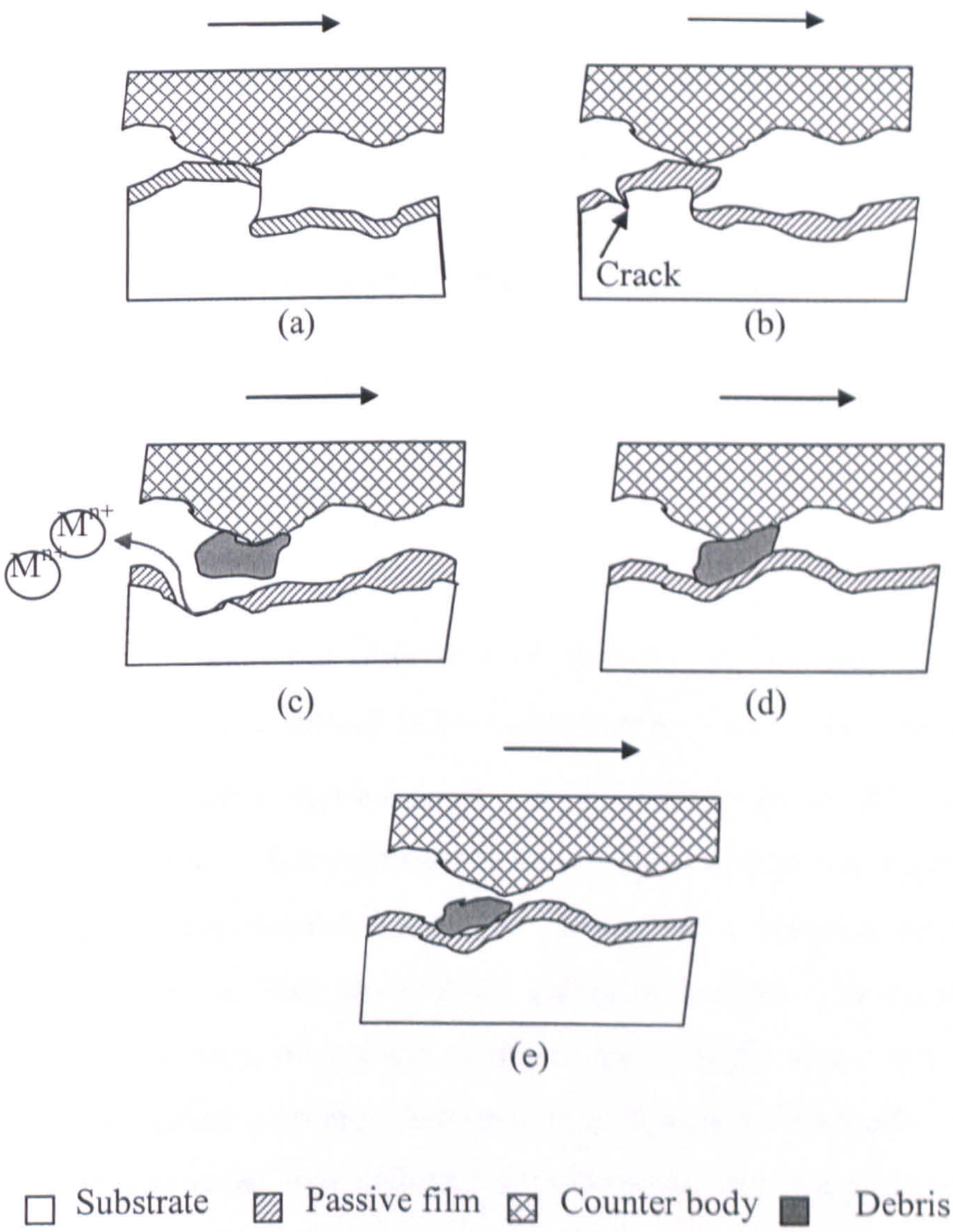

Figure 8-27 Model of adhesive wear and wear debris transfer for 316L

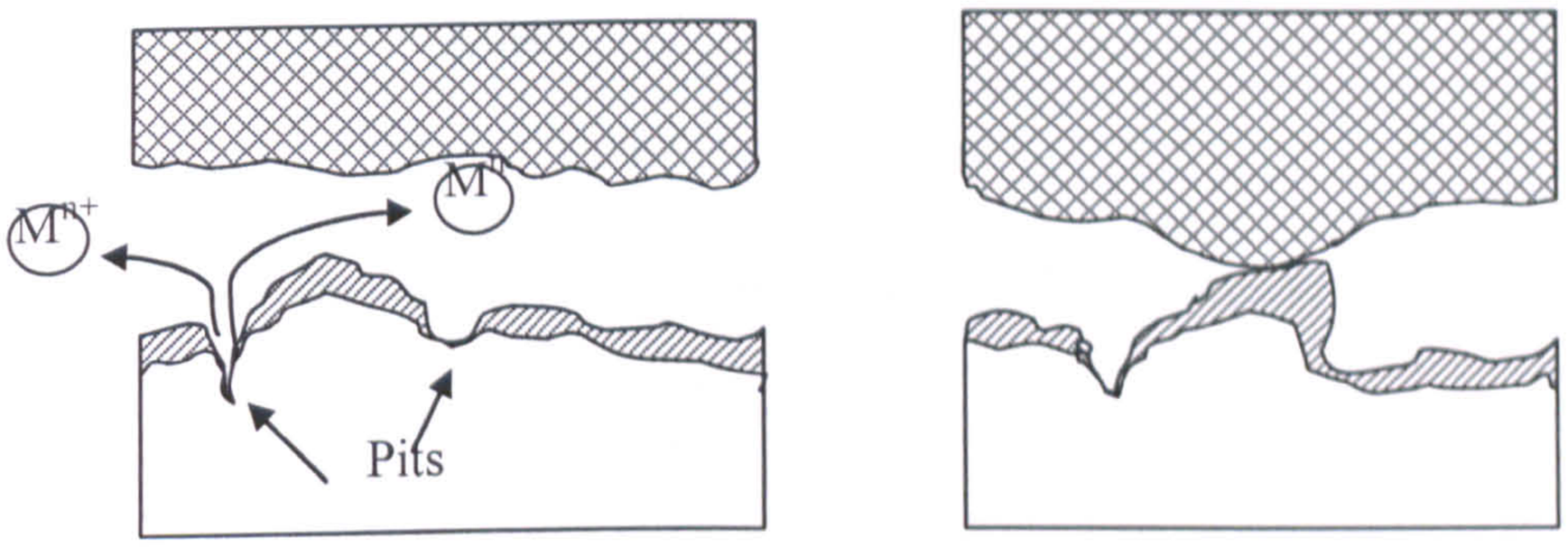

Figure 8-28 Possible effect of corrosion (micro-pits) on adhesive and abrasive wear for 316L

8.6. Surface Energy Effect in Tribocorrosion Systems

8.6.1. Liquid adhesive energy

The adhesion of water molecules or proteins can be characterized by the adhesion work (W_S). It is related to the liquid surface tension (γ_{sl}) and the contact angle (θ). All materials showed greater contact angle with 0.36% NaCl solution than with 50% serum, which indicates that the interaction between organic species is stronger than water molecules. However, whether the interaction was physical or chemical was not clear. Both physical and chemical reactions may be present. From Table 5-2, HC CoCrMo owned the smallest contact angle, thus the attachment of proteins on the surface is stronger and may result in a better lubrication effect. After samples were immersed into different environments, the interaction became the adsorbed proteins with protein molecules in 50% serum and water molecules with hydroxidized sample surface. As immersion progressed, adhesion seemed to increase, which may benefit the low friction in the steady-state.

$$W_S = \gamma_{sl}\left(1+\cos(\theta)\right) \qquad \text{Eq. 8-13}$$

8.6.2. Adhesive energy of solids

To investigate the adhesive behaviour of a solid, adhesive energy was employed and developed by various authors.

$$\Delta\gamma_{AB} = -\gamma_A^0 - \gamma_B^0 + \gamma_{AB}^0 \qquad \text{Eq. 8-14}$$

$$\gamma_{AB}^0 = \gamma^{chem} + \gamma^{geom} \qquad \text{Eq. 8-15}$$

γ^{chem} is the chemical interaction energy

γ^{geom} is the grain boundary energy

γ_A^0 and γ_B^0 are the surface energy of two contacted materials

because $\gamma^{geom} = 0.15(\gamma_A^0 + \gamma_B^0)$

so

$$-\Delta\gamma_{AB} = 0.85(\gamma_A^0 + \gamma_B^0) - \gamma^{chem} \qquad \text{Eq. 8-16}$$

$\Delta\gamma_{AB}$ is the adhesion energy. $-\Delta\gamma_{AB}$ then presents the energy is required to separated two surfaces.

$$\sigma_{max} = \sqrt{\frac{\gamma_{AB}^0 E}{\sqrt[3]{V_m}}} \qquad \text{Eq. 8-17}$$

σ_{max} is the adhesion strength. E is the Young's modulus. $\sqrt[3]{V_m}$ is a measure of the interatomic distance. Generally, the soft material intends to 'stick' on to the hard material, when two different materials are contacted. In this study, silicon nitride is far harder than 316L (passive film). Thus material is always transferred from 316L to the Si_3N_4 ball. The assumption is made that no chemical reactions were found between the attached 316L debris and the counterpart. It is based on XPS studies. Silicon was not found in the wear scar. Due to very low surface energy of the silicon carbide ball (contact angle = 136.7° with distilled water), the adhesive energy of debris on Si_3N_4 was low. Hence the transferred material may be removed by or it is

very difficult to have a transferred material on the silicon nitride ball. If the debris were pulled out from the sample surface, the surface energy of debris can be treated as similar as the passive film. Thus due to the higher value of it in 50% serum, the adhesive wear became more sever than in 0.36% NaCl.

However, from the discussion in the previous section, by preventing corrosion, adhesive wear seemed to be inhibited. It suggests that with the presence of corrosion, the adhesive surface energy of solids is different from materials surface under CP.

8.7. Time Dependence of Corrosion and Wear

The study is to investigate the tribocorrosion behaviour and ultimately to evaluate and help to develop orthopaedic implant materials. The time dependence analysis can explain the tribocorrosion progress over longer times and predict the possible behaviour of such materials in a biological environment.

Two distinct phases are observed. They are the running-in phase and the steady-state phase, which have been reported by many authors for MoM or MoP TJR [82]. The definition of the biphasic character was made based on their wear rate changes. The running-in period had a high wear rate and when materials were in steady-state, a relatively low (comparing with the running-in phase) and stable wear rate was obtained. Many authors have noticed this behaviour both *in vitro* and *in vivo* studies for metal or ceramic bearing implant materials (rigid-on-rigid materials) [25-27]. Before they achieved the steady state, nanometer-scaled debris and metal ions were largely released into the bulk environment [19, 21]. The ultimate goal for MoM implant is to reduce wear and also wear debris. The investigation of the effect of metallic wear debris to the surrounding tissues is still ongoing. However, from the researches on MoM and MoP hip replacements, wear debris remains one of the most important factors affecting the success of total hip arthroplasty. Therefore the initial running-in period is a crucial stage.

From the wear loss tests, CP tests, potentiodynamic tests and potentiostatic tests to ICP tests for the level of released metal ions, all results prove that a bi-phase presents. It has been proved that corrosion plays an important role in tribocorrosion systems. With and without applied CP, all materials present two distinct regions: running-in and steady-state suggesting that the transition is primarily due to mechanical effects. However, 20% to 32% of material degradation in steady-state was attributed to corrosion-related damage. HC CoCrMo showed a not clear transition of the two periods. Therefore, not only the mechanical wear but also the electrochemical corrosion has a different grade between the running-in and the steady-state during the tests. The result was mutual between wear and corrosion. In potentiostatic tests, in the running-in state the metal ions released much more and had a greater extent than in the steady-state. It is also in line with potentiodynamic tests. An activation controlled region was observed then followed by a distinct current reduction with the decrease of the friction. Linear polarization tests also confirm that in the running-in state, the R_p value was not stable until the steady state was reached.

In contact angle measurement, it appears that the adsorption of protein require a period of time. It seems that an hour of pre-adsorption time is needed for proteins to interact with solid surface until equilibrium attained [116]. From this study, the contact angle of serum on metallic surface reduces and stabilized after 1 hour. This also can contribute the transition of the running-in stage to the steady-state.

A stable and thick tribo-film was found in the steady-state by XPS tests. In the running-in stage, the formation of oxides/hydroxides and the organometallic complexes was changing and the thickness of the layers enhanced. It is mainly due to the tribo-chemical reactions in the contact zone and the interaction of protein molecules with the tribo-film

The reduction of friction was due to many factors such as the stable corrosion process, roughness films, tribofilm formations and increased protein adsorption. For

HC CoCrMo, it showed a low wear rate for the whole process. Its higher corrosion resistance (Figure 6-13), higher adhesive energy with proteins (Figure 5-18) and stable formation of metal-protein complexes with Co and Cr oxides (Figure 6-24 and Figure 6-16) are responsible.

CHAPTER 9

CONCLUSIONS AND FUTURE WORK

9.1. Conclusions

The subject of the tribocorrosion performance of implant materials in biological environments is challenging due to its complexity; many physical, chemical and electrochemical processes are involved. However, this study has made some progress towards the understanding of fundamental tribocorrosion processes and material degradation mechanisms in tribocorrosion systems. The link between tribological parameters with electrochemical response has been discussed. The performance of the three widely used implant materials has been evaluated in biological species-rich solutions. How materials are affected by service environment and vice versa have been addressed. The link between the tribofilms and tribocorrosion performance has been identified and discussed. The process – 'biotribocorrosion' is suggested to describe the phenomena of the joint effect of tribology and corrosion in a biological environment. Integrated *in-situ* electrochemical measurements appear to be very useful to determine corrosion and wear interactions. They can evaluate candidate materials in many respects (corrosion, wear and tribocorrosion). Some important findings are summarized in the following section.

9.1.1. Effect of corrosion, tribology and tribocorrosion on material degradation

An important objective of this study is to analyze the interaction between tribology and corrosion in comparing the extent of damage and the process controlling in tribocorrosion systems some conclusions can be derived as follows:

- For the reciprocating wear tests and the materials/solutions considered in this study, corrosion accounts for between 21-49% of the total volume loss, the remainder being attributable to mechanical wear.
- Corrosion-related damage, primarily the effect of corrosion on wear, represents a significant part of the overall tribo-corrosion process, especially on the LC CoCrMo and 316L.
- Corrosion plays a significant role in the overall degradation process in the various simulated biological fluids (and 0.36%NaCl).
- Tribology affects corrosion in various ways. The contact zone becomes more active compared to the rest of the material surface.
- The process of ion release is accelerated by tribological contact (sliding motion in this study). The polarization resistance decreases, which indicates that the protective film in the wear scar is influenced by tribology and tribocorrosion.
- All materials show a running-in and steady-state regime. A lower wear rate and lower fiction is observed in the steady-state regime compared with the running-in regime. This is primarily due to mechanical effects (change in roughness) but the influence of corrosion is also clear. In the steady-state regime, corrosion-related damage contributes 20%-30% of the total material loss.

9.1.2. Effect of biological species on tribocorrosion behaviour

- Proteins and amino acids adversely affect corrosion resistance of all alloys but especially LC CoCrMo and Stainless Steel 316L in static environments. Proteins enhance the static corrosion rate for all materials considered in this study. The passive region for all materials becomes shorter when proteins adsorb on sample surface.
- In wear-corrosion tests, wear behaviour, electrochemical behaviour and the synergy between them are clearly affected by proteins or amino acids for all the materials involved in this study. Some complex mechanisms, involving reactions between ionic species and biological species, are involved and such interfacial processes affect wear and friction response under sliding.
- Proteins can act as a lubricant and reduce friction but due to their effect on corrosion and tribocorrosion processes, they can enhance material degradation.
- Organometallic formations of proteins or amino acids and metal ions are found in the contact area. The formation can cease further ion release by acting as a barrier which also can reduce friction.
- Co^{2+} and Fe^{2+} are the most likely ions to bind with biological molecules and form complex species.
- HC CoCrMo alloy has shown superior resistance to wear-corrosion – primarily due to its ability to resist high rates of corrosion degradation in wear conditions in protein-rich environment.

9.1.3. Evaluation of materials in biotribocorrosion systems

- Due to its excellent wear resistance and high corrosion resistance, HC CoCrMo delivered the best performance in terms of low and stable wear rates, high tribocorrosion resistance and low friction. Even though the biocompatibility of HC CoCrMo is still under long-term investigation and the material degradation for hip replacement depends on many factors (diameter of femoral head,

clearance and the selection of coupling materials), HC CoCrMo is recommended to be employed as a hard bearing MoM prostheses material.

- Surface properties such as their wettability (surface energy) can influence material performance in tribocorrosion systems. High wettability (high surface energy) surfaces tends to absorb proteins more efficiently and form a boundary lubricant under tribological contacts.
- The formation of organometallic complexes (proteins-metal), cobalt sulphide and calcium phosphate during sliding has a tendency to reduce friction. The passive film under tribological rubbing is similar to the spontaneous air-formed passive film but the thickness is greater. For CoCrMo, the passive film contains mainly Cr_2O_3 and minor amounts of CoO/MoO_2. For 316L, Cr_2O_3 and Fe oxides are the major components of passive film.
- The proportion of carbides seems to play an important role in terms of wear resistance and tribocorrosion resistance. Increase of carbides content will increase hardness.

9.2. Suggestions for Future Work

Although the findings from this work are exciting and useful to the understanding and the development of implant materials in biotribocorrosion systems, several new questions have been initiated. Some directions are recommended to continue this study and a few are motioned below:

- An important concern of the use of metallic load bearing implants is the influence of released wear debris and metal ions to patients. In the current study, the awareness of wear debris to tribocorrosion behaviour presents, but further investigation of its exact effect on corrosion behaviour and tribological parameters is necessary.
- The current study is based on a ceramic-on-metal contact because it is the first attempt to understand the biotribocorrosion systems. In MoM joint replacement, the complexity of two metal components can make big difference. However,

the principles of the reaction will not change. Future work can be established in this area.

- The binding of biological molecules (especially proteins) with metal ions is proved to be very important in biotribocorrosion systems. The nature of the film formation (tribofilm) under tribological contact still need more work and attention.
- The current study used a reciprocating ball-on-plate tribometer to investigate the tribocorrosion behaviour of different materials. The ultimate goal in this work should be to instrument a hip simulator to be able to superimpose electrochemical measurements during the movement cycle. As a step towards this the future work will involve tribotesting of metal on metal systems using a multi-station pin-on-plate apparatus to obtain statistically relevant data.
- New materials, new treatments and new combinations and designs of joint replacements are developed fast. Evaluation of those factors is needed.

REFERENCES

[1] *Annual Report of The National Joints Registry (NJR)*, www.njrcentre.org.uk, 2003,

[2] *Annual Report of The Swedish National Hip Arthroplasty Register*, Swedish Orthopaedic Association, 2004,

[3] J. L. Tipper, E. Ingham, Z. M. Jin and J. Fisher, *The science of metal-on-metal articulation*, Current Orthopaedics, 2005, **19**, pp.280-287

[4] C. B. Rieker, R. Schon and P. Kottig, *Development and validation of a second-generation metal-on-metal bearing*, The Journal of Arthroplasty, 2004, **19**, pp.5-11

[5] D. W. Howie and M. A. McGee, *Metal-on-metal resurfacing versus total hip replacement-the value of a randomized clinical trial.*, The Orthopedic clinics of North America, 2005, **36**, pp.195-201

[6] R. W. Revie, *Uhlig's Corrosion Handbook*, 2000, New York, John Wiley & Sons

[7] P. R. Roberge, *Handbook of Corrosion Engineering*, 2000, New York, McGraw-Hill

[8] E. E. Stansbury and R. A. Buchanan, *Fundamentals of electrochemical corrosion*, 2000, Ohio, ASM International

[9] G. W. Stachowiak and A. W. Batchelor, *Engineering Tribology*, 2001, Woburn, Butterworth-Heinemann

[10] J. A. Williams, *Engineering Tribology*, 1998, Oxford, Oxford University Press

[11] Z. M. Jin, P. Firkins, R. Farrar and J. Fisher, *Analysis and modelling of wear of cobalt-chrome alloys in a pin-on-plate test for a metal-on-metal total hip replacement*, Proc Instn Mech Engrs H, 2000, **214**, pp.559-568

[12] Z. M. Jin, D. Dowson and J. Fisher, *Analysis of fluid film lubrication in artificial hip joint replacements with surfaces of high elastic modulus*, Proc Instn Mech Engrs Part H: Journal of Engineering in Medicine, 1997, **211**, pp.247-256

[13] G. E. Totten and H. Liang, *Mechanical Tribology*, 2004, New York, Marcel Dekker, Inc.

[14] D. F. Williams, *Definitions in biomaterials*, Proceeding of Consensus Conference of the European Society for Biomaterials, 1987, Amsterdam, Elsevier

[15] J. B. Park and Y. Kon Kim, *Metallic Biomaterials*, The Biomedical Engineering Handbook, 2000, Boca Raton, CRC Press LLC

[16] B. D. Ratner, *A history of biomaterials*, Biomaterials Science, 2004, London, Elsevier Academic Press

[17] M. Zhang, *Biocompatibility of materials*, Biomaterials and Tissue Engineering, 2004, Heidelberg, Spring-Verlag

[18] D. F. Gibbons, *Biomedical materials*, Annual Review of Biophysics and Bioengineering, 1975, 4, pp.367-375

[19] T. Hanawa and S. Hiromoto, *Surface Modification of metals and Alloys in a Human Body Environment*, Corrosion Engineering, 1998, **47**, pp.895-907

[20] M. A. Jacobs, M. B. Schmidt and R. Farrar, *Comparison of wear rates for metal-on-polyethylene and metal-on-metal hips*, The AAHKS sixth annual meeting, 1998,

[21] A. Yew, M. Jagatia, H. Ensaff and Z. M. Jin, *Analysis of contact mechanics in McKee-Farrar metal-on-metal hip implants*, Proc Instn Mech Engrs Part H: Journal of Engineering in Medicine, 2003, **217**, pp.333-340

[22] I. D. Learmonth, S. Gheduzzi and T. P. Vail, *Clinical experience with metal-on-metal total joint replacements: indications and results*, Proc. IMechE Part H: Engineering in Medicine, 2006, **220**, pp.229-237

[23] D. Dowson and Z. M. Jin, *Metal-on-metal hip joint tribology*, Proc. IMechE Part H: Engineering in Medicine, 2006, **220**, pp.107-118

[24] F. W. Chan, J. D. Bobyn, J. B. Medley, J. J. Krygier and M. Tanzer, *Wear and lubrication of metal-on-metal hip implants*, Clinical Orthopaedics and Related Research, 1999, **369**, pp.10-24

[25] D. Dowson, A. A. J. Goldsmith, C. M. McNie and S. L. Simith, *A tribological study of metal-on-metal total replacement hip joints*, Friction, Lubrication and Wear of Artificial Joints, 2003, London, Professional Engineering Publishing

[26] C. Pabinger, R. Biedermann, B. Stocke, M. Fischer and M. Krismer, *Migration of metal-on-metal versus ceramic-on-polyethylene hip prostheses*, Clinical Orthopaedics and Related Research, 2003, **412**, pp.103-110

[27] S. A. Catledge and Y. K.Vohra, *Structural and mechanical properties of nanostructured metalloceramic coatings on cobalt chrome alloys*, Applied Physics Letters, 2003, **82**, pp.1625-1627

[28] L. L. Hench and S. Best, *Ceramics, glasses, and glass-ceramics*, Biomaterials Science, 2004, London, Elsevier Academic Press

[29] D. F. Williams and R. L. Williams, *Degradative effects of the biological environment on metals and ceramics*, Biomaterials Science, 2004, London, Elsevier Academic Press

[30] D. Dowson, *History of Tribology*, 1998, London, Professional Engineering Pubs

[31] K. S. Katti, *Biomaterials in total joint replacement*, Colloids and Surfaces, 2004, **39**, pp.133-142

[32] M. Long and H.J.Rack, *Titanium alloys in total joint replacement-a materials science perspective*, Biomaterials, 1998, **19**, pp.1621-1639

[33] H. C. Amstutz, P. Campbell, H. McKellop, T. P. Schmalzried, W. J. Gillespie, D. Howie, J. Jacobs and J. Medley, *Metal on metal total hip replacement workshop consensus document*, Clinical Orthopaedics and Related Research, 1996, **319S**, pp.297-303

[34] A. A. J. Goldsmith, D. Dowson, G. H. Isaac and J. G. Lancaster, *A comparative joint simulator study of the wear of metal-on-metal and alternative material combinations in hip replacements*, Proceeding of Insit Mech Engers Part H: Engineering in Medicine, 2000, **214**, pp.39-47

[35] A. P. D. Elfick, I. M. Pinder and a. et, *The influence of femoral head roughness on the wear of UHMWPE sockets in cementless total hip replacement*, Journal of Biomedical Materials Research, 1999, **48**, pp.712-725

[36] V. Saikko and T. Ahlroos, *Wear simulation of UHMWPE for total hip replacement with a multidirectional motion pin-on-disk device: Effects of counterpace material, contact area and lubricant*, Journal of Biomedical Materials Research, 1999, **49**, pp.147-154

[37] S. Santavirta, M. Bohler, W. H. Harris and a. et, *Alternative materials to improve total hip replacement tribology*, Acta Orthop Scand, 2003, **74**, pp.380-388

[38] P. S. M. Barbour, M. H. Stone and J. Fisher, *A hip joint simulator study using simplified loading and motion cycles generating physiological wear paths and rates*, Proc Instn Mech Engrs, 1999, **213**, pp.455-467

[39] M. A. Wimmer, J. Loos, R. Nassutt, M. Heitkemper and A. Fischer, *The acting wear mechanisms on metal-on-metal hip joint bearings: in vitro results*, Wear, 2001, **250**, pp.129-139

[40] T. M. Devine and J. Wulff, *Cast vs Wrought cobalt-chromium surgical implant alloys*, Biomedical Materials, 1974, **9**, pp.151-167

[41] J. R. Goldberg and J. L. Glibert, *The electrochemical and mechanical behavior of passivated and TiN/AlN-coated CoCrMo and Ti6Al4V alloys*, Biomaterials, 2004, **25**, pp.851-864

[42] S. Barril, S. Mischler and D.Landolt, *Influence of fretting regimes on the tribocorrosion behavious of Ti6Al4V in 0.9 wt.% sodium chloride solution*, Wear, 2004, **256**, pp.963-972

[43] S. Hiromoto and S. Mischler, *Effect of albumin on fretting-corrosion mechanism of a Ti-Al-V Alloy*, European Cells and Materials, 2004, **7**, pp.40-41

[44] M. A. Germain, A. Hatton, S. Williams, J. B. Matthews, M. H. Stone, J. Fisher and E. Ingham, *Comparison of the cytotoxicity of clinically relevant cobalt-chromium and alumina ceramic wear particles in vitro*, Biomaterials, 2003, **24**, pp.469-479

[45] J. L. Tipper, J. B. Matthews, E.Ingham, T. D. Stewart and J. Fisher, *Wear and functional biological activity of wear debris generated from UHMWPE-on-Zirconia ceramic, metal-on-metal , and Alumnia ceramic-on ceramic hip prostheses during hip simulator testing*, Friction, Lubrication and Wear of Artificial Joints, 2003, London, Profession Engineering Publishing

[46] J. Yang and K. Meritt, *Detection of antibodies against corrosion products in patients Co-Cr total joint replacement*, Journal of Biomedical Materials Research, 1994, **28**, pp.1249-1258

[47] T. Hanawa, *Evaluation techniques of metallic biomaterials in vitro*, Science and Technology of Advance Materials, 2002, **3**, pp.289-295

[48] J. J. Jacobs, A. K. Skipor, P. A. Campbell, N. J. Hallab, R. M. Urban and H. C. Amstutz, *Can metal levels be used to monitor metal-on-metal hip arthroplasties*, The Journal of Arthroplasty, 2004, **19**, pp.59-65

[49] J. J. Jacobs, N. J. Hallab, A. K. Skipor and R. M. Urban, *Metal degradation products*, Clinical Orthopaedics and Related Research, 2003, **417**, pp.139-147

[50] L. C. Lucas, R. A. Buchanan, J. E. Lemons and C. D. Griffin, *Susceptibility of surgical cobalt-base alloy to pitting corrosion*, Biomedical Materials, 1982, **16**, pp.799-810

[51] B. C. Syrett and S. S. Wing, *Pitting Resistance of new and conventional orthopedic implant materials-effect of metallurgical condition*, Corrosion Nace, 1978, **34**,

[52] U. K. Mudali, T. M. Sridhar and B. Raj, *Corrosion in bio implants*, Sadhana, 2003, **28**, pp.601-637

[53] D. F. Williams, *Corrosion of implant materials*, Annual Review of Materials Science, 1976, **6**, pp.237-266

[54] J. Y. Lin and J. D. Bumgardner, *In vitro biocorrosion of CoCrMo implant alloy by macrophage cells*, Journal of Orthopaedic Research, 2004, **22**, pp.1231-1236

[55] F. Contu, B. Elsener and H. Bohni, *Corrosion behaviour of CoCrMo implant alloy during fretting in bovine serum*, Corrosion Science, 2004, **47**, pp.1863-1875

[56] A. T. Kuhn, *Corrosion of Co-Cr alloys in aqueous environments*, Biomaterials, 1981, **2**, pp.68-77

[57] M. A. Khan, R. L. Williams and D. F. Williams, *Conjoint corrosion and wear in titanium alloys*, Biomaterials, 1999, **20**, pp.762-772

[58] S. Rossi, L. Fedrizzi, F. Deflorian and M. Zen, *Wear-corrosion of nitrided steel:corrosion potential monitoring to evaluate the effect of test parameters*, Materials and Corrosion, 2000, **51**, pp.552-556

[59] M. Stemp, S. Mischler and D. Landolt, *The effect of mechanical and electrochemical parameters on the tribocorrosion rate of stainless steel in sulphuric acid*, Wear, 2003, **255**, pp.466-475

[60] T. Hanawa, *Corrosion Measurements of Biomedical Metallic Materials*, Corrosion Engineering, 2000, **49**, pp.687-699

[61] J. J. Jacobs, A. K. Skipor, L. M. Patterson, N. J. Hallab, W. G. Paprosky, J. Black and J. O. Galante, *Metal release in patients who have had a primary total hip arthroplasty. A prospective, controlled, longitudinal study*, The Journal of Bone and Joint Surgery, 1998, **80**, pp.1447-1458

[62] N. J. Hallab and J. J. Jacobs, *Orthopaedic applications*, Biomaterials Science, 2004, London, Elsevier Academic Press

[63] A. Hensten-Pettersen and N. Jacobsen, *Systemic toxicity and hypersensitivity*, Biomaterials Science, 2004, London, Elsevier Academic Press

[64] W. Brodner, P. Bizan, V. Meisinger, A. Kaider and *et. al*, *Elevated serum cobalt with metal-on-metal articularing surfaces*, J. BONE JT. SURG., 1997, **79**, pp.316-321

[65] C. S. Muniz, J. L. Fernandez-Martin and a. et, *Reference values for trace and ultratrace elements in human serum determined by doublefocusing ICP-MS*, Biol trace Elem Res, 2001, **82**, pp.259-269

[66] J. Black, E. C. Maitin, H. Gelman and D. M. Morris, *Serum concentrations of chromium, cobalt and nickel after total hip replacement : a six month study*, Biomaterials, 1983, **4**, pp.160-164

[67] T. Visuri and M. Koskenvuo, *Cancer risk after McKee total hip replacement*, Orthopedics, 1991, **14**, pp.137-142

[68] H. G. Willert, G. H. Buchhorn and D. Gobel, *Wear behaviour and histopathology of classic cemented metal-on-metal hip prostheses*, Clinical Orthopaedics and Related Research, 1996, **329**, pp.160-186

[69] A. Koegel and J. Black, *Release of corrosion products by F-75 cobalt base alloy in the rat. I:Acute serum elevations*, Society for Biomaterials, 1983,

[70] S. M. d. D. Micheli and O. Riesgo, *Electrochemical study of corrosion in Ni-Cr dental alloys*, Biomaterials, 1982, **3**, pp.209-212

[71] V. Saikko, *A multidirectional motion pin-on-disk wear test method for prosthetic joint materials*, Journal of Biomedical Materials Research, 1998, **41**, pp.58-64

[72] K. W. J. Wright, H. S. Dobbs and J. T. Scales, *Wear studies on prosthetic materials using the pin-on-disc machine*, Biomaterials, 1982, **3**, pp.41-48

[73] J. R. Goldberg and J. L. Gilbert, *Electrochemical response of CoCrMo to high speed fracture of its metal oxide using an electrochemical scratch*, Journal of Biomedical Materials Research, 1997, **37**, pp.421-431

[74] B. Roebuck and E. A. Almond, *The influence of composition, phase transformation and varying the relative f.c.c. and h.c.p. phase contents on the*

properties of Co-W-C alloys, Materials Science and Engineering, 1984, **66**, pp.179-194

[75] A. Kocijan, I. Milosev and B. Pihlar, *Cobalt-based alloys for orthopaedic applications studies by electrochemical and XPS analysis*, Materials in Medicine, 2004, **15**, pp.643-650

[76] J. N. Alhajji and M. R. Reda, *The effect of alloying elements on the electrochemical corrosion of low residual carbon steels in stagnant CO2-saturated brine*, Corrosion Science, 1993, **34**, pp.1899-1911

[77] F. Franks, *Protein stability: the value of 'old literature'*, Biophysical Chemistry, 2002, pp.117-127

[78] K. Kato, *Wear in relation to friction - a review*, Wear, 2000, **241**, pp.151-157

[79] M. Schmidt, H. Weber and R. Schon, *Cobalt chromium Molybdenum metal combination for modular hip prostheses*, Clinical Orthopaedics and Related Research, 1996, **329S**, pp.35-47

[80] H.-Y. Lin and J. D. .Bumgardner, *Changes in the surface oxide composition of Co-Cr-Mo implant alloy by macrophage cells and their released reactive chemical species*, Biomaterials, 2004, **25**, pp.1233-1238

[81] J. Cawley, J. E. P. Metcalf, A. H. Jones, T. J. Band and D. S. Skupien, *A tribological study of cobalt chromium molybdenum alloys used in metal-on-metal resurfacing hip arthroplasty*, Wear, 2003, **255**, pp.999-1006

[82] D. Dowson, C. Hardaker, M. Flett and G. H.Isaac, *A hip joint simulator study of the performance of metal-on-metal joint Part I: The role of Materials*, Arthroplasty, 2004, **19**, pp.124-130

[83] A. Wang, V. K. Polineni and a. et, *Effect of femoral head surface roughness on the wear of UHMWPE acetabular cups*, Journal of Arthroplasty, 1998, **13**, pp.615-625

[84] R. M. Hall and A. Unsworth, *Friction in hip prostheses*, Biomaterials, 1997, **18**, pp.1017-1026

[85] D. M. Elliott, J. Fisher and D. T. Clark, *Effect of counterface surface roughness and its evolution on the wear and friction of PEEK and PEEK-bonded carbon fibre composites on stainless steel*, Wear, 1998, **217**, pp.288-296

[86] N. J. Hallab, K. Bundy, K. O'Connor, R. Moses and J. Jacobs, *Evaluation of Metallic and Polymeric Biomaterial Surface Energy and Surface Roughness Characteristics for Directed Cell Adhesion*, Tissue Engineering, 2001, **7**, pp.55-68

[87] G. W. Stachowiak, A. W. Batchelor and L. J. Griffiths, *Friction and wear changes in synovial joints*, Wear, 1994, **171**, pp.135-142

[88] R. M. Hall, M. J. K. Bankes and G. Blunn, *Biotribology for joint replacement*, Current Orthopaedics, 2001, **15**, pp.281-290

[89] K. R. St.John, L. D. Zardiackas and R. A. Poggie, *Wear evaluation of cobalt-chromium alloy for use in a metal-on-metal hip prosthesis*, Journal of Biomedical Materials Research Part B, 2004, **68B**, pp.1-14

[90] D. Dowson, C. Hardaker, M. Flett and G. H.Isaac, *A hip joint simulator study of the performance of metal-on-metal joint Part II: Design*, Arthroplasty, 2004, **19**, pp.118-123

[91] P. Heilmann and D. S. Rigney, *Running in processes affecting friction and wear*, The running-in process in tribology, 1981, Surry, Butterworth & Co Ltd.

[92] J. K. Lancaster, *On the initial stages of wear of dry-bearing composites*, The running-in process in tribology, 1981, Surry, Butterworth & Co Ltd.

[93] S. C. Scholes, S. M. Green and A. Unsworth, *The wear of metal-on-metal total hip prostheses measured in hip simulator*, Proceeding of Institution Mechanical Engineers Part H, 2001, **215**, pp.523-530

[94] H. Onishi, I. C.Clarke, V. Good, H. Amino and M. Ueno, *Alumina hip joints characterized by run-in wear and steady-state wear to 14 million cycles in hip-simulator model*, Journal of Biomedical Materials Research A, 2004, **70**, pp.523-532

[95] F. Contu, B. Elsener and H. Bohni, *Stability and repassivation of metallic implants in serum bovine*, European Cells and Materials, 2001, **1**, pp.14-15

[96] J. E. Lemons and L. C. Lucas, *Properties of biomaterials*, Arthroplasty, 1986, **1**, pp.143-147

[97] S. Mischler, A. Spiegel and D. Landolt, *The role of passive oxide film on the degradation of steel in tribocorrosion systems*, Wear, 1999, **225-229**, pp.1078-1087

[98] D. Landolt, S. Mischler and M. Stemp, *Electrochemical methods in tribocorrosion: a critical appraisal*, Electrochemica Acta, 2001, **46**, pp.3913-3929

[99] Y. Okazaki, *Effect of friction on anodic polarization properties of metallic biomaterials*, Biomaterials, 2002, **23**, pp.2071-2077

[100] P. Ponthiaux, F. Wenger, D. Dress and J. P. Celis, *Electrochemical techniques for studying tribocorrosion processes*, Wear, 2004, **256**, pp.459-468

[101] I. Garcia, D. Drees and J. P. Celis, *Corrosion-wear of passivation materials in sliding contacts based on a concept of active wear track area*, Wear, 2001, **249**, pp.452-460

[102] A. Neville and T. Hodgkiess, *Characterisation of high-grade alloy behaviour in severe erosion-corrosion conditions*, Wear, 1999, **233-235**, pp.596-607

[103] J. Jiang, M. M. Stack and A. Neville, *Modelling the tribo-corrosion interaction in aqueous sliding conditions*, Tribology International, 2002, **35**, pp.669-679

[104] M. A. Khan, R. L. Williams and D. F. Williams, *The corrosion behaviour of Ti-6A1-4V,Ti-6A1-7Nb and Ti-13Nb-13Zr in protein solutions*, Biomaterials, 1999, **20**, pp.631-637

[105] G. C. F. Clark and D. F.Williams, *The effects of proteins on metallic corrosion*, Biomedical Materials, 1982, **16**, pp.125-134

[106] M. Kobayashi and S. Shimizu, *Cobalt proteins*, Eur. J. Biochem., 1999, **261**, pp.1-9

[107] C. J. v. Oss and R. J. Good, *Orientation of the water molecules of hydration of human serum albumin*, Journal of Protein Chemistry, 1988, **7**, pp.179-183

[108] G. H. Isaac, J. Thompson, S. Williams and J. Fisher, *Metal-on-metal bearings surfaces: materials, manufacture, design, optimization, and alternatives*, Proc. IMechE Part H: Engineering in Medicine, 2006, **220**, pp.119-133

[109] J. b. Medley, *Comparison of alloys and designs in a simulator study of metal on metal implants*, Clinical Orthopaedics and Related Research, 1996, **329S**, pp.148-159

[110] P. S. Walker and b. I. Gold, *The tribology (friction, lubrication and wear) of all-metal artificial hip joints*, Clinical Orthopaedics and Related Research, 1996, **329S**, pp.4-10

[111] S. Affatato, G. Bersaglia, D. Emiliani, I. Foltran and A. Toni, *Sodium-azide versus ProClin 300: influence on the morphology of UHMWPE particles generated in laboratory tests*, Biomaterials, 2004, **25**, pp.835-842

[112] H. C. Amstutz, B. J. Thomas, R. Jinnah and a. et, *Treatment of primary osteoarthritis of the hip. A comparison of total joint and surface replacement arthroplasty*, J. BONE JT. SURG., 1984, **66**, pp.228-241

[113] J. Zhu, N. Xu and C. Zhang, *Characteristics of copper corrosion in simulated uterine fluid in the presence of protein*, Advances in Contraception, 1999, **15**, pp.179-190

[114] T. A. Horbett, *The role of adsorbed proteins in tissue response to biomaterials*, Biomaterials Science, 2004, London, Elsevier Academic Press

[115] J. P. Glusker, *Structural aspects of metal liganding to functional groups of proteins*, Advances in protein, 1991,

[116] V. Hlady and J. Buijs, *Protein adsorption on solid surfaces*, Current Opinion in Biotechnology, 1996, **7**, pp.72-77

[117] B. Kasemo, *Biological surface science*, Materials Science, 1998, **3**, pp.451-459

[118] S. M. Barlow, k. J. Krozer and e. al, *Study of glycine adsorption on a Cu surface using reflection absorption infrared spectroscopy*, Surface Sci, 1998, **401**, pp.322-335

[119] D. F. WIlliams, I. N. Askill and R. Smith, *Protein adsorption and desoption phenomena on clean metal surfaces*, Biomedical Materials, 1985, **19**, pp.313-320

[120] M. P. Heuberger, M. R. Widmer, E Zobeley, R. Glockshuber and N. D. Spencer, *Protein-mediated boundary lubrication in arthroplasty*, Biomaterials, 2005, **26**, pp.1165-1173

[121] T. Hanawa, *Metal ion release from metal implant*, Materials Science and Engineering C, 2004, **24**, pp.745-752

[122] D. Johnson, S. Norman, R. C. Tuckey and L. L. Martin, *Electrochemical behaviour of human adrenodoxin on a pyrolytic graphite electrode*, Bioelectrochemistry, 2003, **59**, pp.41-47

[123] R. L. Williams and D. F. Williams, *Albumin adsorption on metal surfaces*, Biomaterials, 1988, **9**, pp.206-212

[124] R. L. Williams, S. A. Brown and K. Merritt, *Electrochemical studies on the influence of proteins on the corrosion of implant alloys*, Biomaterials, 1988, **9**, pp.181-186

[125] M. J. Swann, L. L. Peel, S. Carrington and N. J. Freeman, *Dual-polarization interferometry: an analytical technique to measure changes in protein structure in real time, to determine the stoichiometry of binding event, and to differentiate between specific and nonspecific interactions*, Analytical Biochemistry, 2004, **329**, pp.190-198

[126] P. Bernabeu and A. Capramo, *Influence of surface charge on desorption of fibrinogen and/or albumin on a rotating disc electrode of platinum and carbon*, Biomaterials, 1990, **11**, pp.258-264

[127] K. Merritt and S. A. Brown, *Distribution of cobalt chromium wear and corrosion productions and biological reactions*, Clinical Orthopaedics and Related Research, 1996, **329S**, pp.233-243

[128] B. Adelina, *An innovative method based on the difference of material wettability to gain an efficient lubricant condition*, Synopses of the International Tribology, 2005, Kobe

[129] T. H. Muster, A. K. Neufeld and I. S. Cole, *The protective nature of passivation films on zinc: wetting and surface energy*, Corrosion Science, 2004, **46**, pp.2337-2354

[130] B. A. Ivarsson, P.-O. Hegg, K. I. Lundstrom and U. Jonsson, *Adsorption of proteins on metal surfaces studied by ellipsometric and capacitance measurements*, Colloids and Surfaces, 1985, **13**, pp.169-192

[131] D. Y. Wu, Y. Xie and a. et, *Surface enhanced Raman scattering from bare cobalt electrode surfaces*, PhyschemComm, 2001, **18**, pp.1-13

[132] N. J. Hallab, A. Skipor and J. Jacobs, *Interfacial kinetics of titanium- and cobalt-based implant alloys in human serum: Metal release and biofilm formation*, Journal of Biomedical Materials Research Part A, 2003, **65**, pp.311-318

[133] G. H. Cross, A. A. Reeves, S. Brand, J. F. Popplewell, L. Peel, M. J. Swann and N. J. Freeman, *A new quantitative optical biosensor for protein characterisation*, Biosensors and Bioelectronics, 2003, **19**, pp.383-390

[134] G. Beamson, D. Briggs, S. F. Davies, I. W. Fletcher, D. T. Clark, J. Howard, U. Gelius, B. Wannberg and P. Balzer, *Performance and application of the Scienta ESCA300 spectrometer*, Surface and Interface Analysis, 1990, **15**, pp.541-549

[135] C. D. Wagner, A. V. Naumkin, A. Kraut-Vass, J. W. Allison and C. J. Powell, *NIST X-ray Photoelectron Spectroscopy Database*, NIST Standard Reference Database 20, Version 3.4 (Web Version),

[136] http://lasurface.com/Data_base/Aw_test_princ_database.htm, *La Surface Database*

[137] T. Hanawa, S. Hiromoto and K. Asami, *Characterization of the surface oxide film of Co-Cr-Mo alloy after being located in quasi-biological environments using XPS*, Applied Surface Science, 2001, **183**, pp.68-75

[138] B. S. Becker and J. D. Bolton, *Corrosion behaviour and mechanical properties of functionally gradient materials developed for possible hard-tissue applications*, Materials Science, 1997, **8**, pp.793-797

[139] B. C. Syrett and S. S. Wing, *An electrochemical investigation of fretting corrosion of surgical implant materials*, National Association of Corrosion Engineers, 1978, **34**, pp.379-383

[140] R. L. Williams, *The interfacial reaction between implantable materials and proteins*, 1986, University of Liverpool

[141] X. Hu and A. Neville, *An examination of the electrochemical characteristics of two stainless steels (UNS S32654 and UNS S31603) under liquid-solid impingement*, Wear, 2004, **256**, pp.537-544

[142] M. Browme, P. J. Gregson and R. H. West, *Characterization of titanium alloy implant surfaces with improved dissolution resistance*, Materials Science, 1996, **7**, pp.323-329

[143] C. S. Abreu, M. S. Amaral, F. J. Oliveira, A. Tallaire, F. Benedic, O. Syll, G. Cicala, J. R. Gomes and R. F. Silva, *Tribological testing of self-mated nanocrystalline diamond coatings on Si3N4 ceramics*, Surface and Coatings Technology, 2006, **200**, pp.6235-6239

[144] J. Yang and J. Black, *Competitive binding of chromium, cobalt and nickel to serum proteins*, Biomaterials, 1994, **15**, pp.262-268

[145] G. Fagan, H. Wayment, D. Morris and P. Crosby, *The albumin cobalt binding test: analytical performance of a new automated chemistry assay for the detection of ischemia modified albumin*, Journal of Clinical Ligand Assay, 2002, **25**, pp.178-187

[146] L. J. Yang, *Prediction of net steady-state wear coefficient in an Al-Al2O3/stell system with an integrated wear model*, Tribology Letters, 2004, **17**, pp.105-118

[147] T. Hanawa, K. Asami and K. Asaoka, *Repassivation of titanium and surface oxide film regenerated in simulated bioliquid*, John Wiley, 1998, **98**, pp.530-538

[148] T. Hanawa and M. Ota, *Calcium Phosphate naturally formed on titanium in electrolyte solution*, Biomaterials, 1991, **12**, pp.767-774

[149] J. D. Andrade, V. Hlady and A. P. Wei, *Adsorption of complex proteins at interfaces*, Pure and applied chemistry, 1992, **64**, pp.1777-1781

[150] H. J. Mueller, *The binding of corroded metallic ions to salivary-type proteins*, Biomaterials, 1983, **4**, pp.66-71

[151] K. Merritt, S. A. Brown and N. A. Sharkey, *The binding of metal salts and corrosion products to cells and proteins in vitro*, Biomedical Materials, 1984, **18**, pp.1005-1015

[152] N. J. Hallab, J.J.Jacobs, S. A, J. Black, M. K and J. O. Galante, *Systemic metal-protein binding associated with total joint replacement arthroplasty*, Journal of Biomedical Materials Research, 2000, **49**, pp.353-361

[153] B. Chan, N. Dodsworth, J. Woodrow, A. Tucker and R. Harris, *Site-specific N-terminal auto-degradation of human serum albumin*, Eur. J. Biochem., 1995, **227**, pp.524-528

[154] D. Bar-Or, G. Curtis, N. Rao, N. Bampos and E. Lau, *Characterization of the Co^{2+} and Ni^{2+} binding amino-acid residues of the N-terminal of human albumin*, Eur. J. Biochem., 2001, **268**, pp.42-47

[155] W. Stopford, J. Turner, D. Cappelini and T. Brock, *Bioaccessibility testing of cobalt compounds*, Jour. Envir. Moni., **2003**, pp. 675-680

[156] P. A. Dearnley, *A review of metallic, ceramic and surface-treated metals used for bearing surfaces in human joint replacements*, Proc. Instn. Mech. Engrs. H, **1999**, 213, pp. 107-135.

[157] C.G.F. Pina, *Tribology of nitrogen S-phase coated stainless steel for UHMWPE hip joints*, University of Leeds, 2005